Appendix B Addendum

Marine Processes Technical Report

ORIEL WINDFARM
OFFSHORE RENEWABLE ENERGY

rps
A TETRA TECH COMPANY

JERA NEX BP

ESB Energy for generations

ORIEL WIND FARM PROJECT

Natura Impact Statement Addendum

Appendix B Addendum: Marine Processes Technical Report

MDR1520C
NIS –
Appendix B Addendum
A1 C01
December 2025

Contents

Figures

Tables

Glossary

Term	Meaning
Ebb tide	Changing of the tides from high to low.
Flood tide	Changing of the tides from low to high.
Littoral current	Flow derived from tide and wave climate.
Offshore Cable Corridor	This is where the offshore cable will be located.
Shields parameter	A nondimensional number used to calculate the initiation of motion of sediment in a fluid flow
Significant wave height	Mean wave height (trough to crest) of the highest third of the waves.
Spring tide	Tide that occurs when the sun and moon are directly in line with the Earth and their gravitational pulls reinforce each other.
Residual current	The resulting flow over the course of a tidal cycle.

Acronyms

Term	Meaning
ADCP	Acoustic Doppler Current Profiler
AEP	Annual Exceedance Probability
BERR	Department for Business Enterprise and Regulatory Reform
BODC	British Oceanographic Data Centre
CD	Chart Datum (generally defined as LAT)
CEFAS	Centre for Environment, Fisheries and Aquaculture Science
CIRIA	Construction Industry Research and Information Association
DHI	Danish Hydraulic Institute
ECMWF	European Centre for Medium Range Forecasts
EMODnet	European Marine Observation and Data Network
EPA	Environmental Protection Agency
FLiDAR	Floating Light Detection and Ranging
GSI	Geological Survey of Ireland
HAT	Highest Astronomical Tide
HWM	High Water Mark – the level reached by the sea at high tide
ICPSS	Irish Coastal Protection Strategy Study
INFOMAR	Integrated Mapping for the Sustainable Development of Ireland's Marine Resource
LAT	Lowest Astronomical Tide
LIDAR	Light Detection and Ranging
LWM	Low Water Mark – the level reached by the sea at low tide
MEDIN	Marine Environmental Data and Information Network
MHWN	Mean High Water Neaps
MHWS	Mean High Water Springs
MI	Marine Institute
MLWN	Mean Low Water Neaps
MLWS	Mean Low Water Springs
MRFS	Mid-Range Future Scenario
MT	Mud Transport

Term	Meaning
OPW	Office of Public Works
ORE	Offshore Renewable Energy
SPM	Suspended Particulate Matter
WTG	Wind Turbine Generator

Units

Unit	Description
mm	Millimetre (distance)
m	Metre (distance)
km	Kilometre (distance)
mm/s	Millimetres per second (speed)
m/s	Metres per second (speed)
mg/l	Milligrams per litre (suspended sediment concentration)
g/l	Grams per litre (suspended sediment concentration)

PREFACE

This Addendum provides supplementary information in response to a Request for Further Information (RFI) from An Coimisiún Pleanála (ACP) (formerly An Bord Pleanála) regarding the planning application (case reference ABP-319799-24) for the Oriel Wind Farm Project (hereafter referred to as "the Project"). Due to the nature of the additional information requested which involved replotting many of the figures and providing additional information throughout, the marine processes modelling study documented in appendix B: Marine Processes Technical Report of the Natura Impact Statement (NIS) has been reproduced in its entirety with the inclusion of the supplementary information. Thus, this document supersedes appendix B: Marine Processes Technical Report.

To facilitate the reader in understanding the changes to appendix B: Marine Processes Technical Report, supplementary text in blue is included in this Addendum.

Many of the figures presented in appendix B: Marine Processes Technical Report have been updated in response to the further information request e.g. to show the offshore cable corridor or with increased resolution. To aid the reader in identifying where changes have been made three figure and table caption types have been applied within the document, as follows:

- Text of title in black - no change has been made to the figure.
- Text of title in blue (e.g. Figure 2 2: Model bathymetry to mean sea level) – figure updated but no material change, e.g. plotting at increased resolution or including reference data.
- Text of title in blue with the inclusion of 'A', e.g. Figure 2A-9, indicates one of the following:
  - New figure in response to RFI;
  - Updated model output; or
  - Updated figure with amendment, e.g. a change to plotting scale or parameter unit.

The reader should note that due to the inclusion of additional information dispersed throughout the document the figure and table numbers will vary from those presented in appendix B: Marine Processes Technical Report.

1 INTRODUCTION

This Marine Processes Technical Report presents information relating to marine processes associated with the Oriel Wind Farm Project (hereafter referred to as the Project). It describes the current baseline conditions and quantifies the potential changes due to the Project. It covers the numerical modelling undertaken in respect of design parameters for the construction, operational and maintenance, and decommissioning phases of the Project.

The numerical modelling study undertaken was designed to provide supporting information for the marine processes environmental assessment. The approach adopted is in line with that for other Offshore Renewable Energy (ORE) developments in the UK and across Europe, whereby the modelling is undertaken to determine the potential magnitude of impact by a comparative study of selected infrastructure and activities. Modelling has not been undertaken for activities which are scoped out of the assessment and it is also noted that if an activity or installation is not modelled this does not mean it was excluded from the assessment. This may be because it is not anticipated to have a significant effect, can be inferred from modelling undertaken or that in-built mitigation measures will be adopted to avoid significant impacts, e.g. the use of shallow profile tapered cable protection which enables sediment transport regime to continue uninterrupted. Sample, but representative, activities have been modelled to determine the magnitude of potential impacts and no significant impacts were identified nor did these impacts result in an effect on a sensitive area or coastal feature. As a result of the determination of no significant impacts, more detailed modelling was not justified, required for assessment or undertaken.

The offshore wind farm area is located east of Dundalk Bay, to the east of the Dundalk Patch (as shown on Admiralty Charts), with the landfall located south of Dunany Point. The offshore wind farm area is characterised by relatively **weak tidal currents** with water depths ranging between approximately 16 m and 33 m. Seabed sediments within the offshore wind farm area range from muddy sand to coarse gravel, with exposed rock outcrops at some locations.

This Technical Report is presented in three main sections:

- Baseline conditions – describing current hydrography and sedimentology (see section 2).
- Potential environmental effects – describing changes to the baseline arising from the construction and operational phases of the Project (see Section 3).
- Model verification – describing model calibration and validation (see section 4).

1.1 Study area

Section 2 outlines the physical conditions associated with the Marine Processes Study Area which is based on one tidal excursion from the offshore wind farm area and the offshore cable corridor. The tidal excursion was quantified by utilising the calibrated numerical model described in section 2: Baseline conditions. Specifically, neutrally buoyant particles were released across the extent of the modelled offshore wind farm area and offshore cable corridor. The excursion of these particles was examined over the course of a spring tide cycle and used to define the extent of a typical tidal excursion.

1.2 Methodology

The study utilised a range of data types from multiple sources as summarised in Table 1-1.

The MIKE numerical modelling suite was used to assess and describe the tide, wave and sediment transport processes both individually and in combination using a single model domain as described in section 2.1. The MIKE suite of models is a widely used industry standard modelling package developed by the Danish Hydraulic Institute (DHI). It has been approved for use by industry and government bodies including the Environmental Protection Agency (EPA). The MIKE suite is a modular system that contains different but complementary modules encompassing different gridding approaches and representing different physical processes.

Table 1-1: Summary of data sources.

Sources	Study	Data type	Format
UK Hydrographic Office	Admiralty	Tidal statistics and harmonics	Tide tables
Integrated Mapping for the Sustainable Development of Ireland's Marine Resource (INFOMAR)	Seabed Mapping Programme	Bathymetry / Light Detection and Ranging (LIDAR)	Digital source
Office of Public Works (OPW)	Irish Coastal Protection Strategy Study	Bathymetry / LIDAR	Digital source
	Catchment Flood Risk Assessment Management Studies	Bathymetry / LIDAR	Digital source
	Wave, tide and surge forecast trial for Dundalk	Bathymetry	Digital source
	Port Oriel and Giles Quay gauge data	Water level data	Digital source
MEDIN	Seabed Mapping Programme	Bathymetry / LIDAR	Digital source
CMap	Digital Charts	Bathymetry	Digital source
RPS	Irish Sea Surge model	Water level and current speed boundary data	Digital source
European Centre for Medium Range Forecasts (ECMWF)	ERA-40	Wave data	Digital source
	ERA5	Wind data	Digital source
Marine Institute	M2 buoy	Wave and wind data	Digital source
Gavin and Doherty Geosolutions (2018)	Oriel Wind Farm Project Site Data Review	Sedimentology Information: including Geological Survey Ireland (GSI) Foreshore Licence Area survey analysis	PDF Document
Gavin Doherty Geosolutions (2020)	Oriel Ground Model Update and Cable Route Interpretation	Sedimentology Information: geophysical data, geotechnical data, grab samples and boreholes collected for Oriel wind farm	PDF Document
PARTRAC (2020)	Oriel Wind Farm – Floating LiDAR Buoy 12 Month Measurement Campaign Data Report	Wave, current and wind data	Digital source and PDF Document
European Marine Observation and Data Network (EMODnet)	Sedimentology	Seabed classification	PDF Spatial data

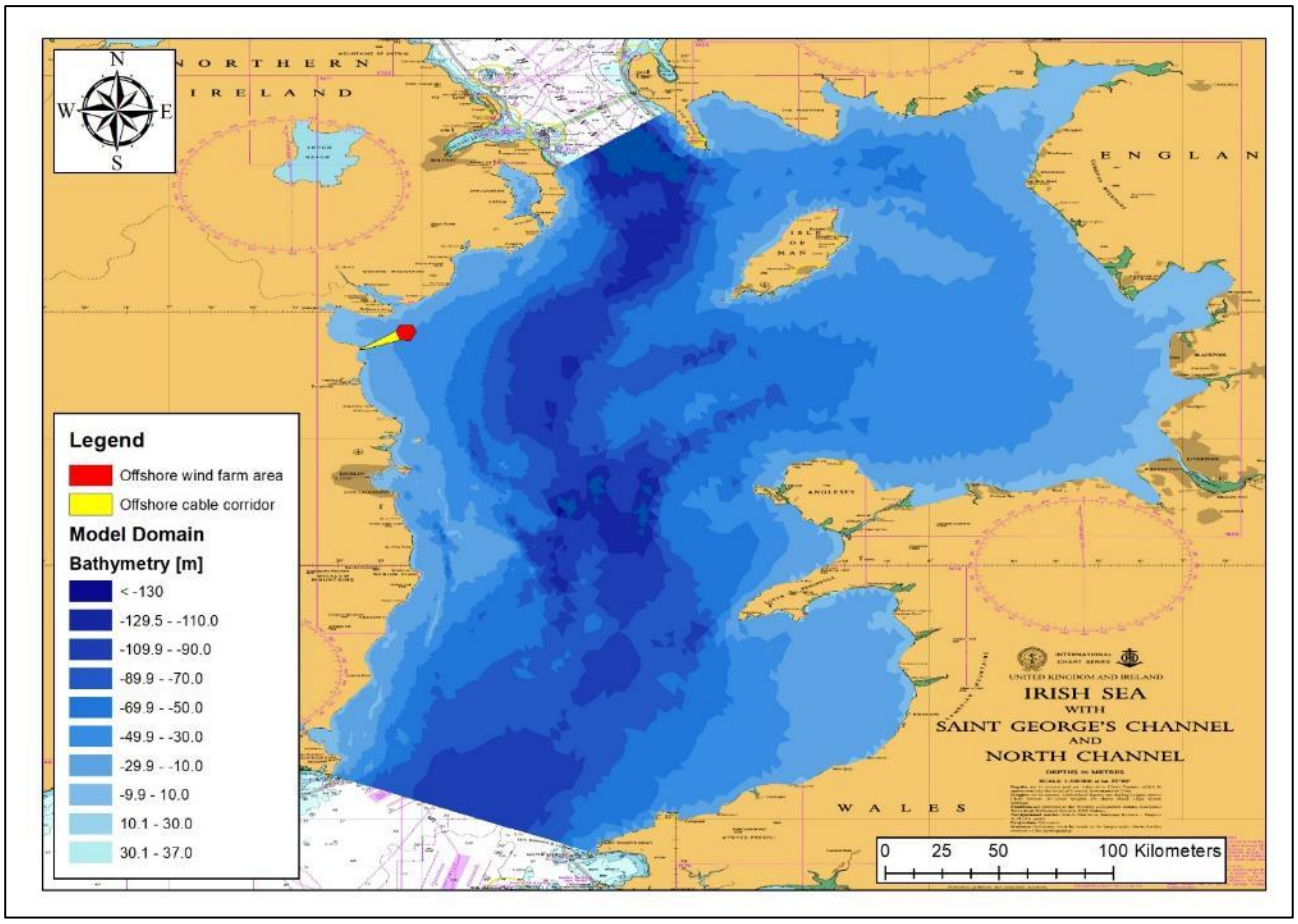

Figure 1-1: Numerical model domain used to assess marine processes in context of the Project.

2 BASELINE CONDITIONS

This section outlines the numerical modelling that was undertaken to determine baseline conditions. It describes the physical environment in terms of the sea state and existing sediment transport regime.

2.1 Bathymetry

The model domain had full bathymetry data coverage and was developed utilising data from a range of sources. This included data from the European Inspire project provided by INFOMAR, a joint programme between the GSI and the Marine Institute, which incorporated high resolution surveys which included the offshore wind farm area. Additionally, these surveys also provided coverage of the offshore banks along the east coast of Ireland which is important for the development of the wave climate in the Irish Sea.

The model also utilised Lidar and bathymetric data collected for the Irish Coastal Protection Strategy Study, the Catchment Flood Risk Assessment Management Studies and the wave, tide and surge forecast trial for Dundalk undertaken on behalf of the OPW.

Figure 2-1 illustrates a section of the bathymetric data used to develop the model whilst the inset shows the INFOMAR datasets for the Marine Processes Study Area.

Where additional data was required, digital chart data supplied by C-Map was included. The data was prioritised in order so that the most recent data was used where there was data overlay and all data was adjusted to the mean sea level datum.

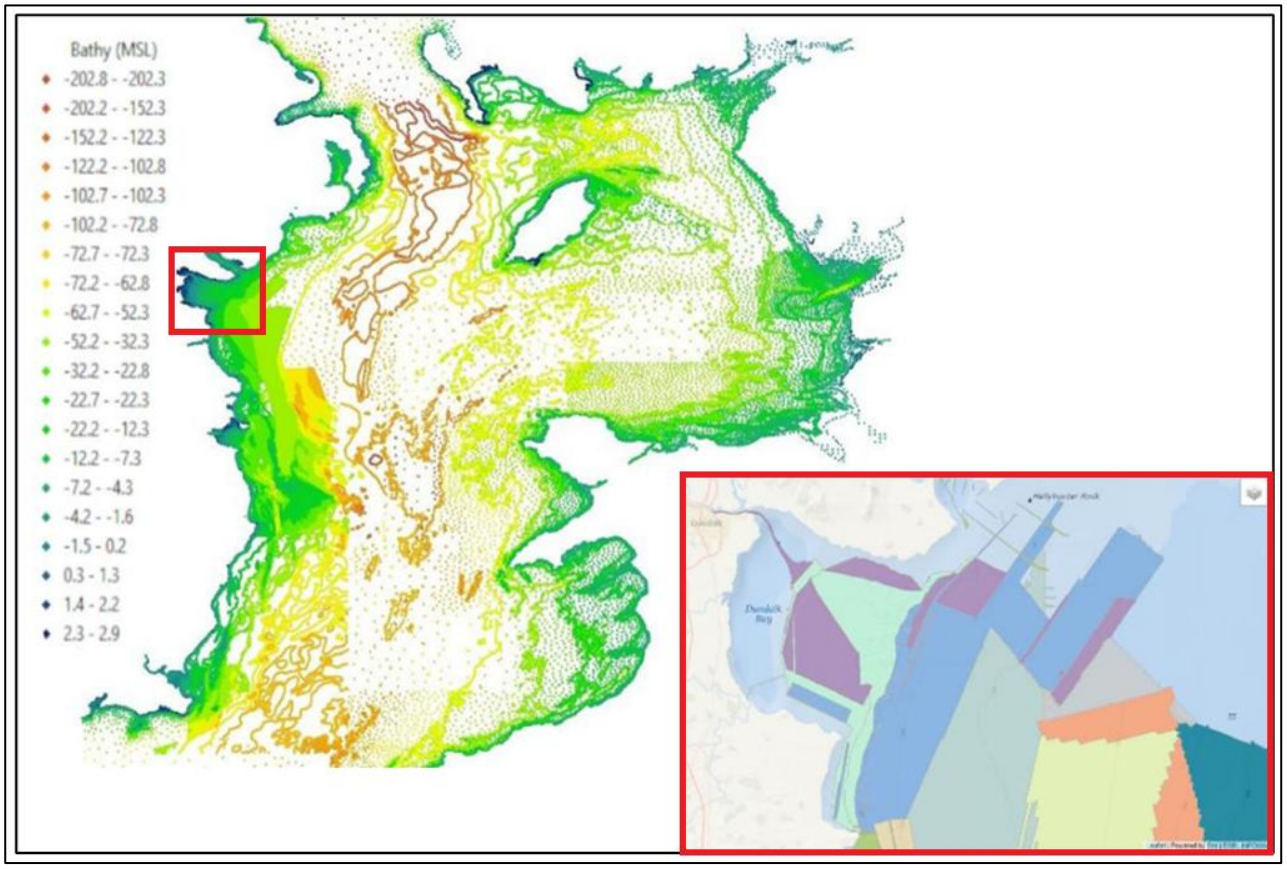

Figure 2-1: Sample of bathymetric data (left) detail of INFOMAR datasets within study area (inset).

The resolution of the model bathymetry was designed to provide accurate simulation of tidal currents. The model resolution was increased in areas where rapid changes in bathymetry occur. This included Arklow Bank, Codling Bank and Blackwater Bank to the south. Additionally, the model resolution was increased to <5 m across the offshore wind farm area in order that the influence of scour protection may be included within the sediment transport modelling in the post-construction modelling.

The extent of the domain was designed to provide a suitable basis for tide, wave and sediment transport modelling. The focus of the study is one tidal excursion from the offshore wind farm and offshore cable corridor area. However, a larger domain was required to develop wave fields and ensure that tidal currents were simulated accurately at the offshore wind farm area.

As illustrated in Figure 2-1, the model extends across the entire Irish Sea from the North Channel to Saint George's Channel. This extent ensured a stable tidal model due to the larger range and also enabled fetch limited wave modelling to be undertaken. Figure 2-2 shows the variation in bathymetry across the model domain whilst Figure 2-3 shows the detail of the Marine Processes Study Area with mesh data inset. In each case the offshore wind farm and offshore cable corridor areas are shown in red.

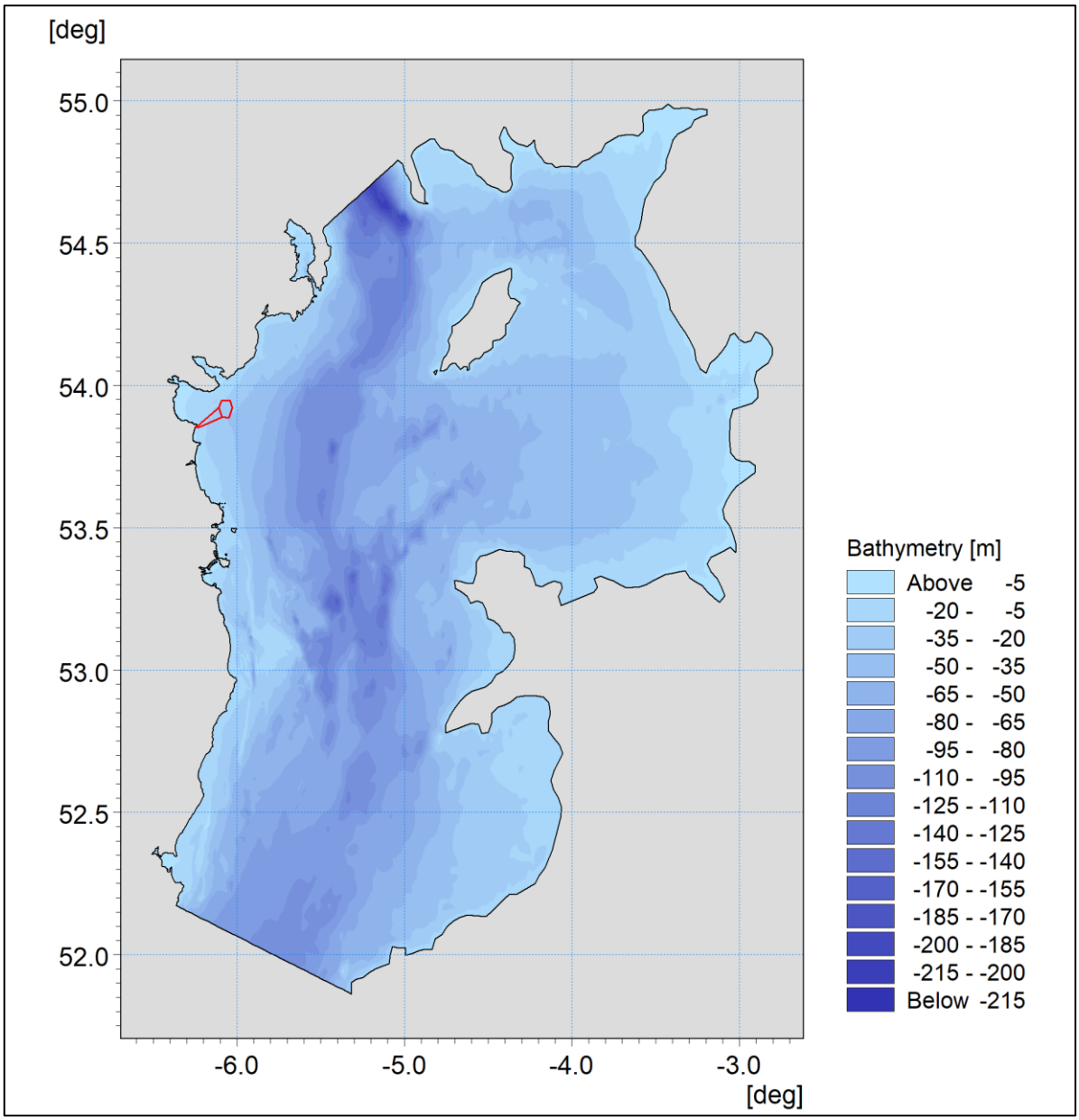

Figure 2-2: Model bathymetry to mean sea level.

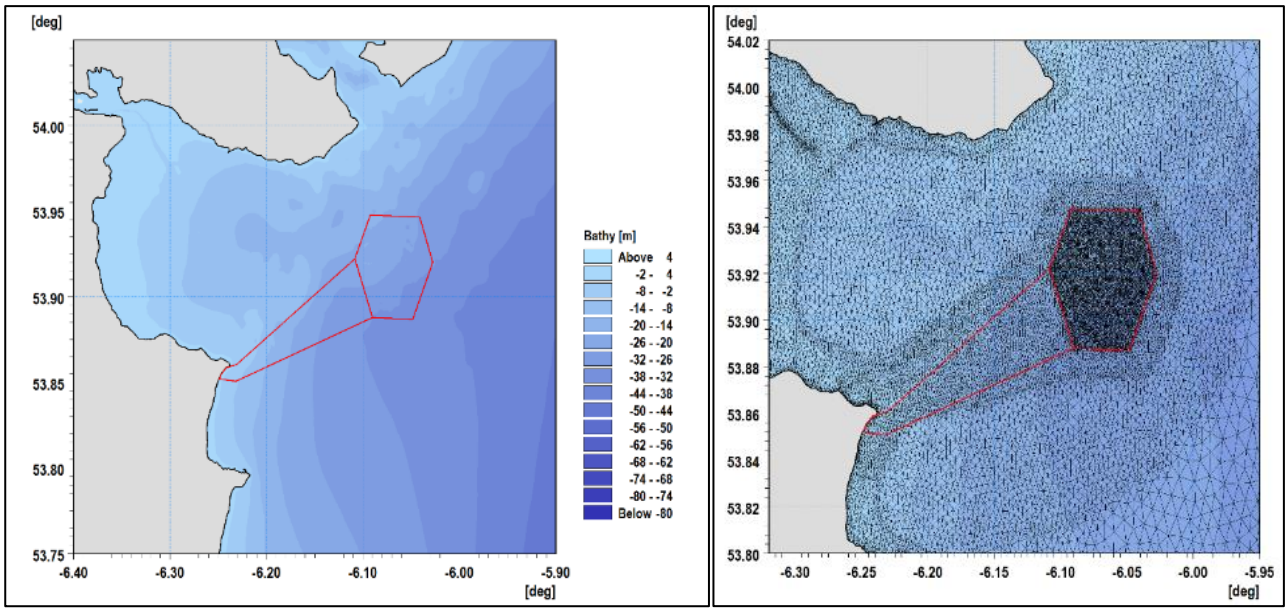

Figure 2-3: Model bathymetry within Marine Processes Study Area and with mesh detail.

2.2 Hydrography

2.2.1 Tidal flows

The UK Hydrographic Office states that the mean tidal range at the closest Standard Port of Dublin is approx. 2.65 m with the following characteristics in metres referenced to Chart Datum (CD):

- Lowest Astronomical Tide (LAT): +0.1;
- Mean Low Water Springs (MLWS): +0.7;
- Mean Low Water Neaps (MLWN): +1.5;
- Mean Sea Level (MSL): +2.4;
- Mean High Water Neaps (MHWN): +3.4;
- Mean High Water Springs (MHWS): +4.1; and
- Highest Astronomical Tide (HAT): +4.5.

Furthermore, Figure 2-4 shows the tidal ranges at the OPW gauges at Giles Quay, to the north of the offshore wind farm area and Port Oriel to the south. The flat bottom of the Port Oriel trace indicates that the gauge dried out at lower water levels.

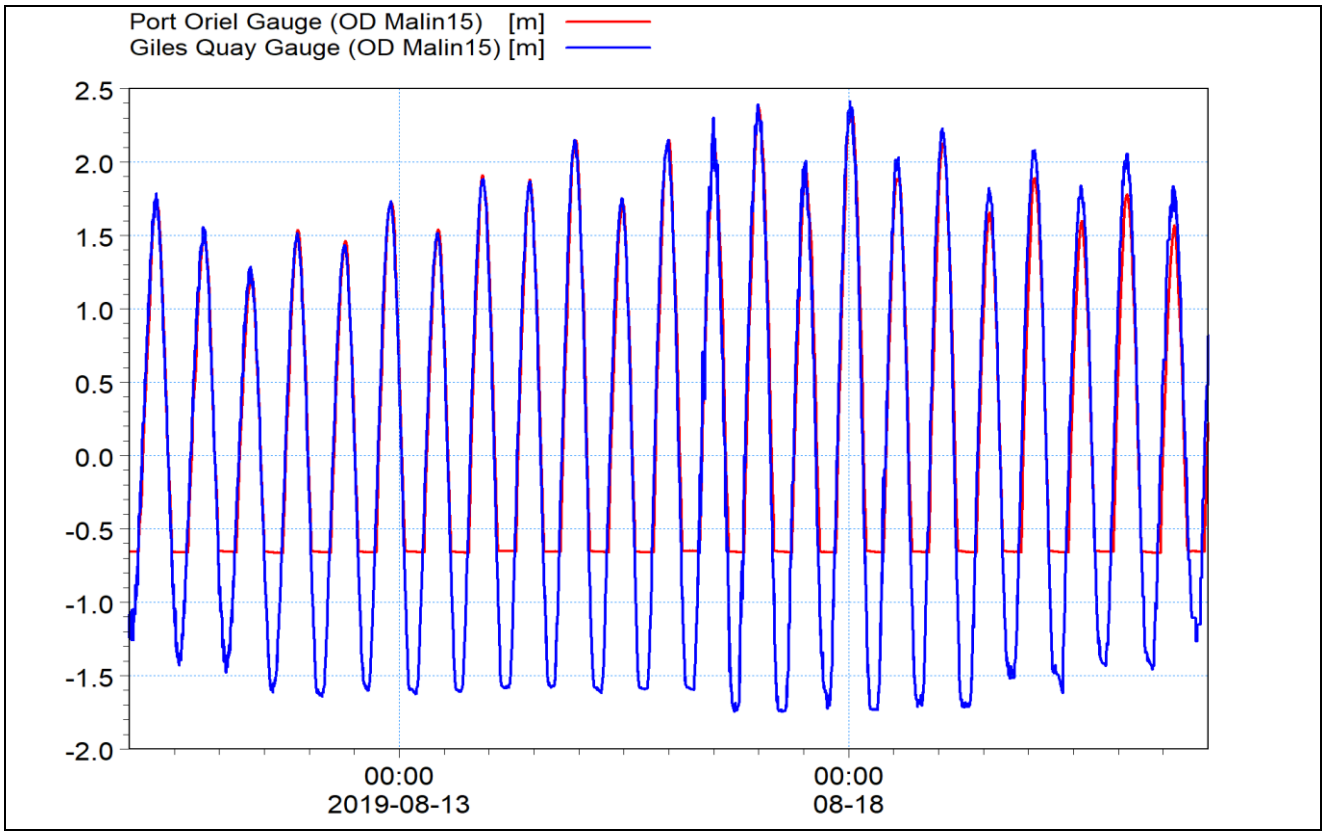

Figure 2-4: Gauge records from Port Oriel and Giles Quay.

The tidal flow simulations which form the basis of the study were undertaken using the MIKE21 Hydrodynamic (HD) module based on a Flexible Mesh (FM) modelling system. The HD Module is a 2-dimensional, depth averaged hydrodynamic model which simulates the water level variations and flows in response to a variety of forcing functions in lakes, estuaries and coastal areas. The water levels and flows are resolved on a mesh covering the area of interest when provided with bathymetry, bed resistance coefficient, wind field, hydrodynamic boundary conditions, etc.

The Marine Processes Study Area is characterised by shallower banks surrounded by deep areas of open water. The mesh resolution was therefore defined with sufficient detail to resolve the spatial variations in tidal flow. There are no counter currents or strong density stratified flows that would necessitate the use of three-dimensional modelling. It is however recognised that the Project is located to the west of the location where long term seasonal effects give rise to the western Irish Sea Gyre during the summer months (Hill *et al.,* 1996). Tidal flows enter the Irish Sea from both the North Channel and St. Georges channel to the south. During the winter months winds which are dominant from the south counter residual tidal currents and provide mixing. In summer months, in the absence of wind driven mixing and coupled with the surface warming, stratification occurs giving rise to density driven currents. The gyre is a near-surface circulation which occurs in summer months above the deep western basin where depths exceed 100 m. Both field measurement and modelling studies have indicated that the seasonal thermocline is located at circa 20 m to 40 m depth within the deep trough. The outer extent of the Gyre is located in circa 80 m water depth which is situated in excess of 40 km from the Project whilst the centre of the Gyre is almost double this distance (Brown *et al*, 2000).

Even though the model used for this assessment is depth averaged, the MIKE modules include the influence of depth of wind, bed shear and current profiles when modelling of the movement of particles within the. water column. The tidal model was driven using boundary conditions extracted from RPS' Irish Sea Surge model which is used for live storm surge forecasting on behalf of the OPW. These boundaries were fully defined 'flather' boundaries for which both surface elevation and current vectors are specified. The model was calibrated using the gauged water level data, Admiralty tidal data and field data collected as part of the

OPW forecast trial for Dundalk. The model was then verified against floating Lidar and Acoustic Current Doppler Profiler (ADCP) measurements collected within the offshore wind farm area. Further detail relating to model calibration and validation is presented in Section 4. The model was calibrated using a constant bed friction of Manning's number 36 $m^{1/3}/s$. Due to the application of flather boundaries damping was not required to provide model stability.

Across the offshore wind farm area, the tidal current floods in a northwest direction and ebbs to the southeast. The flows are relatively weak with tidal current speeds typically less than 0.2 m/s; with ebb and flood currents being of a similar magnitude. This was confirmed by ADCP survey data which showed current speeds were below 0.2 m/s for 80% of the 12 month monitoring period. This is illustrated in Figure 2-5 and Figure 2-6 which present the tidal patterns for flood and ebb tides respectively across the Marine Processes Study Area. In each case (and in all subsequent figures) the offshore wind farm area is outlined in red.

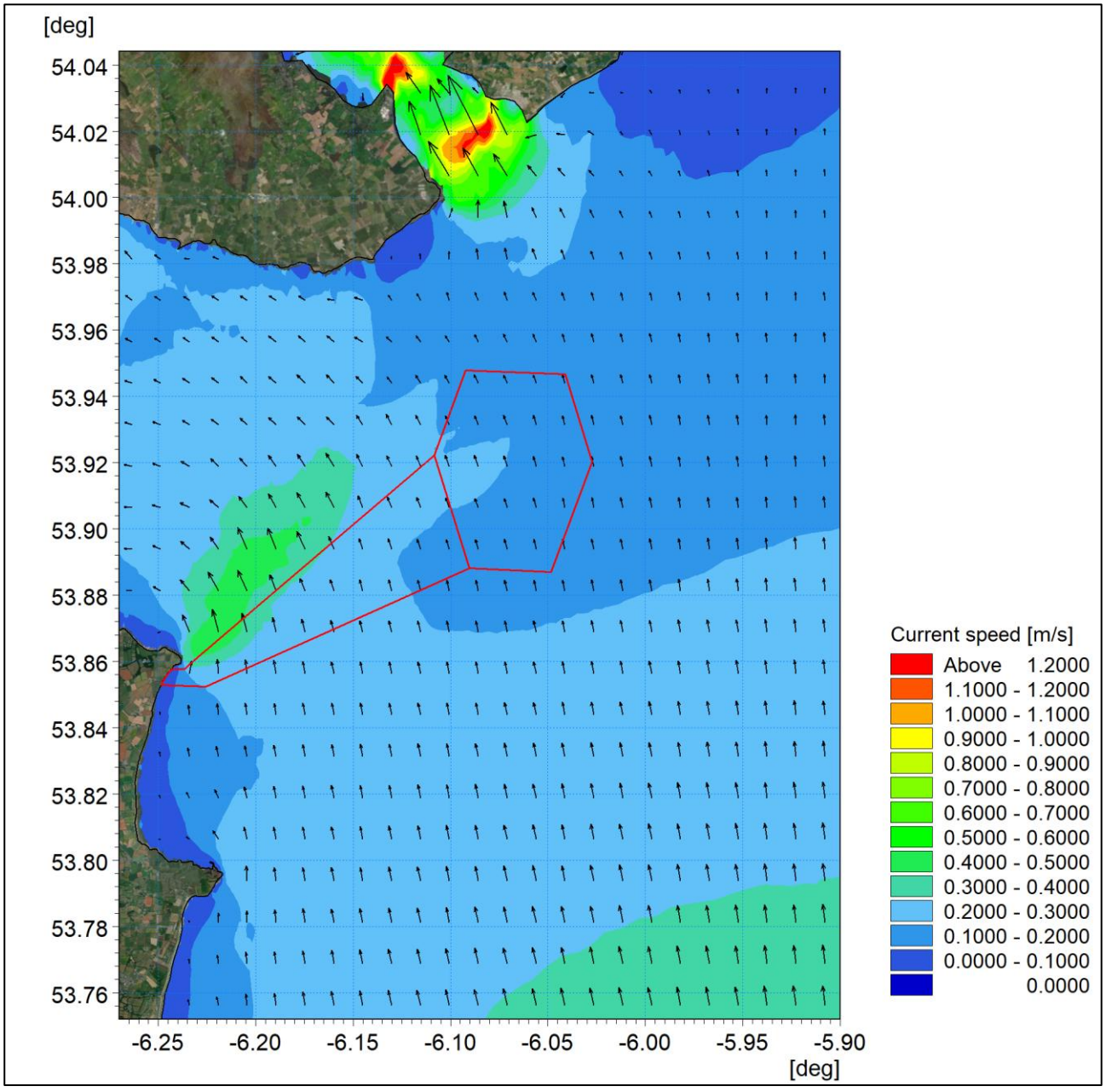

Figure 2-5: Baseline tidal flow patterns - mid-flood.

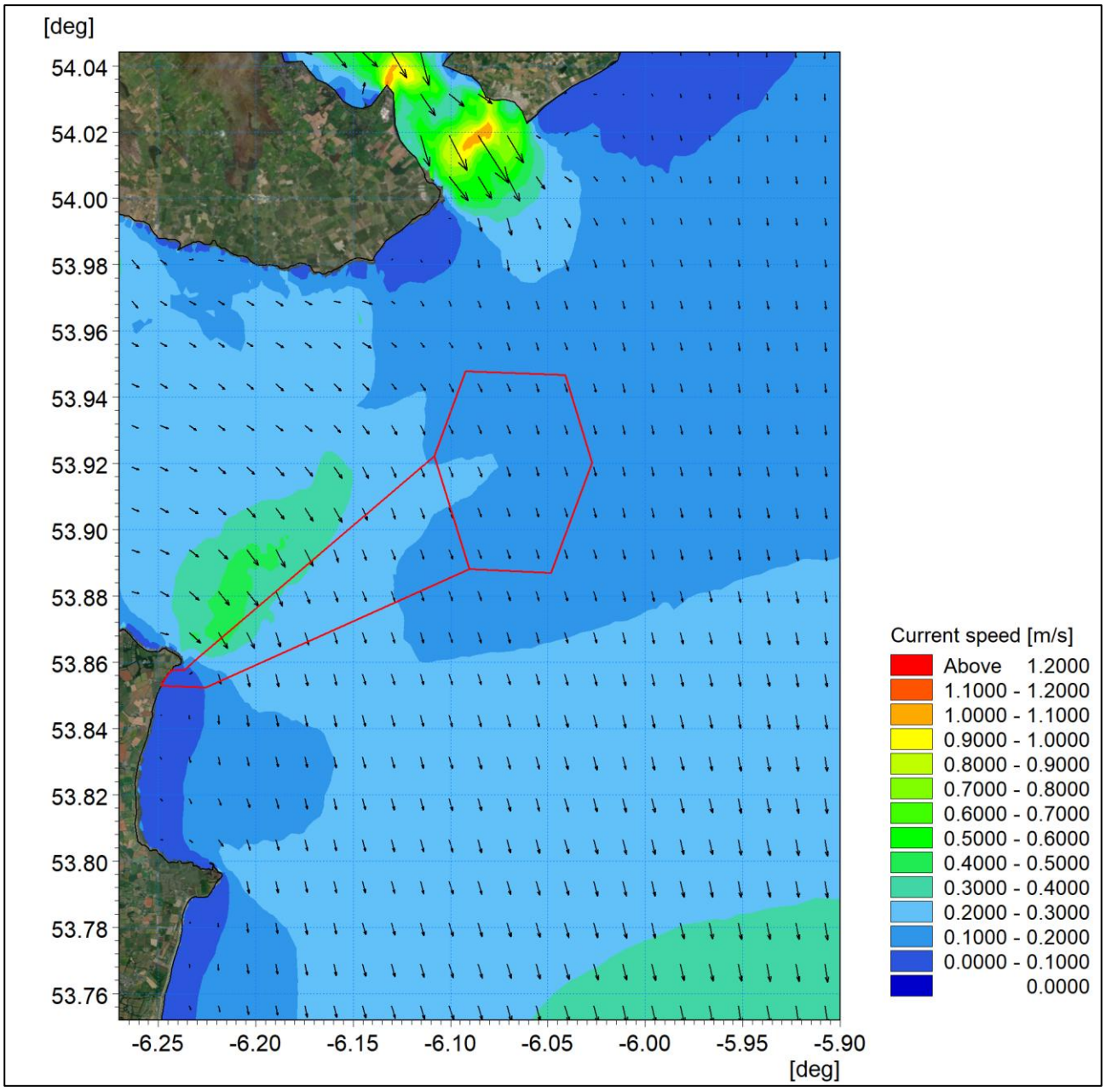

Figure 2-6: Baseline tidal flow patterns - mid-ebb.

2.2.2 Wave climate

The offshore wind farm area is sheltered from incoming waves from northerly fetches however larger waves may reach the offshore wind farm area from the south due to a greater fetch length. This is shown in Figure 2-7 which presents the significant wave height and directionality of waves in the vicinity of the Marine Processes Study Area. This wave rose was produced using data from the ECMWF ERA-40 model for a 22-year period.

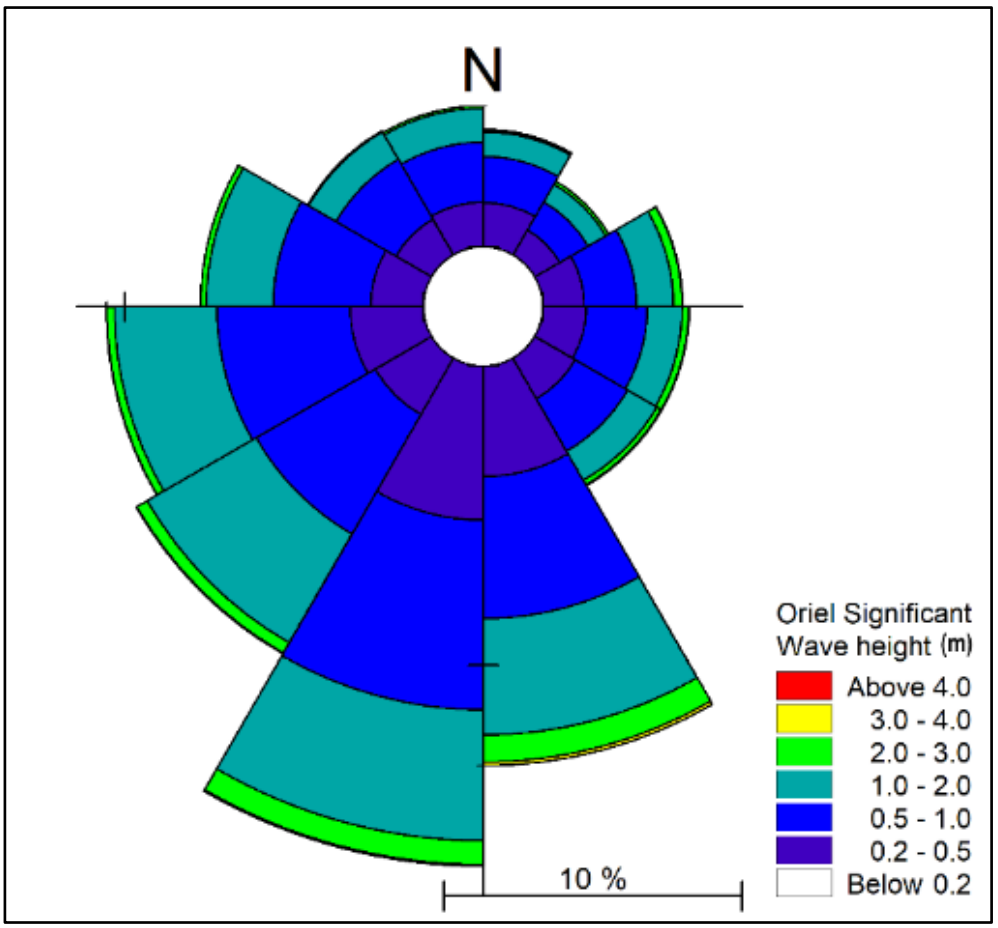

Figure 2-7: Wave rose for the offshore wind farm area based on a 22-year wave climate.

The waves reaching the offshore wind farm area are fetch limited. An analysis was therefore undertaken to determine the wind conditions in the Irish Sea for a number of scenarios in order to develop baseline wave conditions.

Thirty-nine years of data were obtained from the ECMWF's ERA5 reanalysis dataset for a location near to the M2 buoy location to the southeast of Dundalk Bay. The wind rose for this period is presented in Figure 2-8. An Extreme Value Analyses (EVA) was undertaken for the principal sectors to determine the 1 in 2 and 1 in 50-year wind speeds. These return periods were selected to identify the magnitude of typical events and more extreme events from the principal directions (i.e. 015°, 090° and 165°). These data were then used as boundary condition input for wave simulations to establish the potential impacts under a range of wave conditions.

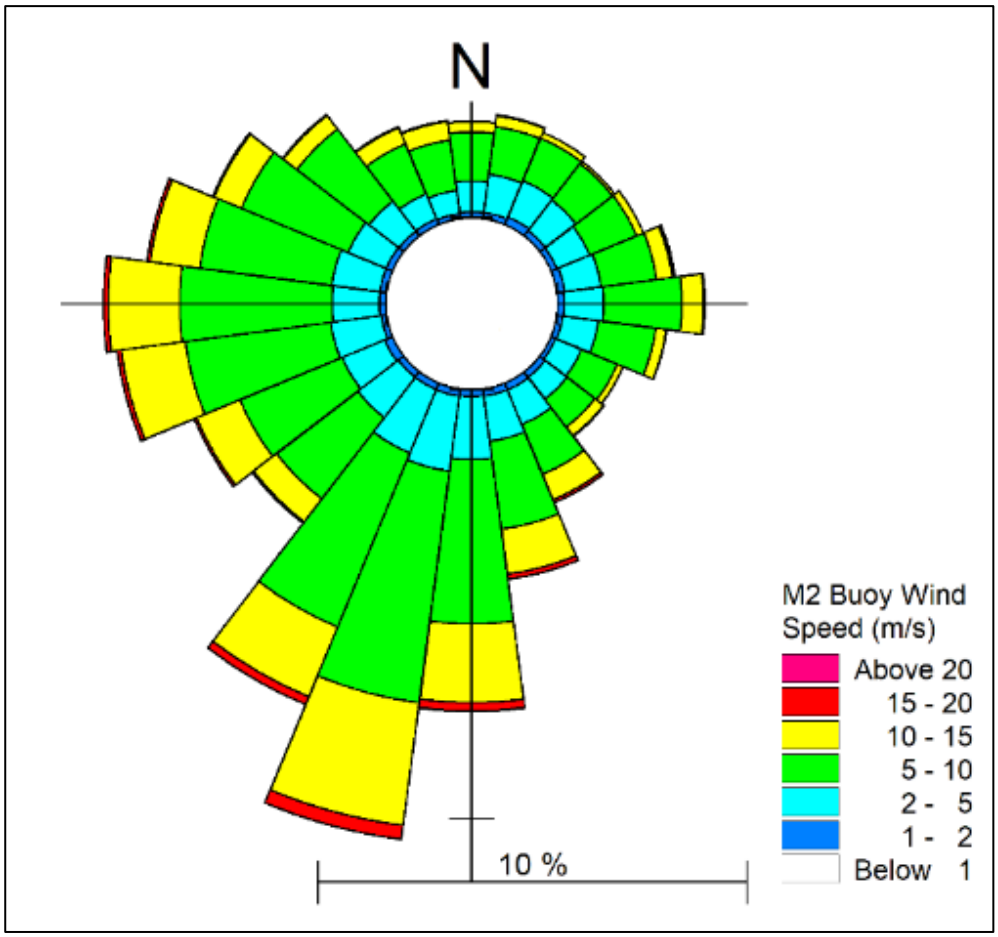

Figure 2-8: Wind rose for a location near the M2 wave buoy in the Irish Sea based on 39-year dataset.

The wave modelling was undertaken using the MIKE21 Spectral Save (SW) module. The waves were computed on the same grid as the tidal flows and were resolved by simulating wind generation of waves within the model domain. Figure 2A-9 to Figure 2A-14 illustrates the wave climate for three 1 in 2 and three 1 in 50 year return period events; from approximately a northerly (015°), easterly (090°) and southerly (165°) direction. These wave simulations were undertaken during a typical high water (HW) spring tide scenario.

Figure 2A-9 shows the waves approaching from the north. Based on these results, significant wave heights of around 2.5 m were found to occur at the offshore wind farm area from a north-easterly direction. As illustrated in Figure 2A-10, significant wave heights were larger at the offshore wind farm area during easterly storm events owing to the more exposed fetch. Storm events from the south were found to produce the largest significant waves of *c.* 3.2 m at the offshore wind farm area as illustrated in Figure 2A-11.

Figure 2A-12 to Figure 2A-14 presents similar results for the 1 in 50-year wave events. It will be seen from these figures that the wave patterns are generally similar, albeit significant wave heights are greater. The significant wave heights in the offshore wind farm increases from 3.2 m during a 1 in 2 year event to *c.* 4.0 m during a 1 in 50 year event from the south.

The floating Lidar data was collected over a period of 12 months and therefore the magnitude and variation with direction may be utilised to confirm the model results (albeit for a reduced return period). This survey data recorded significant wave heights of 1.5 – 2 m for the largest events from the northeast. Significant wave heights of 2.5 – 3 m and 3.5 – 4 m were recorded during arduous events from the east and southeast respectively. In general, this survey data correlated well with the example events modelled. Further detail relating to model calibration and validation is presented in section 4.

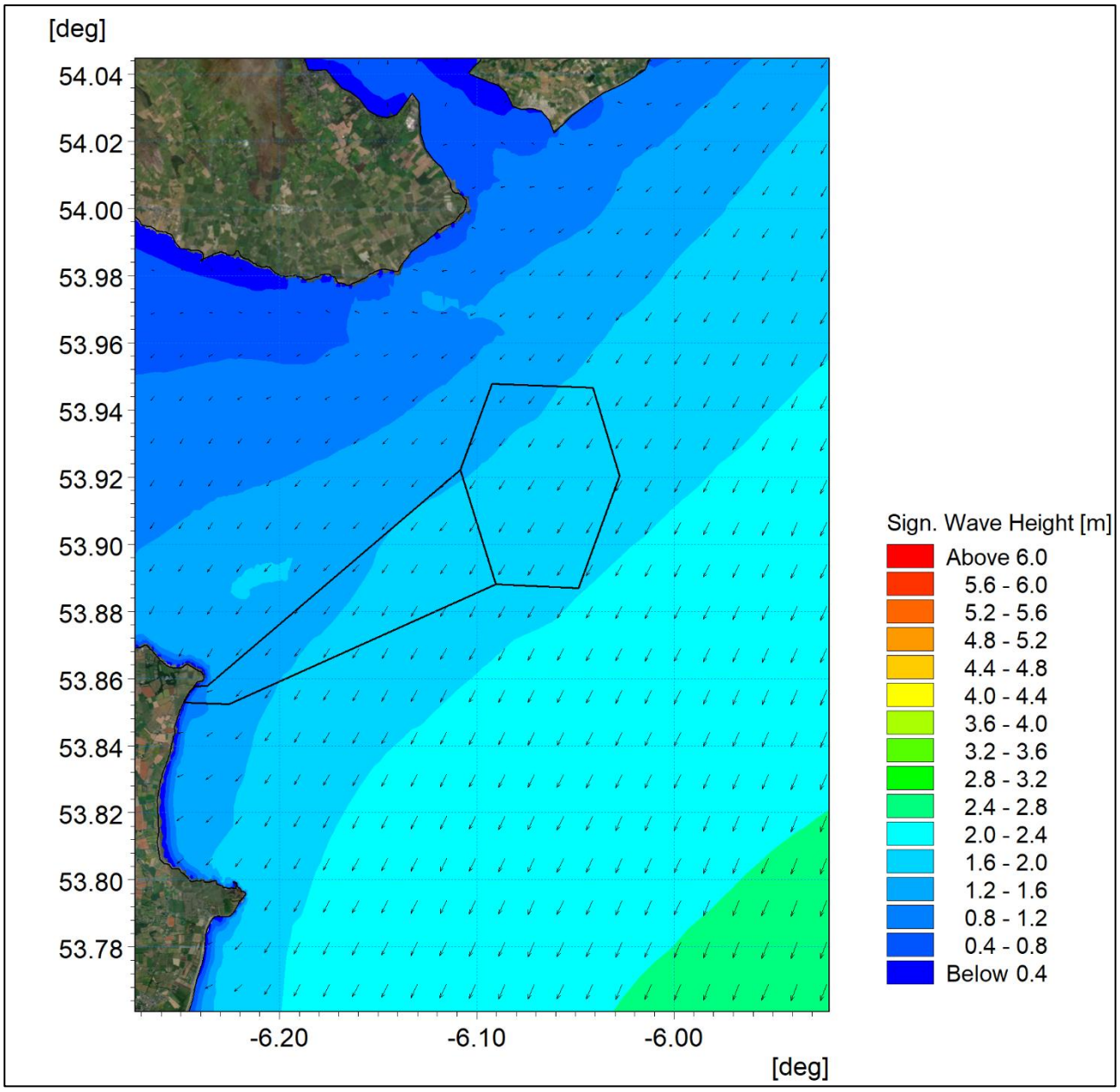

Figure 2A-9: Baseline wave climate 1 in 2 year storm from 015°.

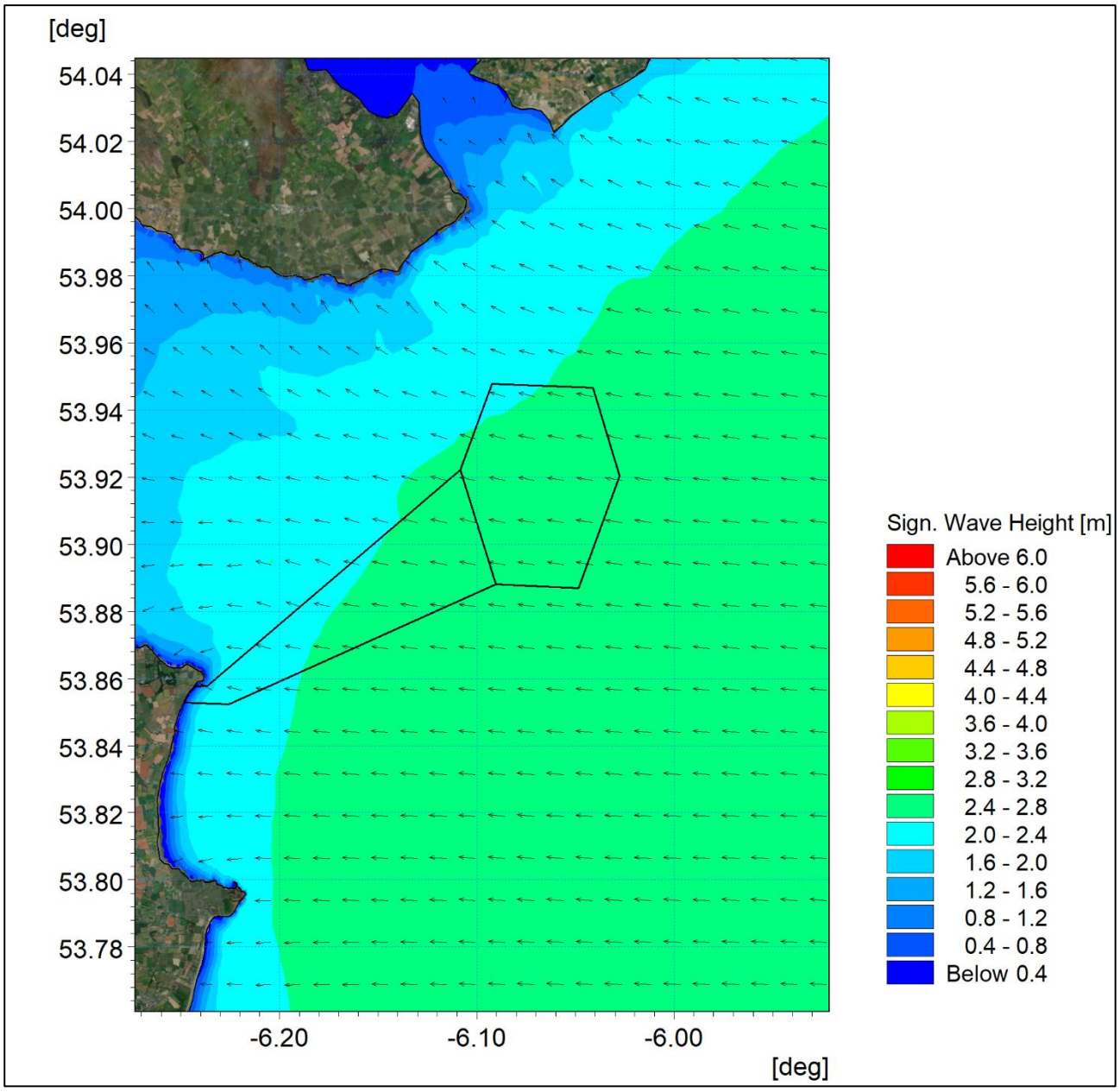

Figure 2A-10: Baseline wave climate 1 in 2 year storm from 090°.

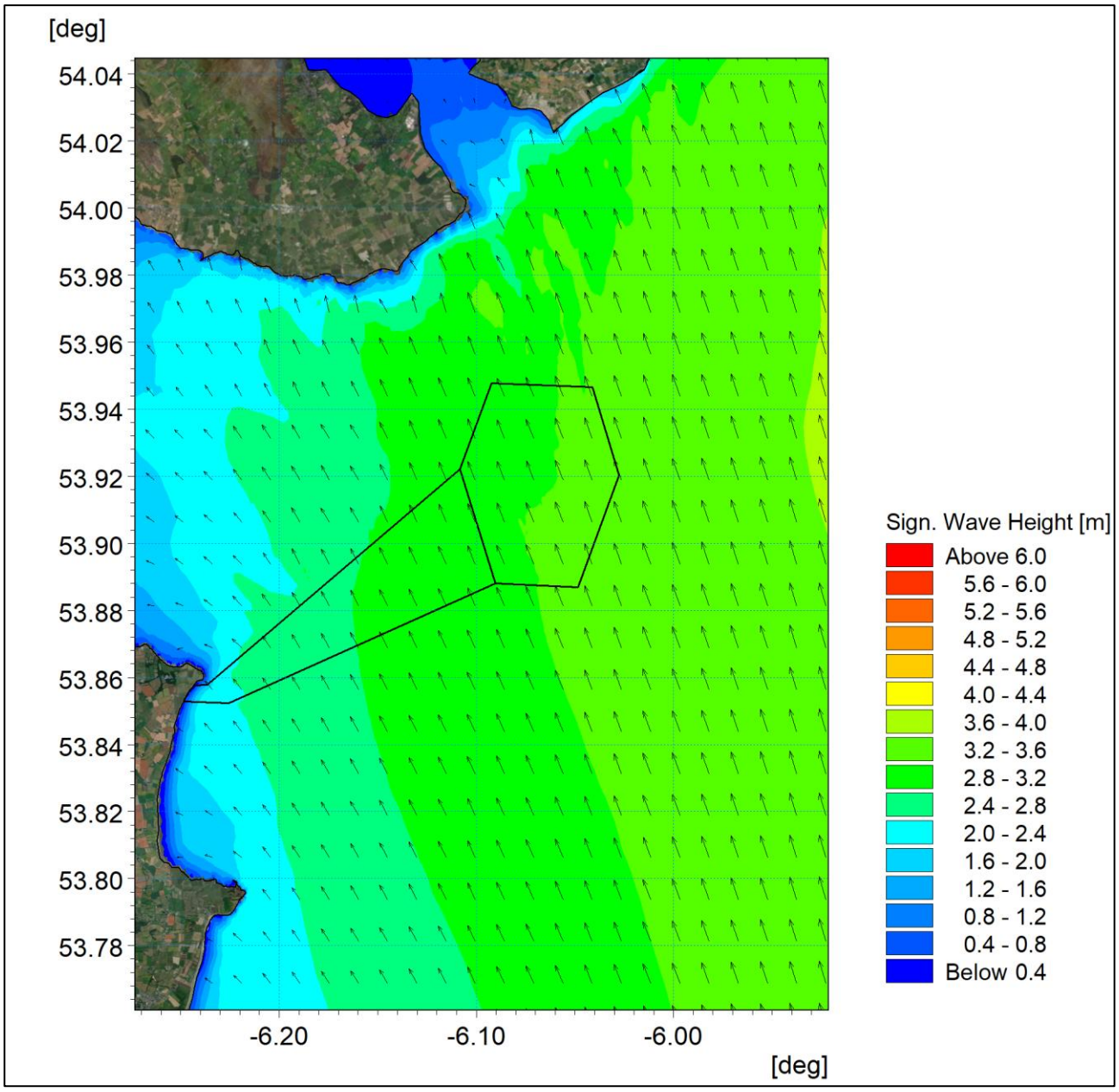

Figure 2A-11: Baseline wave climate 1 in 2 year storm from 165°.

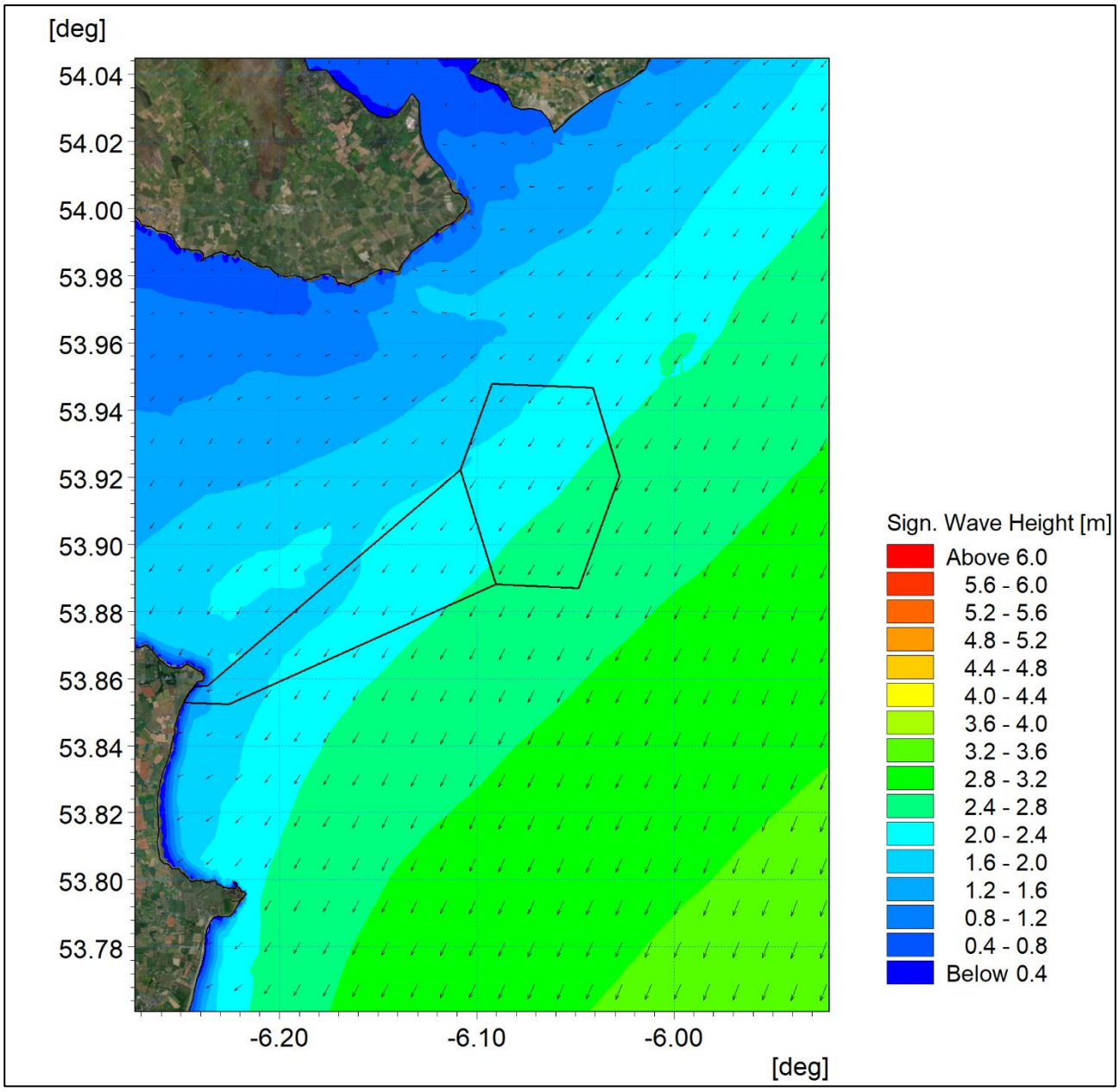

Figure 2A-12: Baseline wave climate 1 in 50 year storm from 015°.

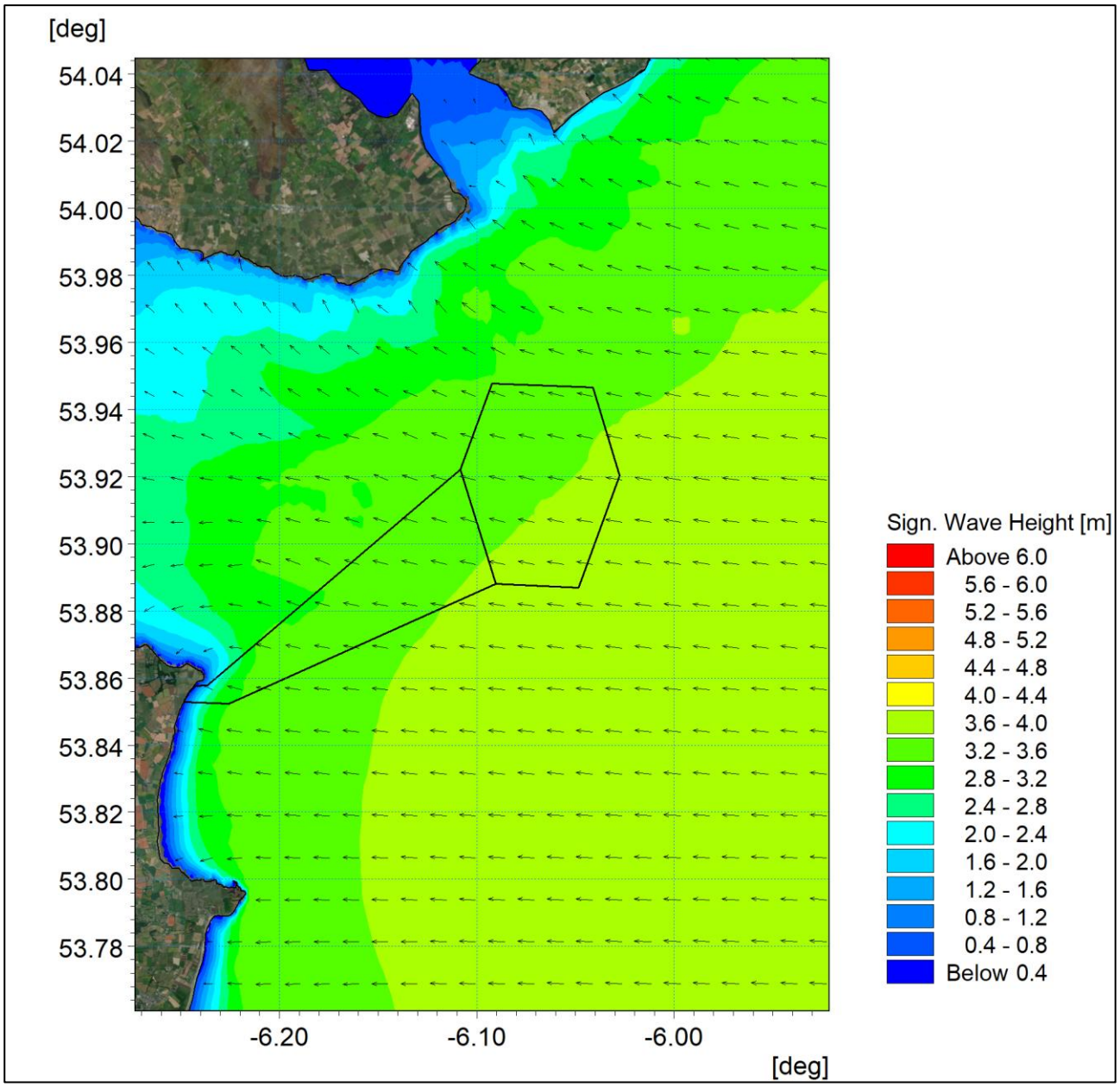

Figure 2A-13: Baseline wave climate 1 in 50 year storm from 090°.

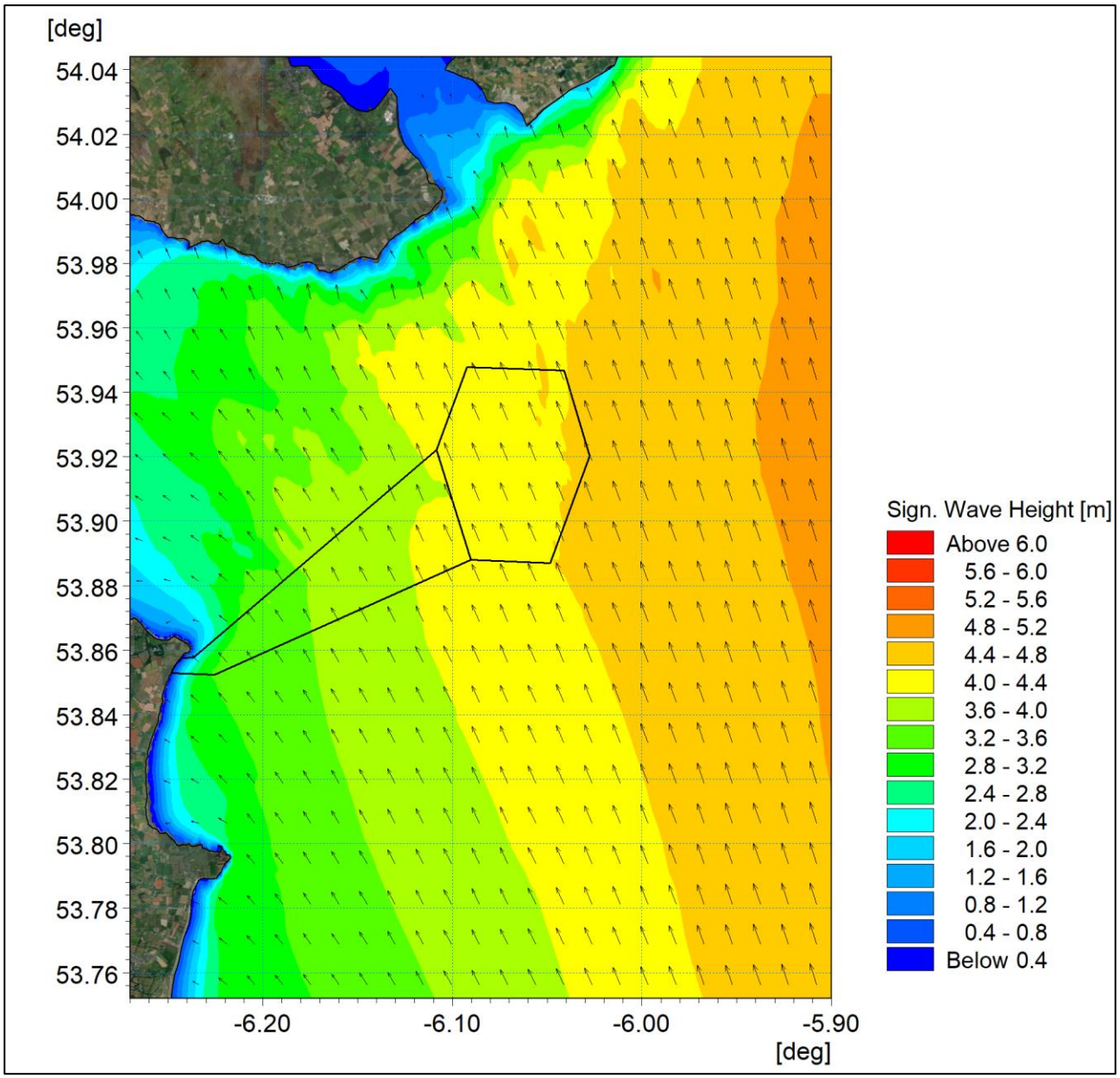

Figure 2A-14: Baseline wave climate 1 in 50 year storm from 165°.

Sensitivity of wave climate

In response to a request for further information (RFI) 6.D additional wave climate modelling was carried out. Sensitivity modelling was undertaken for intermediate return periods and return periods greater than those presented in the previous section for the critical, dominant 165º directional sector. It is noted that the offshore infrastructure is proposed to be located in an average water depth in excess of 20 m and therefore the wave climate is not depth limited and therefore joint probability assessment of waves and water level (i.e. storm surge) was not applicable. However, by way of example, an additional simulation was undertaken to examine the influence of sea level rise on wave climate.

Twenty-four years of measured wind data were obtained from the M2 buoy located to the southeast of Dundalk Bay. An Extreme Value Analyses (EVA) was undertaken for the critical 165º sector to determine the 1 in 50 year return period wind speed. This was verified against the datasets used for the initial modelling. Three times the record length is typically the maximum period for which extreme value analysis may be reliably applied. Due to the requirement to provide modelled data up to 1 in 200 year return period (0.2%

annual exceedance probability (AEP)), the 1 in 50 year (2% AEP) value was scaled to provide 1 in 10, 20, 100, 200 and 500 year return period winds (i.e. 10%, 5%, 1%, 0.5%, 0.2% AEP) by applying the British Standard Method (BS EN 1991-1-4:2005). Simulations were then undertaken using the process described in previously in this section. Furthermore, an additional run was undertaken for the 1 in 200 year return period wave climate with the application of sea level rise. The water depth was adjusted in line with the Mid-Range Future Scenario (MRFS) of +0.5m.

Figure 2A-15 and Figure 2A-16 show the intermediate return period storms with significant waves heights of 3.8 m and 3.9 m for the 10 and 20 year return period wave climate respectively. As anticipated they lie within the range of those previously presented for the 1 in 2 and 1 in 50 return period from the critical 165º direction. Figure 2A-17 to Figure 2A-19 show the less frequent wave climates. Within the offshore wind farm area (array area) these are 4.4 m, 4.8 m and 5.0 m for the 1 in 100, 200 and 500 year return period respectively. Whilst Figure 2A-20 illustrates that there are only minor changes in the 1 in 200 return period wave climate due to sea level rise, with typical significant wave height remaining 4.8 m within the array area.

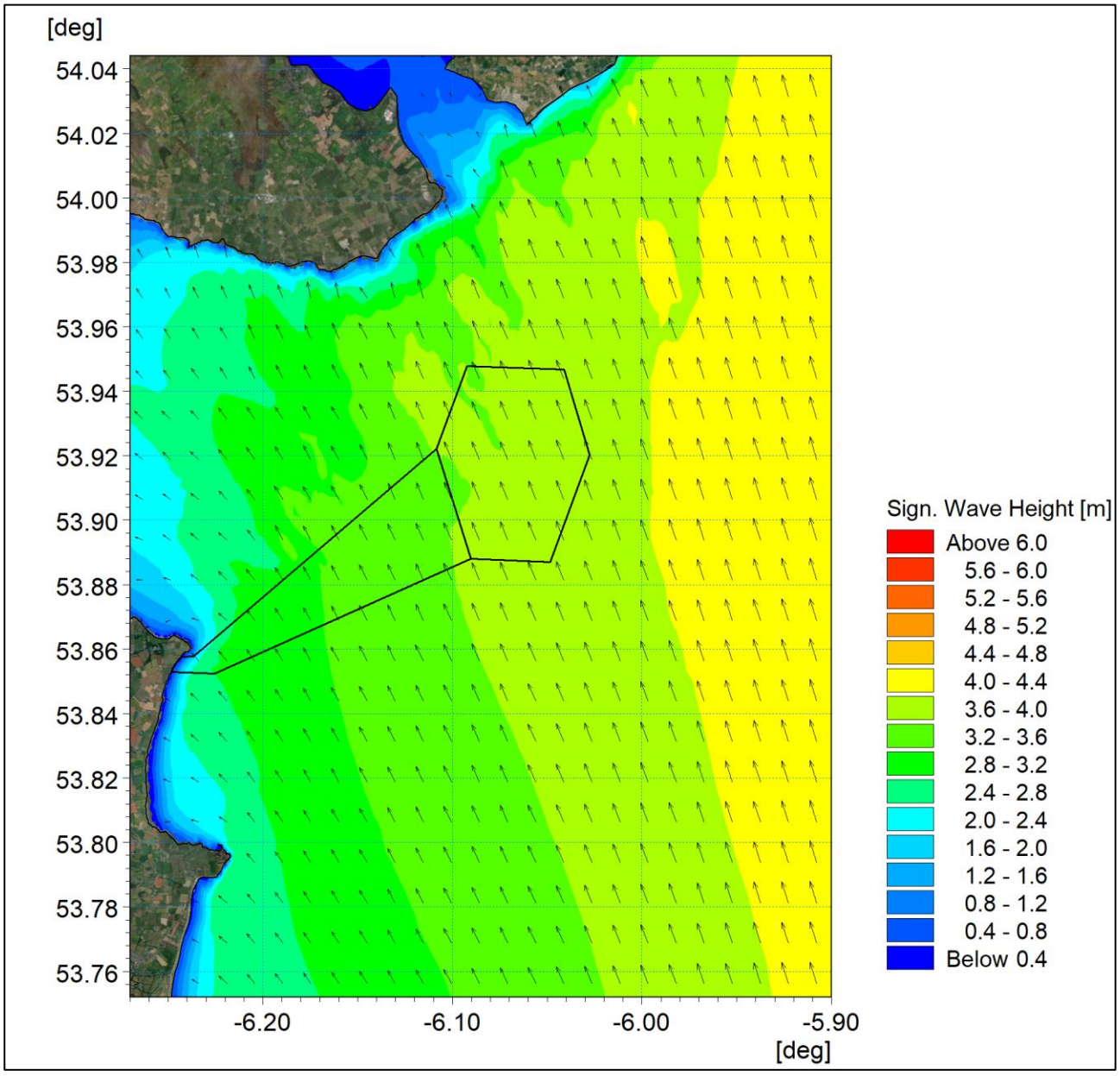

Figure 2A-15: Baseline wave climate 1 in 10 year storm from 165°.

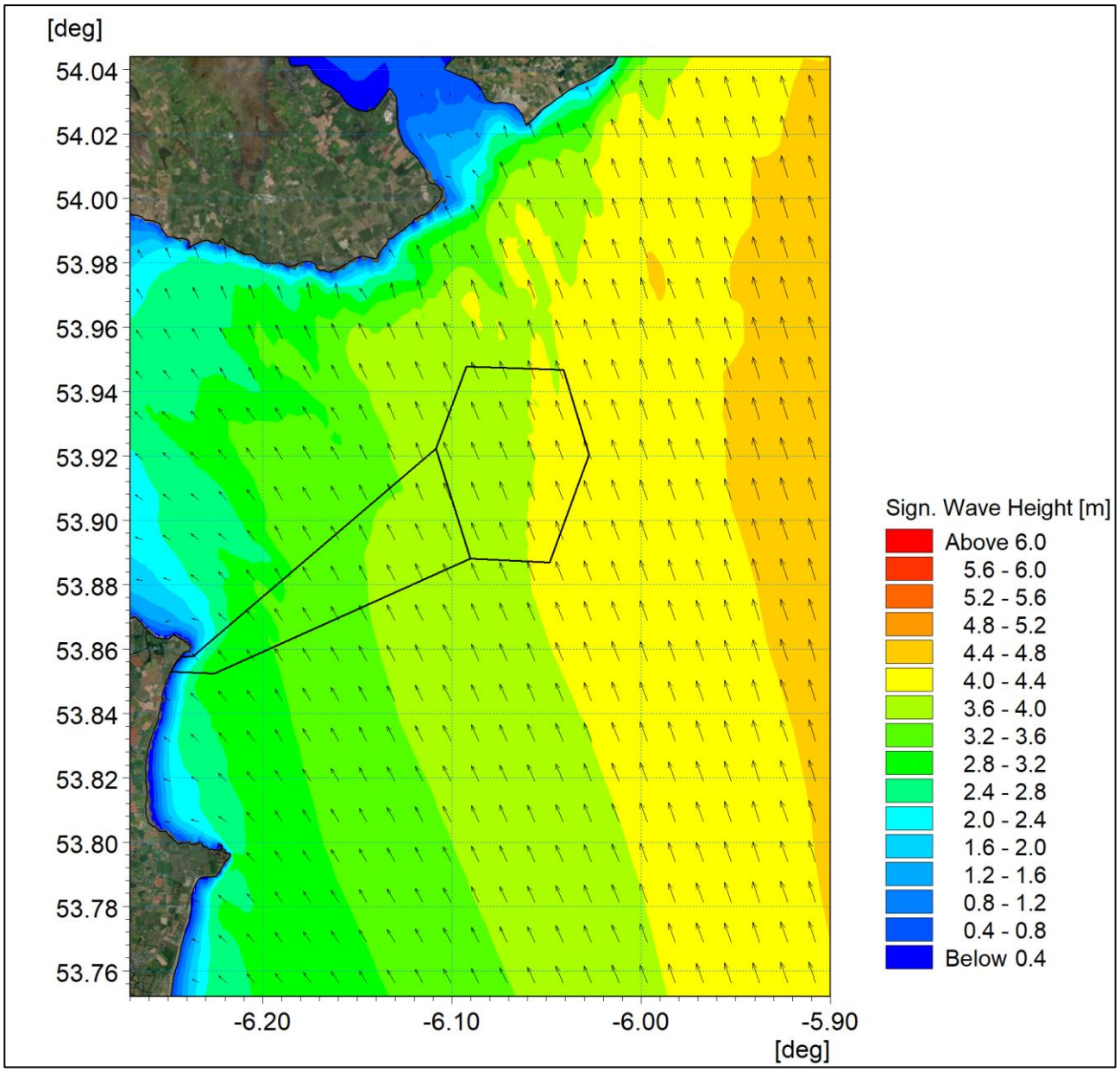

Figure 2A-16: Baseline wave climate 1 in 20 year storm from 165°.

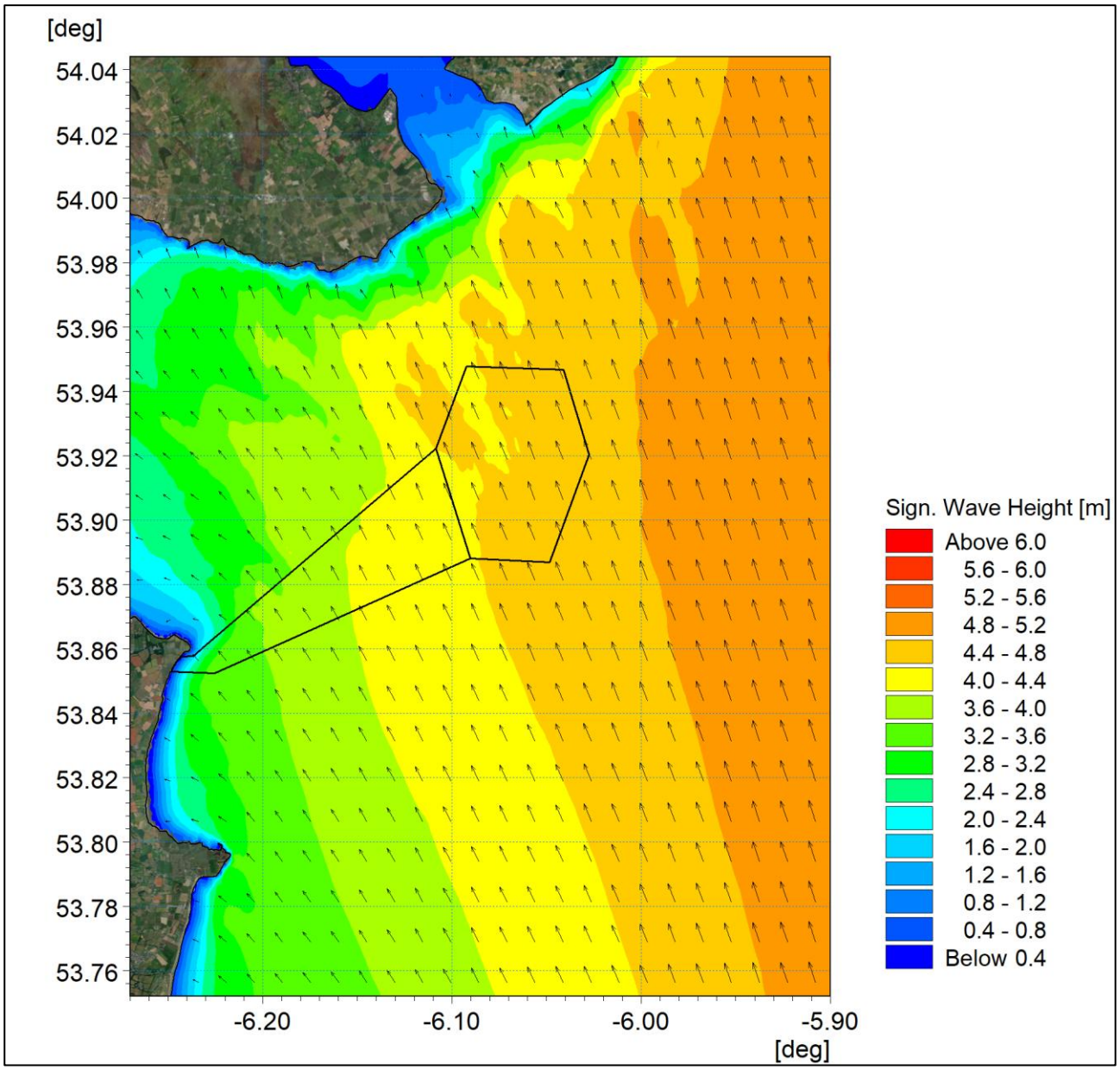

Figure 2A-17: Baseline wave climate 1 in 100 year storm from 165°.

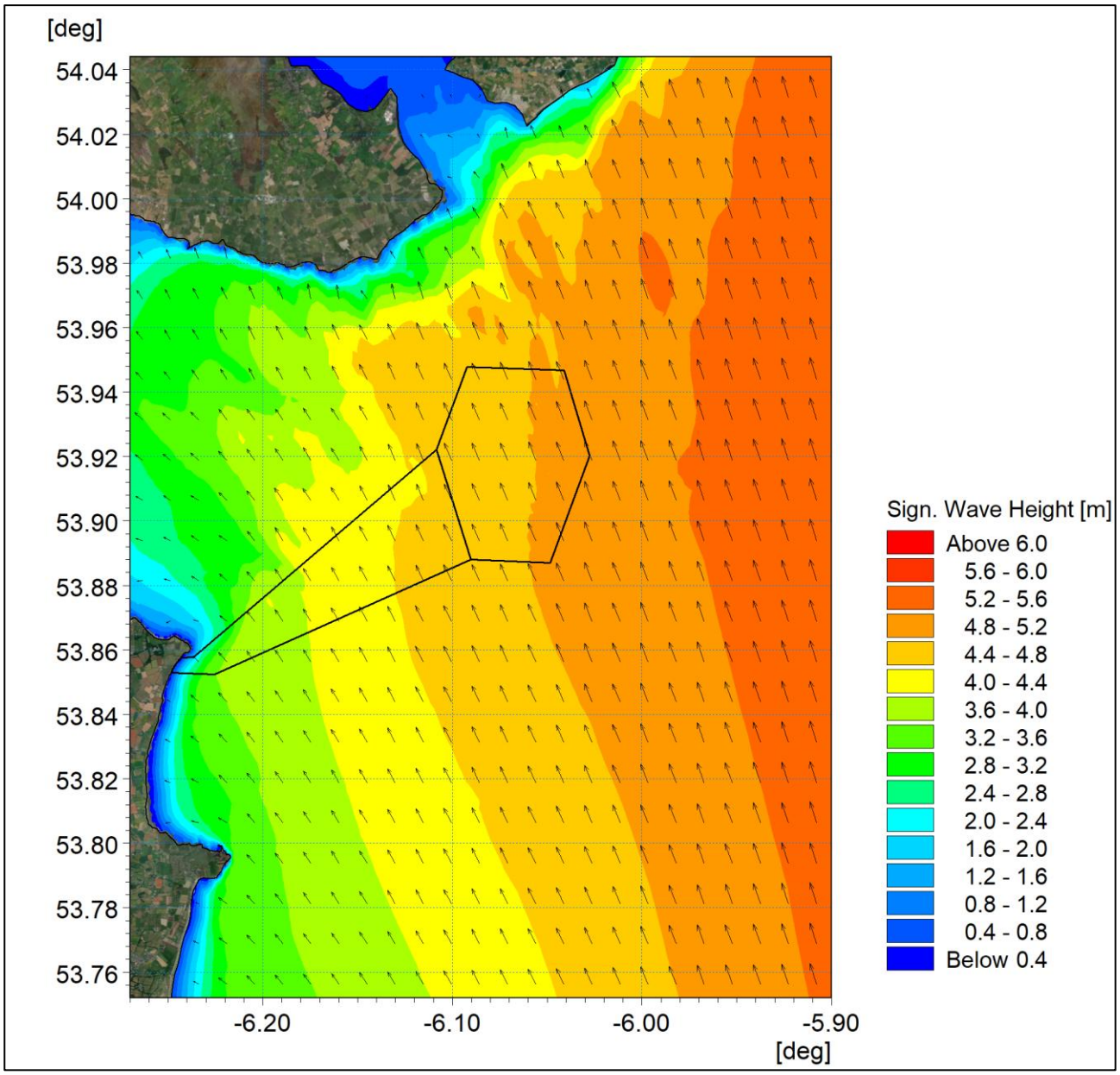

Figure 2A-18: Baseline wave climate 1 in 200 year storm from 165°.

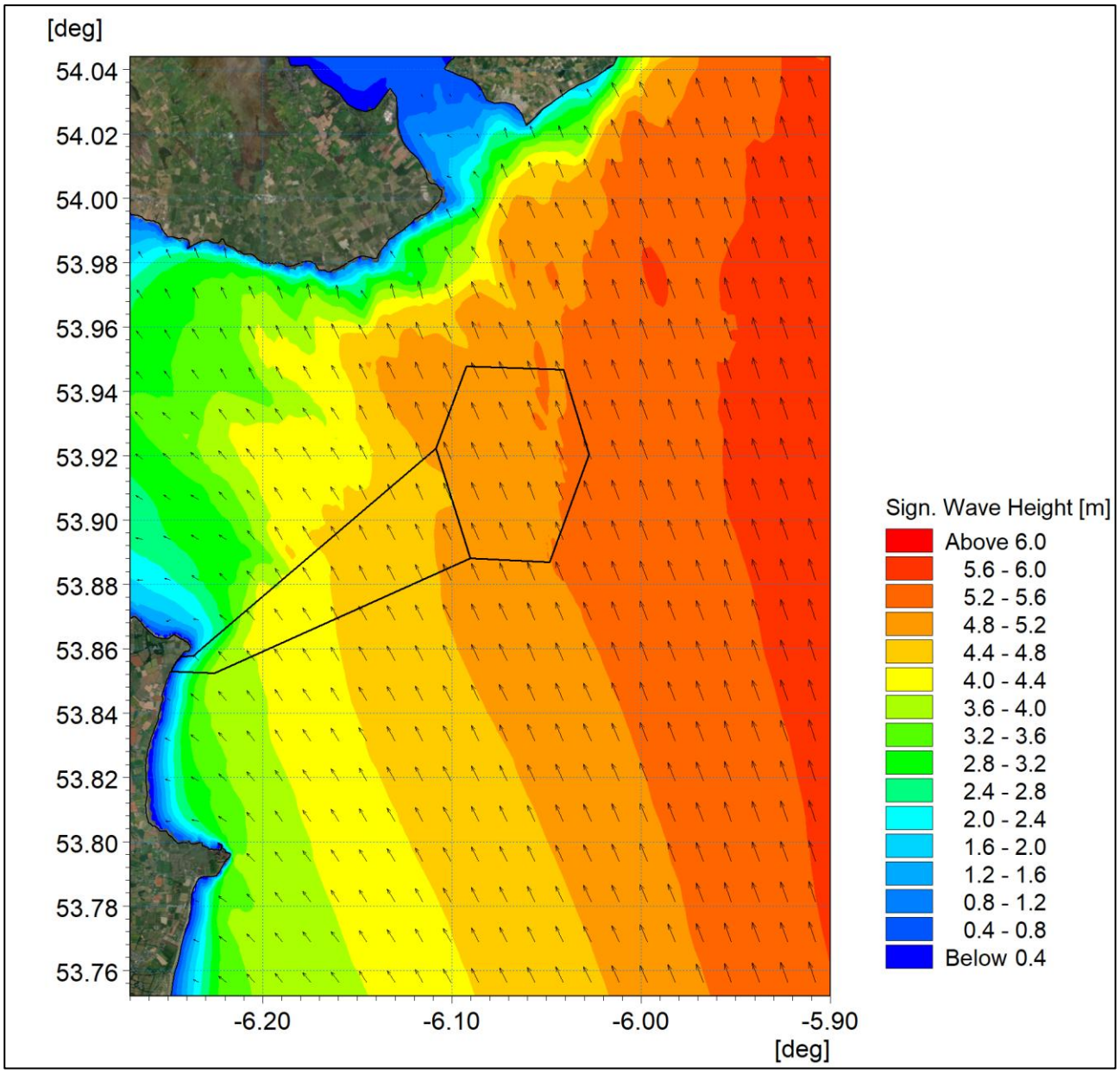

Figure 2A-19: Baseline wave climate 1 in 500 year storm from 165°.

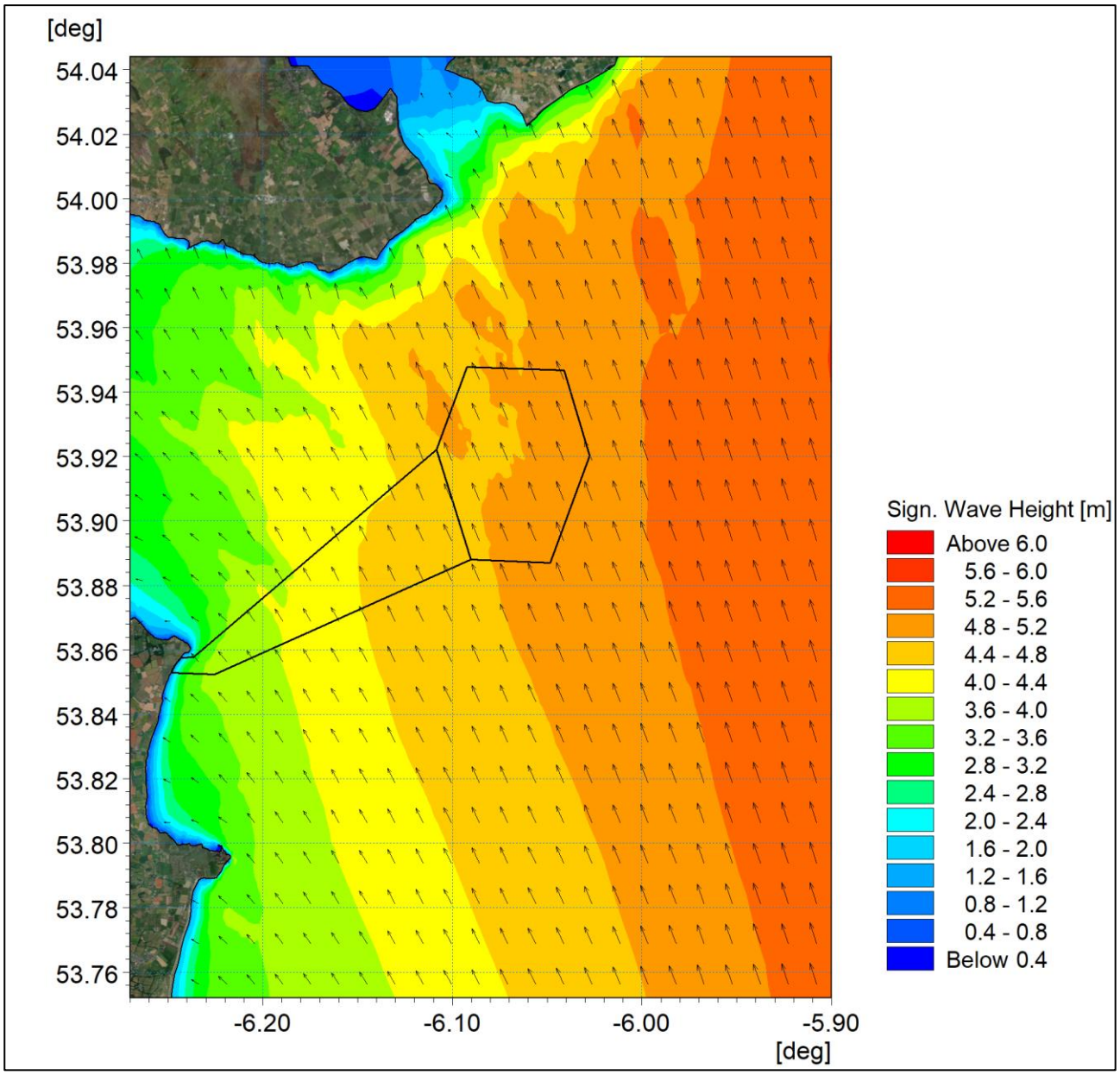

Figure 2A-20: Baseline wave climate 1 in 200 year storm from 165° with sea level rise.

2.2.3 Littoral currents

The MIKE suite facilitates the coupling of models. The depth averaged hydrodynamic model, used for the tidal modelling, coupled with the spectral wave model provides a full wave climate incorporating the impact of water levels and currents on waves and wave breaking. Using this, the littoral currents (i.e. currents driven by tidal, wave and meteorological forces) were examined.

The 1 in 2 year storm from 165° was simulated with the inclusion of spring tides. The resultant mid-flood and mid-ebb currents are presented in Figure 2-21 and Figure 2-22 respectively. These correspond with the (calm) tidal plots presented previously in Figure 2-5 and Figure 2-6. As expected, the effect of the north going waves increase the current velocities on the flood tide whilst reducing them on the ebb. In both cases, increased velocities are seen along the coastlines and eddying is induced at headlands and promontories such as Clogher Head and Cooley Point.

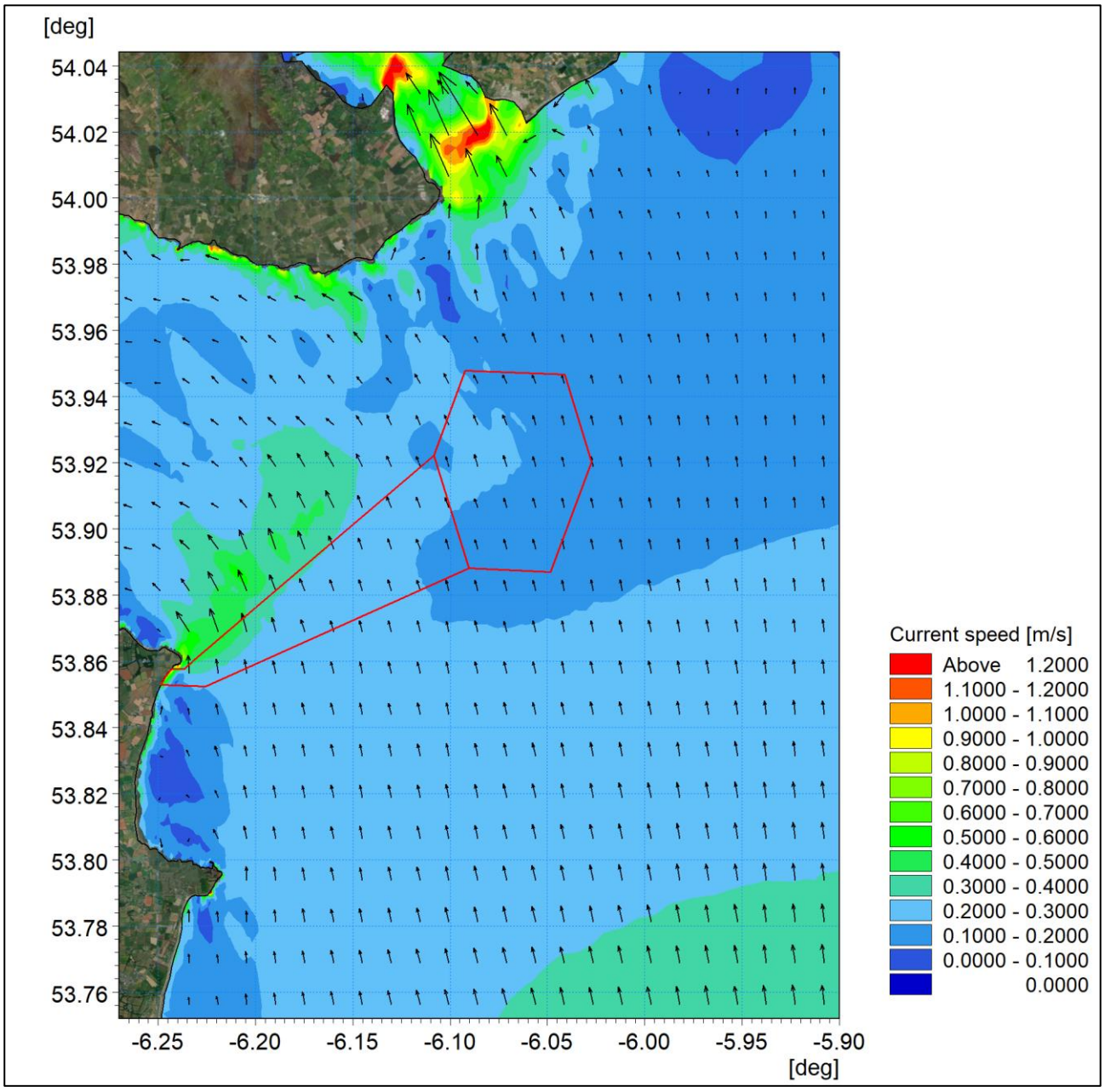

Figure 2-21: Baseline littoral current 1:2 year storm from 165° - flood tide.

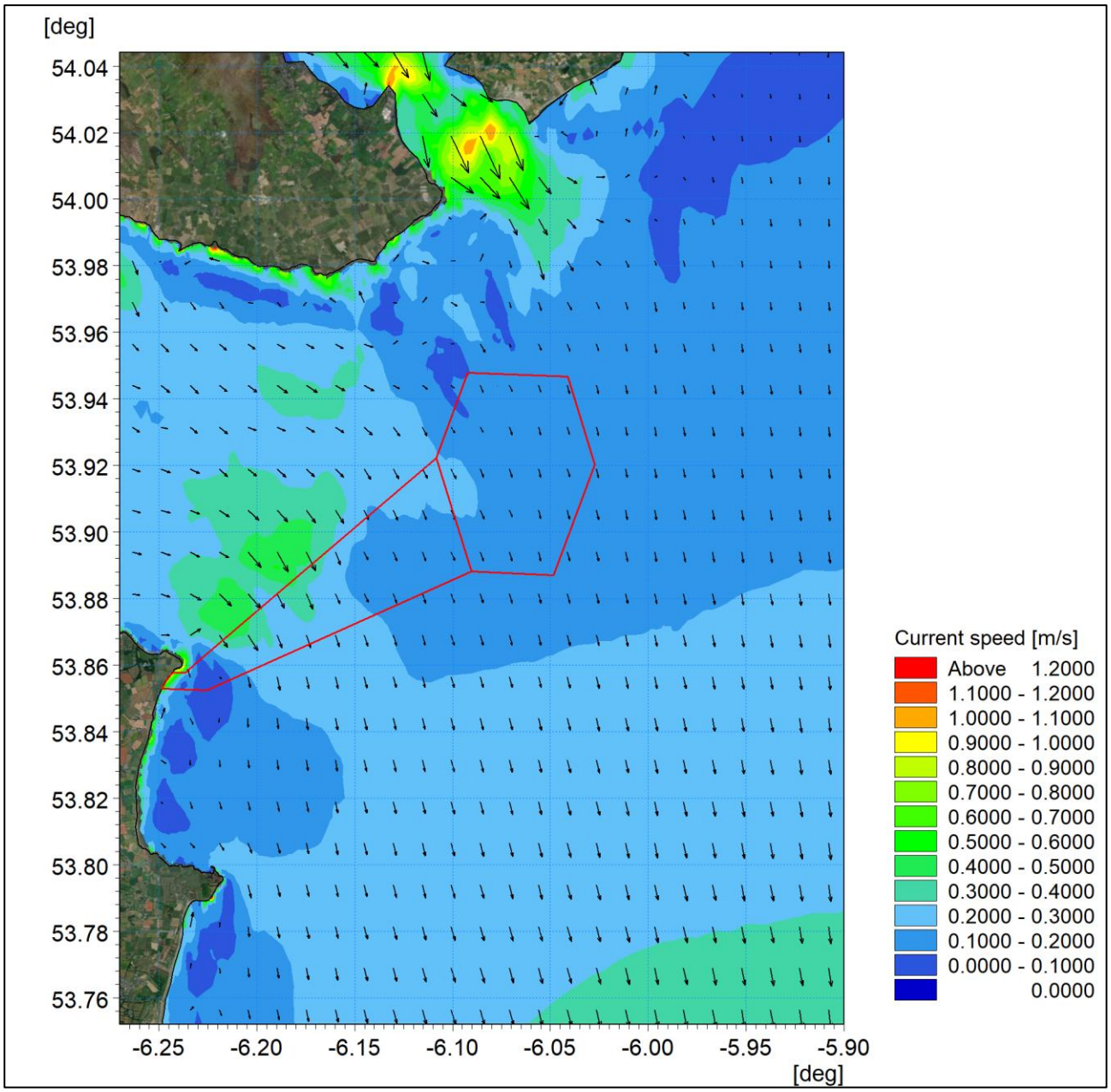

Figure 2-22: Baseline littoral current 1:2 year storm from 165° - ebb tide.

Sensitivity of littoral currents

In response RFI 6.D additional littoral current modelling was undertaken. Sensitivity modelling was carried out for a higher return period event, namely 1 in 200 year return period, and also to examine the influence of sea level rise on littoral currents. The simulations undertaken as outlined in the previous section were repeated with the 1 in 200 year return period wind speed.

Figure 2A-23 and Figure 2A-24 present the flood and ebb tide littoral currents for the 1 in 200 year storm event respectively. It is apparent that increased radiation stresses due to higher wind speed significantly increase current speeds along the shoreline in comparison to the calm condition. This is also the case within Dundalk Bay and in outer Carlingford Lough. However it is noted that offshore tidal currents are not appreciatively altered.

A further scenario was examined whereby the simulation was repeated with the inclusion of an increased water level corresponding to the MRFS of 0.5m. Similarly, Figure 2A-25 and Figure 2A-26 show the flood and ebb tide littoral currents respectively. There is little in the way of variation from the present day water levels scenario as decreases in current speed afforded by increased water depth are countered by increased radiation stresses due to greater wave penetration.

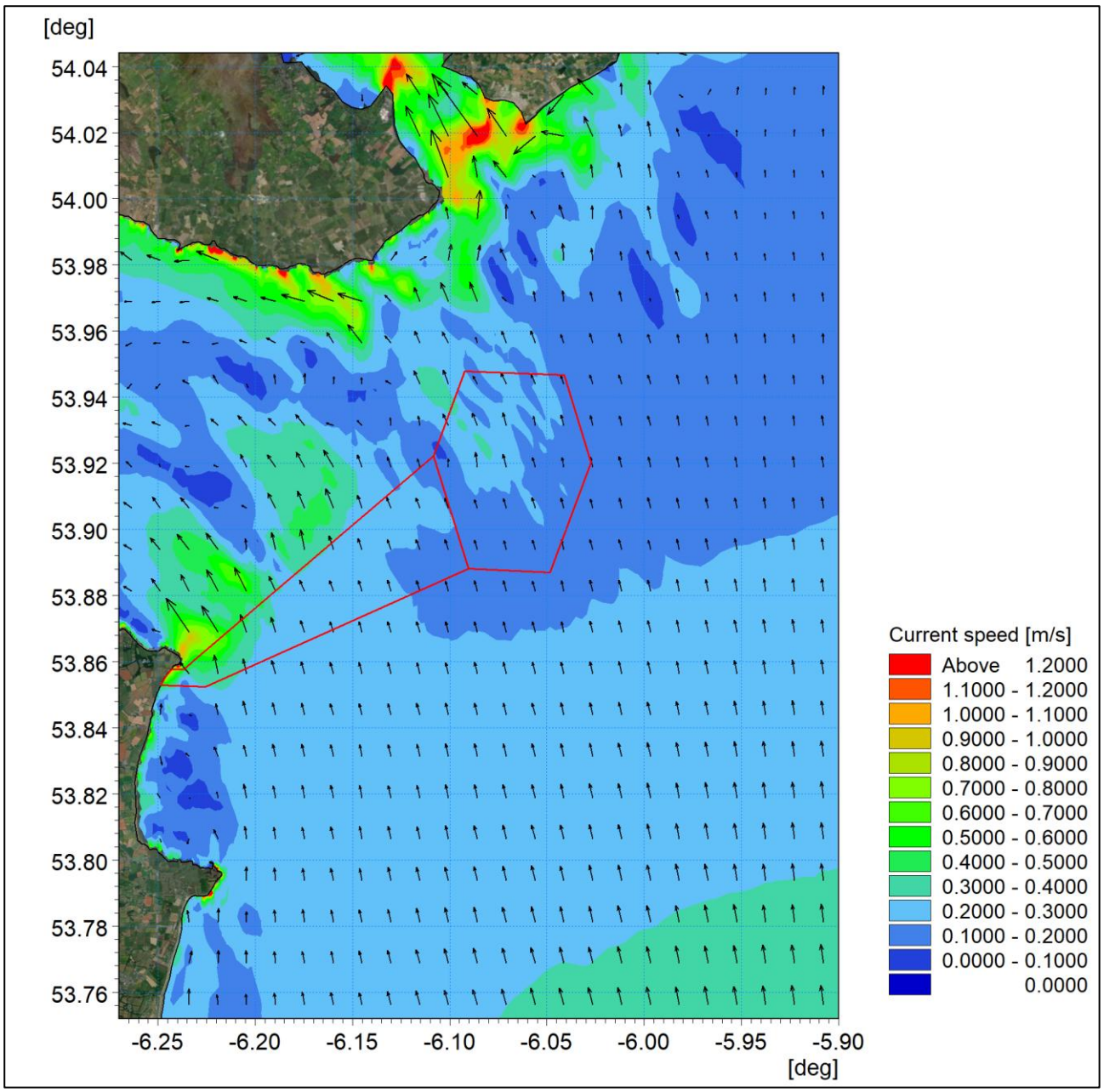

Figure 2A-23: Baseline littoral current 1:200 year storm from 165° - flood tide.

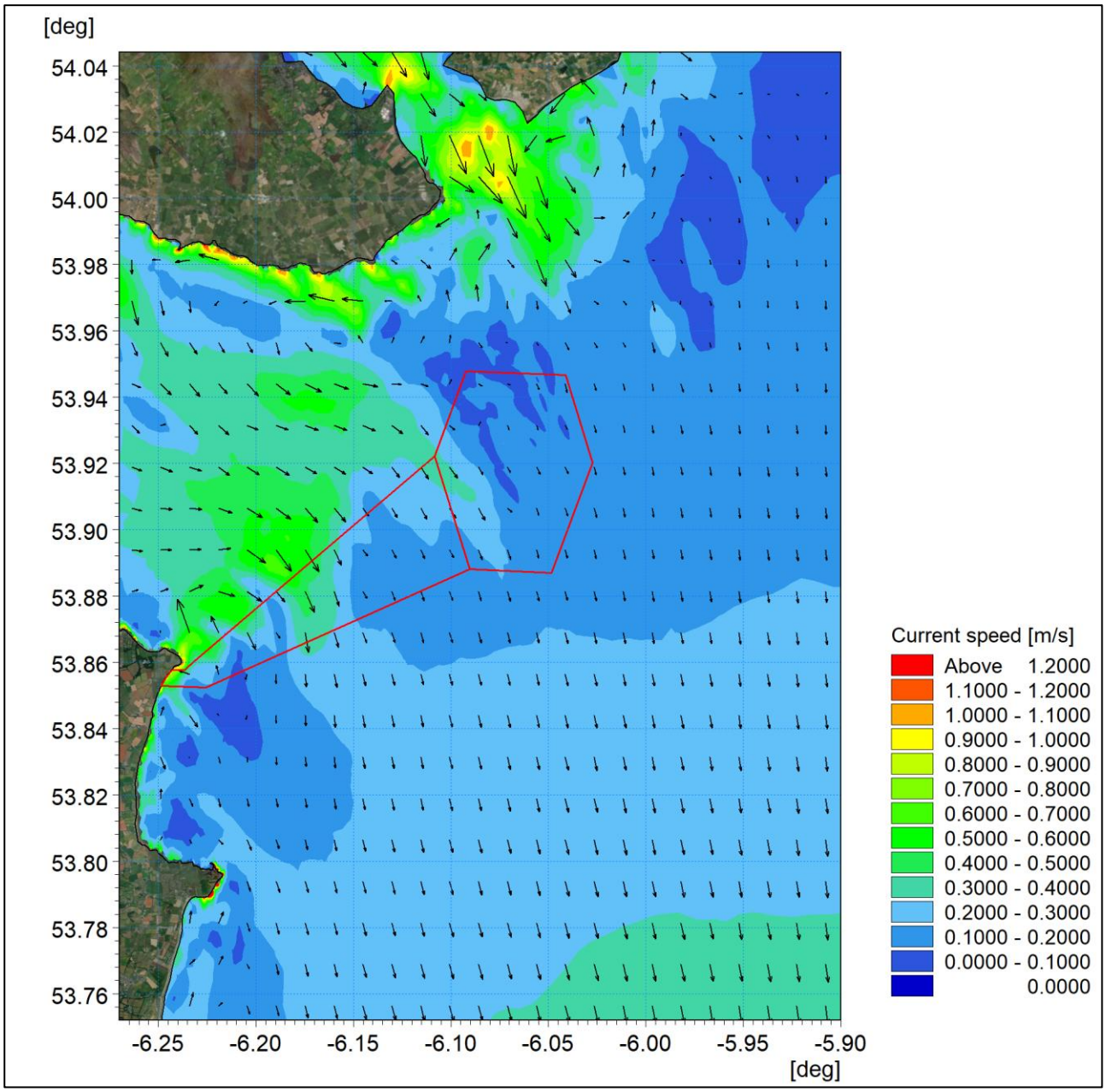

Figure 2A-24: Baseline littoral current 1:200 year storm from 165° - ebb tide.

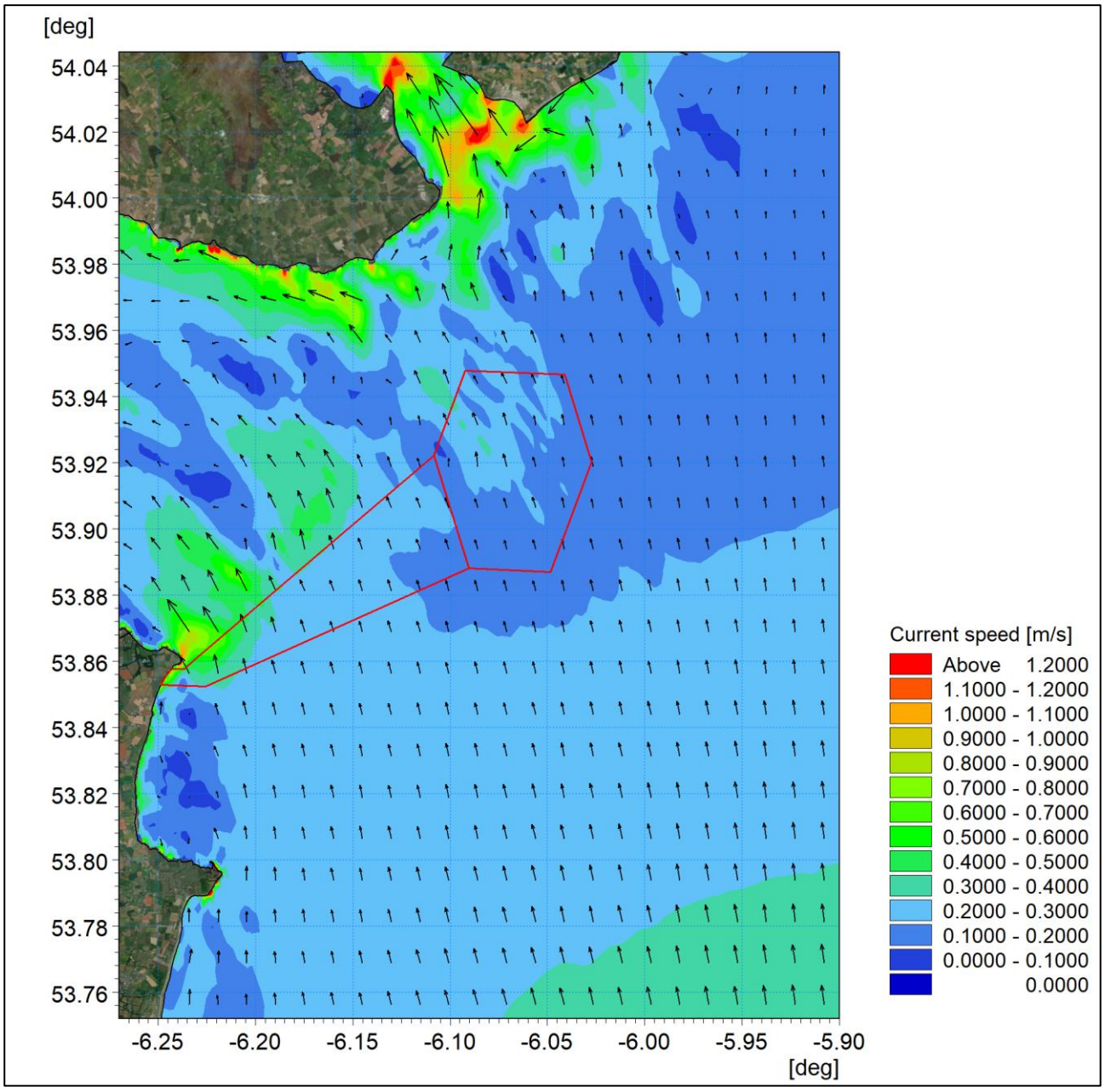

Figure 2A-25: Baseline littoral current 1:200 year storm from 165° with sea level rise - flood tide.

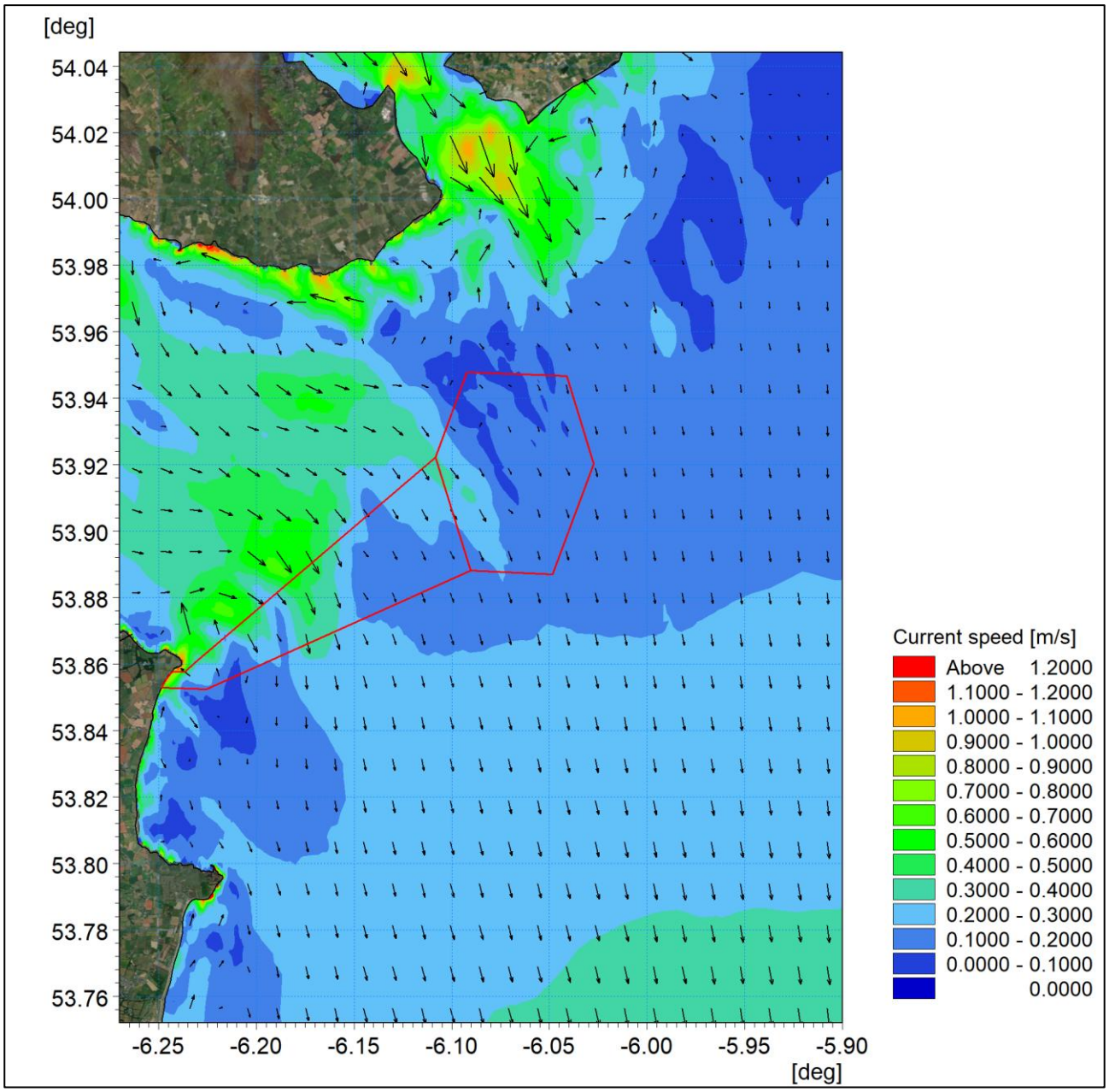

Figure 2A-26: Baseline littoral current 1:200 year storm from 165° with sea level rise - ebb tide.

2.3 Sedimentology

2.3.1 Overview

Before undertaking sediment modelling, it was necessary to first define characteristics for the seabed sediment. To this end a number of data sources were used including site-specific sediment sampling data, as documented in Gavin and Doherty Geosolutions (2020). For the zones beyond the Offshore wind farm area, data was accessed via the EMODnet online database (also collected by GSI). The INFOMAR data on seabed substrate is shown in Figure 2-27 whilst the extended composite data from EMODnet is shown in Figure 2-28.

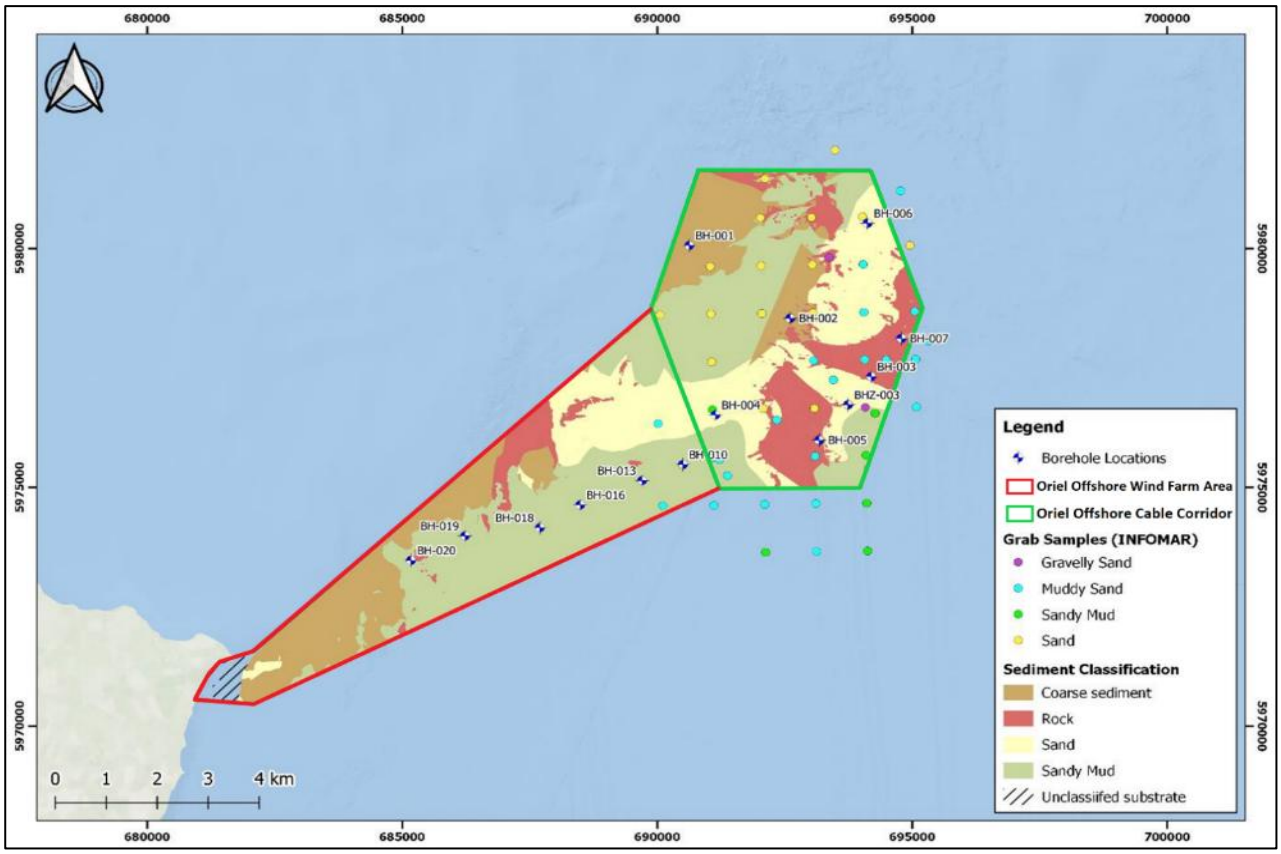

Figure 2-27: INFOMAR Sediment classification with Grab Samples used to ground-truth (Source: Gavin and Doherty Geosolutions, 2020).

Figure 2-28: Sediment classification EMODnet.

2.3.2 Sediment transport

Seabed sediments within the offshore wind farm area range from muddy sand to coarse gravel, with exposed rock outcrops at some locations. It has been noted however that there is little evidence of significant sediment transport within this area as average current speeds of less than 0.2 m/s would not be sufficient to mobilise and transport the coarse sandy material. The Shields critical shear parameter indicates the typically coarse sand (1 mm diameter) requires bed currents greater than those present for sediment to be mobilised. This is corroborated by the smooth bed formation and lack of significant sand wave features in the field data within the offshore wind farm area although some sand waves are visible to the south of the offshore wind farm area.

The MIKE 21 Sediment Transport (ST) module enables assessment of seabed sediment transport rates and initial rates of seabed level change for non-cohesive sediment resulting from currents or combined wave-current flows. It was used to determine the sediment transport pattern in the Marine Processes Study Area. The model combines inputs from both the hydrodynamic model and, if required, the wave propagation model. The model was setup using a layer of mobile bed material based on the sediment types (sizes and gradation) as illustrated in Figure 2-28.

Two sediment transport scenarios were examined, one relating to calm conditions and a second relating to the 1 in 2 year return period event from 165°. In each case the evaluations were undertaken over the course of a spring tide. These simulations included a period for the hydrodynamics and wave fields to stabilise and develop across the domain, i.e. a “warm-up” period.

For each scenario three aspects were examined. Firstly, the residual current, which is the net flow over the course of the tidal cycle. This is effectively the driving force of the sediment transport. The second aspect was the potential annual sediment transport as a result of this residual current. The net sediment transported during the tidal cycle was used to assess the annual net load. The use of an annual figure is standard when presenting sediment transport data however it does assume the same hydraulic conditions persist for an entire year. Whilst this is unrealistic for individual storm events, the magnitudes are still useful for comparative purposes. The unit of transport is $m^3/yr/m$; this represents the volume of material displaced over a period of one year and is presented per metre width perpendicular to the direction of that movement. These net values do not provide a full picture of the transport mechanism.

For the tidal current alone the depth average residual current is presented in Figure 2-29. It is characterised by minimal residual current at the offshore wind farm area, as anticipated, and elevated values along the coastline. The resultant transport rate as illustrated in Figure 2-30 further demonstrates that there is very little movement of sediment at the offshore wind farm area due to the low current speed.

When a storm approaches from 165°, the flood tide currents are enhanced by the wave climate. This is reflected in an increase in the residual currents along the coastline as illustrated in Figure 2-31. There is movement of the sandy material in the centre of the offshore wind farm area however the magnitude of the transport is smaller than that along the coastline as illustrated in Figure 2A-32.

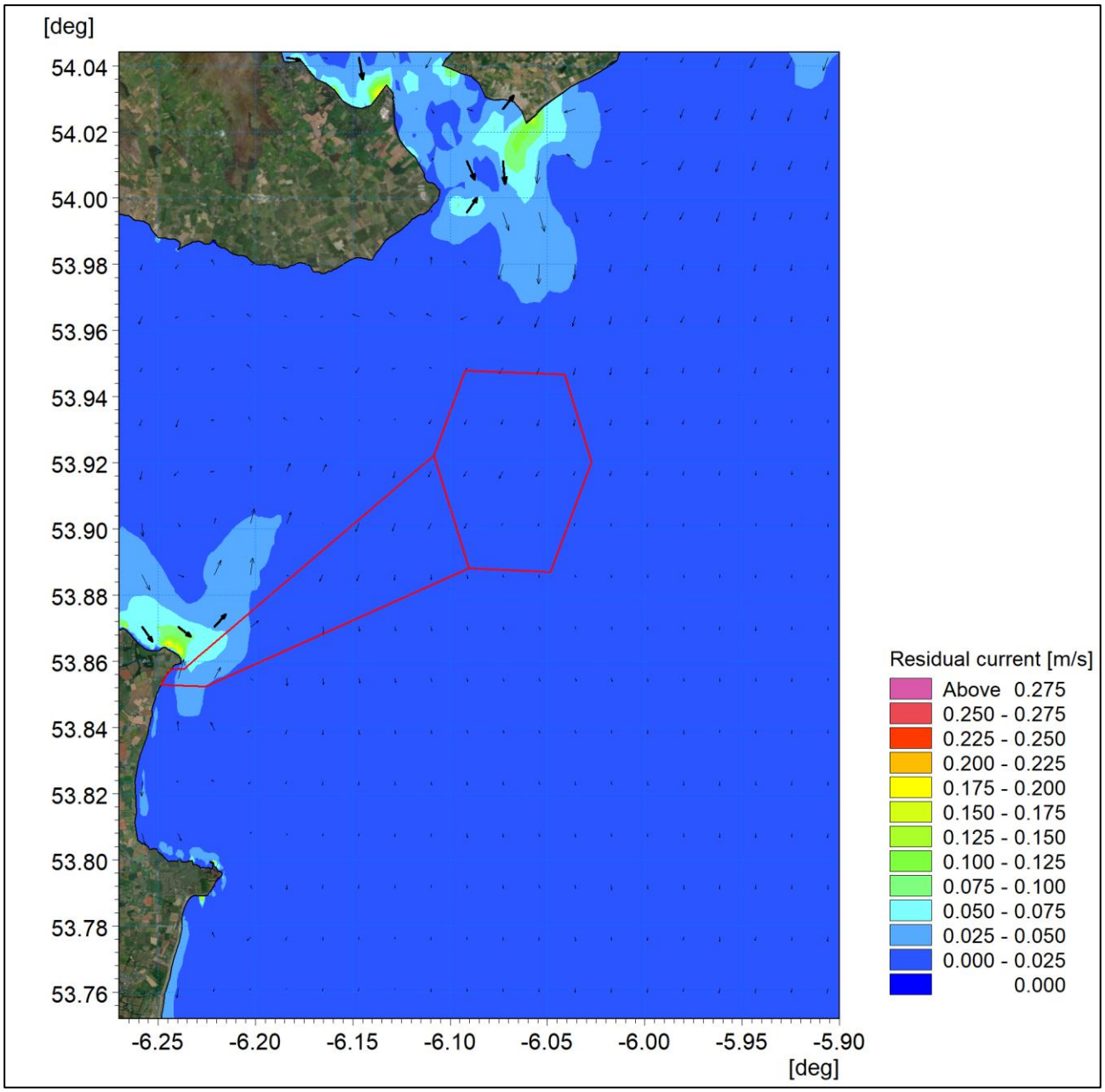

Figure 2-29: Baseline residual current spring tide.

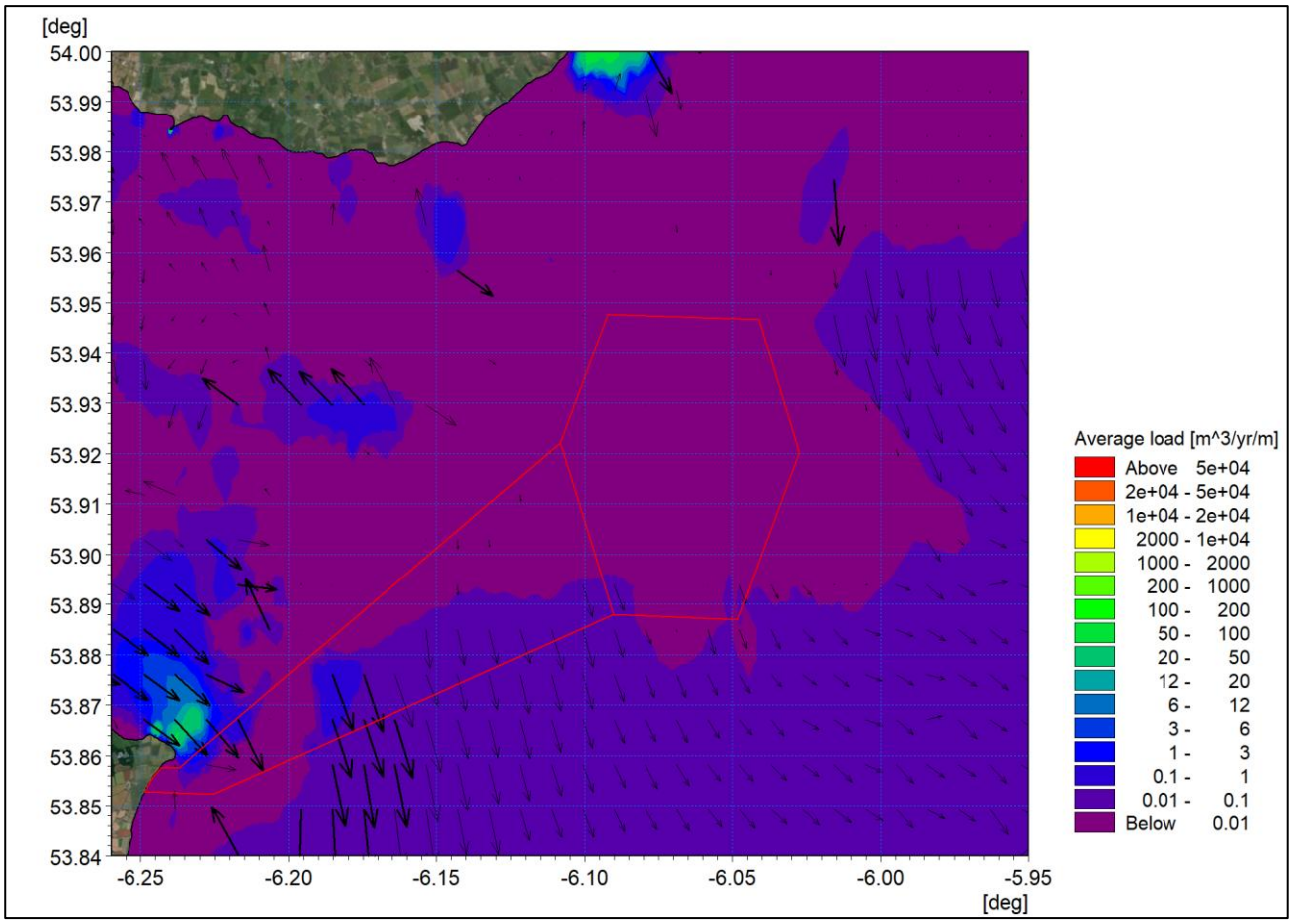

Figure 2-30: Baseline potential net sediment transport - spring tide.

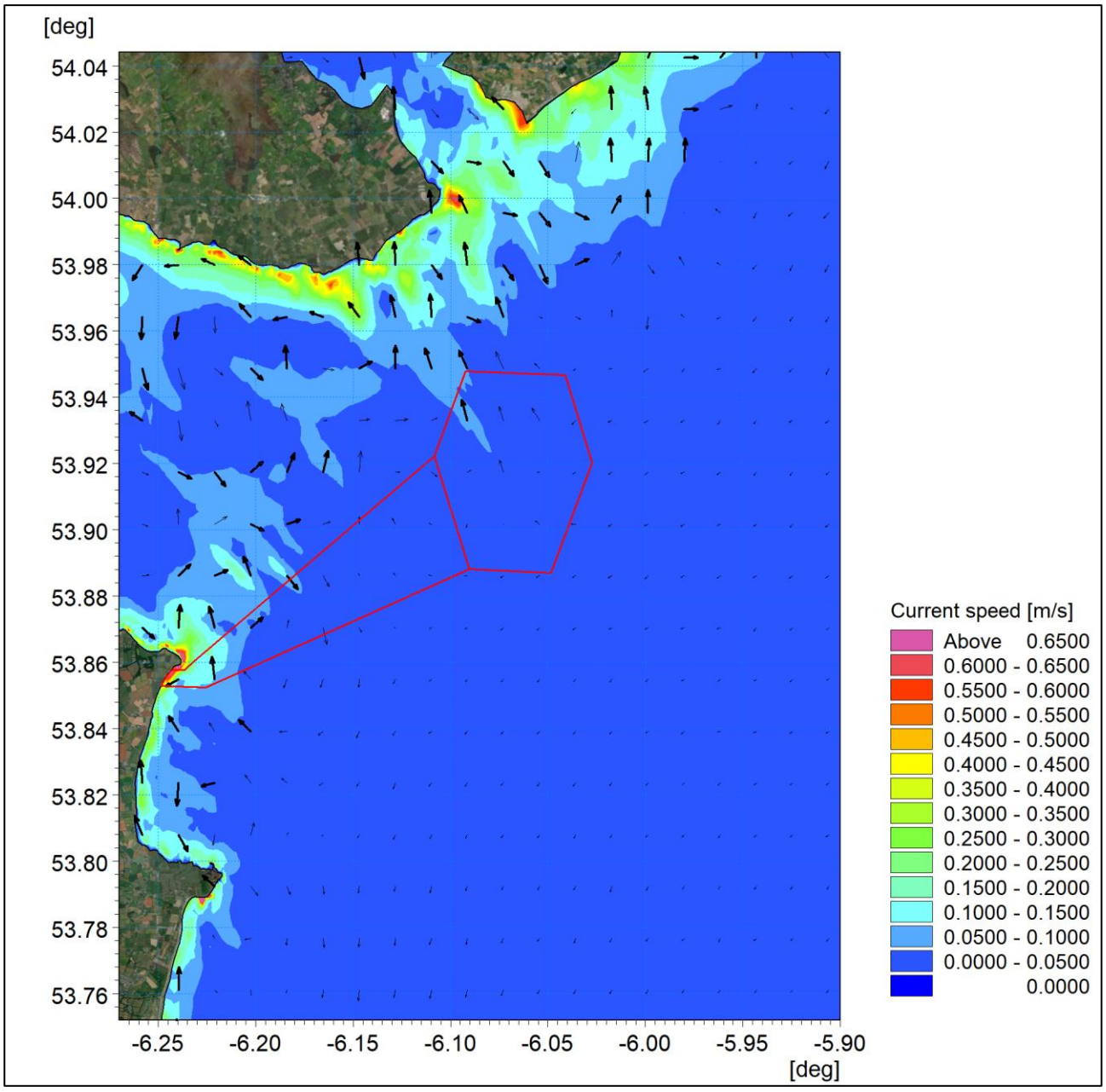

Figure 2-31: Baseline residual current spring tide with 1:2 year storm from 165°.

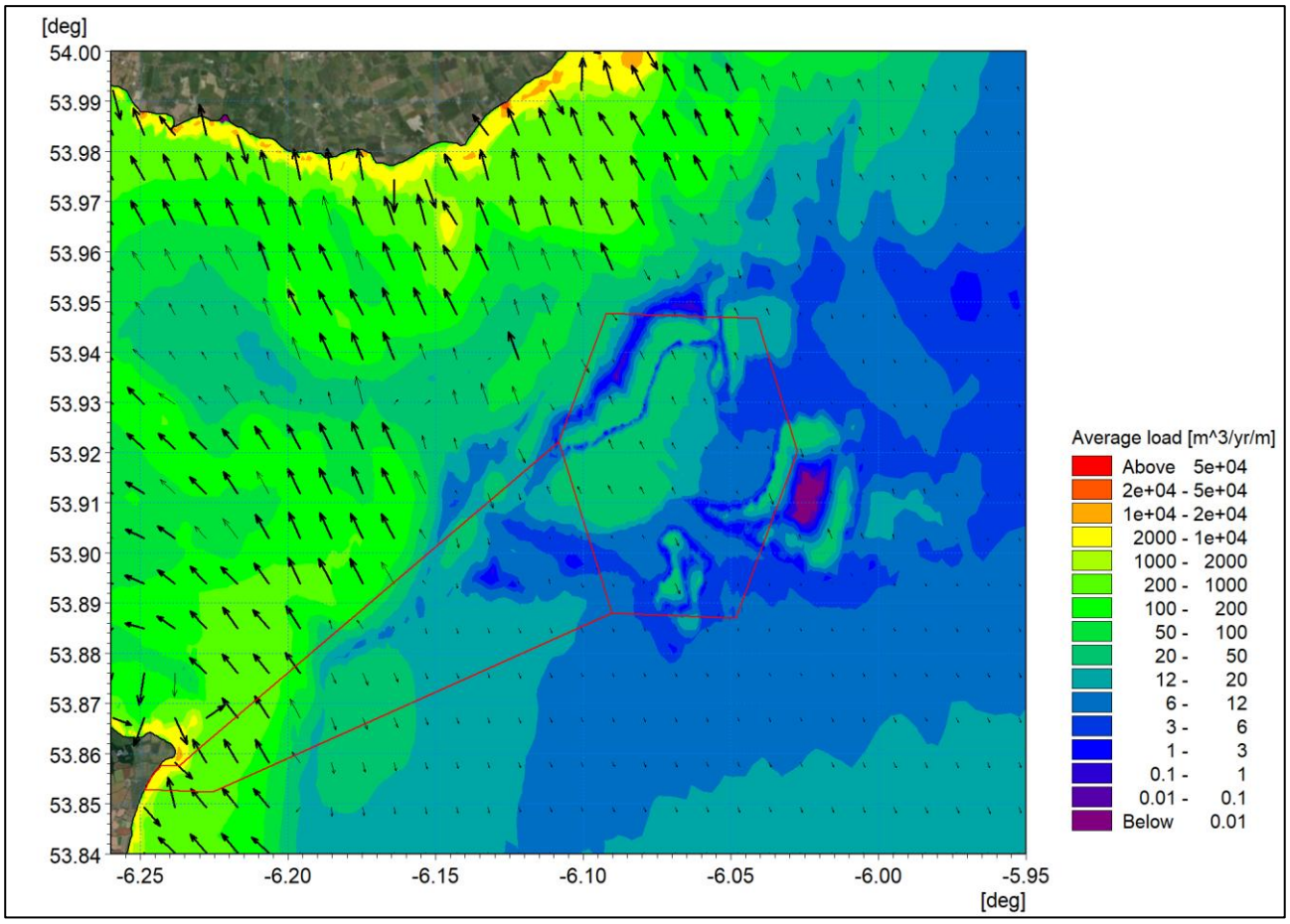

Figure 2A-32: Baseline potential net sediment transport - spring tide with 1:2 year storm from 165°.

Sensitivity of sediment transport

In response to RFI 6.H and by way of a sensitivity analysis, the potential for the longer term impact on sediment transport was examined. A sediment map which extended beyond the immediate vicinity of the proposed development was created based on the EMODnet data presented in Figure 2-28. It should be noted by the reader that in the longer term simulation there was no limit on sediment sources, i.e. the bed was assumed to be comprised of mobile bed sediment as classified on the surface to an unlimited depth. In reality where significant erosion occurs consolidated and more cohesive sediment would be encountered. Additionally, the model did not account for sediment input from riverine sources, such as the Castletown River which deposits silt into the navigation channel within Dundalk Bay. Any longer term model is therefore conservative in terms of sediment transport but remains a valuable indicator for a comparison with the post development scenario.

A period of one month was selected whereby the tidal range was representative of that exhibited across the year. The sediment transport simulation was then undertaken for a month of tides with the application of a speed-up factor to provide the equivalent of annual sediment transport rates. The change in bed levels over this period was used to indicate the sediment transport and seabed morphology. The baseline scenario is presented in Figure 2A-33. As anticipated, there is very little change in bed levels across the Project area, particularly within the array area. As presented in Figure 2-27 and Figure 2-28, across much of this region the bed is composed of sand, muddy sand and coarse sediments. Both the modelled and measured current speeds indicate depth averaged values of typically less than 0.2 m/s (which would be further reduced at the seabed), whilst the threshold for movement of even fine to medium sand is in excess of 0.2 m/s at 1 m above the bed (Hjulstrøm, 1939).

There is some limited change in bed level approximately half way along the cable corridor, where both the increased current speed and extent of the rocky outcrop are located. As noted previously, there is exaggerated erosion and deposition within Dundalk Bay where the finer sands and mud are eroded from the channel where current speeds are elevated and then deposited in the outer Bay where current speeds are reduced. In reality sediment sources from the Castletown River would replenish this eroded material.

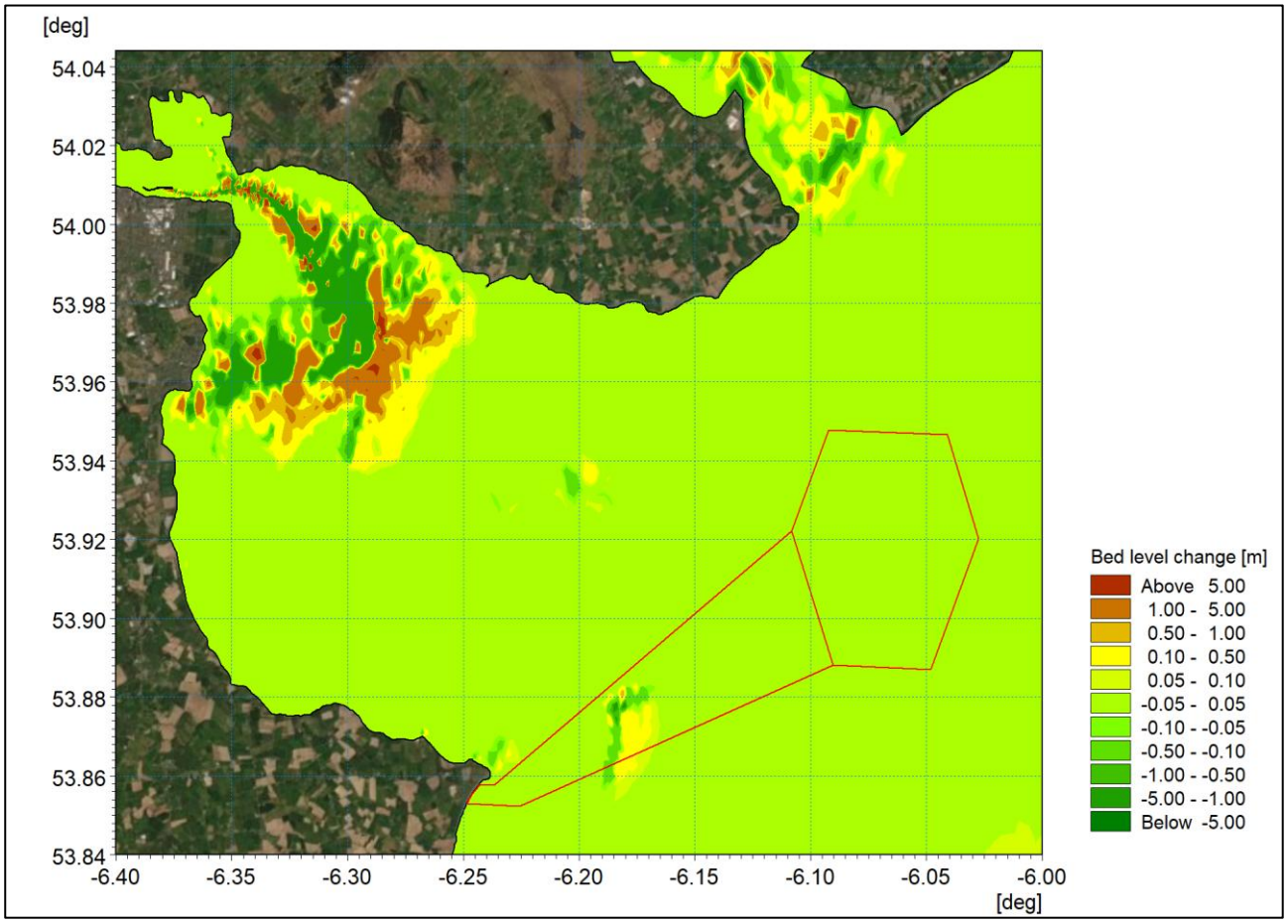

Figure 2A-33: Baseline change of bed level for one year of tidal currents.

In response to RFI 6.D the additional littoral current modelling was extended to examine residual currents and sediment transport patterns. Sensitivity modelling was undertaken for the 1 in 200 year return period and also to examine the influence of sea level rise. As before, the simulations undertaken as outlined in the previous section were repeated with an increased wind speed to examine the effect on residual currents which form the driver for sediment transport.

Figure 2A-34 illustrates the residual currents for the 1 in 200 year event from the 165º sector. It is noted that peak residual current speeds along the shoreline reach 0.9 m/s when compared to 0.6 m/s for the 1 in 2 year storm therefore an alternate contour palette was required. Figure 2A-35 shows the corresponding sediment transport pattern. It is observed that there is an increase in sediment transport across the rocky outcrop within the array area to circa 100 m^3/year/m however it should be noted that this remains significantly less than transport rates along the shoreline which are in excess of 10000 m^3/year/m for the same event. A log palette was required to illustrate the range of transport magnitude.

Figure 2A-36 and Figure 2A-37 show the corresponding information for the same storm condition with the inclusion of sea level rise. Given that littoral currents remained largely unchanged due to the increase in water level it is not unexpected that the residual currents and sediment transport patterns are also akin to the present day counterparts.

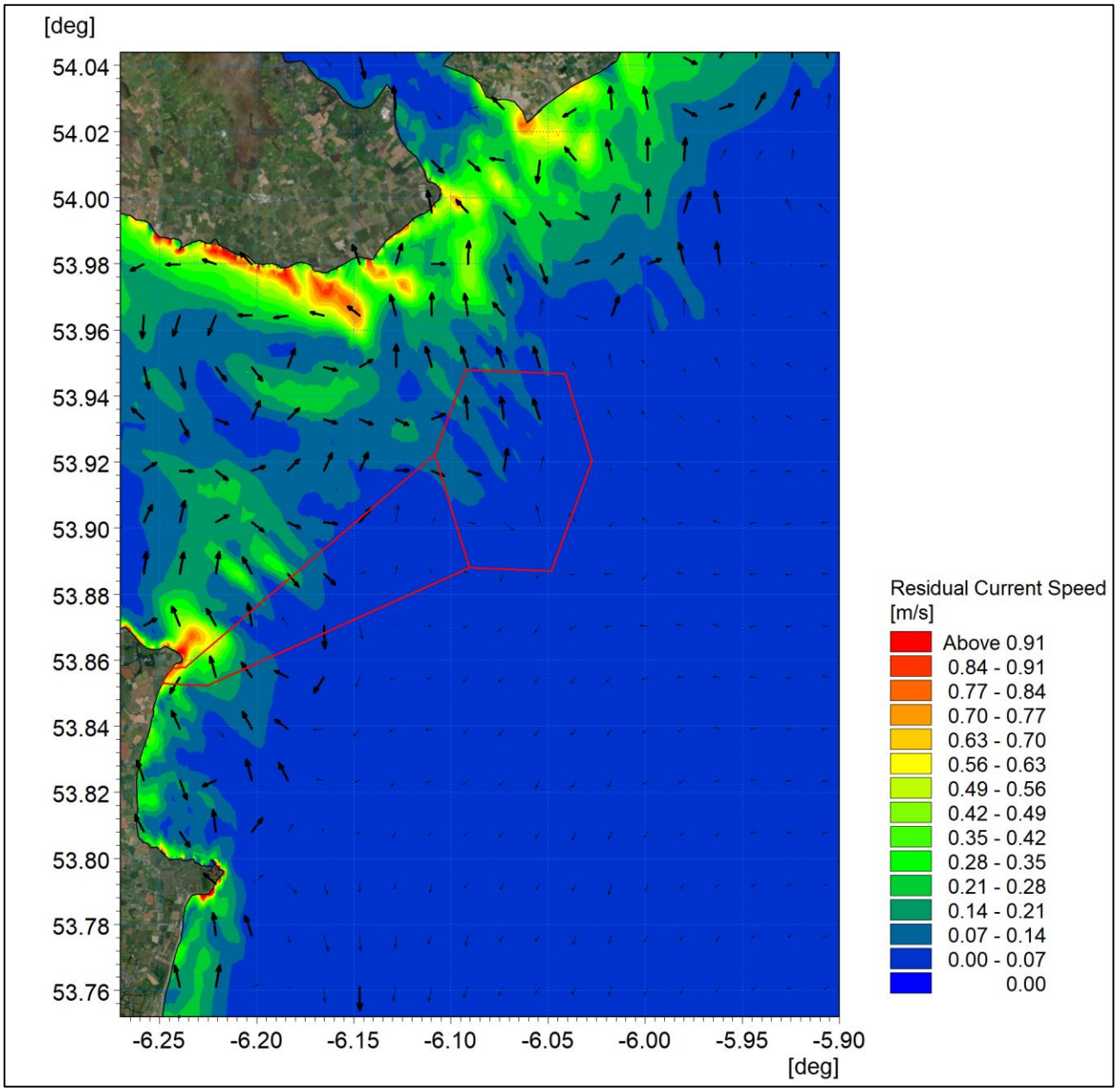

Figure 2A-34: Baseline residual current spring tide with 1:200 year storm from 165°.

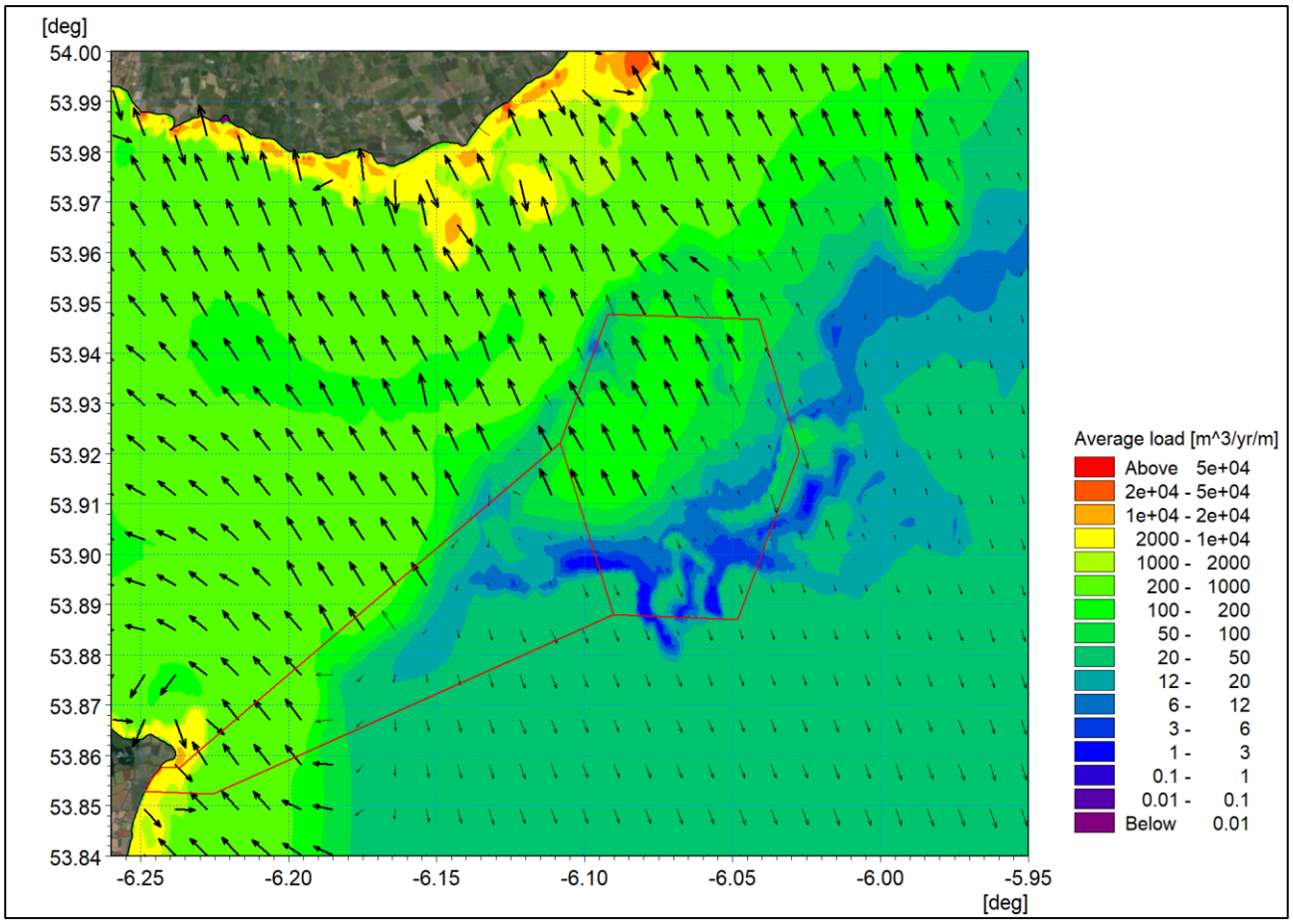

Figure 2A-35: Baseline potential net sediment transport - spring tide with 1:200 year storm from 165°.

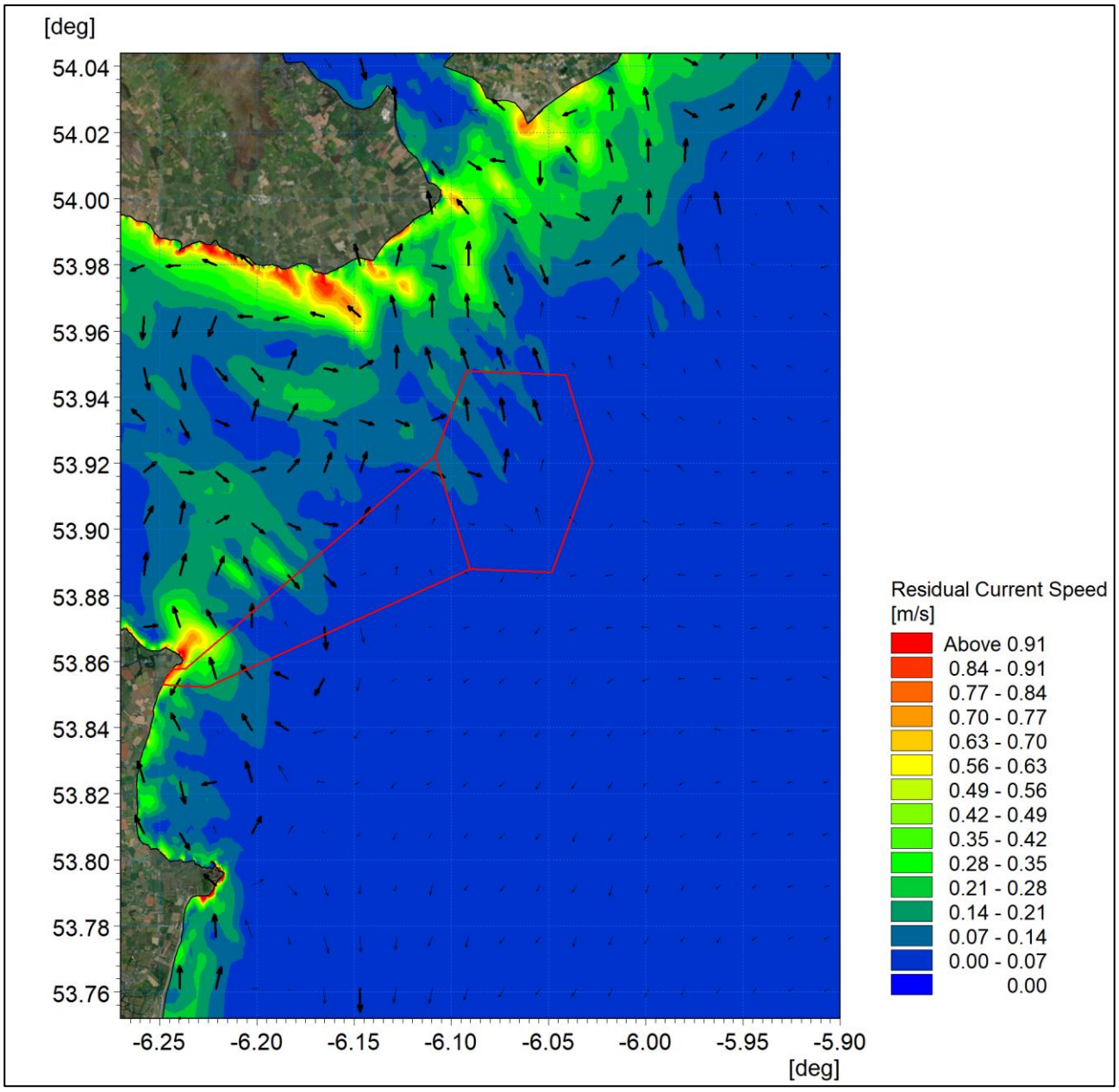

Figure 2A-36: Baseline residual current spring tide with 1:200 year storm from 165° with sea level rise.

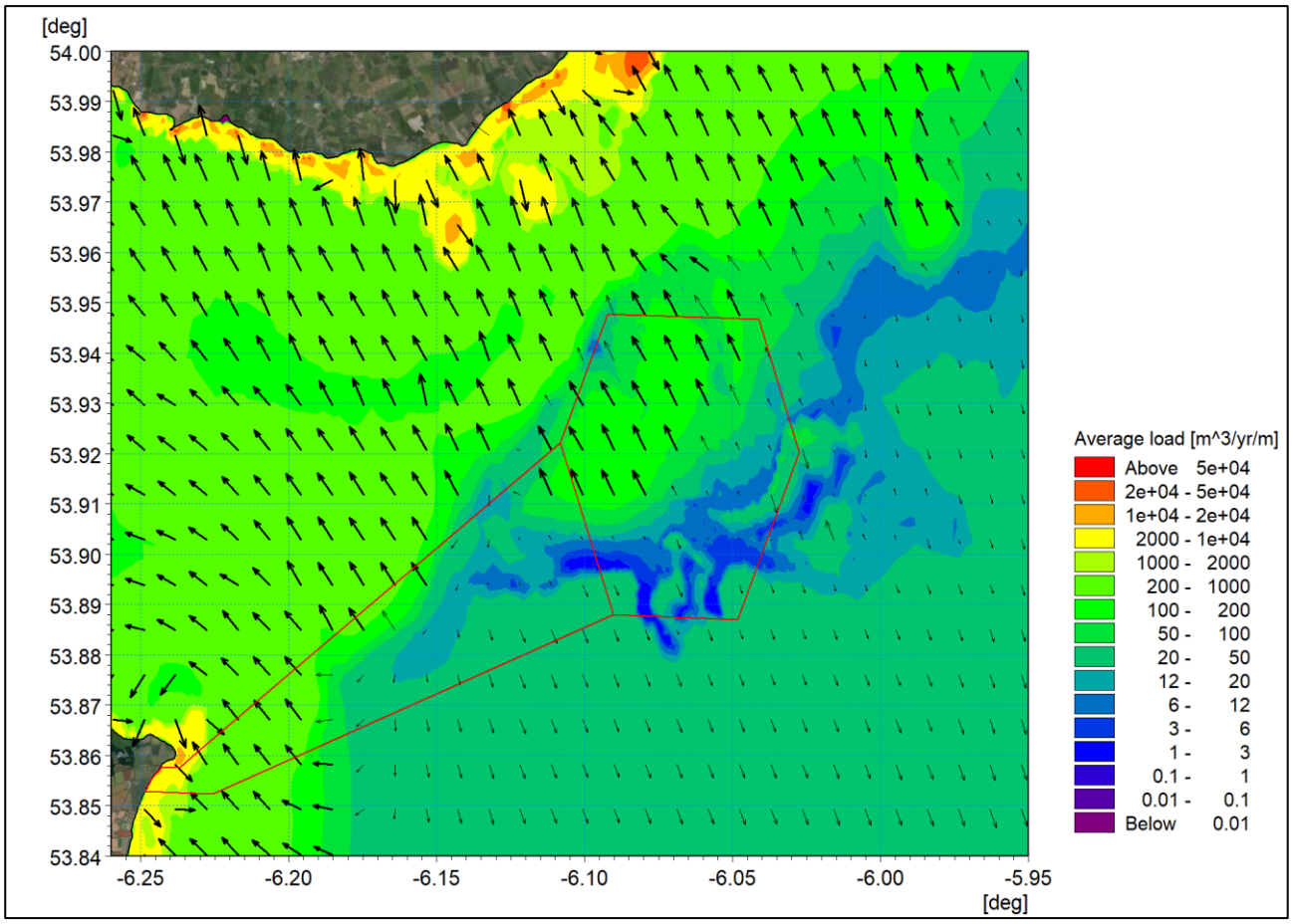

Figure 2A-37: Baseline potential net sediment transport - spring tide with 1:200 year storm from 165° with sea level rise.

2.3.3 Suspended sediments

Sediment in the Marine Processes Study Area is dominated by sand and gravel and it has been seen that tidal currents are not sufficiently strong to give rise to high turbidity. The Centre for Environment, Fisheries and Aquaculture Science (CEFAS) Climatology Report 2016 (CEFAS, 2016) shows the spatial distribution of average non-algal Suspended Particulate Matter (SPM) for the majority of the UK continental shelf.

For the period 1998-2005 the largest plumes are associated with large rivers such as the Thames Estuary, the Wash and Liverpool Bay, which show mean values of SPM above 30 mg/l. Based on this information it is estimated that the average SPM within Dundalk Bay over this period is *c.* <3 mg/l as shown in Figure 2-38.

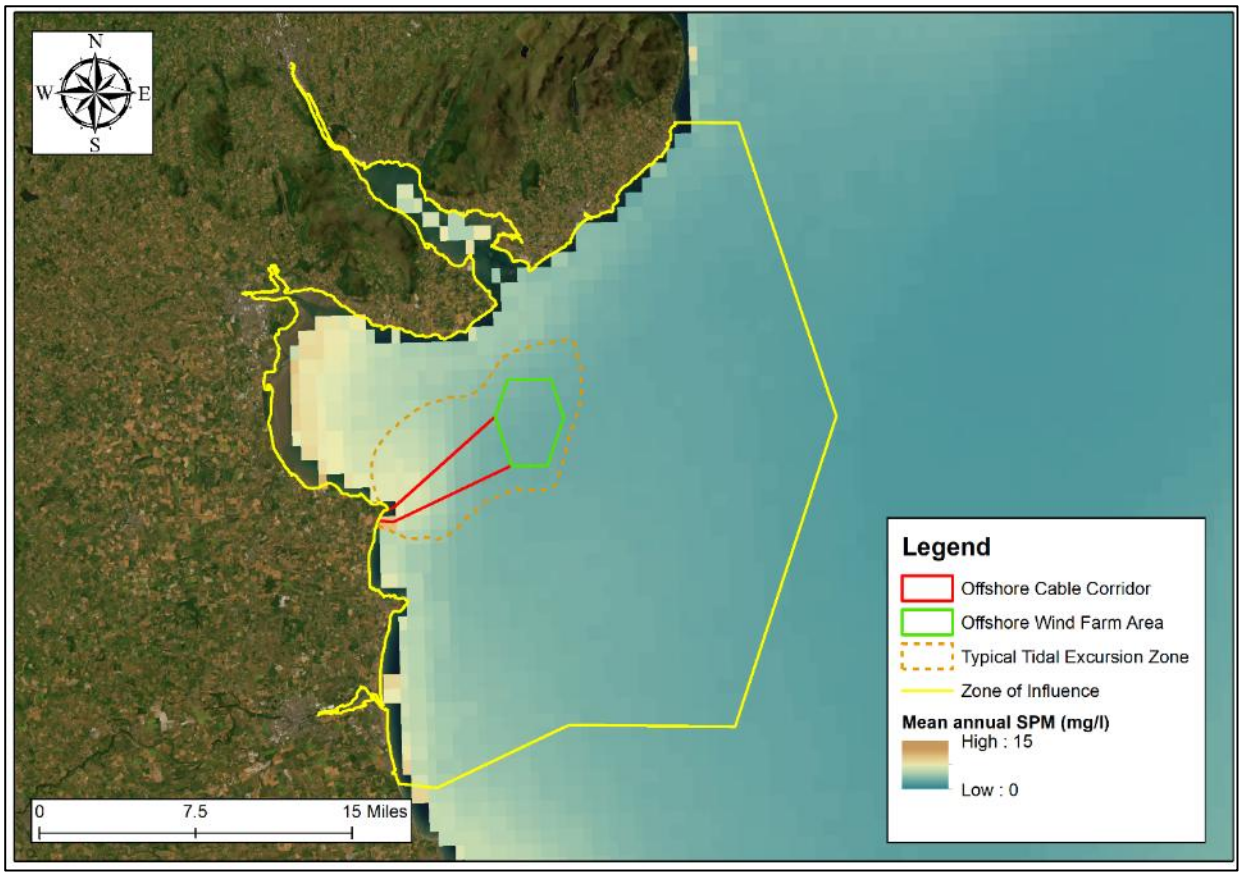

Figure 2-38: Distribution of average non-algal Suspended Particulate Matter.

3 POTENTIAL ENVIRONMENTAL EFFECTS

3.1 Overview

The potential changes to baseline conditions as a result of the construction and operation of the Project are quantified in the following sections. The potential changes to sea state and sediment transport regime were established by repeating the modelling undertaken in the previous section with the proposed turbine and OSS foundation structures in place. The foundation structures were modelled by including sub-grid structures within the model at each location and, in the case of sediment transport, the scour protection was simulated using an area of fixed seabed around each structure.

For the purposes of modelling, the offshore wind farm layout as described in section 2 of the NIS was used to define the location of structures within the numerical model. It should be noted that the scale of the model mesh meant that the general flow and sediment patterns around the structures could be observed on the wider scale.

However, the localised nature of the scour meant that a detailed assessment of the effectiveness of the scour protection at each foundation structure was not undertaken as this was not the purpose of the computational modelling. The scour protection does not have implications on the global scale and is restricted to reducing sediment erosion in the vicinity of the foundation structures; there would be larger implications if scour protection were not provided, as detailed by Whitehouse *et al.* (2006).

A description of the modelling methodology used to assess impact of the offshore wind farm on specific marine processes, i.e. tidal regime, wave climate and sediment transport regime, is outlined in the following Sections.

3.2 Post-construction hydrography

3.2.1 Tidal Flow

The obstruction created by monopile foundations has the potential to alter tidal flows within the offshore wind farm area. Therefore, each of the 26 structures (25 turbines and one offshore substation) were defined in the numerical model as sub-grid features. The geometry and locations used to define each monopile are summarised in Figure 3-1 and Figure 3-2 respectively. This approach enabled potential changes in tidal flows to be resolved at an appropriate scale that accounted for the presence of the structures. Using this method, the baseline spring tide simulation described in section 2.2.1 was repeated but with the offshore wind farm in place.

Figure 3-3 and Figure 3-4 illustrate the post-construction flood tide flow patterns during mid-flood and mid-ebb tidal flows respectively. Due to the limited magnitude of the changes relative to baseline conditions, difference plots have also been provided for post-construction mid-flood and mid-ebb flows in Figure 3-4 to Figure 3-6 respectively. Difference plots are produced by subtracting baseline conditions from conditions with the Project in place. Thus, positive changes in difference plots reflect areas whereby the magnitude of that process (i.e. tidal currents, waves or sediment transport rates) have increased as a result of the Project and vice versa for negative changes. The same procedure for calculating differences has been implemented throughout this Technical Report.

This assessment found that the Project resulted in a localised acceleration of tidal flows within the immediate vicinity of the structures. However, it should be noted that these values (i.e. changes to velocity; magnitude and direction) are generally <4 mm/s which constitutes less than 2% at the peak flows. These changes are also limited to the immediate Project offshore wind farm area. Due to the limited magnitude and spatial extent of these changes and a return to baseline conditions within close proximity (in the order of <1 km of the Project boundary) the predicted impact on the North Western Irish Sea Gyre, which is present at a distance of over 40 km to the east of the Project during summer months, is expected to be negligible.

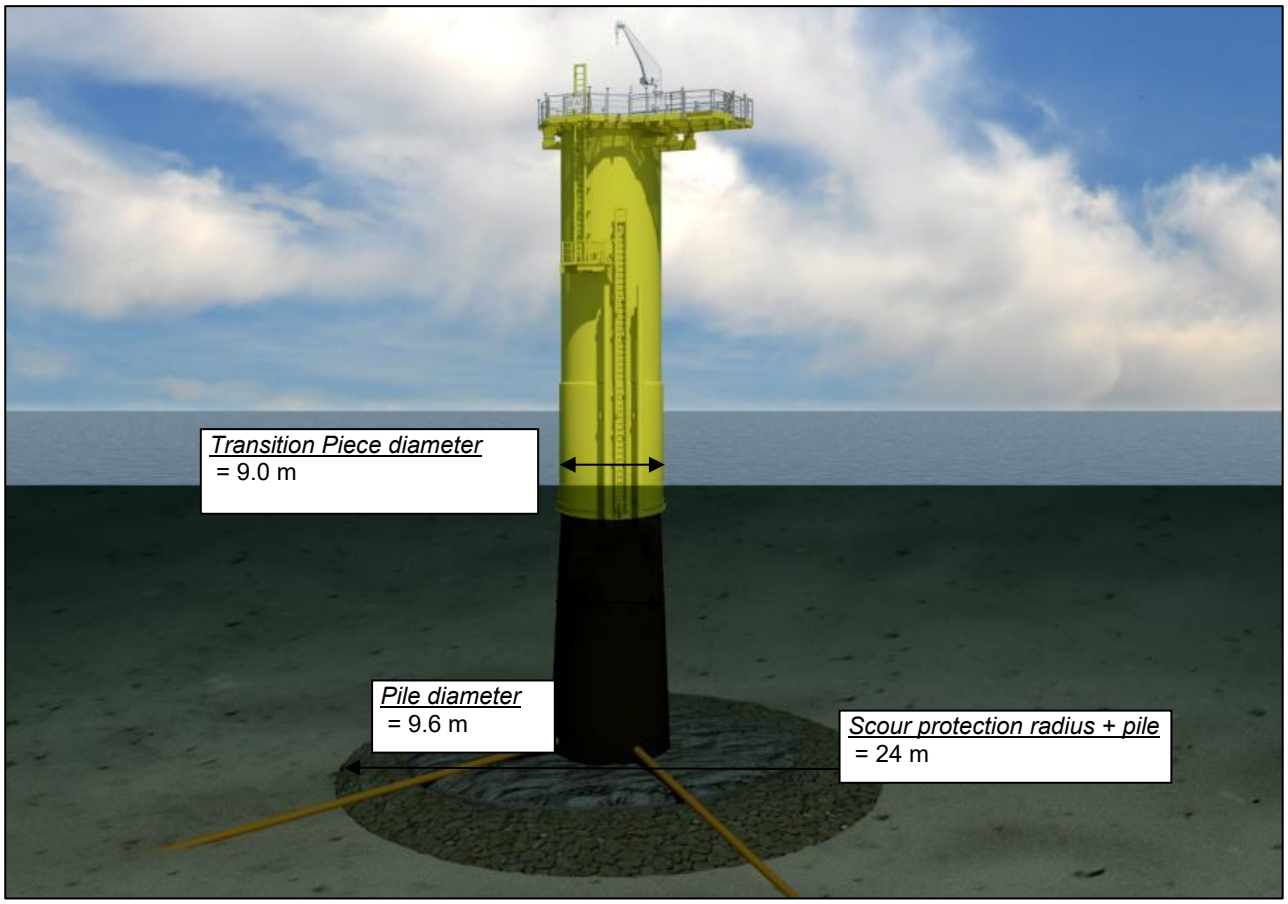

Figure 3-1: Geometry of a monopile foundation (not to scale).

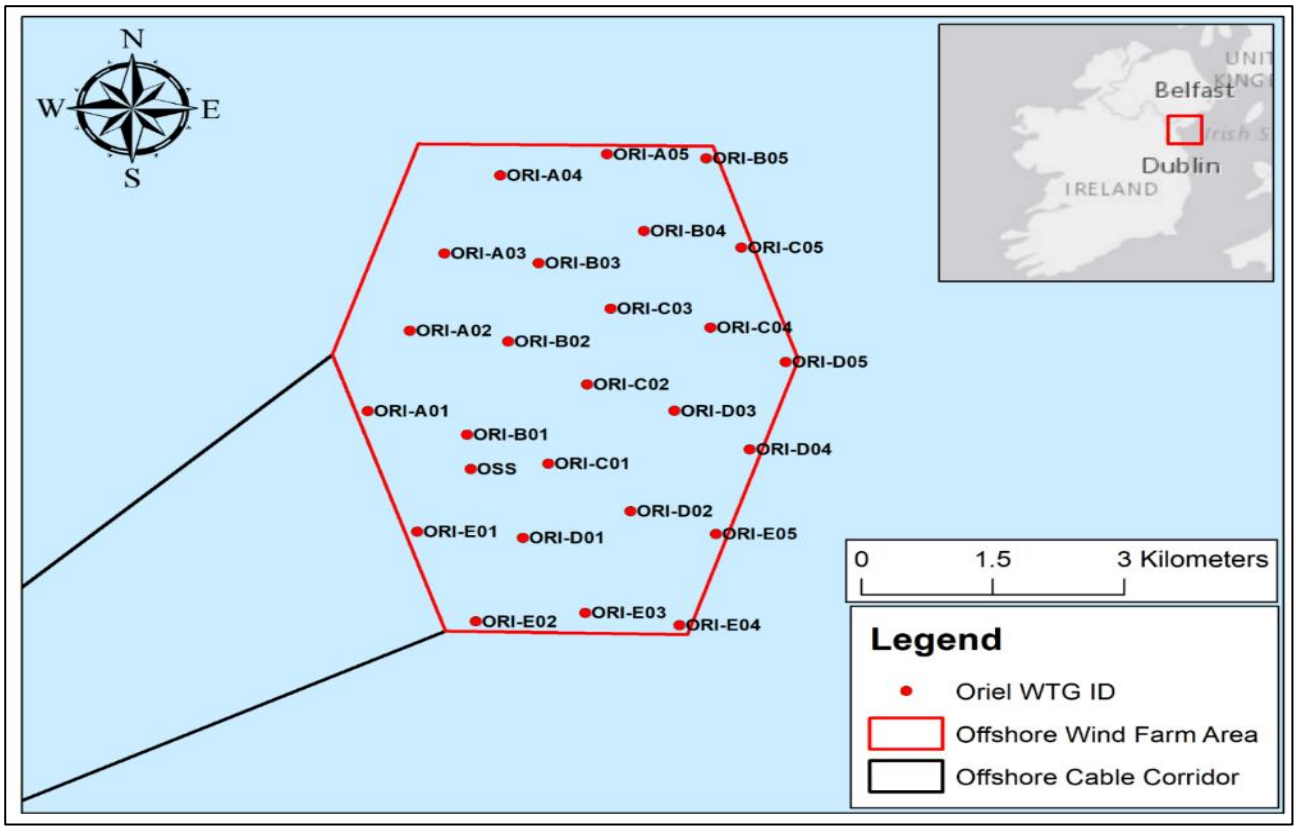

Figure 3-2: WTG and OSS locations within the offshore wind farm area.

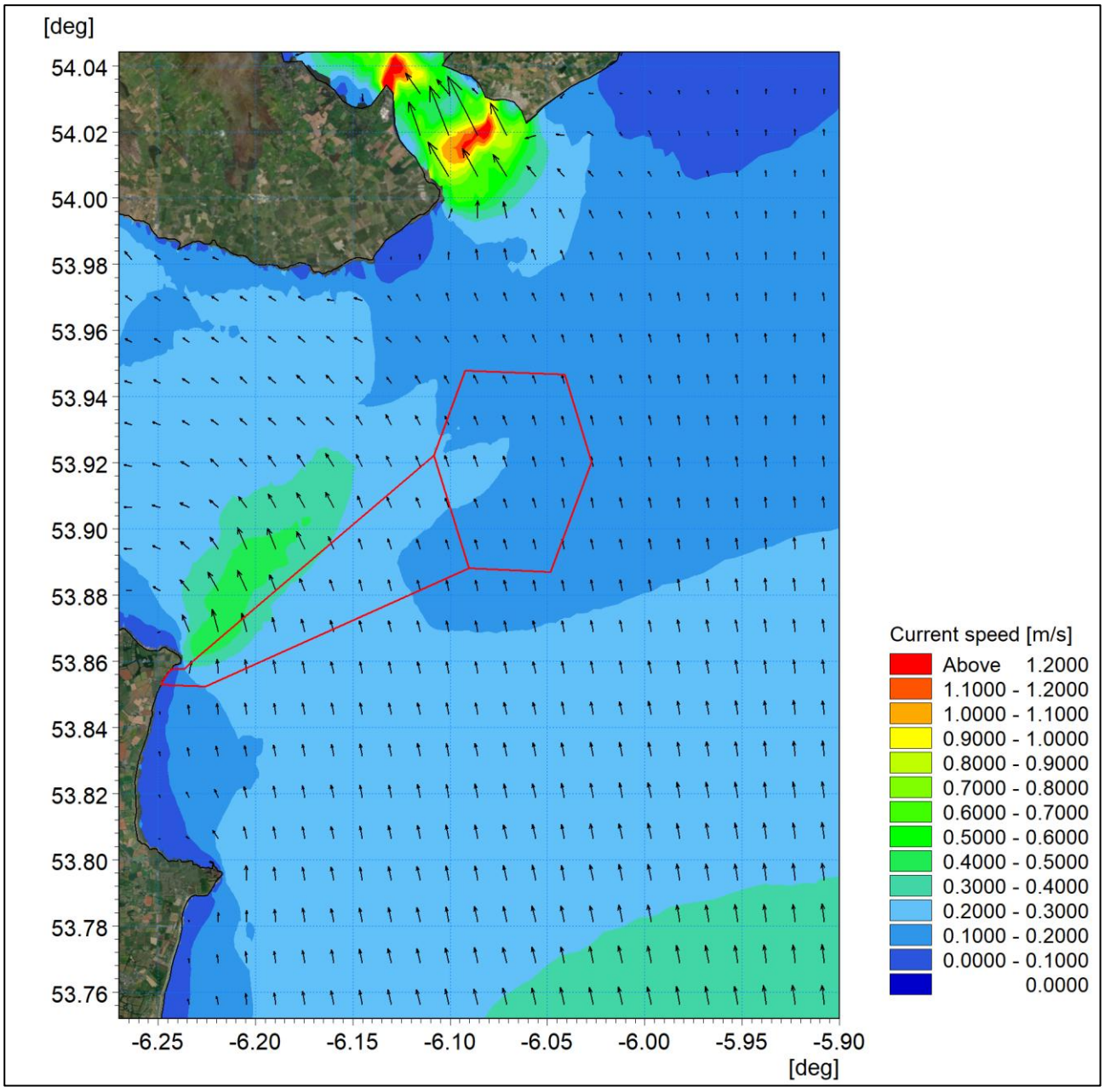

Figure 3-3: Post-construction tidal flow patterns - mid-flood.

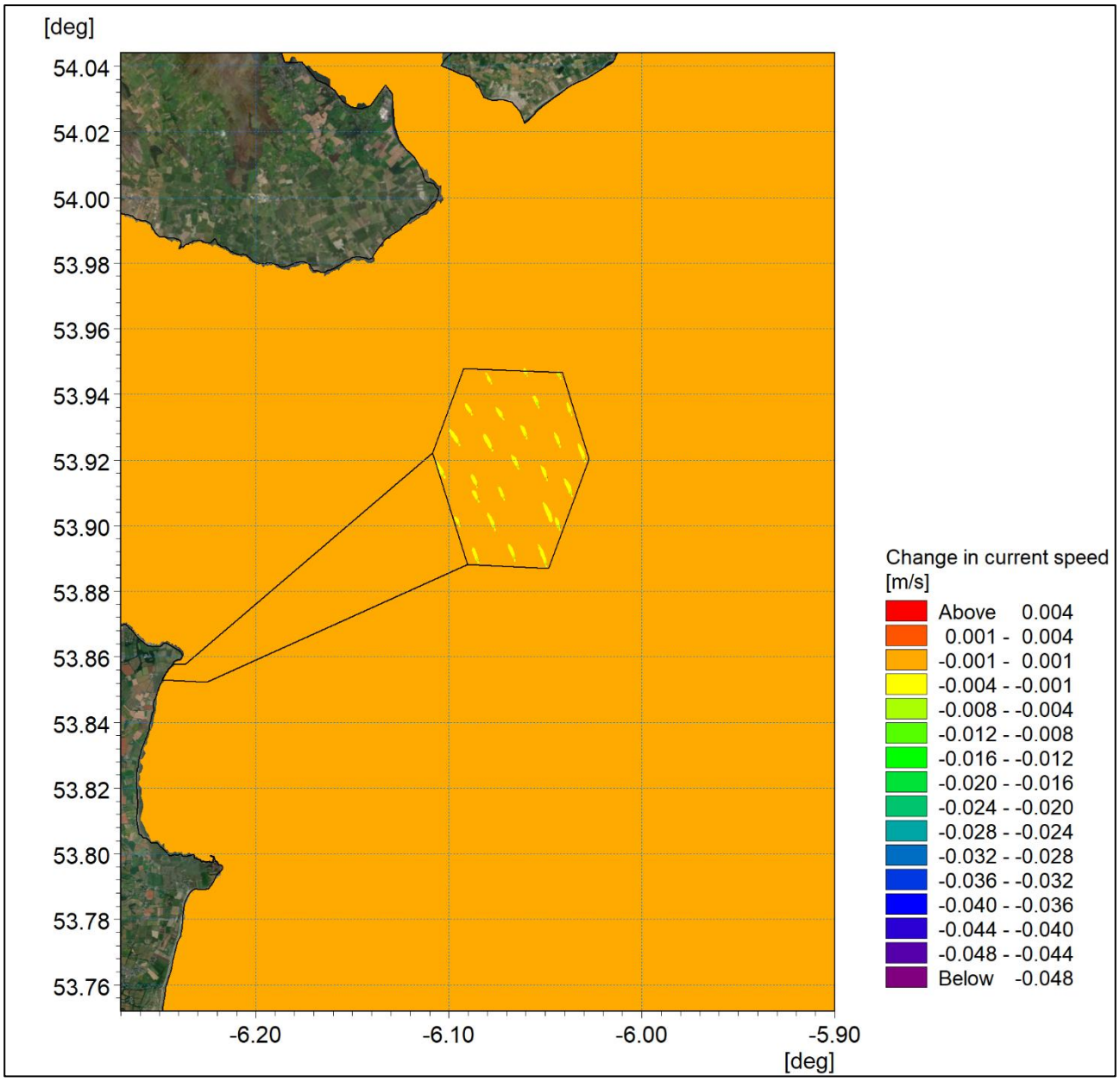

Figure 3-4: Change in tidal flow (post-construction minus baseline) - mid-flood.

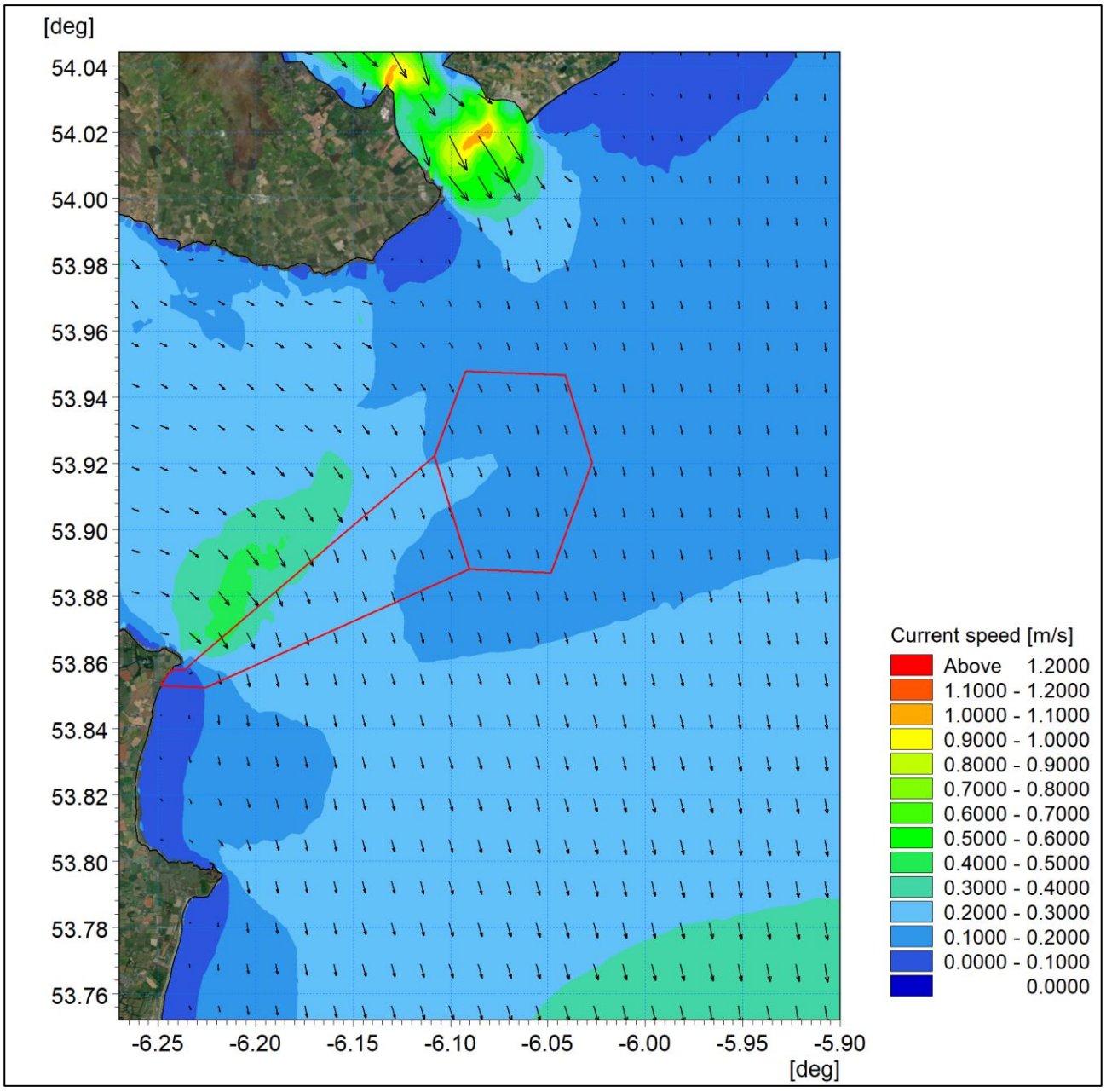

Figure 3-5: Post-construction tidal flow patterns - mid-ebb.

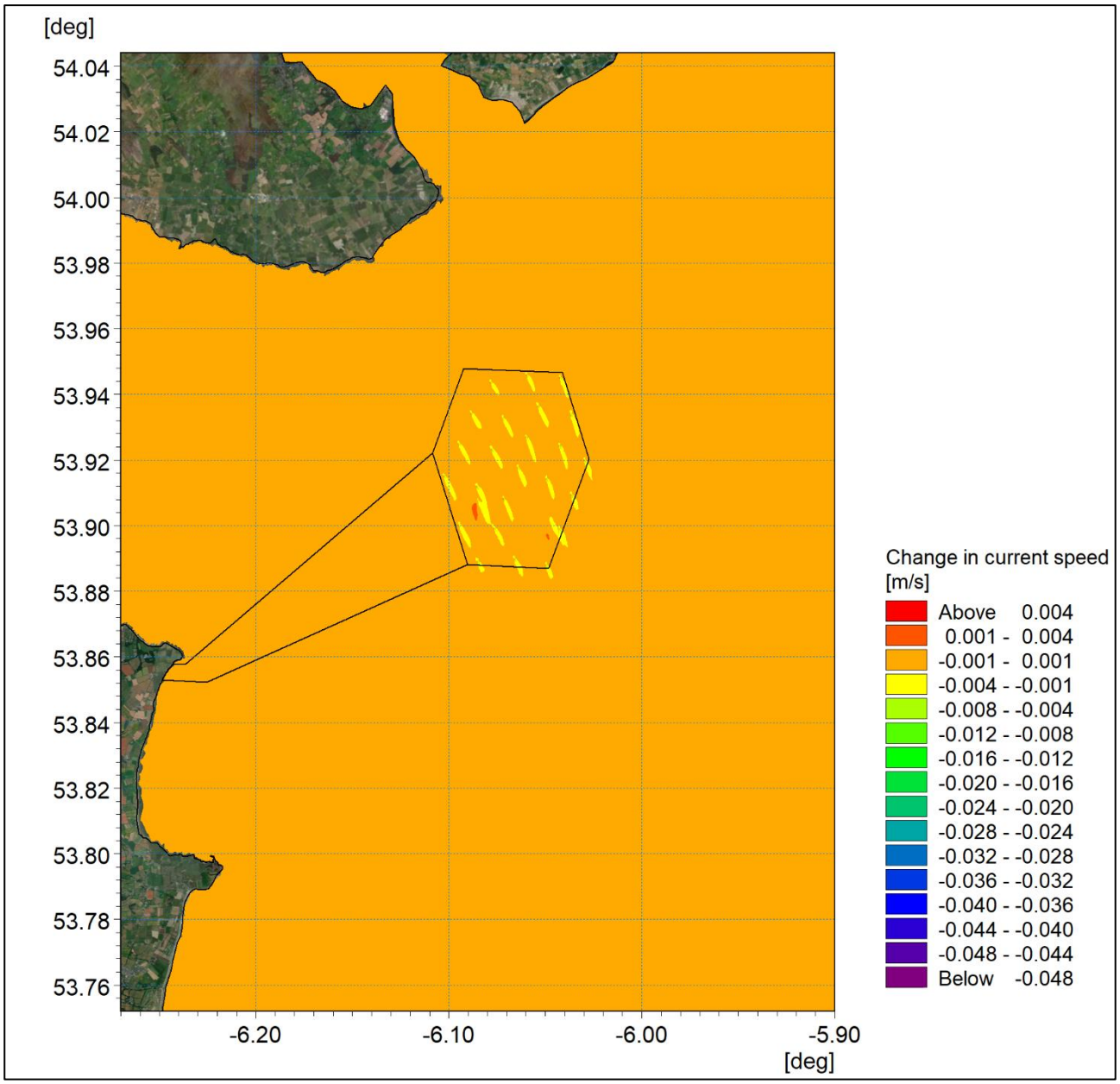

Figure 3-6: Change in tidal flow (post-construction minus baseline) - mid-ebb.

3.2.2 Wave Climate

Using the same principle as for the tidal modelling, the wave climate modelling was repeated with the 25 turbines and one offshore substation defined in the numerical model as sub-grid features. Again, changes were found to be indiscernible from the baseline scenario by visual inspection therefore difference plots have been provided.

The 1 in 2 year storms for the three principal directions (015°, 090° and 165°) are presented in Figure 3A-7, Figure 3A-9 and Figure 3A-11 respectively. It should be noted that these correspond to the baseline wave climate figures presented in Figure 2A-9, Figure 2A-10 and Figure 2A-11 for each direction respectively.

For all wave scenarios, the reduction in significant wave height is around 40 mm, typically less than 2% and is limited to the vicinity of the structure. The difference in baseline and post construction wave climates is presented in Figure 3-8, Figure 3-10 and Figure 3-12 for the three principal directions 015°, 090° and 165°

respectively. It should be noted that a log scale palette has been used to accentuate differences in these results.

Further modelling was undertaken for a more severe 1 in 50-year storm, with the results presented in Figure 3A-13 to Figure 3A-18. In each case the post-construction wave climate is followed by the difference plot and, as indicated with the 1 in 2-year plots, the larger the wave climate the less significant the changes resulting from the structures (i.e. the changes in wave height magnitude remain similar whilst the baseline increases).

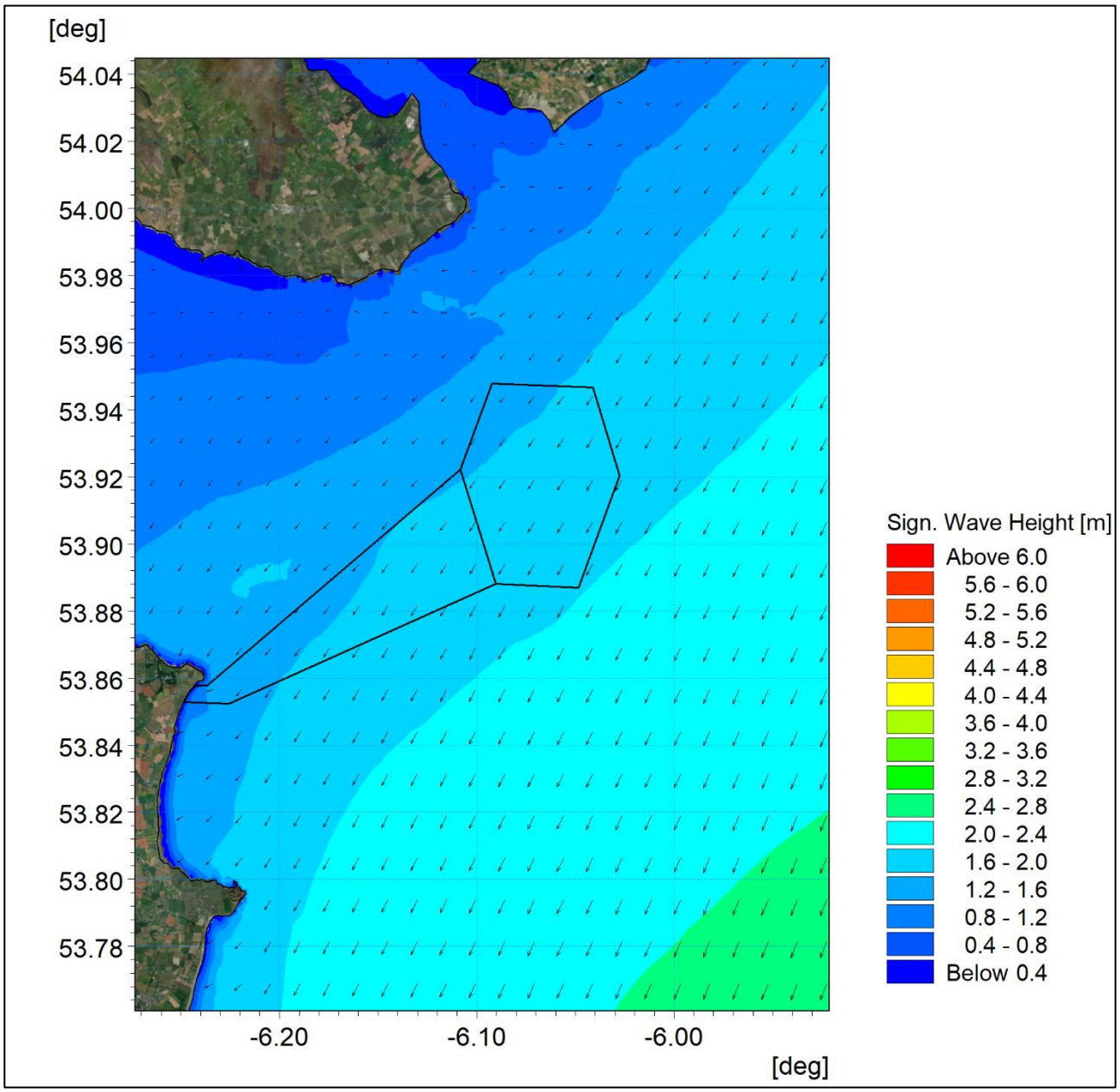

Figure 3A-7: Post-construction wave climate 1 in 2 year storm 015°.

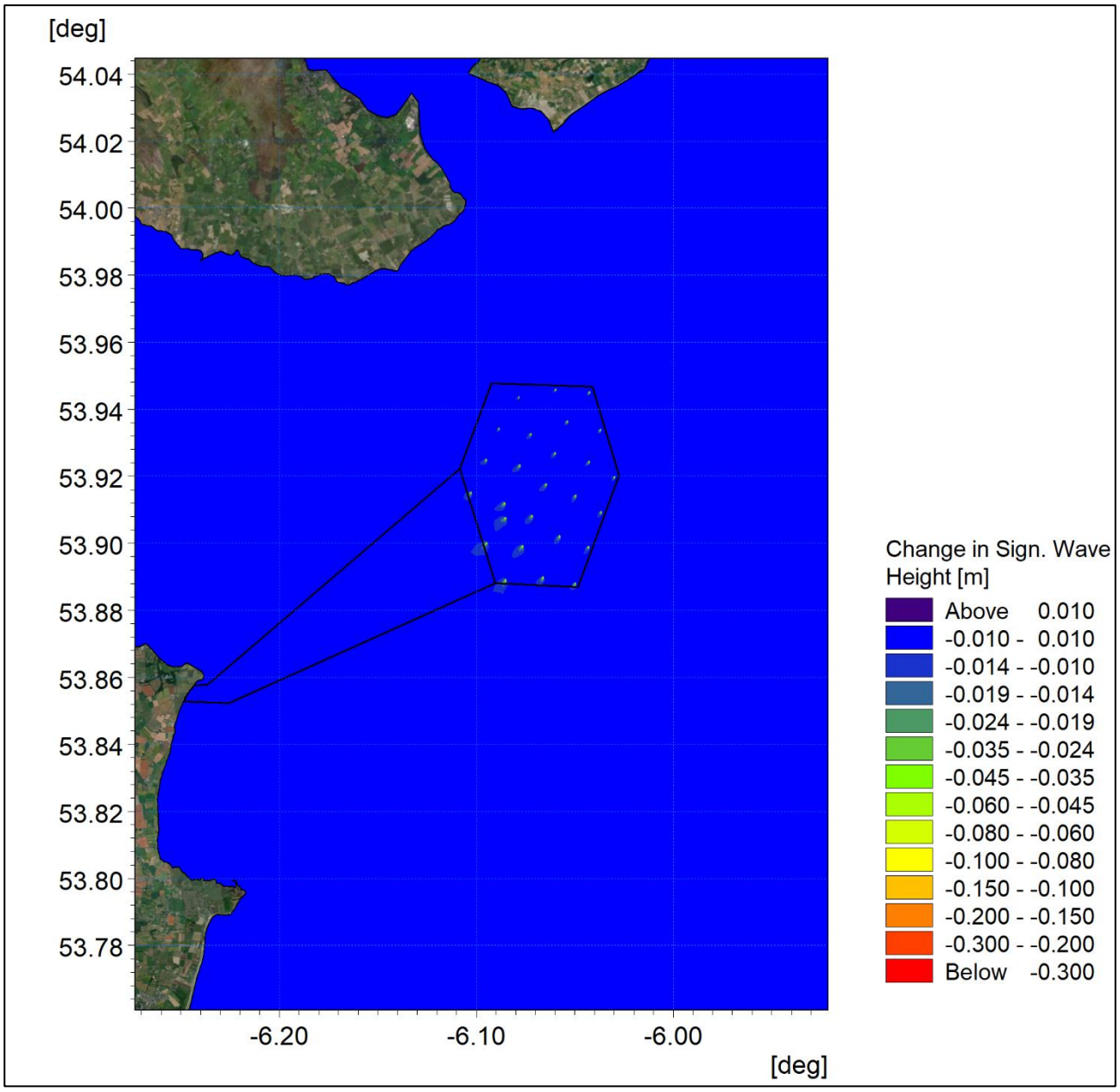

Figure 3-8: Change in wave climate 1 in 2 year storm 015° (post-construction minus baseline).

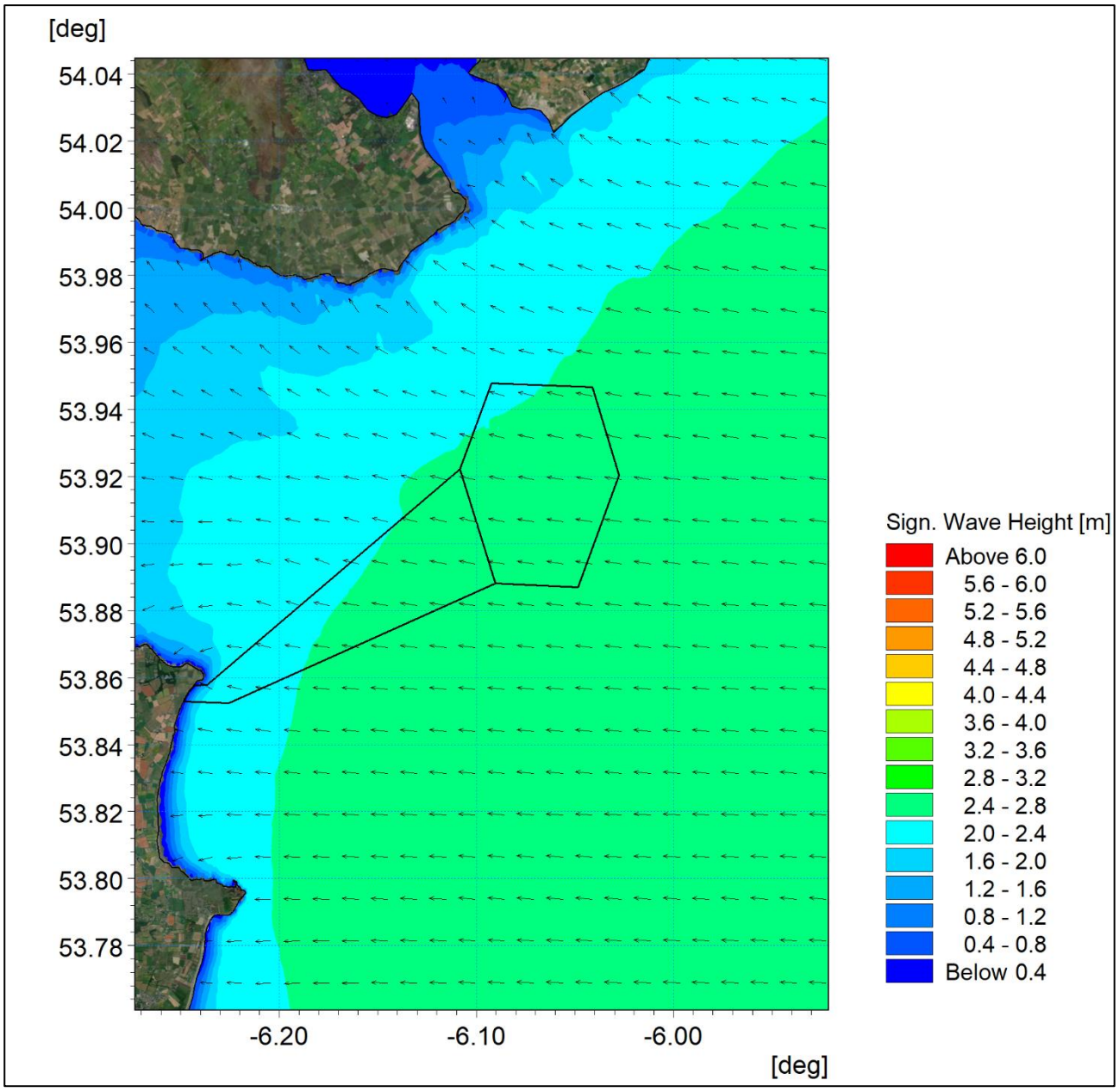

Figure 3A-9: Post-construction wave climate 1 in 2 year storm 090°.

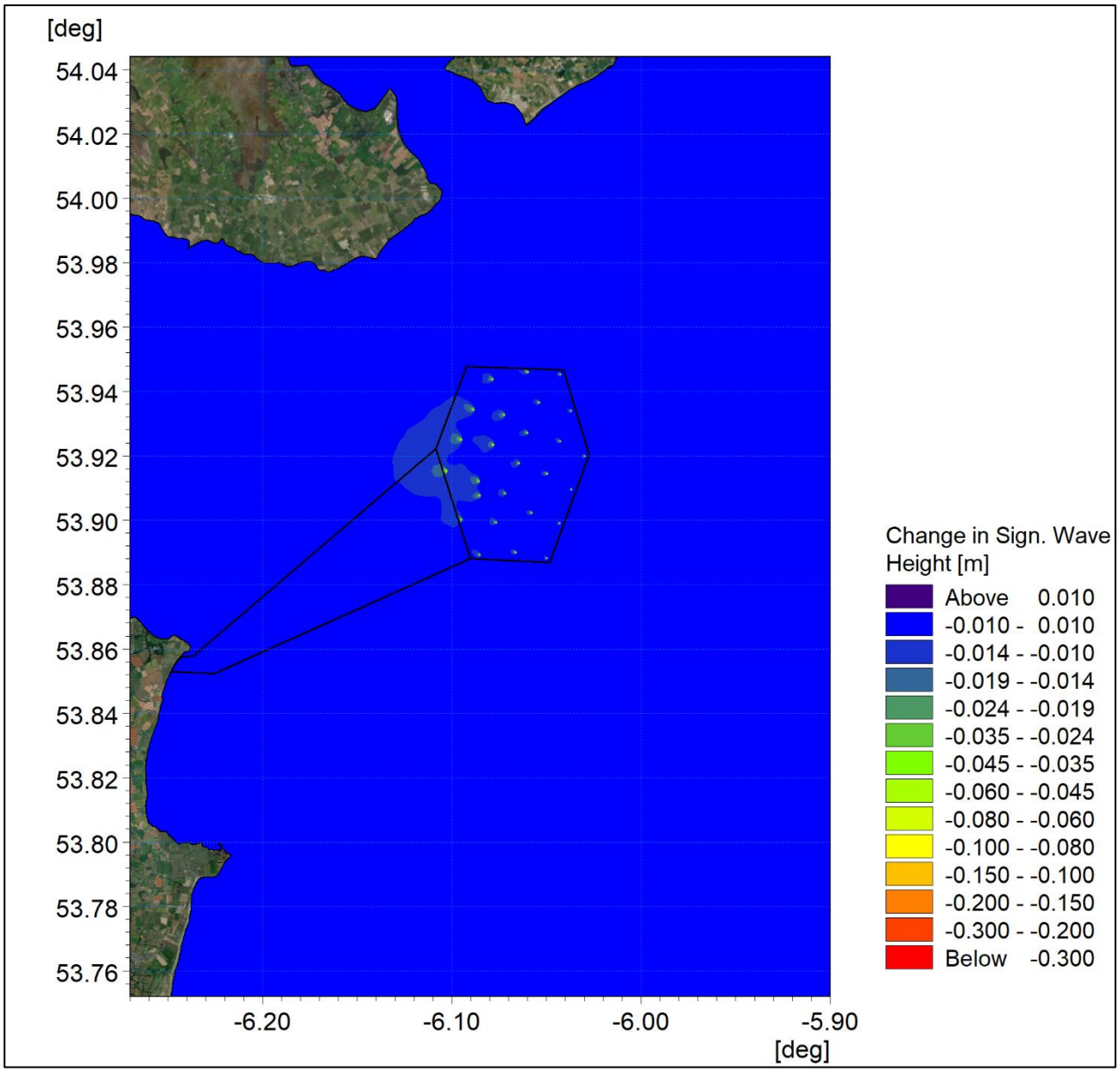

Figure 3-10: Change in wave climate 1 in 2 year storm 090° (post-construction minus baseline).

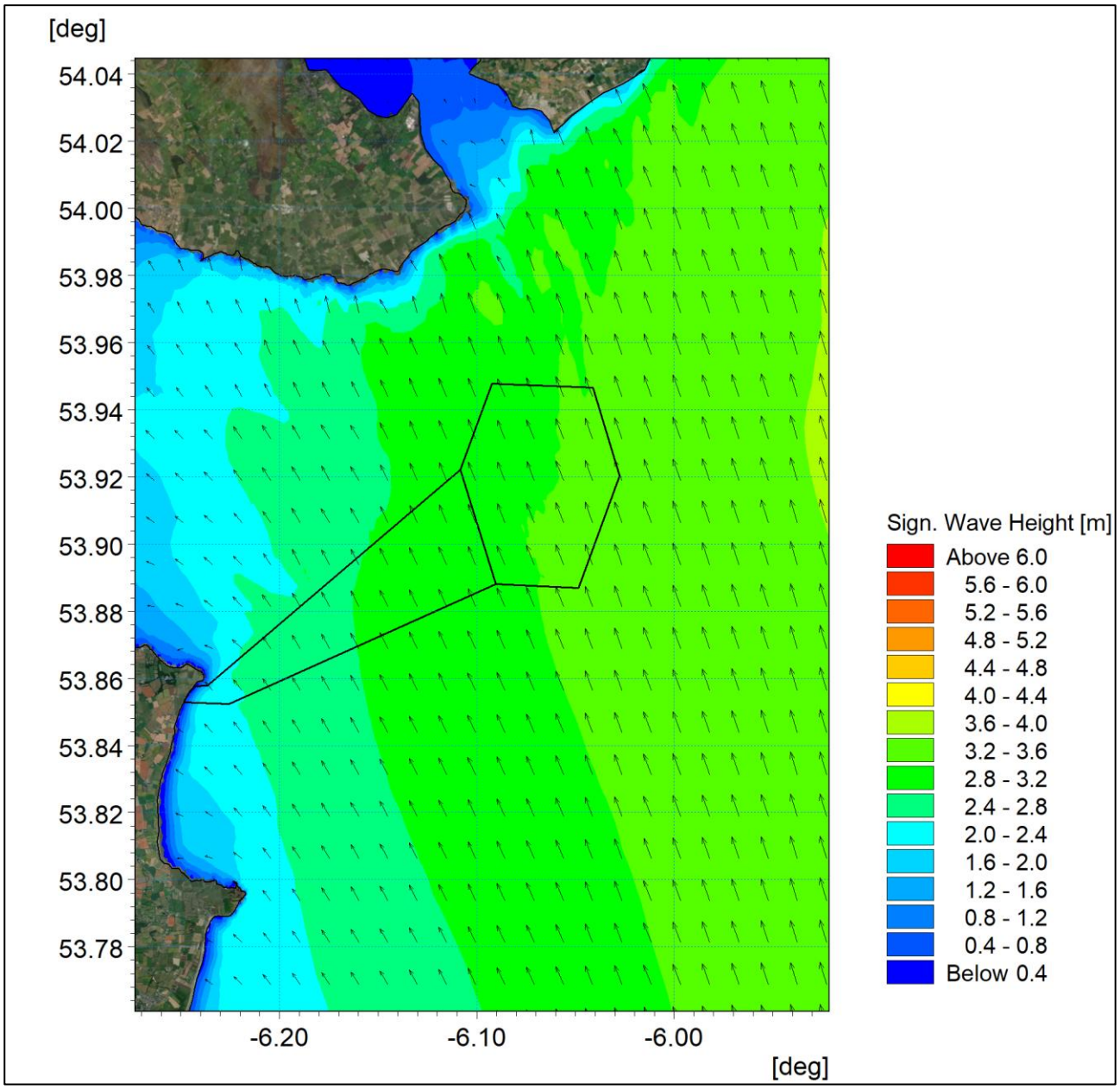

Figure 3A-11: Post-construction wave climate 1 in 2 year storm 165°.

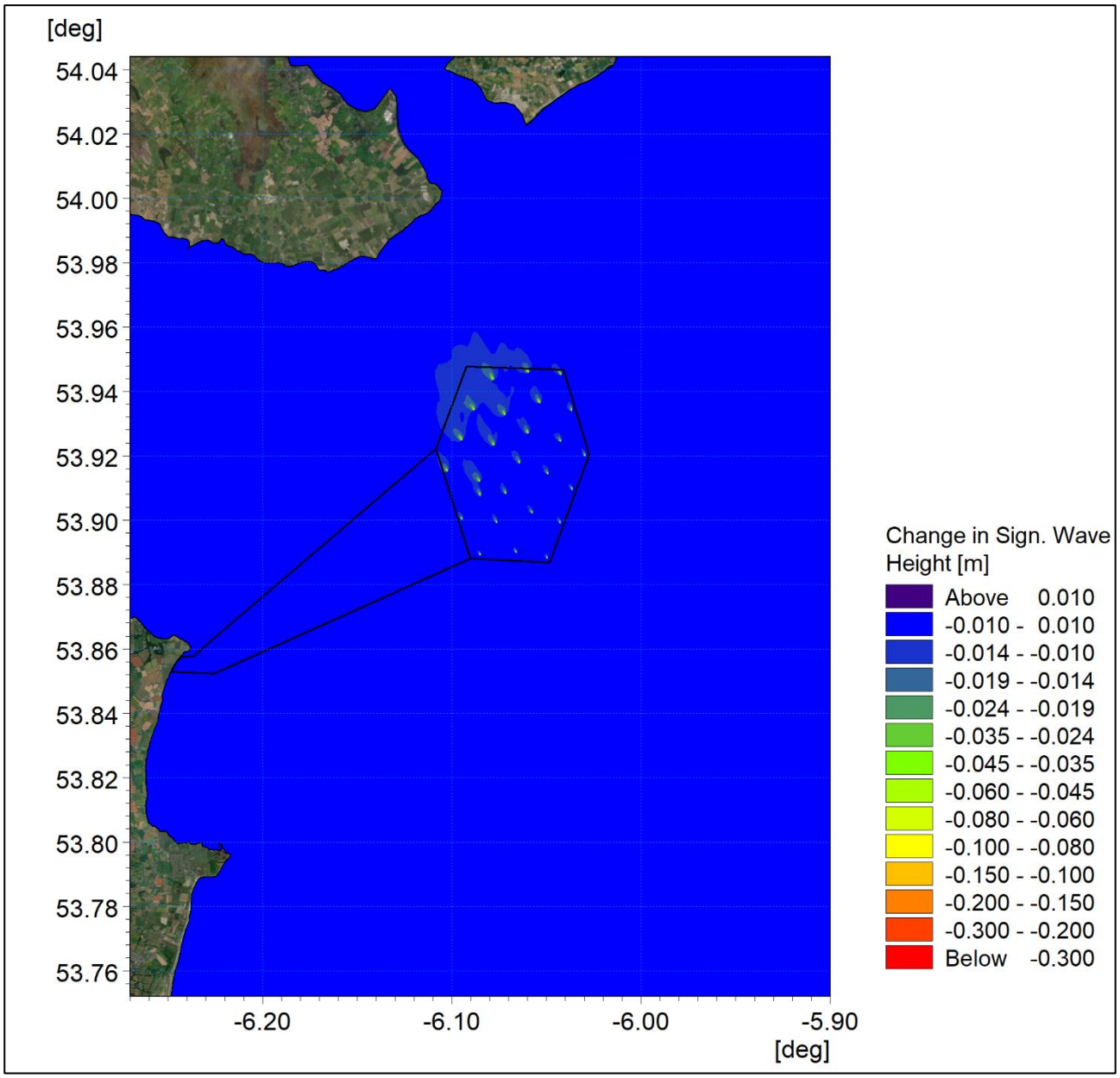

Figure 3-12: Change in wave climate 1 in 2 year storm 165° (post-construction minus baseline).

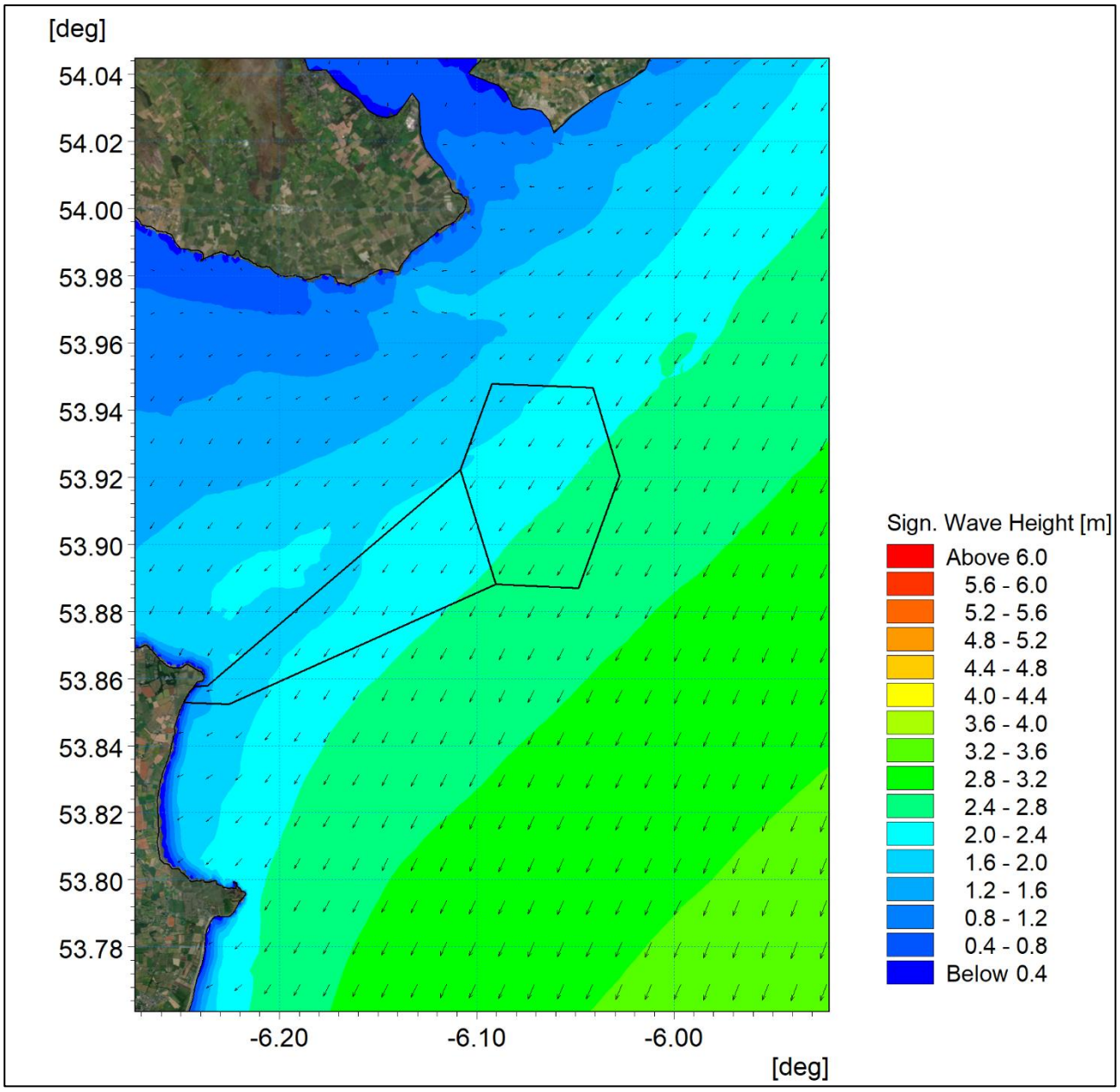

Figure 3A-13: Post-construction wave climate 1 in 50 year storm 015°.

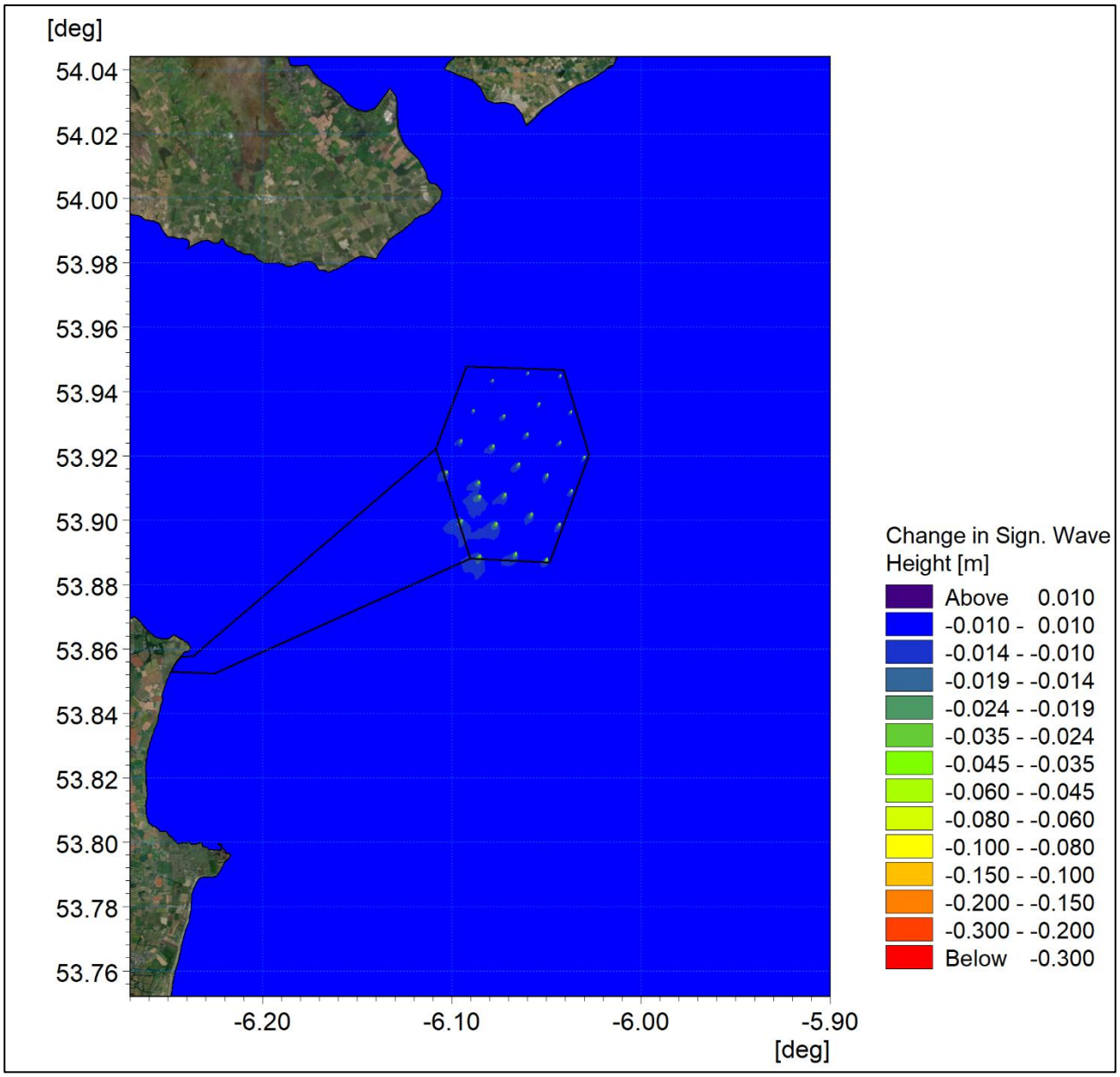

Figure 3-14: Change in wave climate 1 in 50 year storm 015° (post-construction minus baseline).

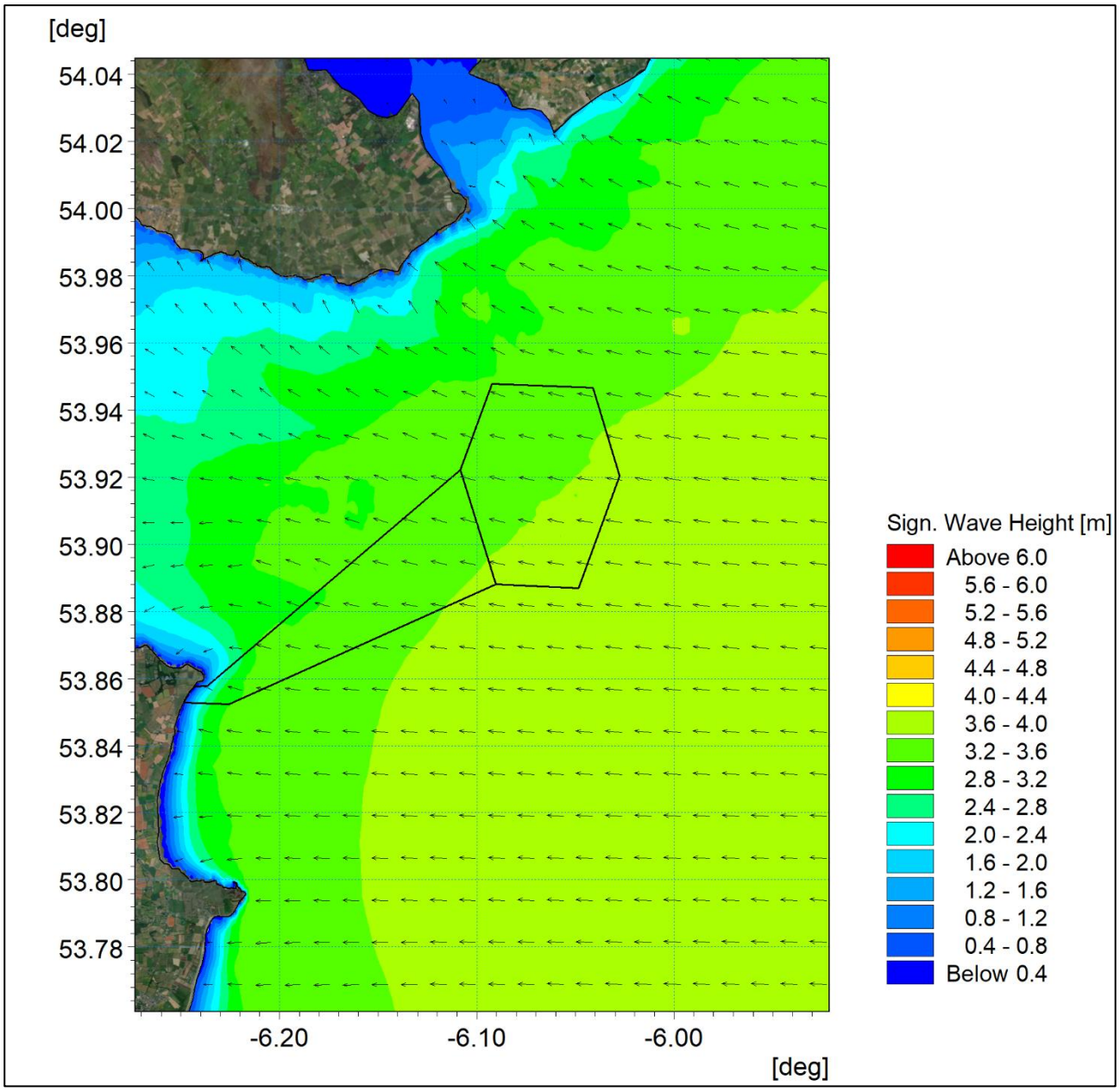

Figure 3A-15: Post-construction wave climate 1 in 50 year storm 090°.

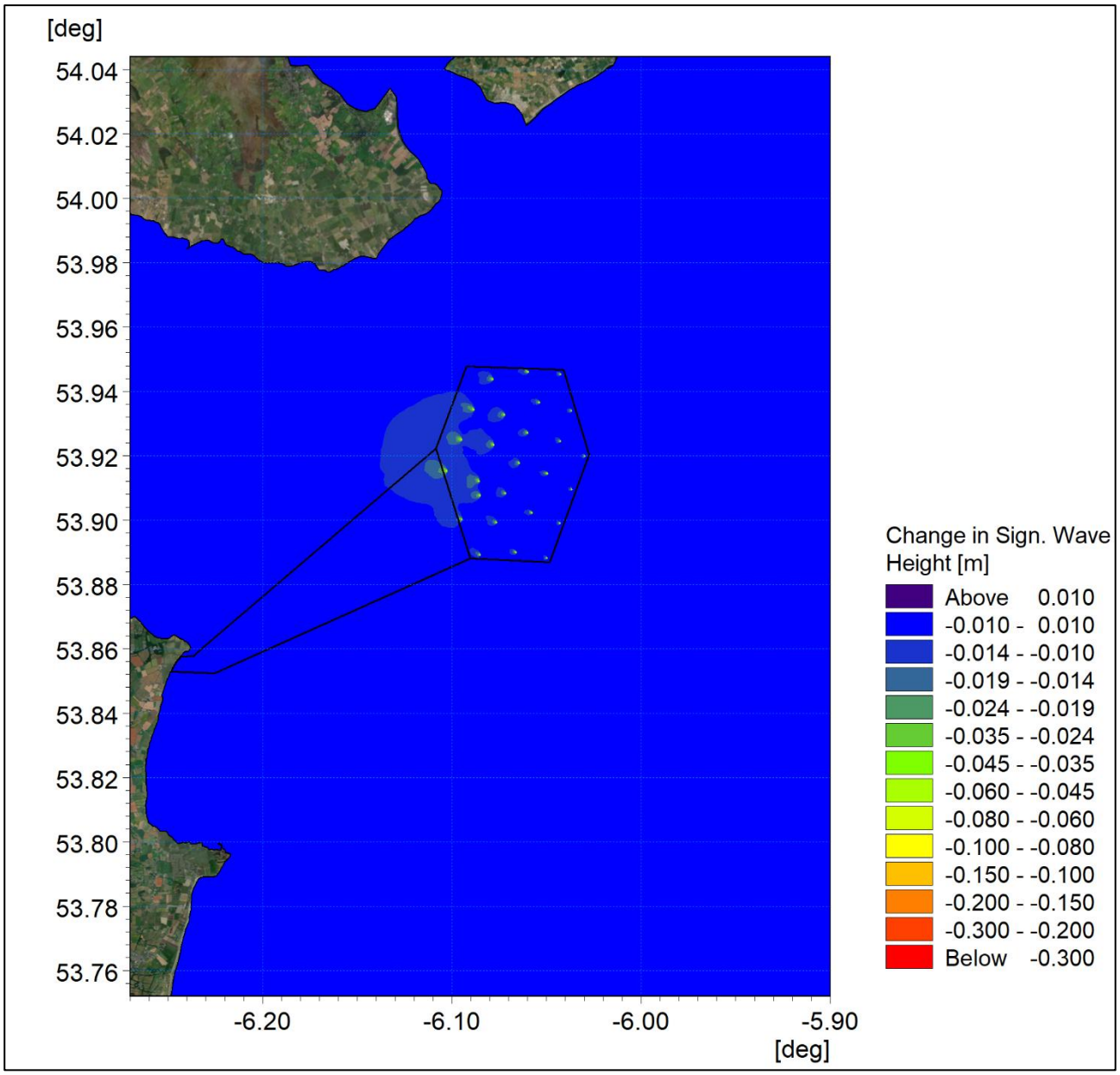

Figure 3-16: Change in wave climate 1 in 50 year storm 090° (post-construction minus baseline).

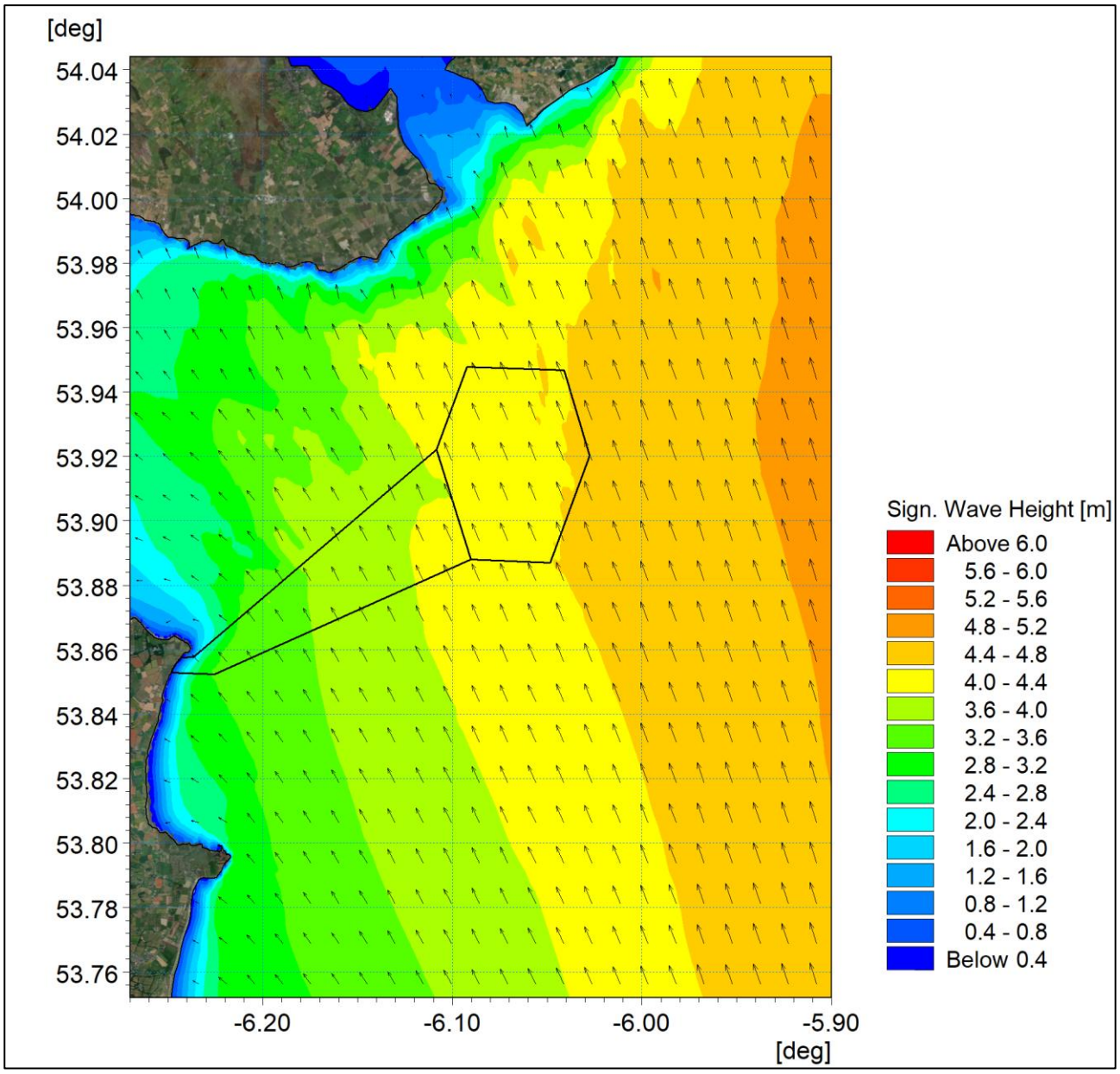

Figure 3A-17: Post-construction wave climate 1 in 50 year storm 165°.

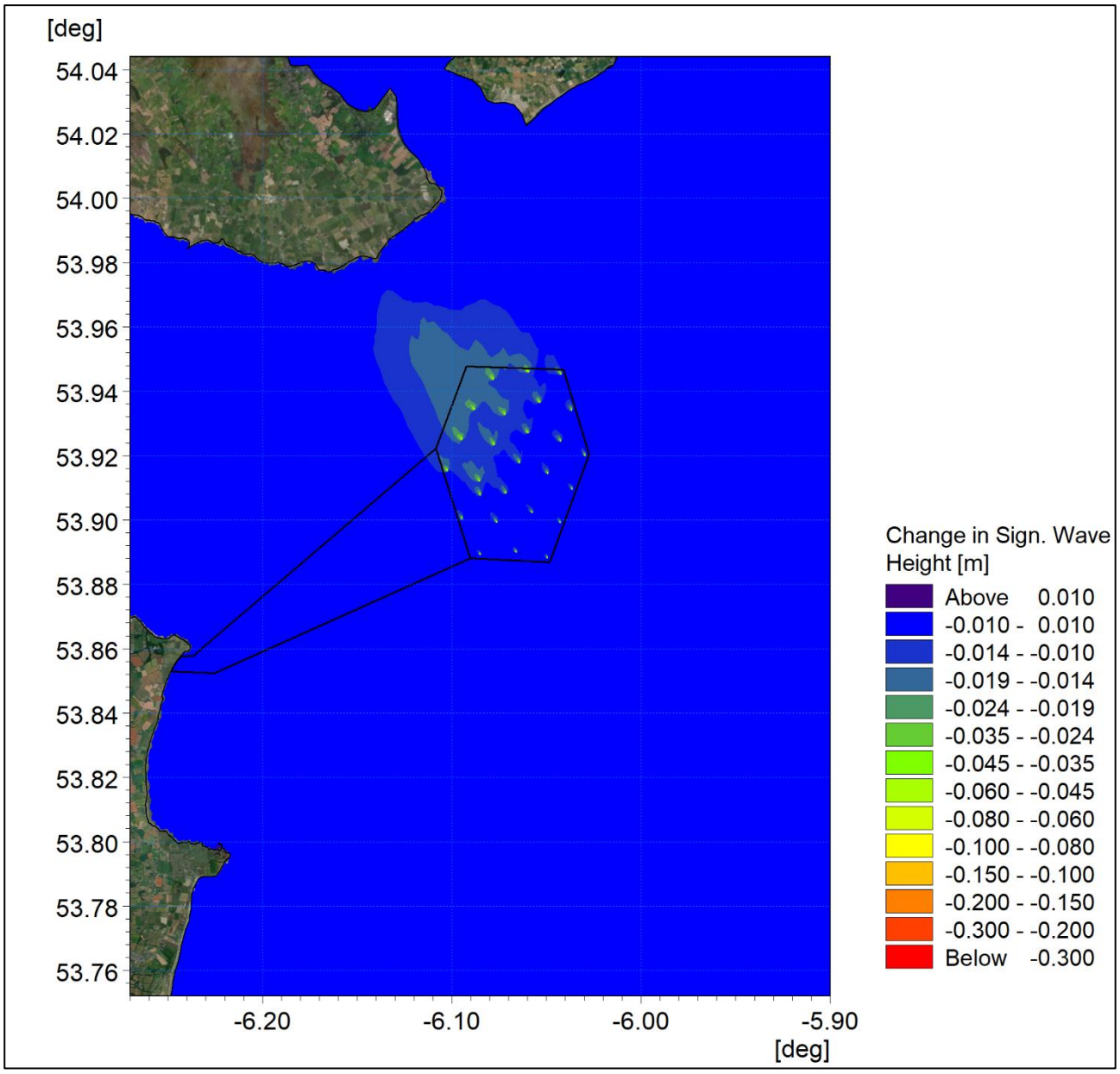

Figure 3A-18: Change in wave climate 1 in 50 year storm 165° (post-construction minus baseline).

Sensitivity of wave climate

In accordance with RFI 6.D, additional wave climate modelling was undertaken for the post-construction scenario for the extended range of wave climates as outlined in Section 2.2.2. As outlined in the previous section, a pair of plots is provided for each return period, the first relating to the post-construction wave climate and the second showing the change from the baseline scenario due to the presence of the offshore infrastructure.

The 1 in 10 and 1 in 20 year return period plots shown in Figure 3A-19 to Figure 3A-22 echo the findings from the previous modelling undertaken for this sector. Changes in wave height at the location of the turbine foundations are typically <40mm, however the wakes are more discrete than the 1 in 2 year storm event. It is however recognised that the wakes which extend beyond the boundary of the offshore wind farm area are less than 0.5% change from the baseline scenarios.

A similar pattern is shown in the longer term return period events for 1 in 100, 200 and 500 years presented in Figure 3A-23 to Figure 3A-28. The extent of the change in wave climate for the 100 year event is slightly larger than the 200 year event scenario, whilst the 500 year event is more akin to the 50 year return period storm. It is however noted that, in absolute terms, the change at site of the infrastructure is <40mm and wakes extending beyond the array boundary exhibit less than *circa* 0.5% change from baseline conditions. There is no discernible difference for the 1 in 200 year return period event including sea levels rise (Figure 3A-29 and Figure 3A-30).

The corresponding baseline conditions for 1 in 10, 20, 100, 200 and 500 year return periods are presented in Figure 2A-15 to Figure 2A-19, whilst the 1 in 200 year return period event with sea level rise is presented in Figure 2A-20.

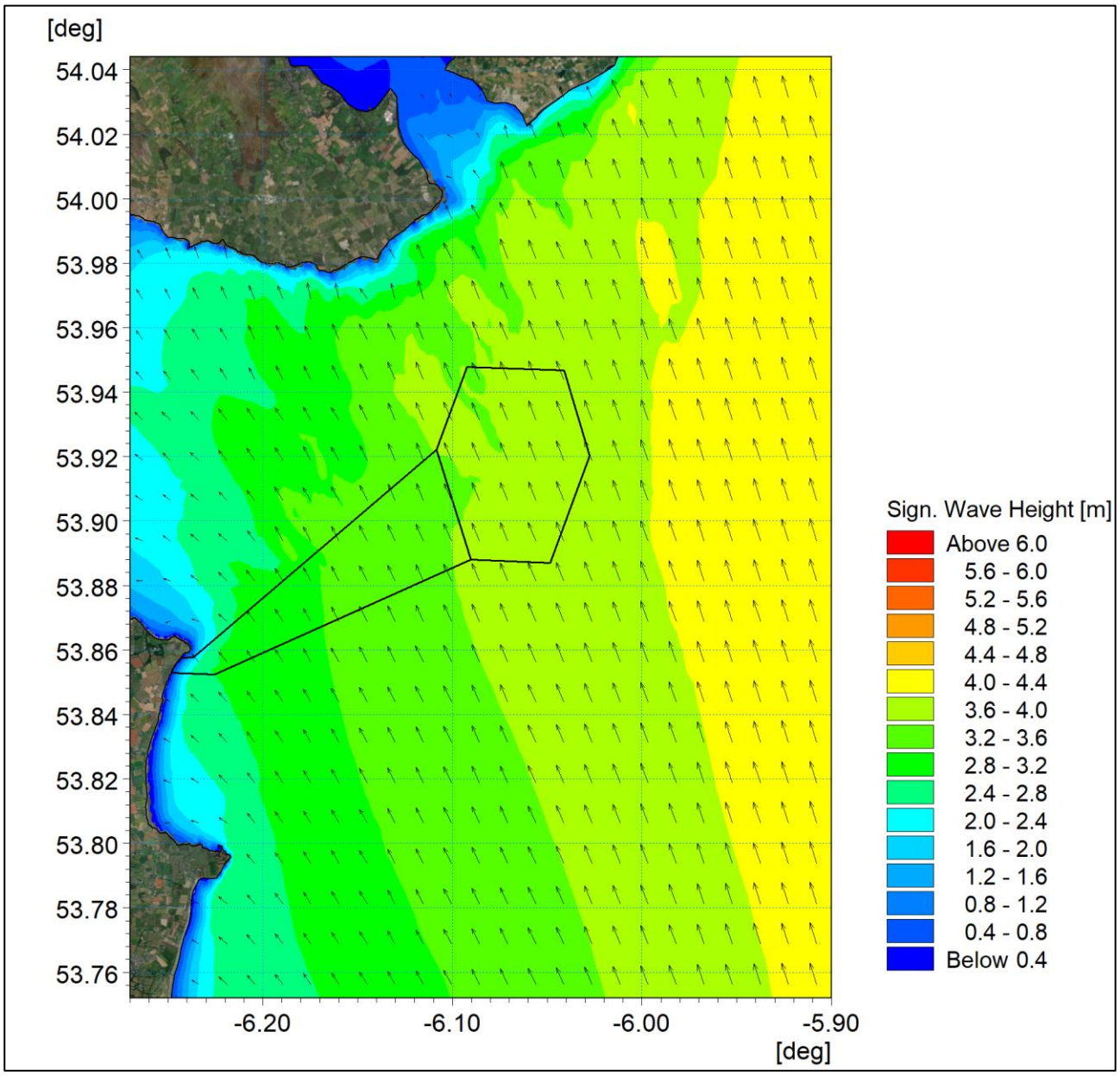

Figure 3A-19: Post-construction wave climate 1 in 10 year storm 165°.

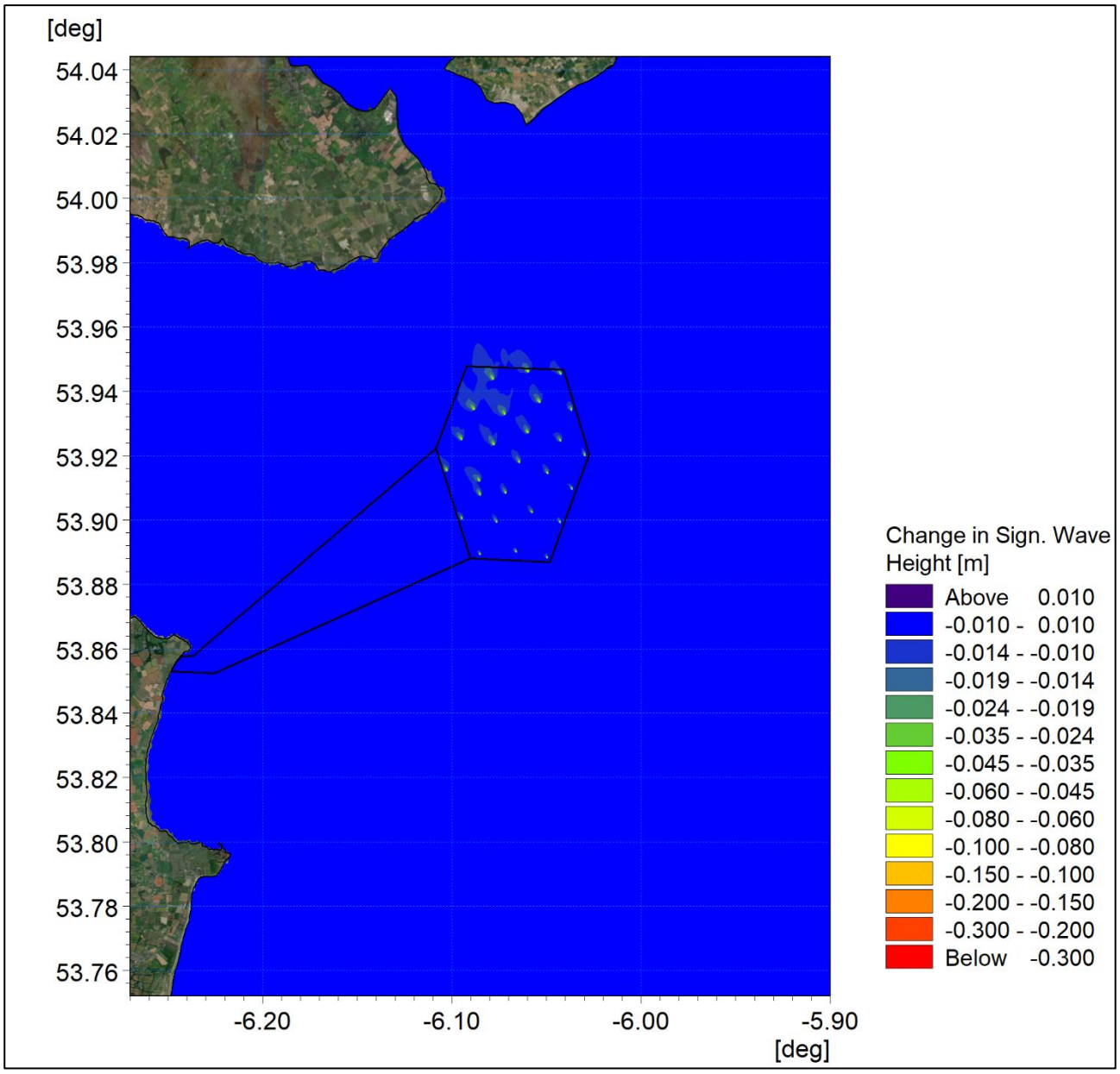

Figure 3A-20: Change in wave climate 1 in 10 year storm 165° (post-construction minus baseline).

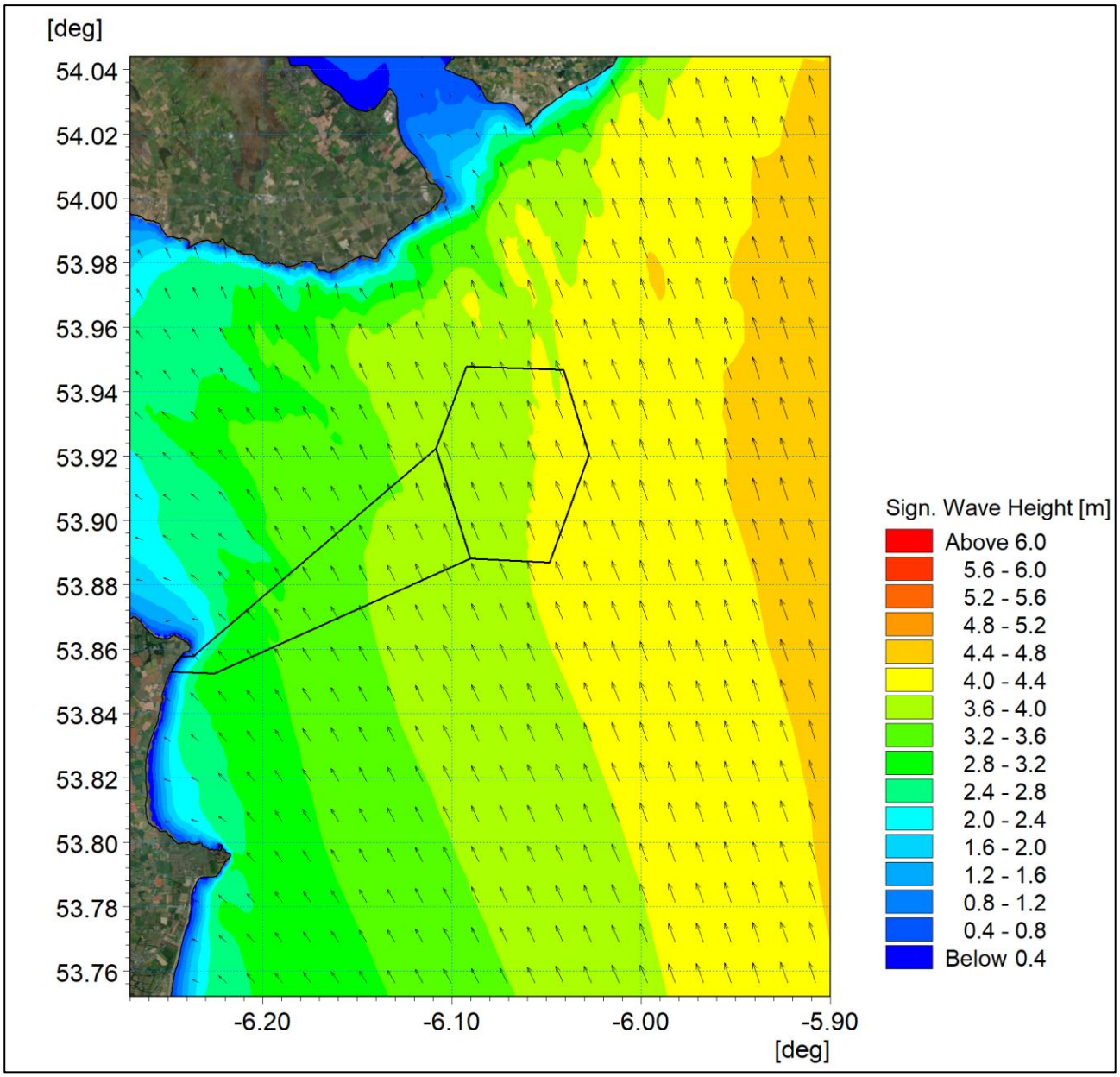

Figure 3A-21: Post-construction wave climate 1 in 20 year storm 165°.

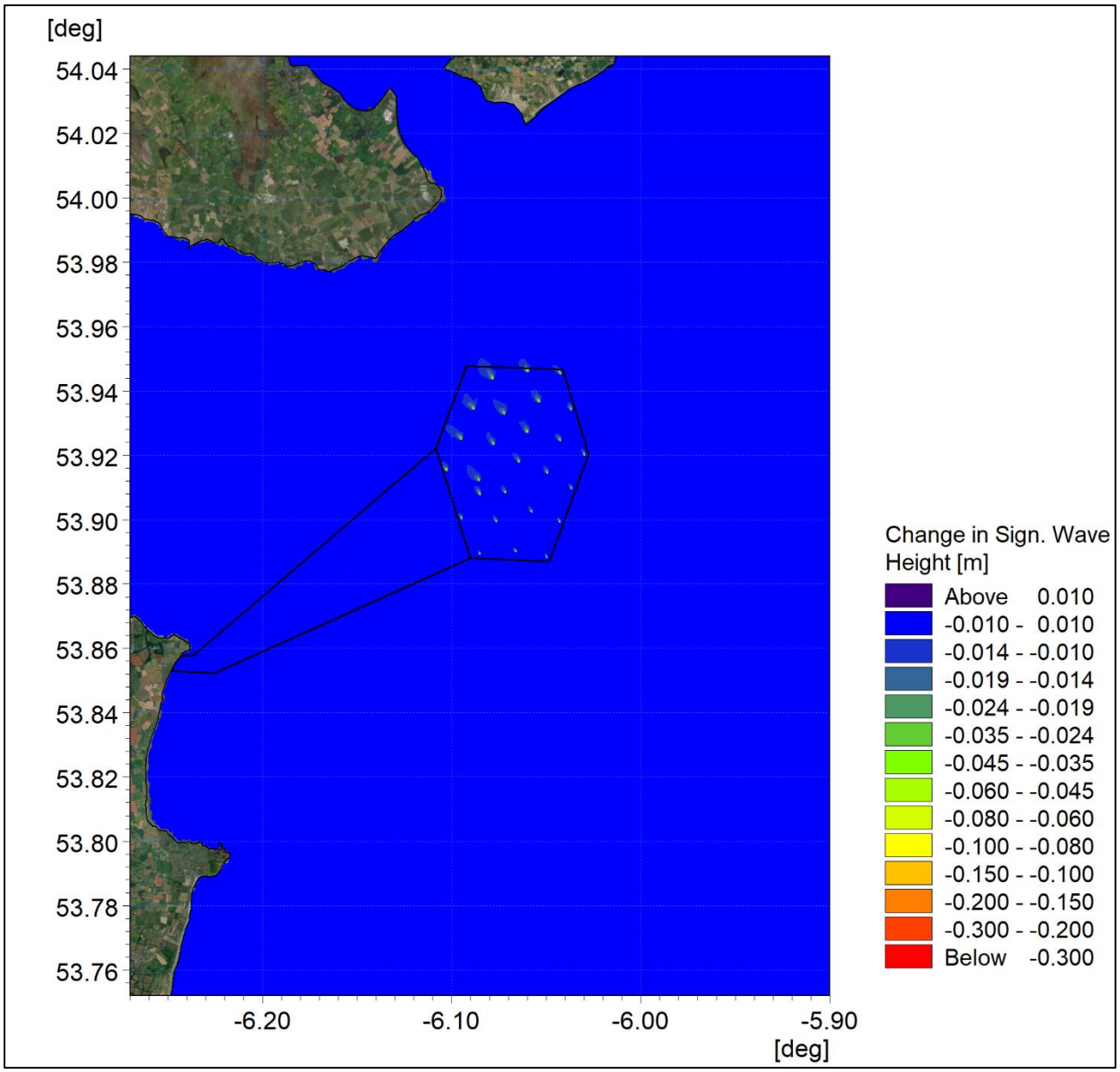

Figure 3A-22: Change in wave climate 1 in 20 year storm 165° (post-construction minus baseline).

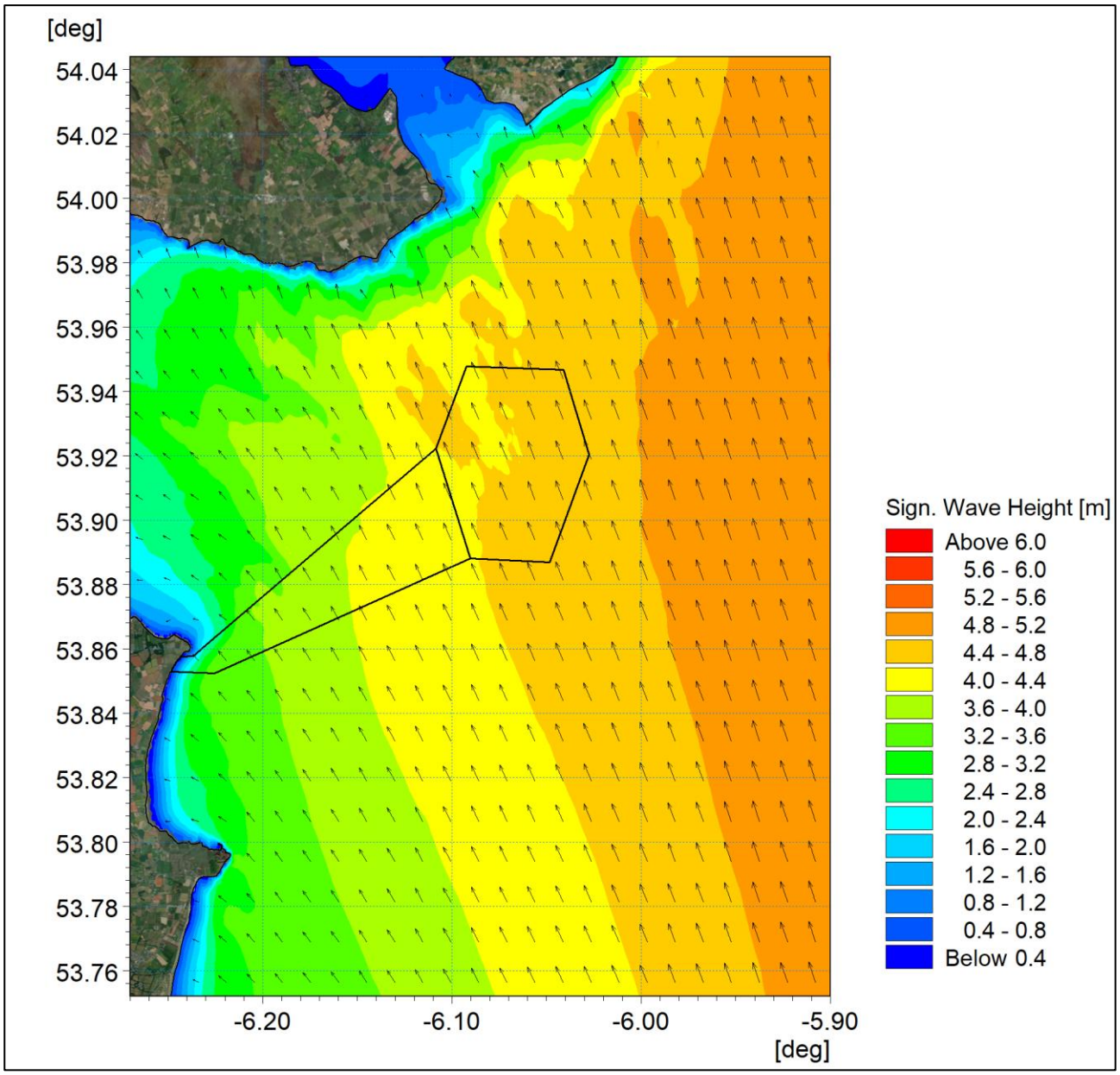

Figure 3A-23: Post-construction wave climate 1 in 100 year storm 165°.

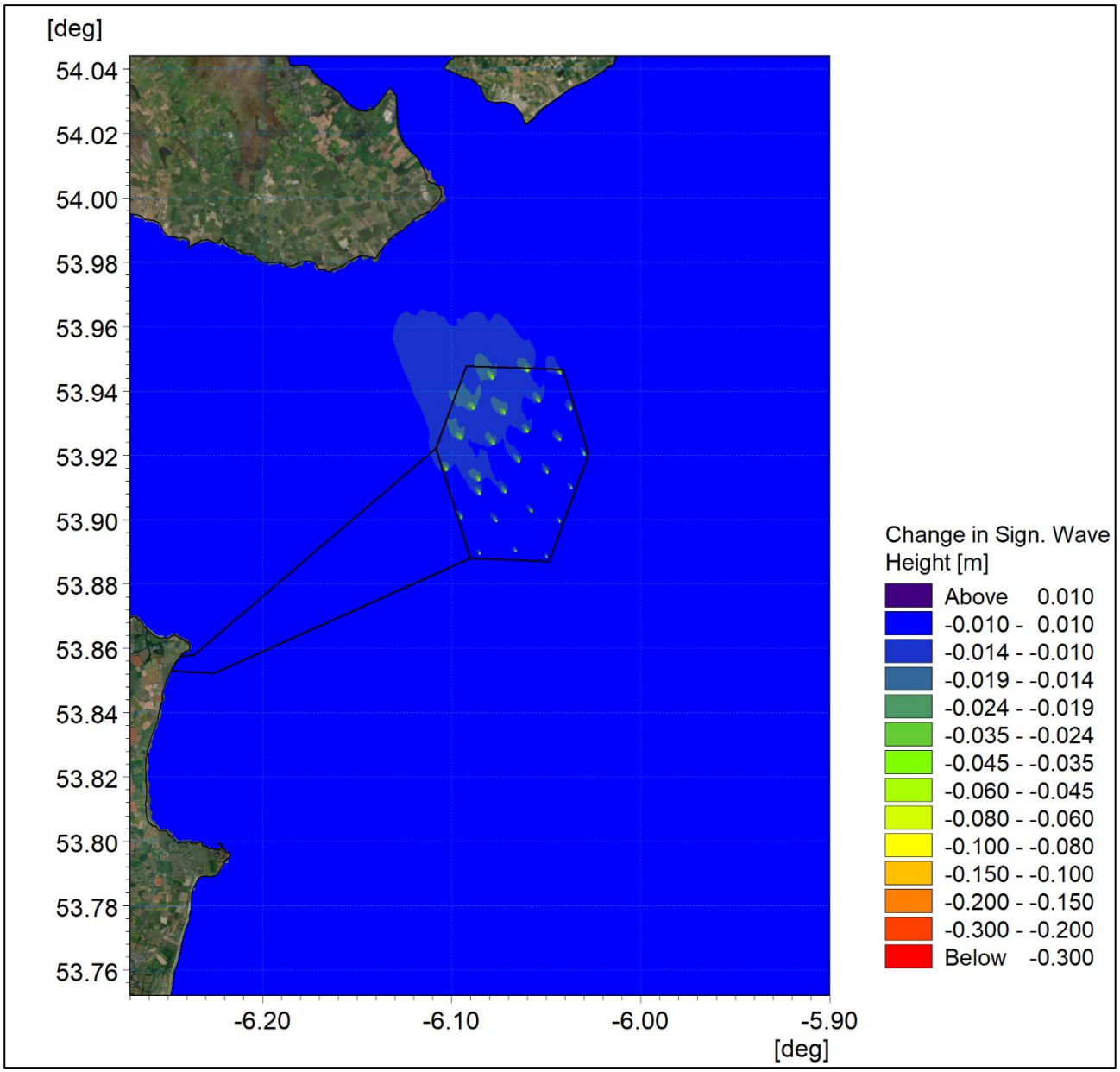

Figure 3A-24: Change in wave climate 1 in 100 year storm 165° (post-construction minus baseline).

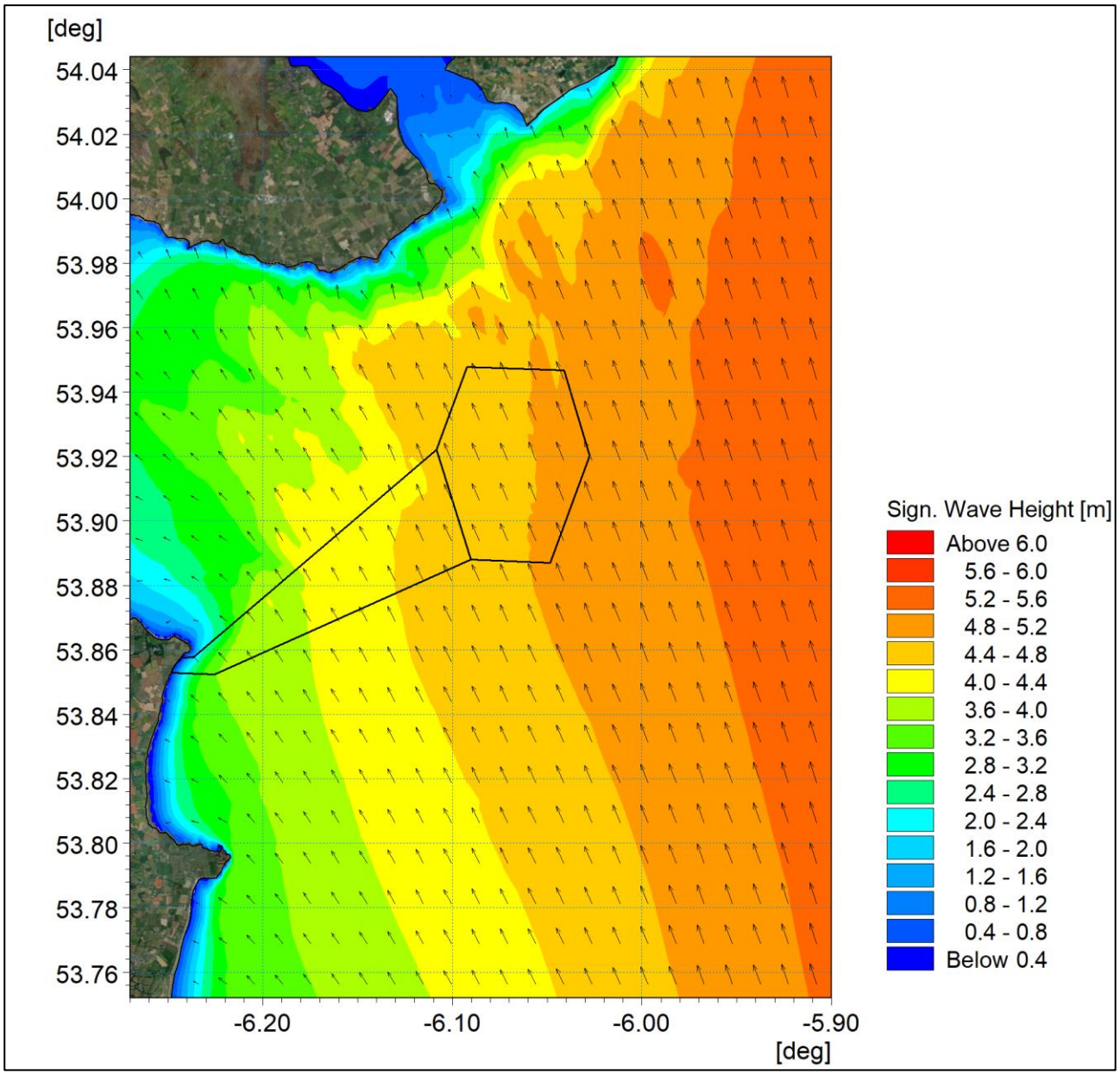

Figure 3A-25: Post-construction wave climate 1 in 200 year storm 165°.

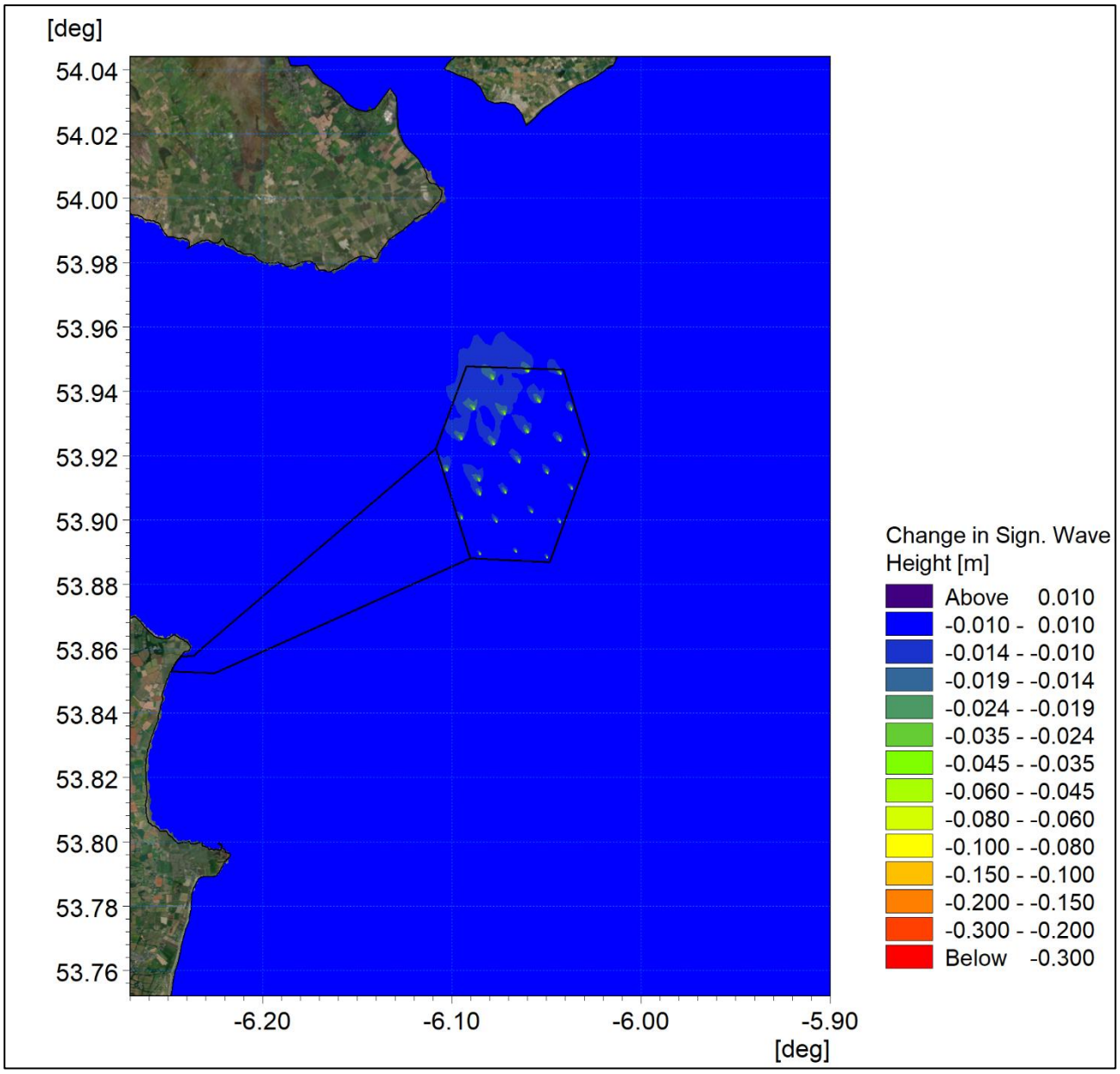

Figure 3A-26: Change in wave climate 1 in 200 year storm 165° (post-construction minus baseline).

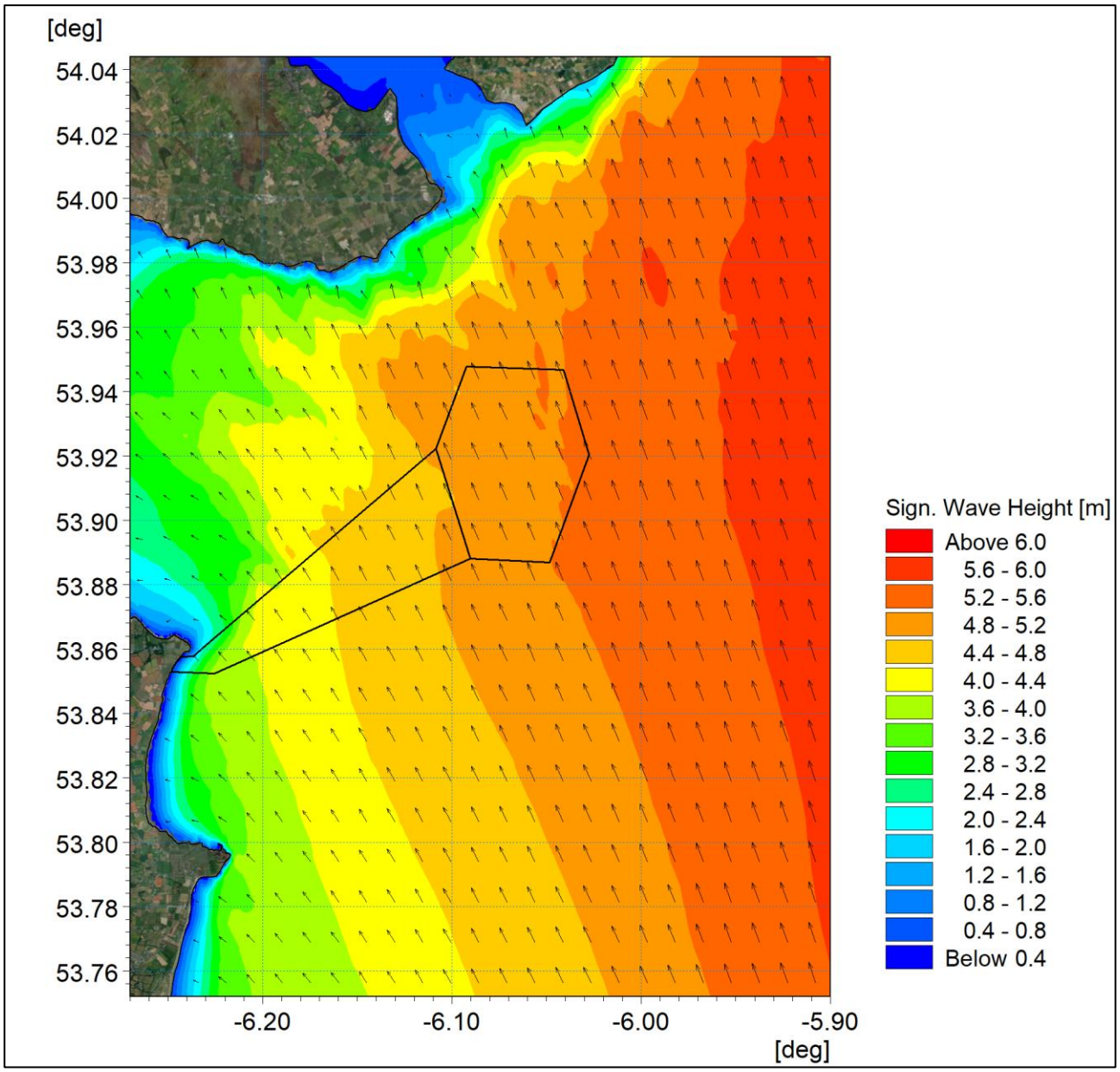

Figure 3A-27: Post-construction wave climate 1 in 500 year storm 165°.

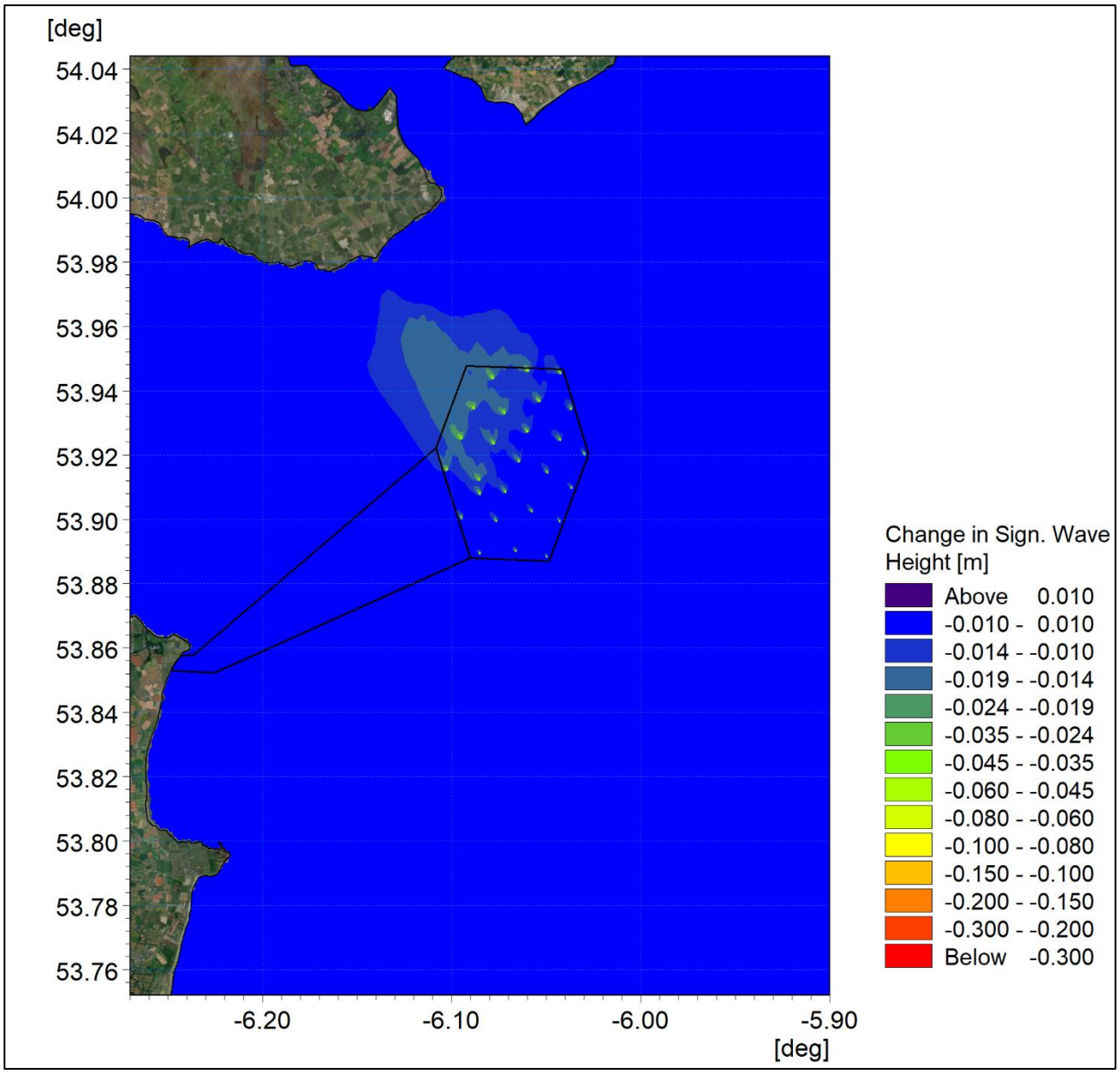

Figure 3A-28: Change in wave climate 1 in 500 year storm 165° (post-construction minus baseline).

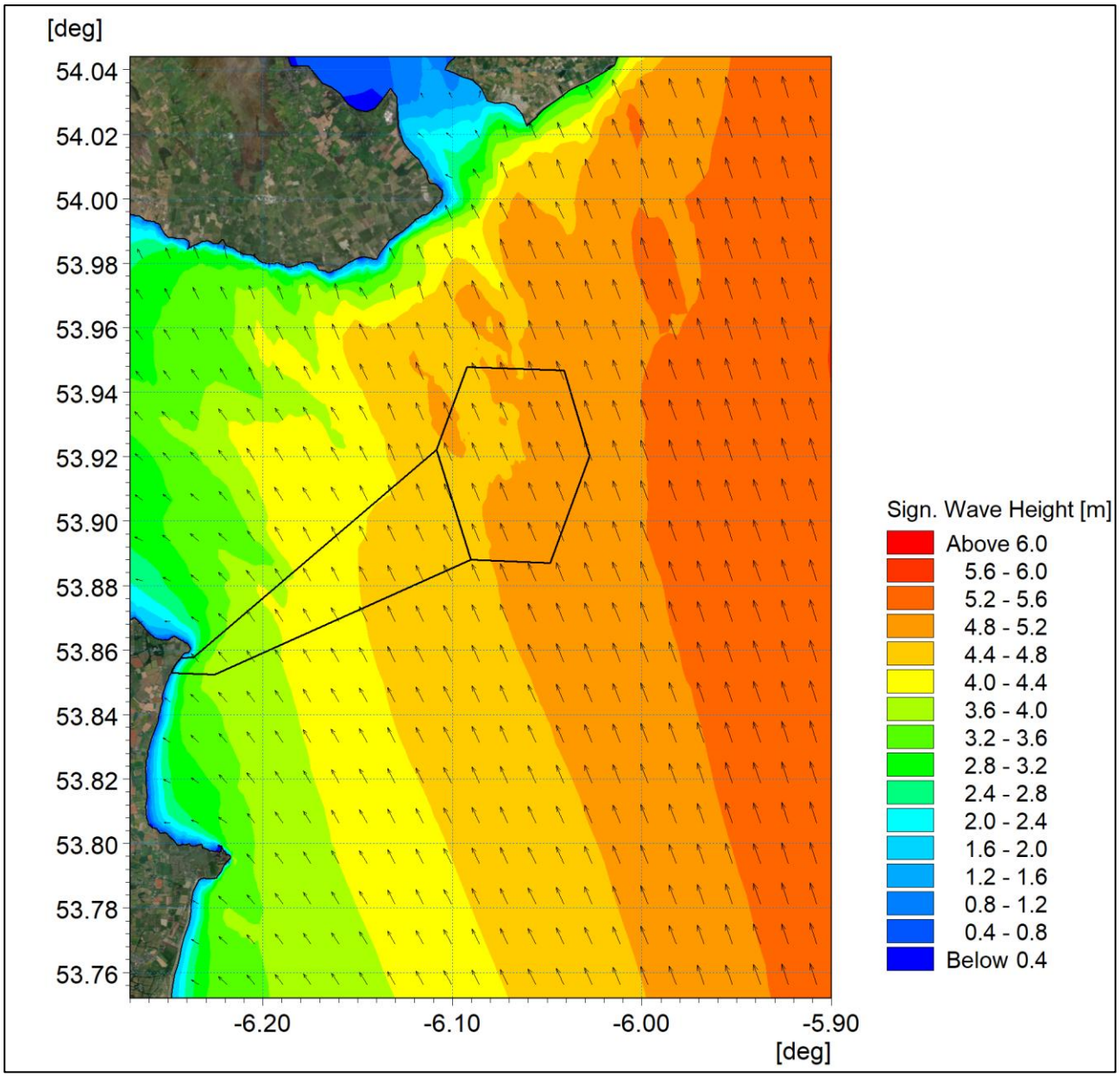

Figure 3A-29: Post-construction wave climate 1 in 200 year storm 165° with sea level rise.

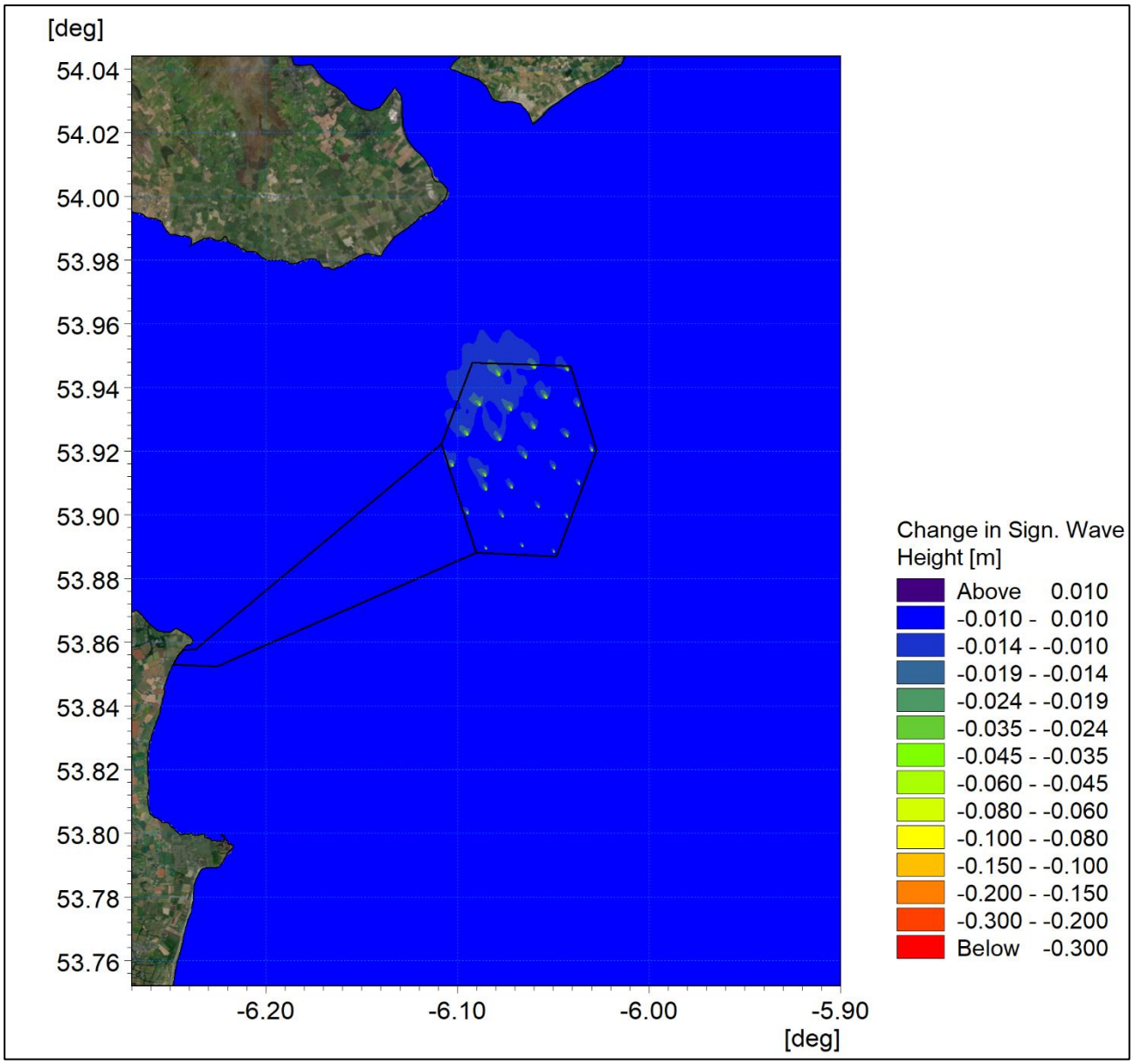

Figure 3A-30: Change in wave climate 1 in 200 year storm 165° with sea level rise (post-construction minus baseline).

3.2.3 Littoral Currents

The previous sections established the magnitude of the changes in tidal currents and wave conditions individually. However, sediment transport regime are driven by a combination of these factors. For completeness, the influence on littoral currents was examined and has been presented in this section.

The modelling was extended to include the Project design parameters for the post-construction period, i.e. with 26 structures in place for a 1 in 2 year storm from 165°. The baseline littoral currents for mid flood and mid ebb are presented in Figure 2-21 and Figure 2-22 respectively whilst the equivalent post-construction littoral currents are shown in Figure 3-31 and Figure 3-32 for the flood and ebb tides respectively.

During the flood tide the direction of tidal flow is aligned with the wave climate and the difference in littoral currents from the baseline to post-construction is presented in Figure 3-33. These changes are both limited in magnitude (to around ~~30~~ 10 mm/s) and also spatially, with the alteration in flows limited to the offshore wind farm area. During ebb tide the tidal flow is in opposition to the wave direction and the resulting flow field

is more unsteady. The changes in littoral currents due to the structures were found to be smaller than the convergence criteria for the mode (i.e. indiscernible).

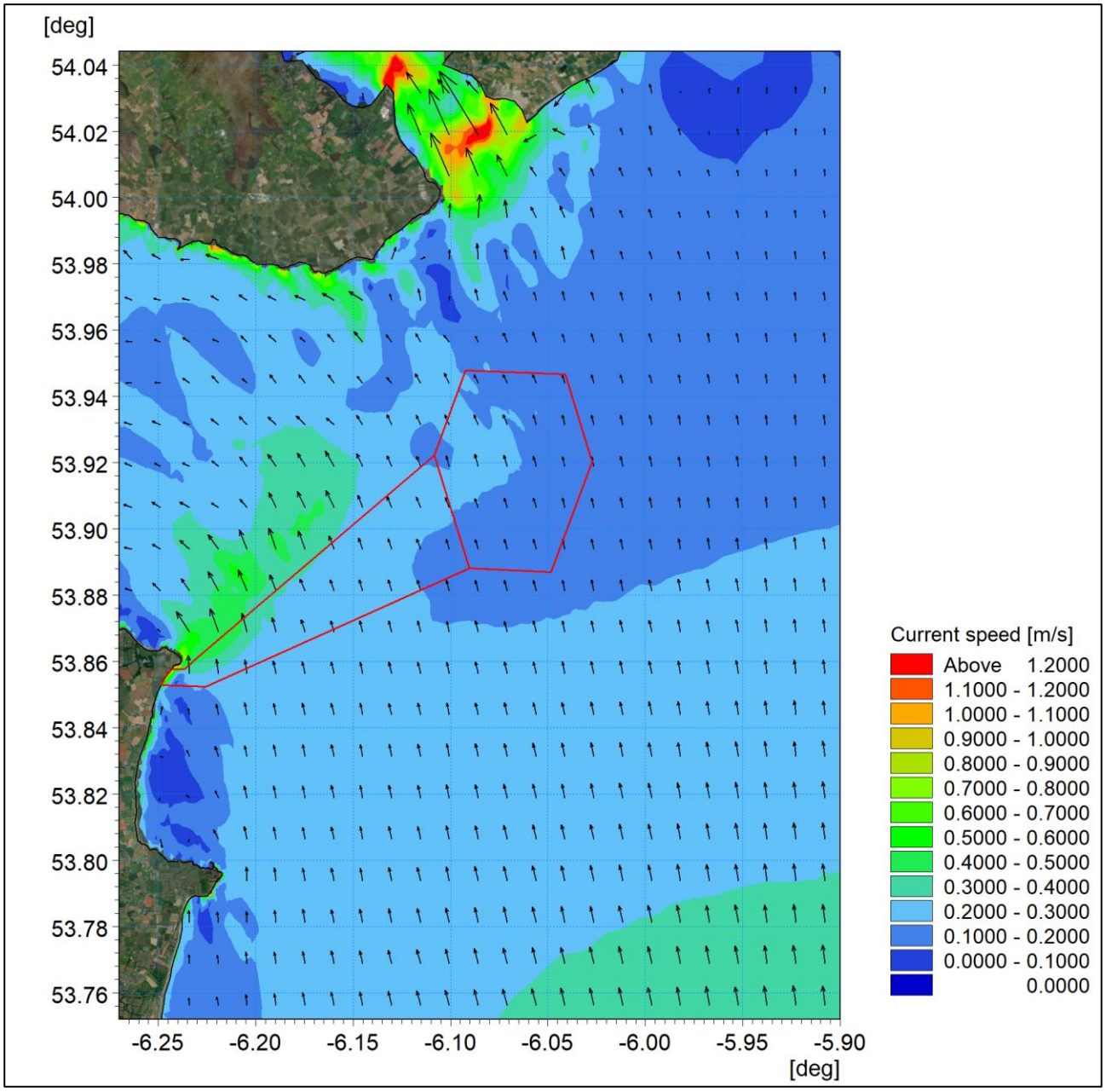

Figure 3-31: Post-construction littoral current 1 in 2 year storm from 165° - flood tide.

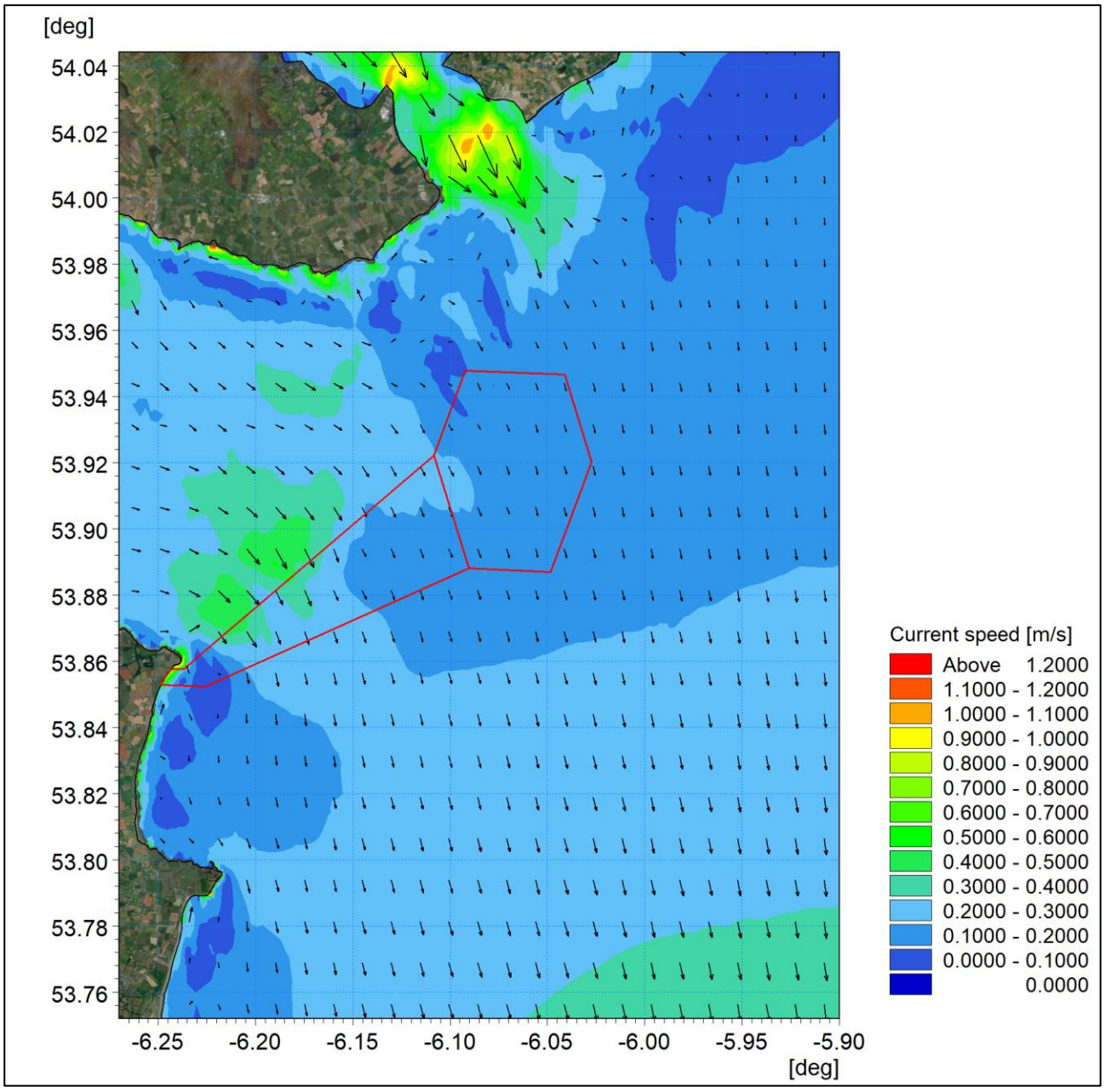

Figure 3-32: Post-construction littoral current 1 in 2 year storm from 165° - ebb tide.

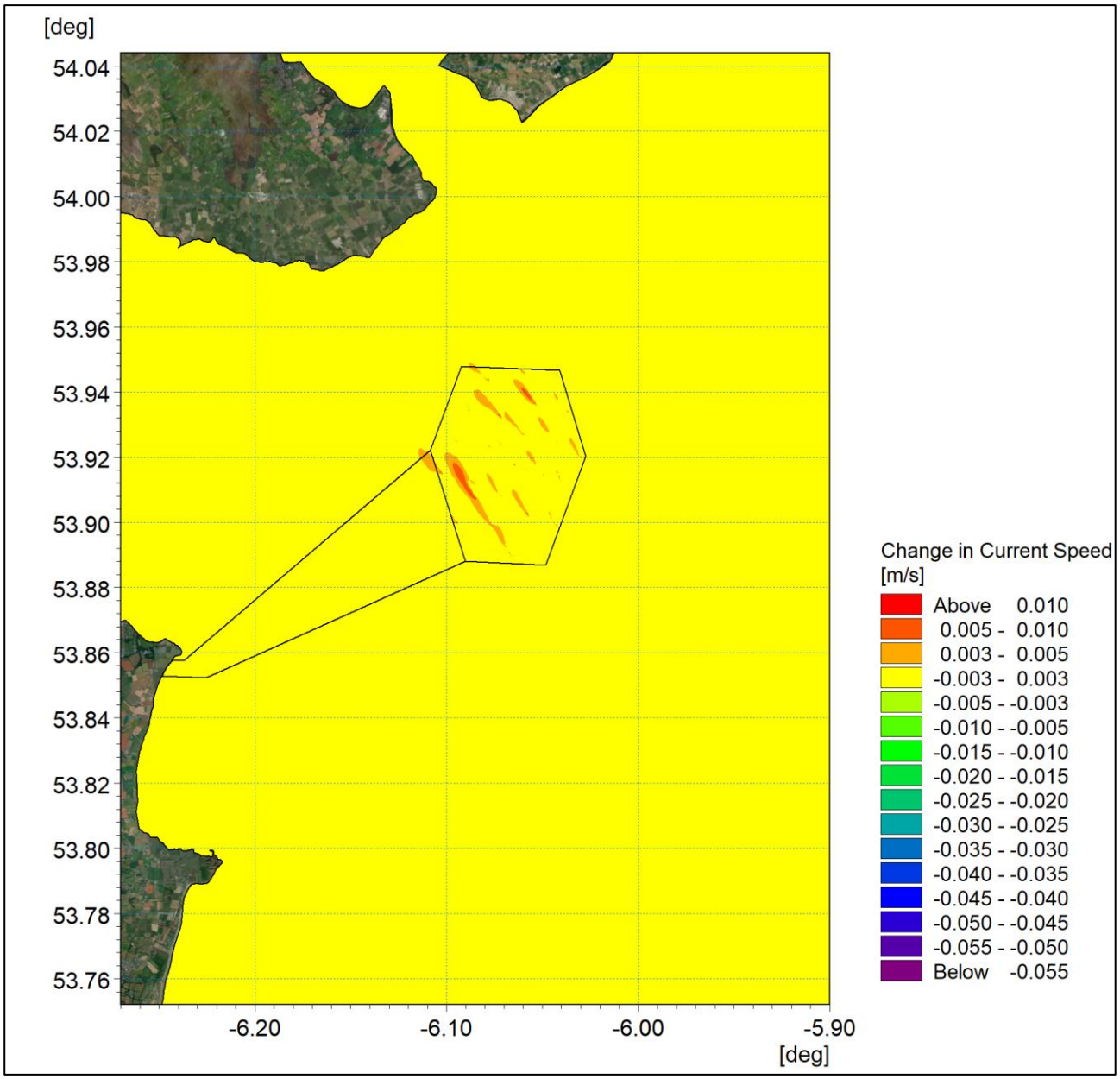

Figure 3-33: Change in littoral current 1 in 2 year storm from 165° - flood tide (post-construction minus baseline).

Sensitivity of littoral currents

In accordance with RFI 6.D, additional return period modelling was undertaken for the post-construction scenario which corresponds with the baseline scenarios presented in Section 2.2.3. The post construction littoral flood and ebb tides for the 1 in 200 year event from the 165º sector are presented in Figure 3A-34 and Figure 3A-35 respectively, whilst Figure 3A-36 illustrates the change in residual current during the flood tide. As previously noted, the changes from the baseline conditions are not visible unless the difference plot is considered. Changes of a similar form and extent as those exhibited in the more frequent 1 in 2 year return period storm. The change is of slightly increased magnitude, hence the use of an alternate palette, however they are still limited to less than 15 mm/s in proximity to the installed infrastructure.

As with the underlying tides and wave climate, the application of a sea level rise of 0.5 m, presented in Figure 3A-37 to Figure 3A-39, showed no discernible difference from the present day scenario on terms of littoral currents within the study area.

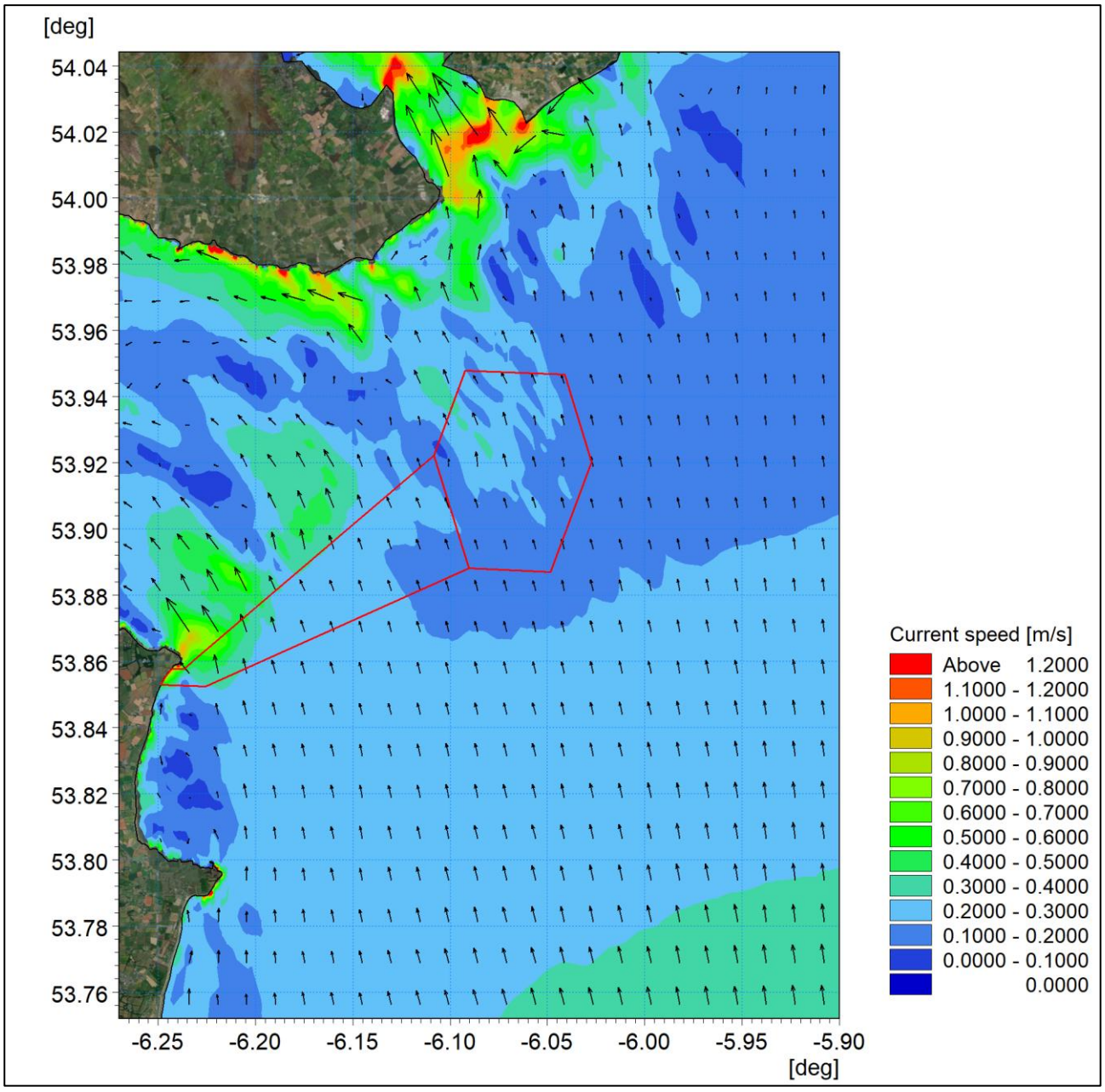

Figure 3A-34: Post-construction littoral current 1 in 200 year storm from 165° - flood tide.

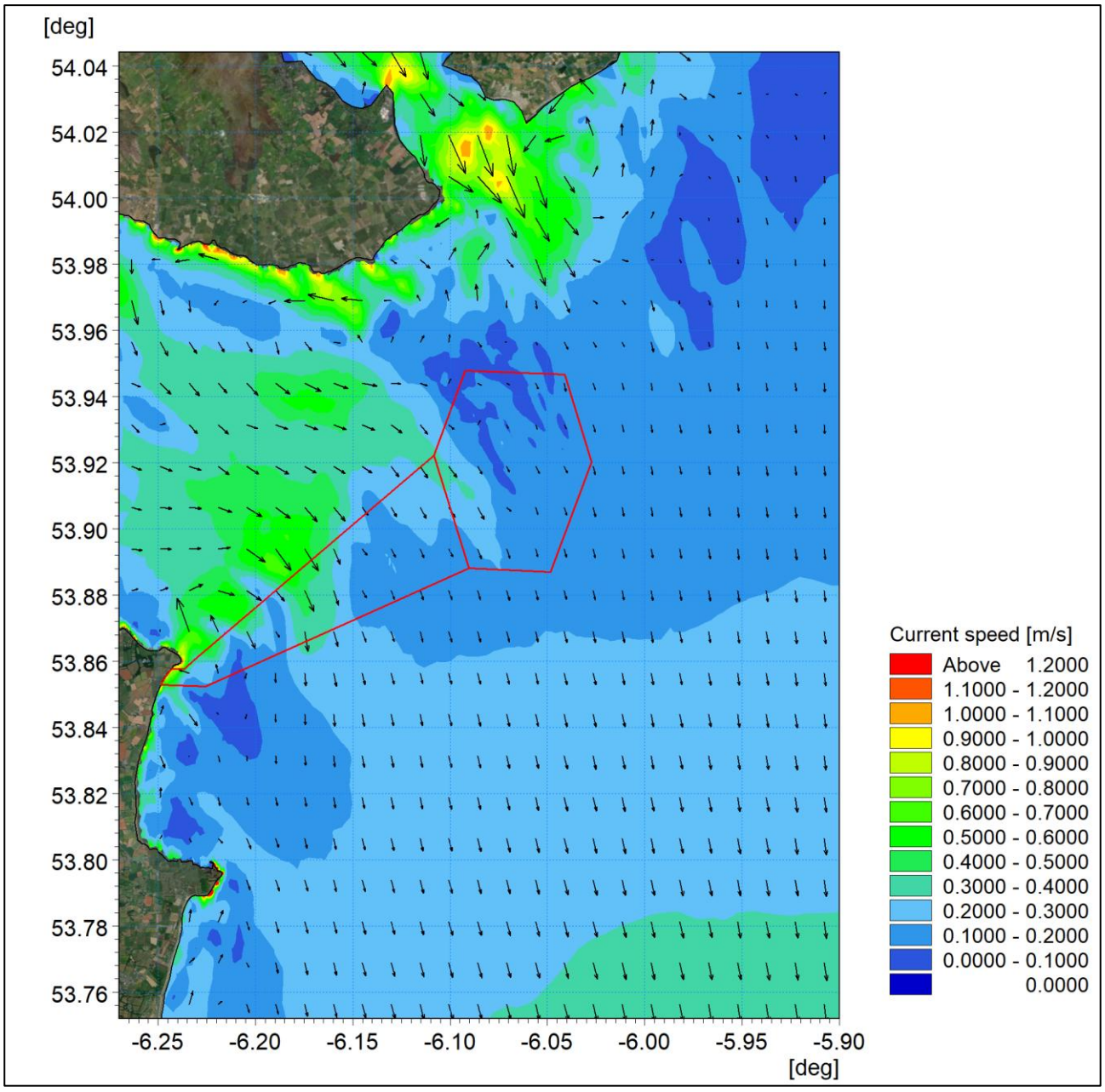

Figure 3A-35: Post-construction littoral current 1 in 200 year storm from 165° - ebb tide.

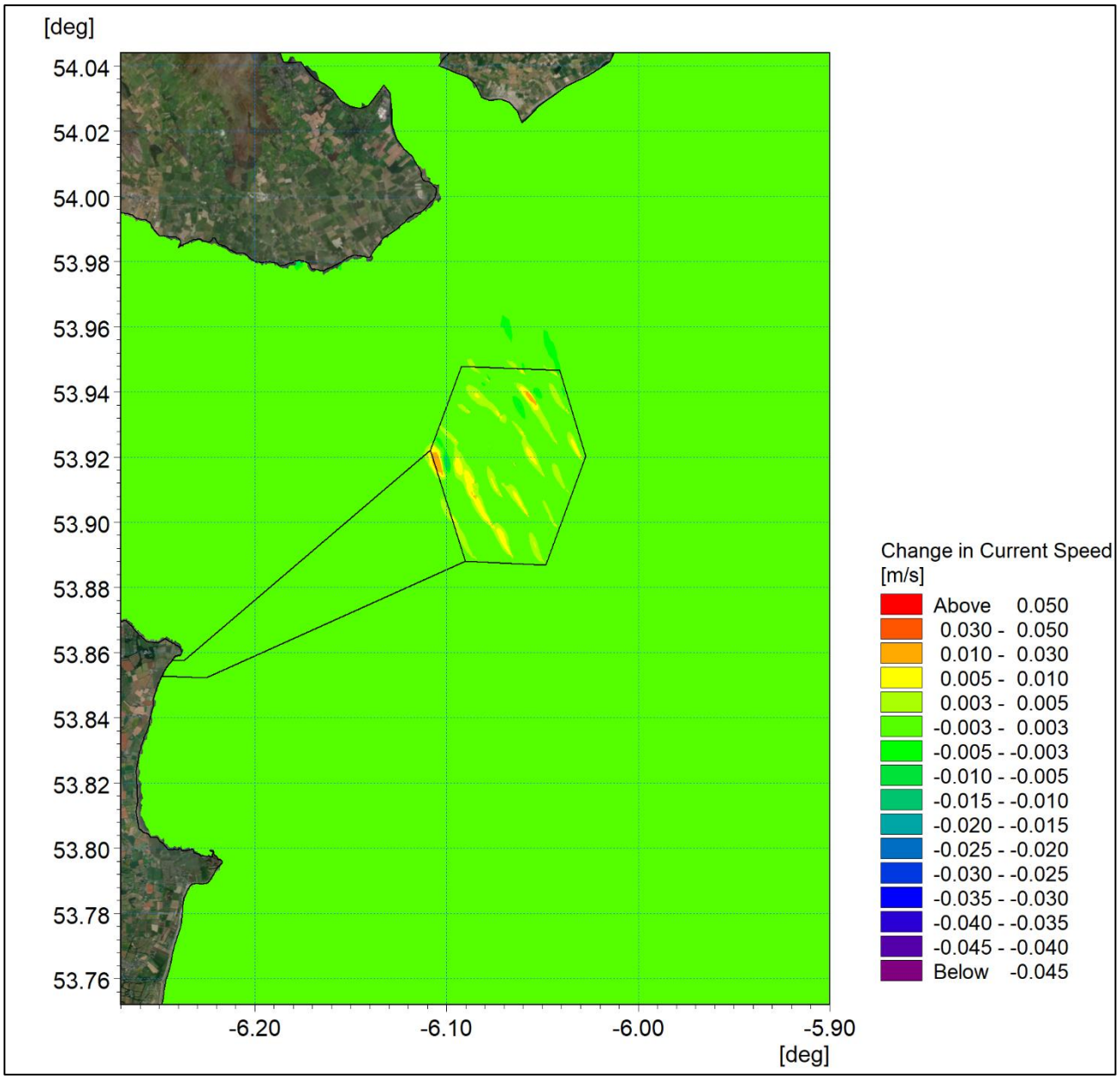

Figure 3A-36: Change in littoral current 1 in 200 year storm from 165° - flood tide (post-construction minus baseline).

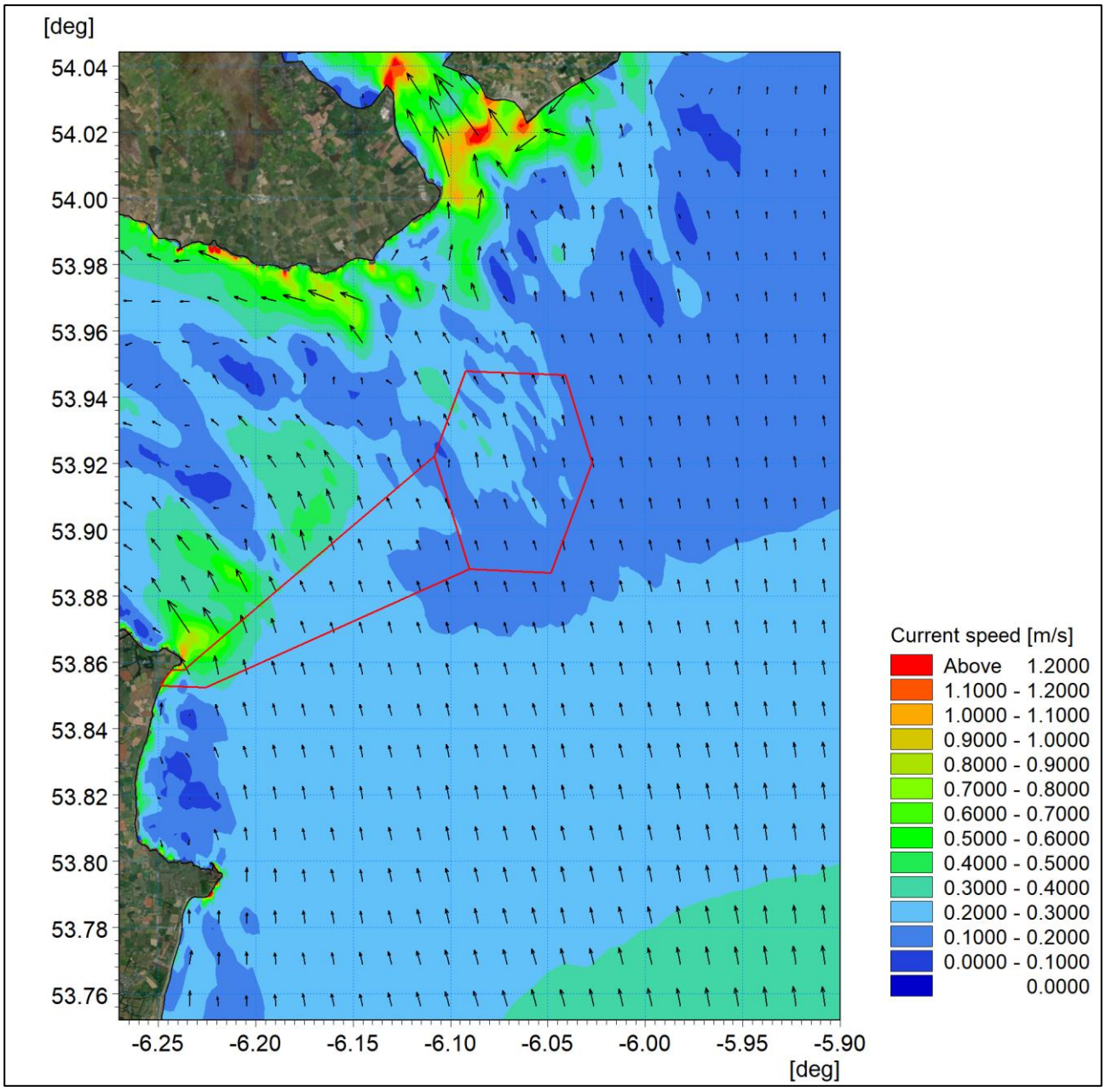

Figure 3A-37: Post-construction littoral current 1 in 200 year storm from 165° with sea level rise - flood tide.

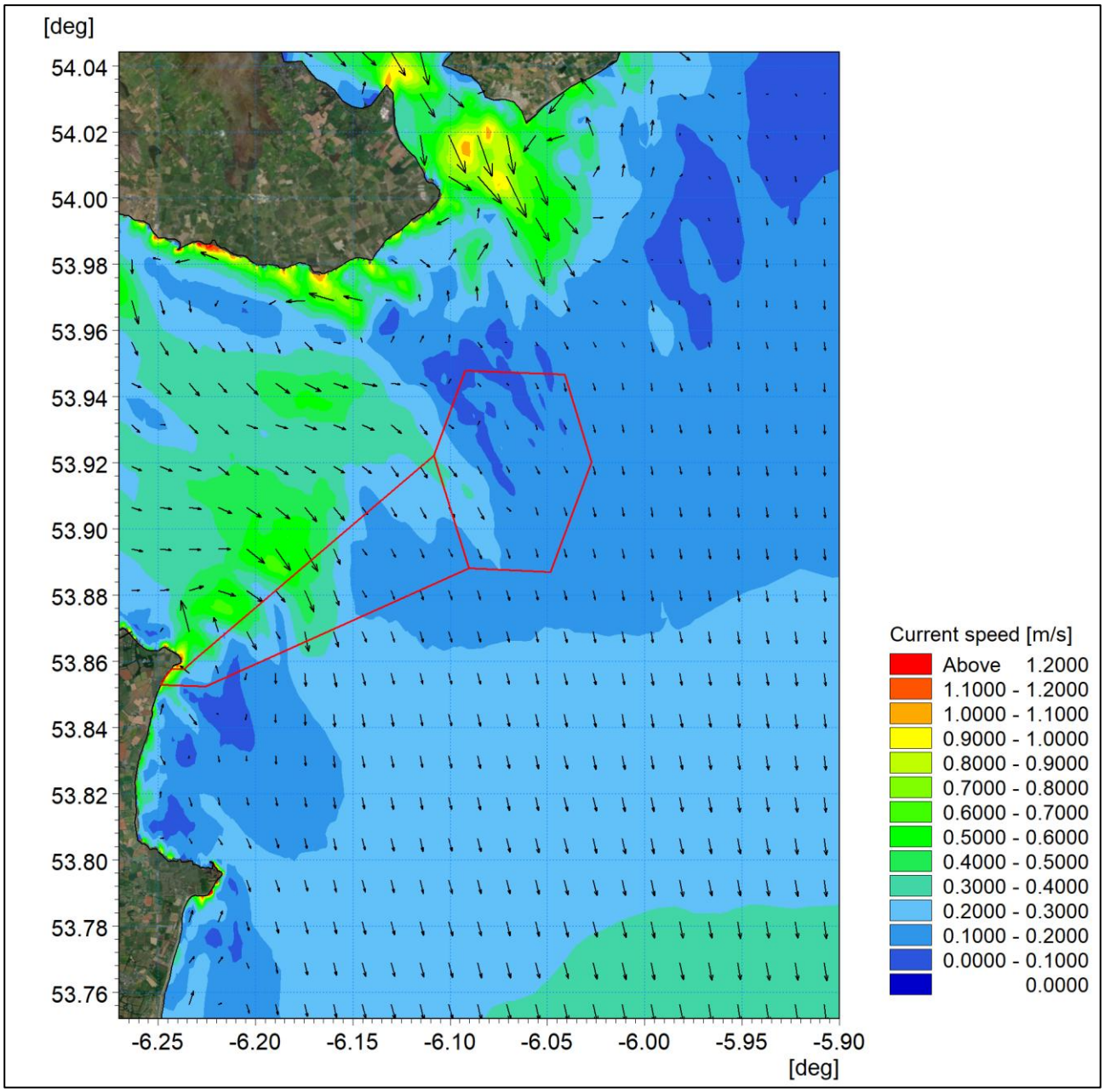

Figure 3A-38: Post-construction littoral current 1 in 200 year storm from 165° with sea level rise - ebb tide.

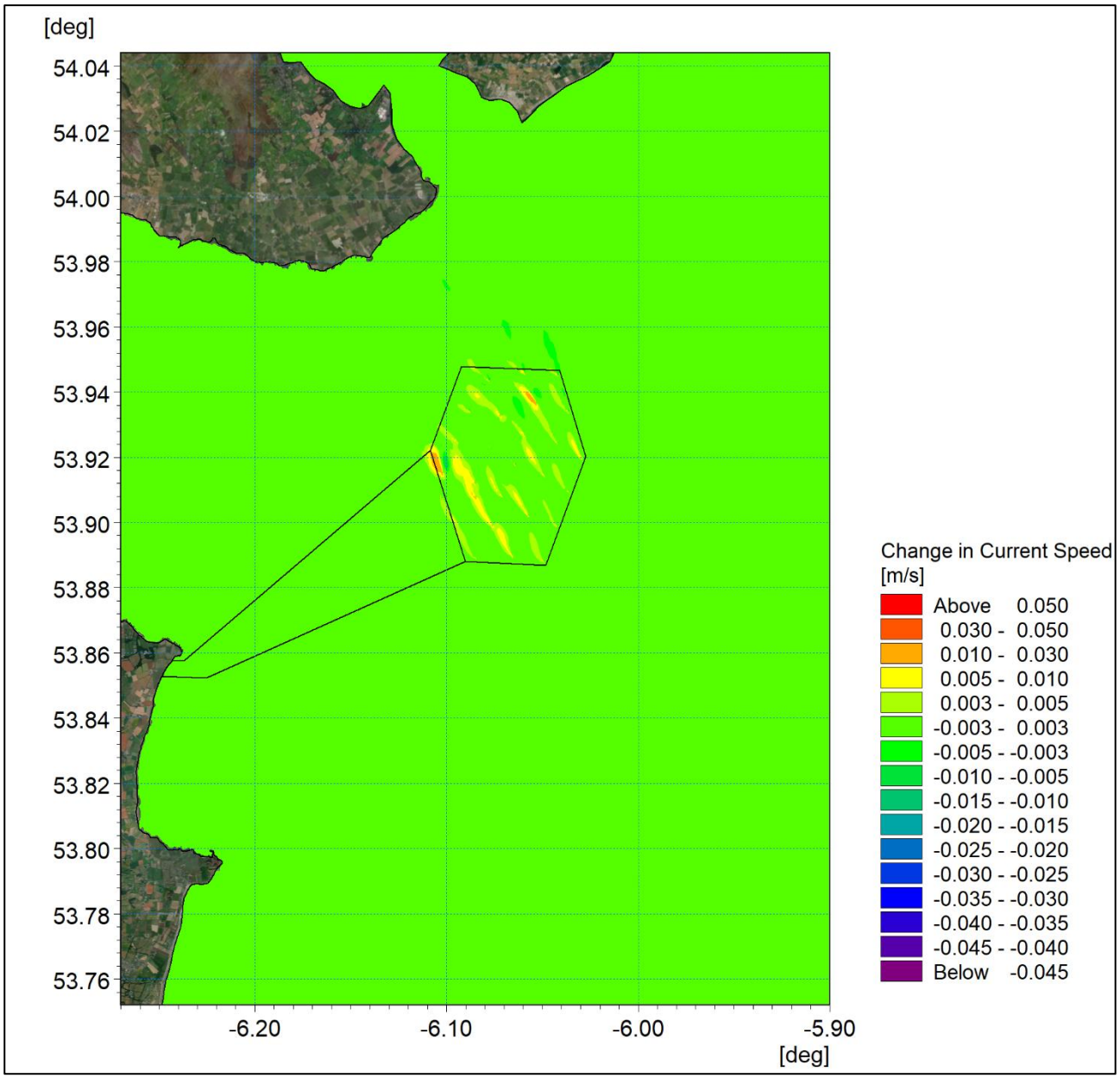

Figure 3A-39: Change in littoral current 1 in 200 year storm from 165° with sea level rise - flood tide (post-construction minus baseline).

3.2.4 Post-construction sedimentology

Sediment Transport

The numerical modelling methodology for sediment transport was described in section 2.2. For the post-construction scenario, in addition to the structures being included in the tide and wave models, the seabed material map was edited to include a non-erodible hard layer to represent the scour protection. Modelling did not include the cable armouring as the proposed armouring is of limited height and it is anticipated not to have a significant effect as in-built mitigation measures will be adopted to avoid significant impacts, e.g. the use of shallow profile tapered cable protection which enables sediment transport regime to continue uninterrupted.

With regards to scour protection, an area of fixed seabed was overlain with a thin layer of sand to initialise the model and avoid instabilities. The scour protection was defined as described in section 2 of the NIS (i.e. scour protection radius + pile =24 m). The models were then re-run for a spring tide under calm conditions and also for a 1 in 2 year storm from 165°.

For this analysis the post-construction residual current was calculated over the course of one complete typical tidal cycle and compared with the baseline (Figure 2-29). The post-construction residual current and changes from the baseline are shown in Figure 3-40 and Figure 3-41 respectively. These figures demonstrate that the structures have little influence on the flow domain under calm conditions.

The residual currents are the driving force for sediment transport and if the structures do not have a significant influence on either tide or wave conditions, they cannot therefore have a significant effect on the sediment transport regime. For completeness the sediment transport was simulated with the structures in place and then factored to indicate the loading over the course of one year to provide representative quantities. The baseline annual sediment transport rate is shown in Figure 2-30, whilst the post-construction rate is shown in Figure 3-42. As anticipated these figures demonstrate that the regime remains unchanged with little sediment transport potential across the domain.

This process was repeated for the 1 in 2 year storm. The baseline residual current (Figure 2-31) and annual potential sediment transport (Figure 2A-32) were compared with the equivalent post-construction residual current pattern as shown in Figure 3A-43 with the difference in Figure 3A-44. As discussed previously, the changes due to the presence of the structures are very small (often in the order of the model convergence criteria). During storm conditions the variation in residual littoral currents and therefore sediment transport processes is limited both in magnitude and spatially. The post-construction sediment transport regime presented in Figure 3A-45 shows only a small amount of variation from the baseline scenario. To the north west of the offshore wind farm area where a rocky outcrop is present the current speed is reduced to below the level required for transport. This is corroborated by the reduction in wave height in the shadow of the installed infrastructure, shown in Figure 3-12. It should be noted that the log scale palette applied in the figures which range from 0.01 to 50,000 m^3/year/m exaggerates the potential changes particularly at very low magnitudes.

This analysis demonstrates that the Project will have no significant effect on sediment transport, given that the baseline transport is limited and that any changes to the residual currents which drive transport are minimal.

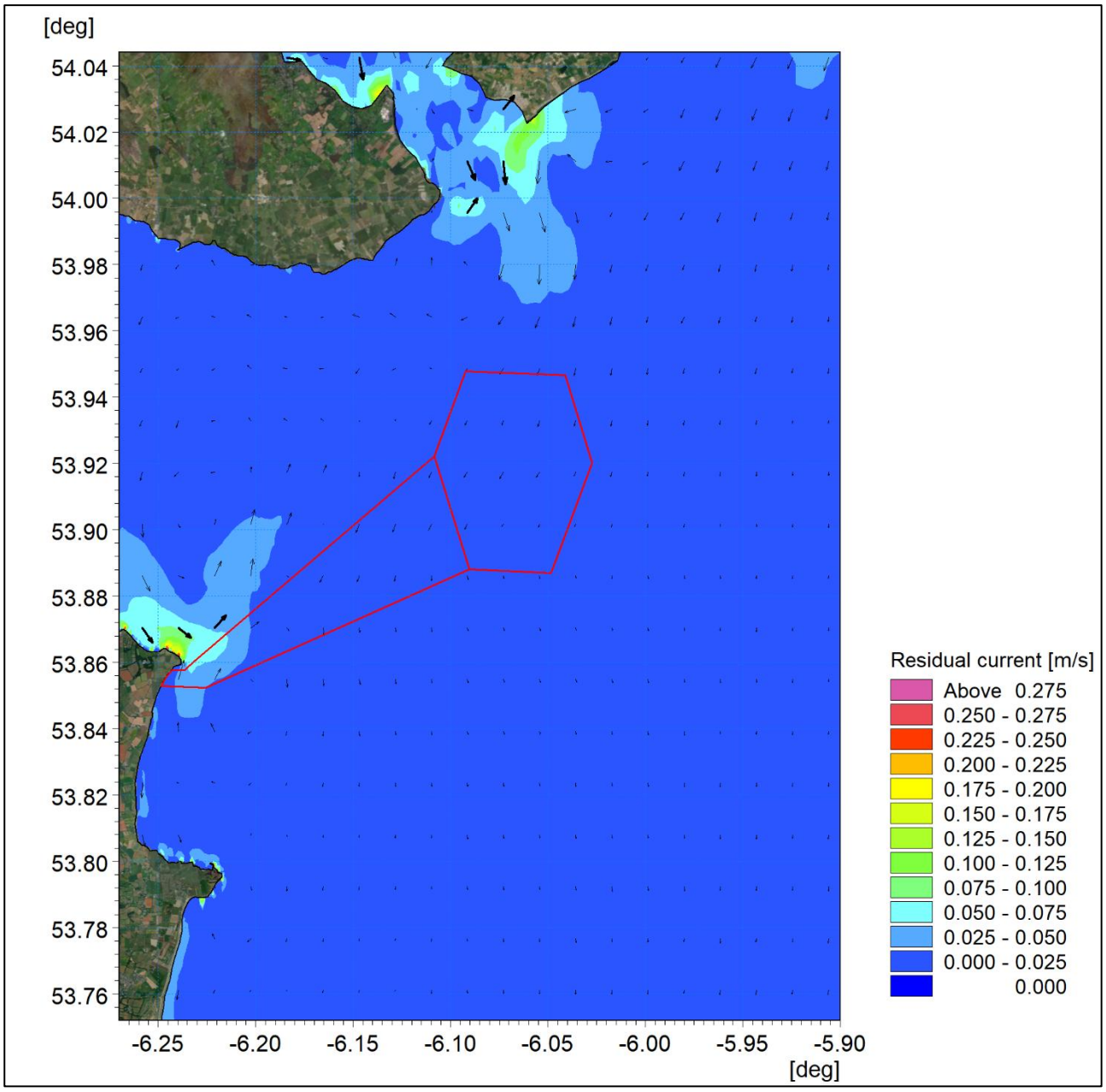

Figure 3-40: Post-construction residual current spring tide.

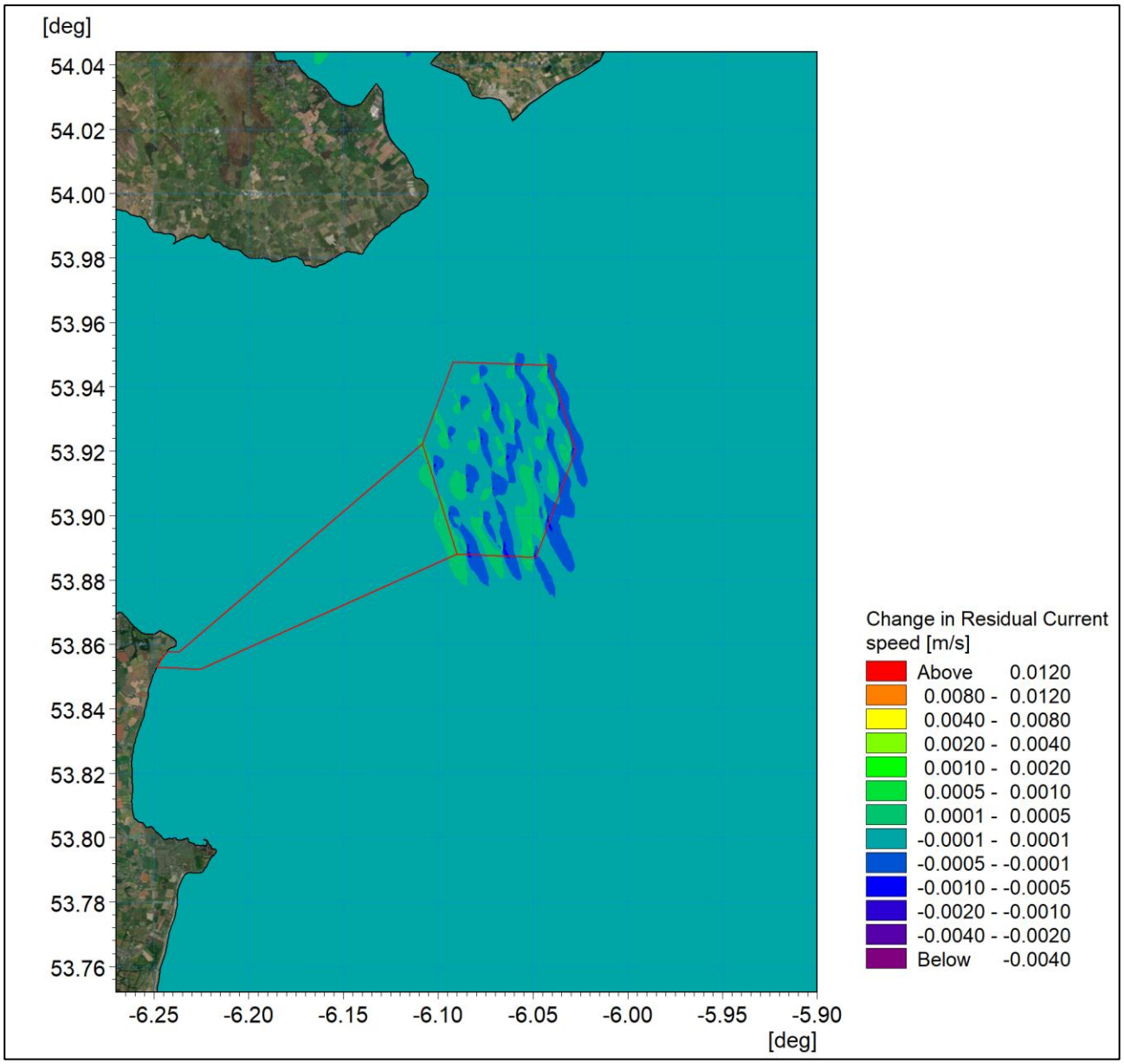

Figure 3-41: Change in residual current spring tide (post-construction minus baseline).

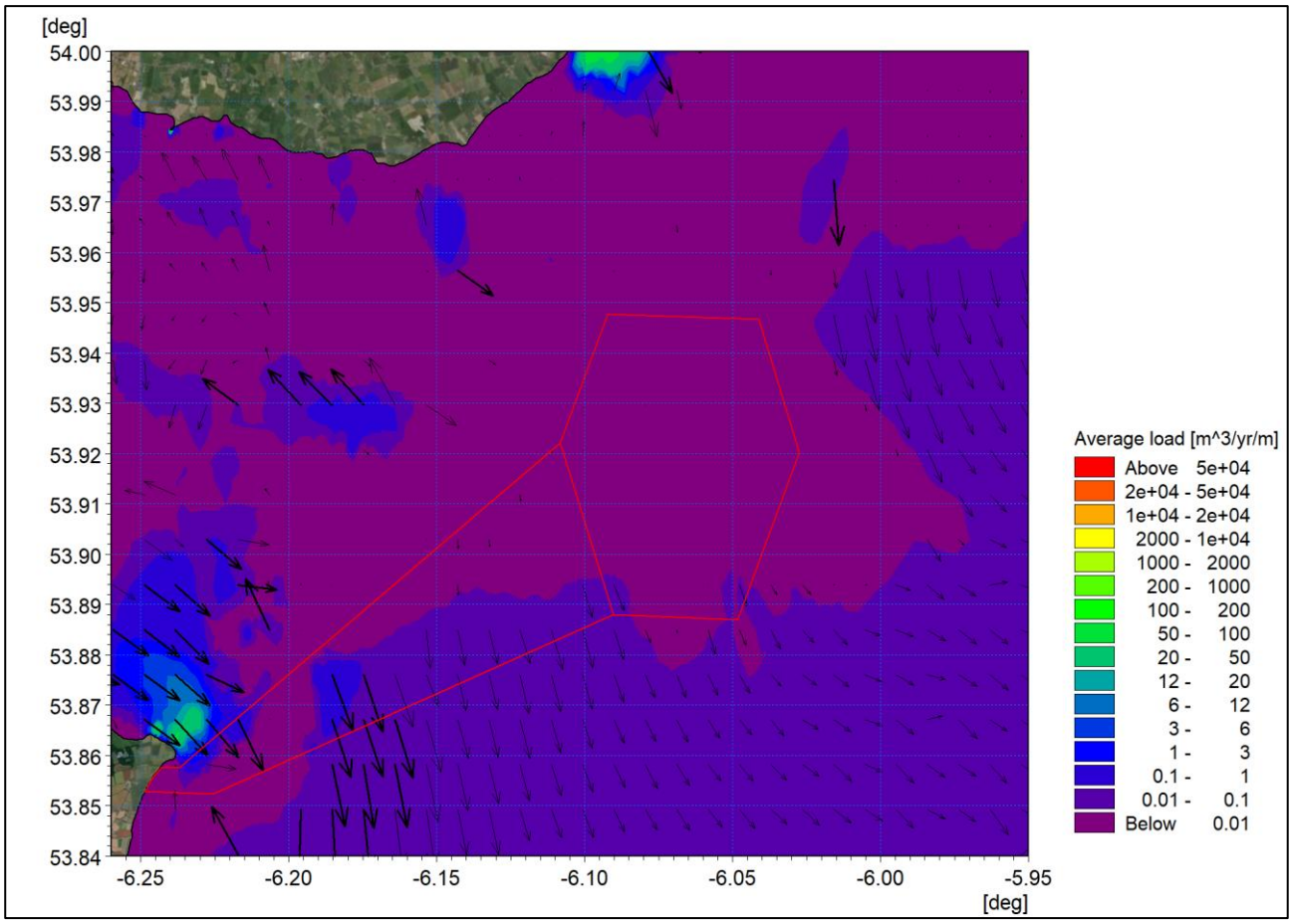

Figure 3-42: Post-construction net sediment transport - spring tide.

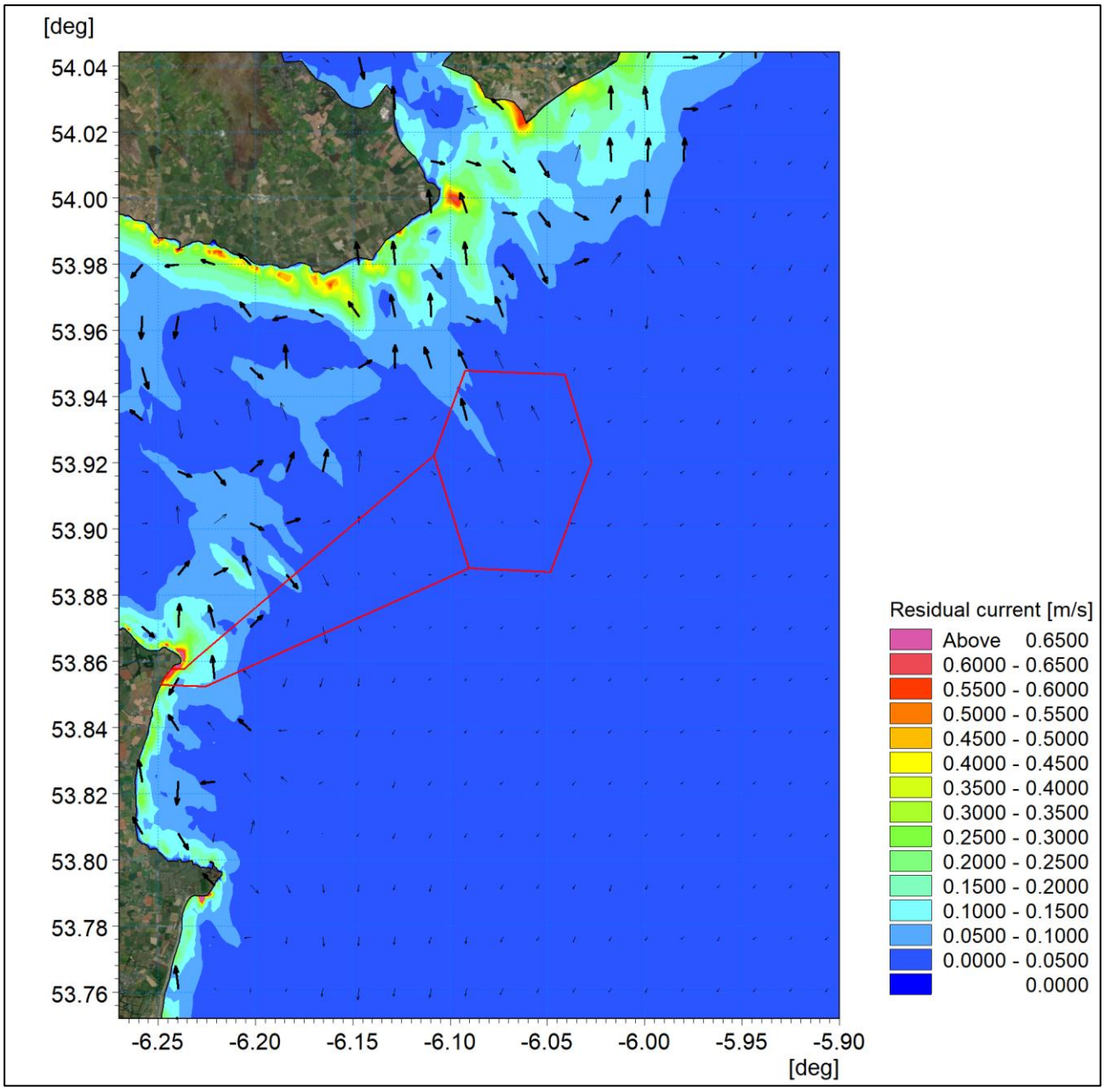

Figure 3A-43: Post-construction residual current 1 in 2 year storm from 165° spring tide.

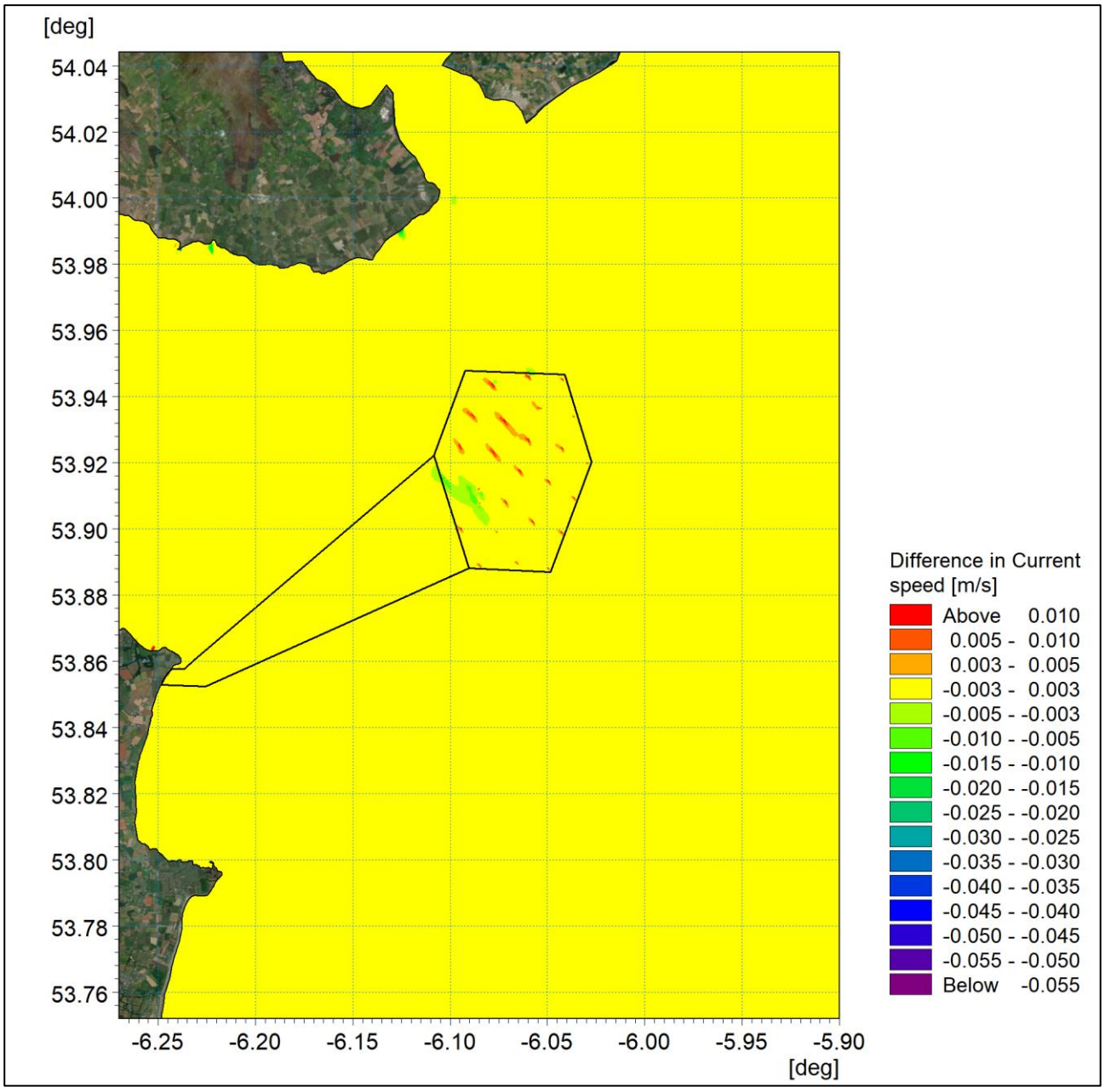

Figure 3A-44: Change in residual current 1 in 2 year storm from 165° spring tide (post-construction minus baseline).

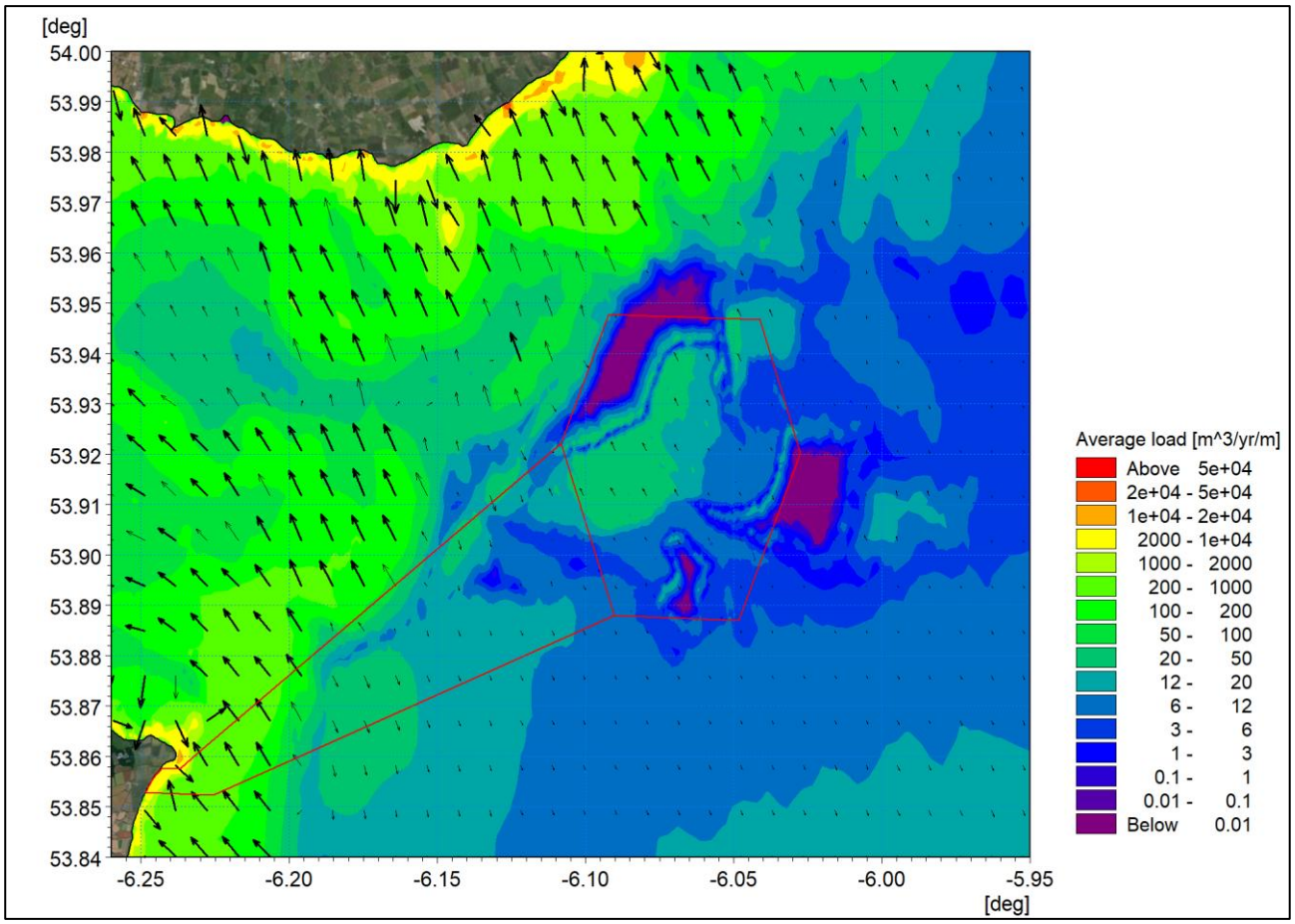

Figure 3A-45: Post-construction net sediment transport - spring tide with 1 in 2 year storm from 165°.

Sensitivity of sediment transport

In response to RFI 6.H, the potential for impact on the longer term sediment transport regime was examined. The simulation of annual seabed morphology described in Section 2.3.2 was repeated for the post construction scenario. The change in bed level following one year of tidal forcing is shown in Figure 3A-46 and is comparable with the baseline figure, Figure 2A-33. As noted previously, the omission of riverine sediment sources results in somewhat exaggerated erosion within the river channel, however the morphological development mechanisms are captured within the model. The difference in the seabed level change between the post-construction and baseline scenario is shown in Figure 3A-47. There are small changes, circa 1 mm in the immediate vicinity of the foundation structures where the tidal currents are marginally stronger and seabed sediment is comprised of finer material (as shown in Figure 2-28). However even at these locations the variations are within the limits of the model accuracy and impacts on seabed morphology in the region would be negligible.

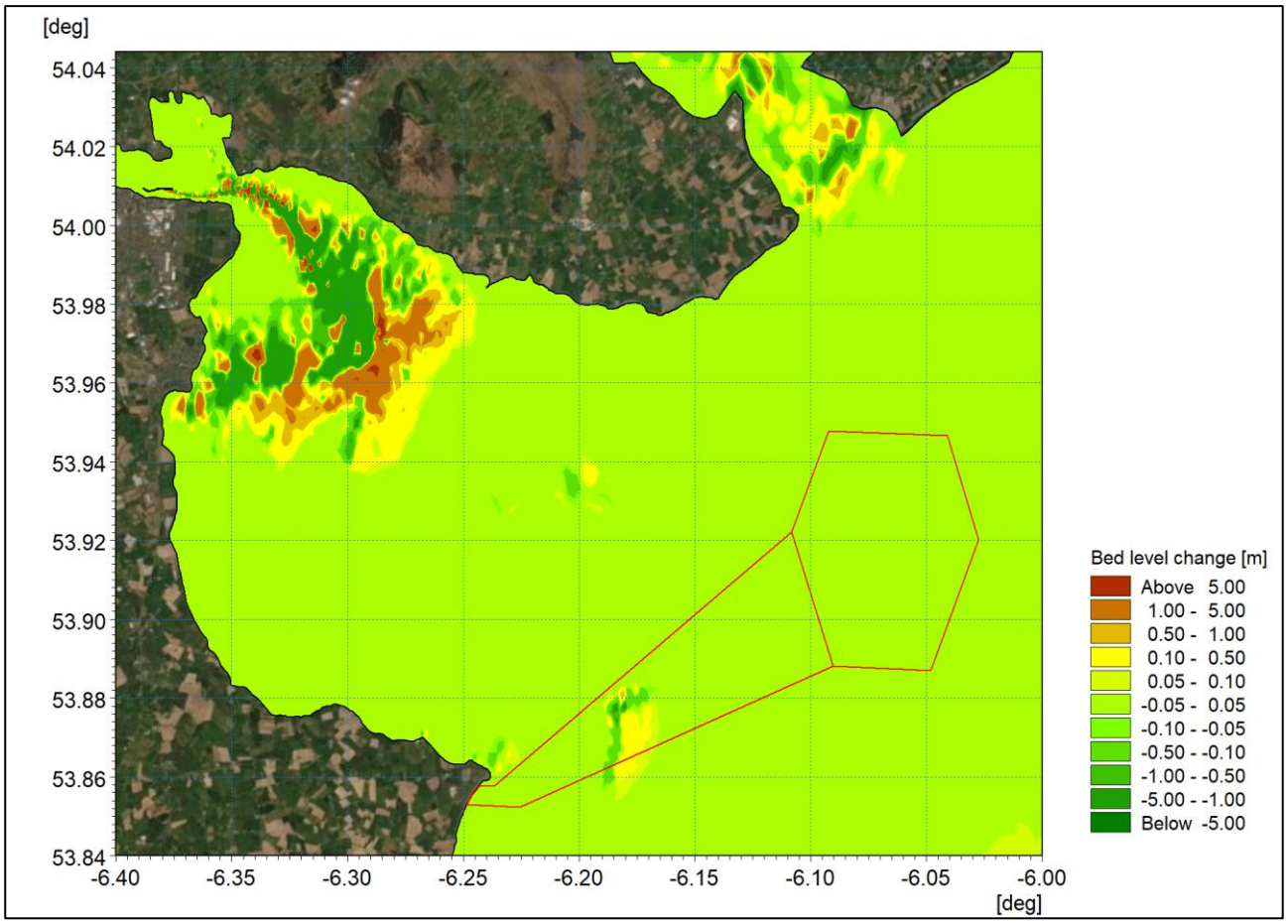

Figure 3A-46: Post-construction change of bed level for one year of tidal currents.

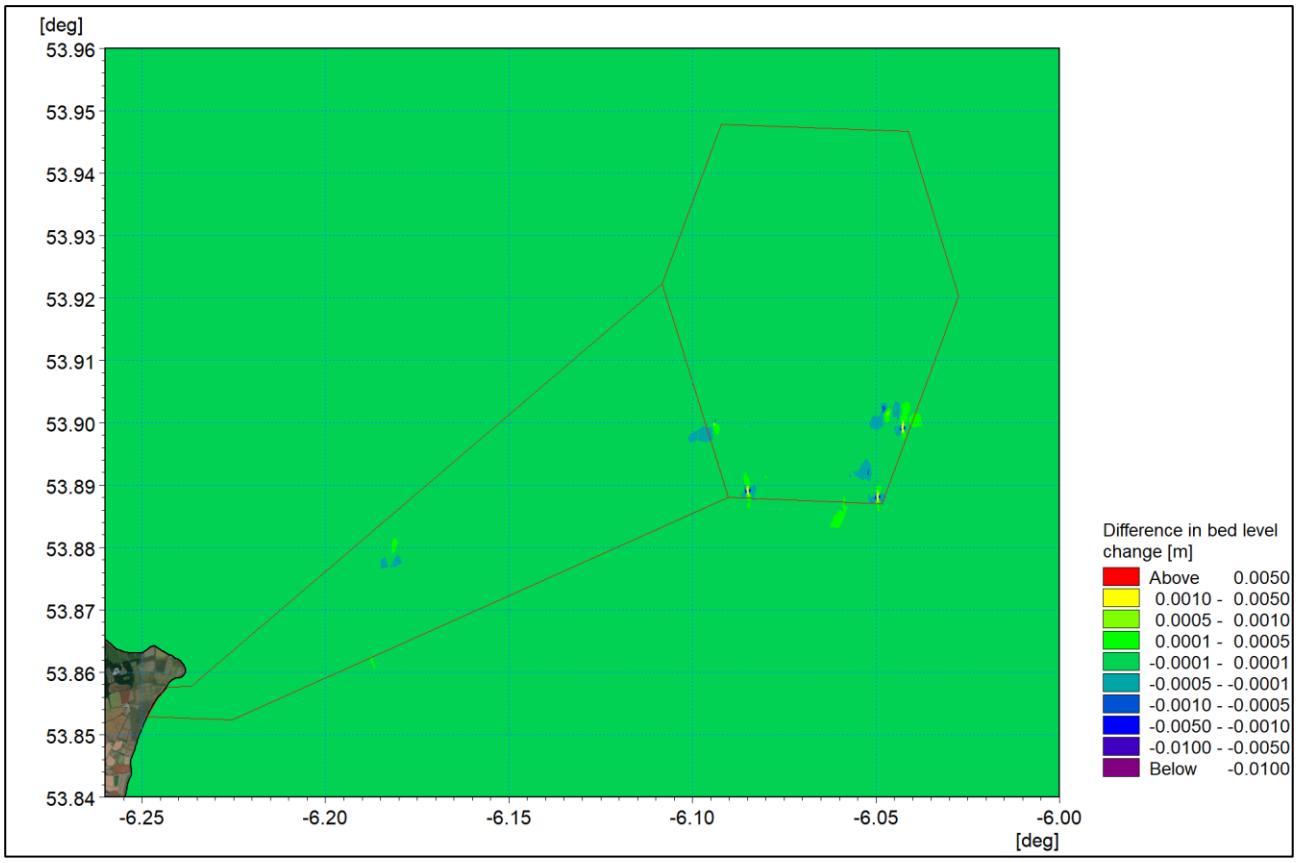

Figure 3A-47: Difference in change of bed level for one year of tidal currents.

In accordance with RFI 6.D, additional return period modelling was undertaken for the post-construction scenario which corresponds with the baseline scenarios presented in Section 2.3.2. As outlined in the previous section, simulation and analysis of residual currents was undertaken for the 1 in 200 year return period storm for 165º. Figure 3A-48 illustrates the post-construction residual current, whilst Figure 3A-49 shows the difference from the baseline condition presented in Figure 2A-34. There are localised changes within the offshore wind farm area of up to 10%, however beyond the boundary of the Project this is reduced to less than 3%. As previously noted, variation in coupled models (particularly wave, tide and sediment transport combined) may occur due to model closure. Figure 3A-50 shows the post construction sediment transport demonstrates very limited change from the baseline condition presented in Figure 2A-35.

For completeness, the modelling was extended to the scenario which incorporates a 0.5m increase in water depth to account for sea level rise. The residual current and change in residual current are presented in Figure 3A-51 and Figure 3A-52 respectively, whilst the sediment transport is shown in Figure 3A-53. These figures correspond with the baseline figures presented in Figure 2A-36 and Figure 2A-37. As with underlying tidal and littoral current simulations, the residual current and sediment transport regimes do not indicate any discernible difference from the 1 in 200 year return period event with present day sea levels.

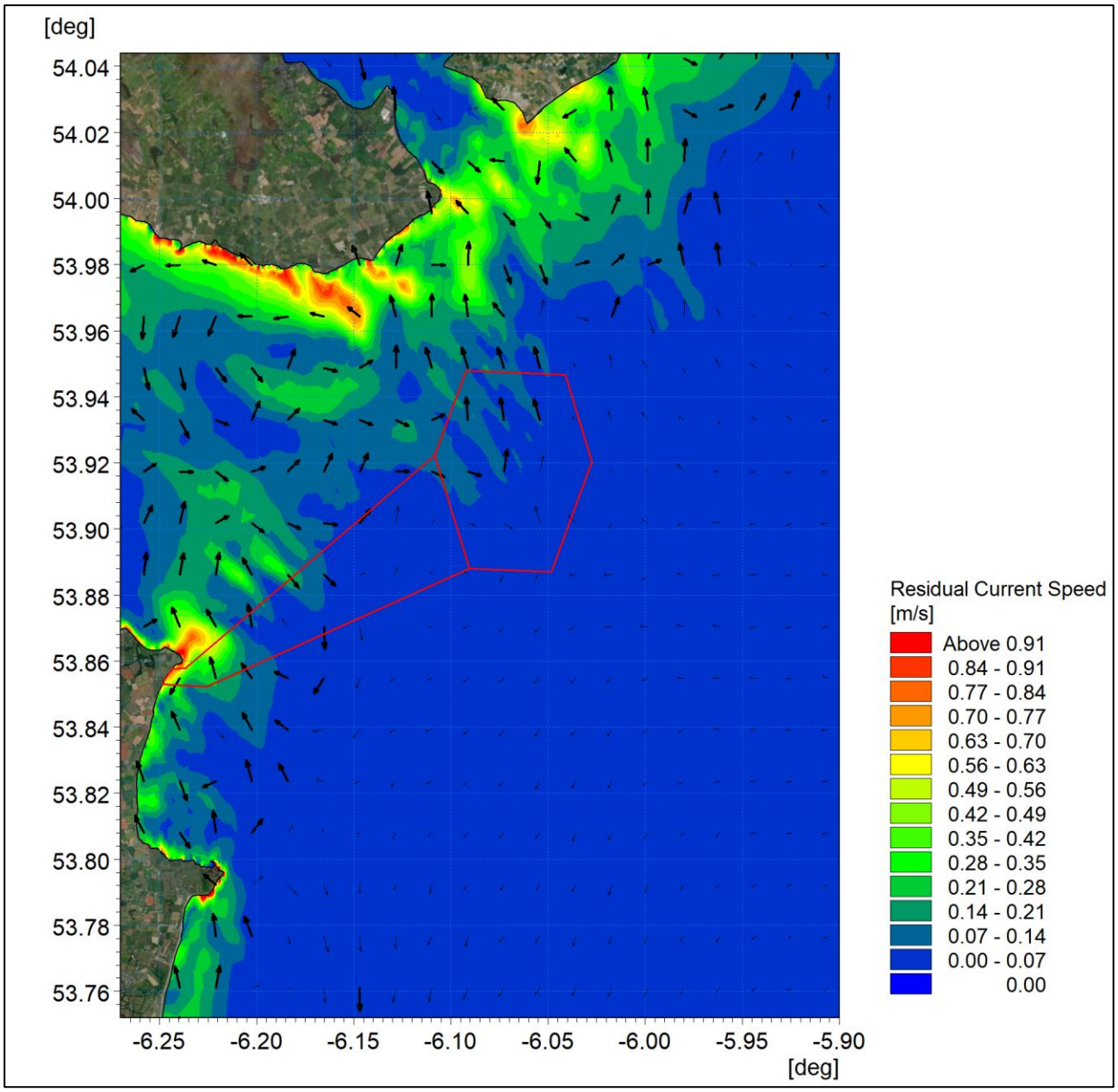

Figure 3A-48: Post-construction residual current 1 in 200 year storm from 165° spring tide.

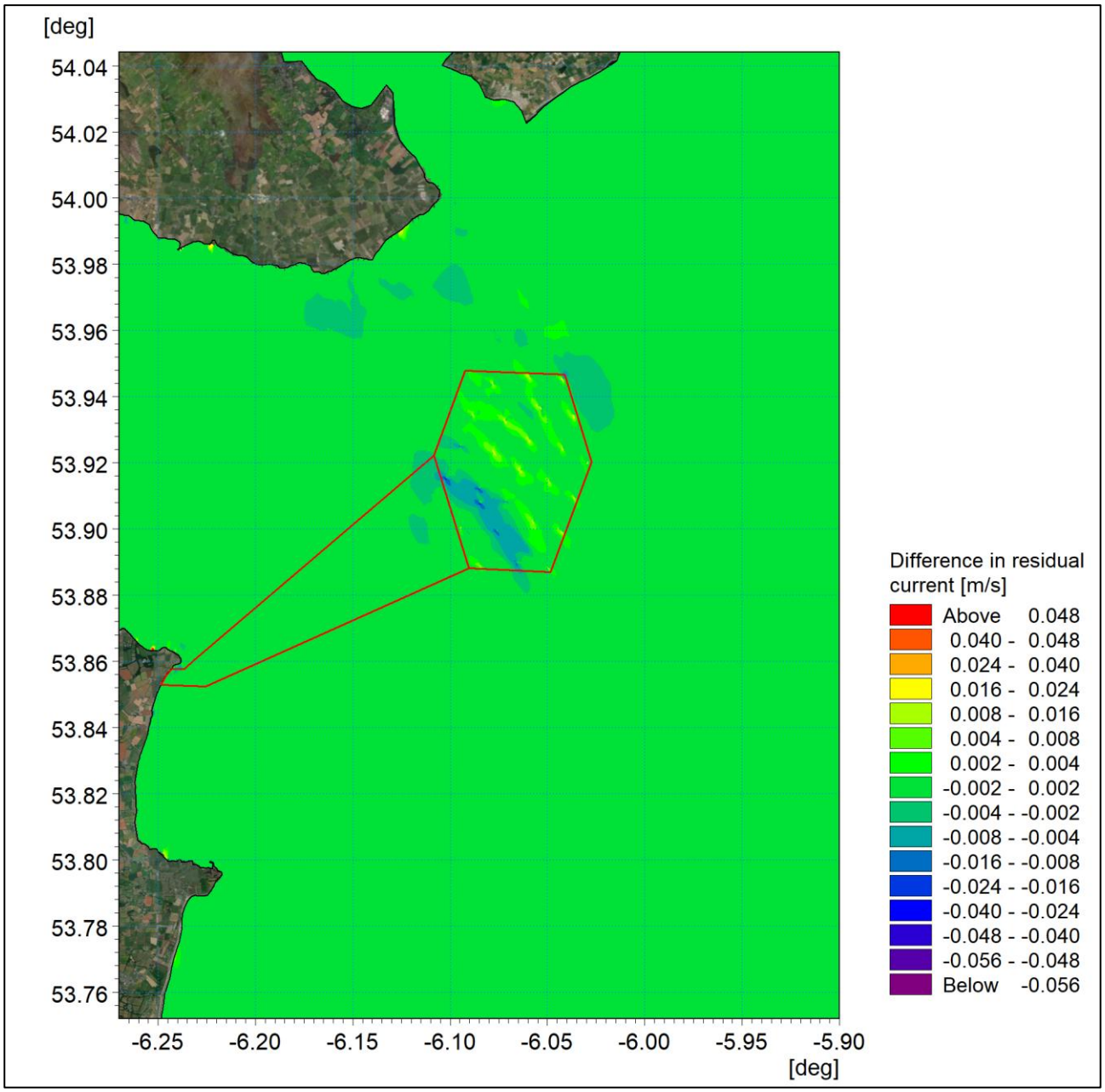

Figure 3A-49: Change in residual current 1 in 200 year storm from 165° spring tide (post-construction minus baseline).

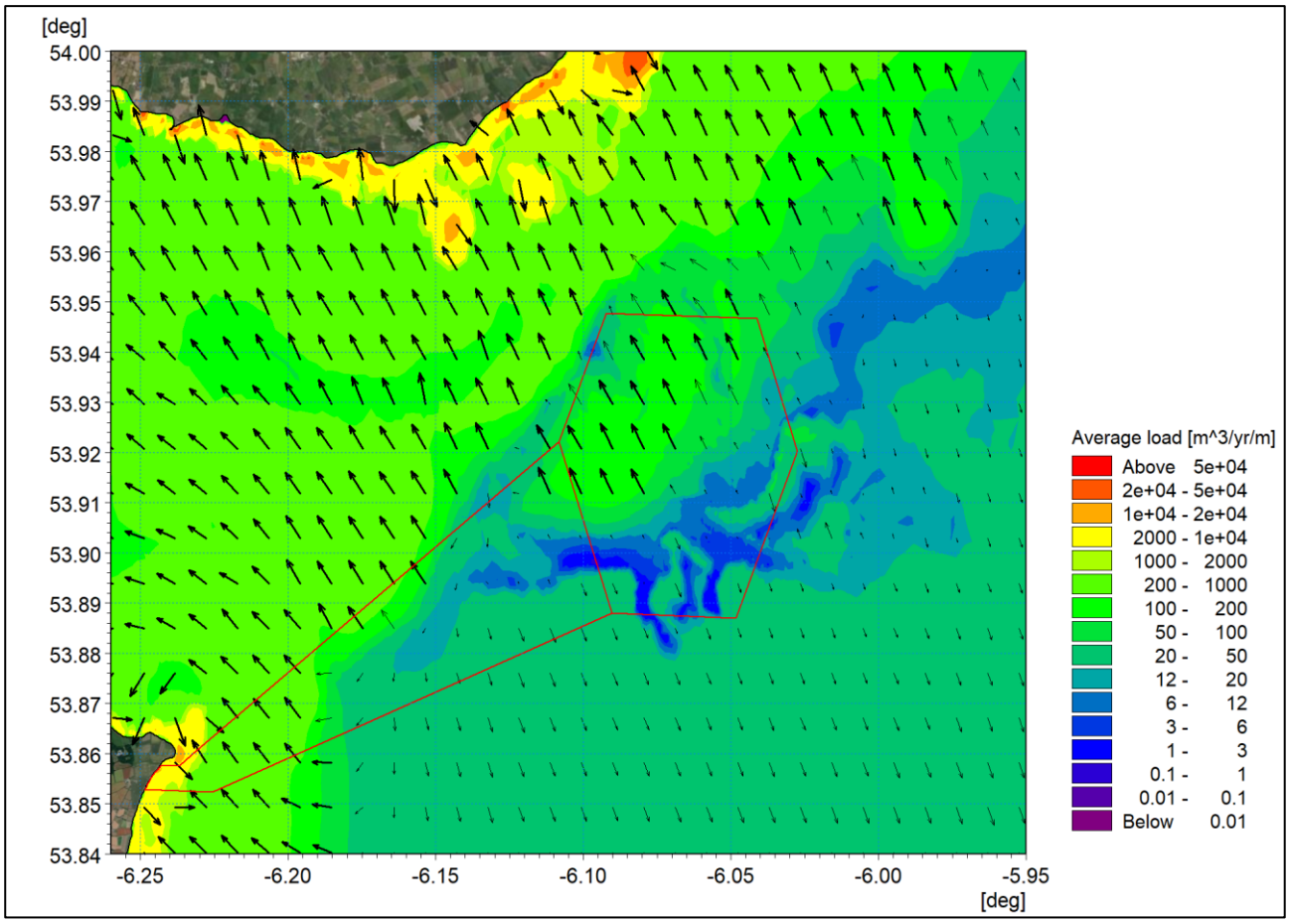

Figure 3A-50: Post-construction net sediment transport - spring tide with 1 in 200 year storm from 165°.

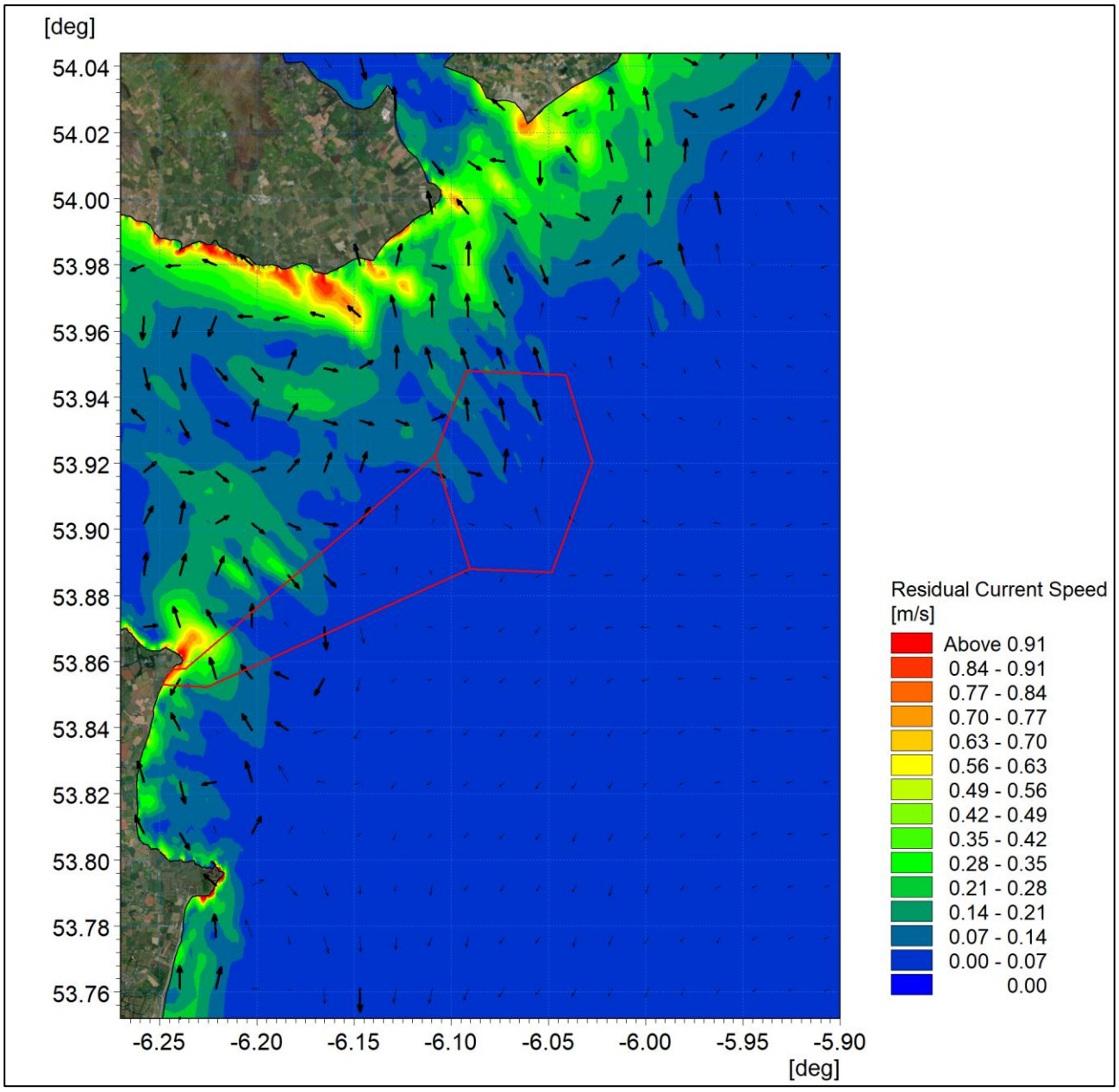

Figure 3A-51: Post-construction residual current 1 in 200 year storm from 165° with sea level rise - spring tide.

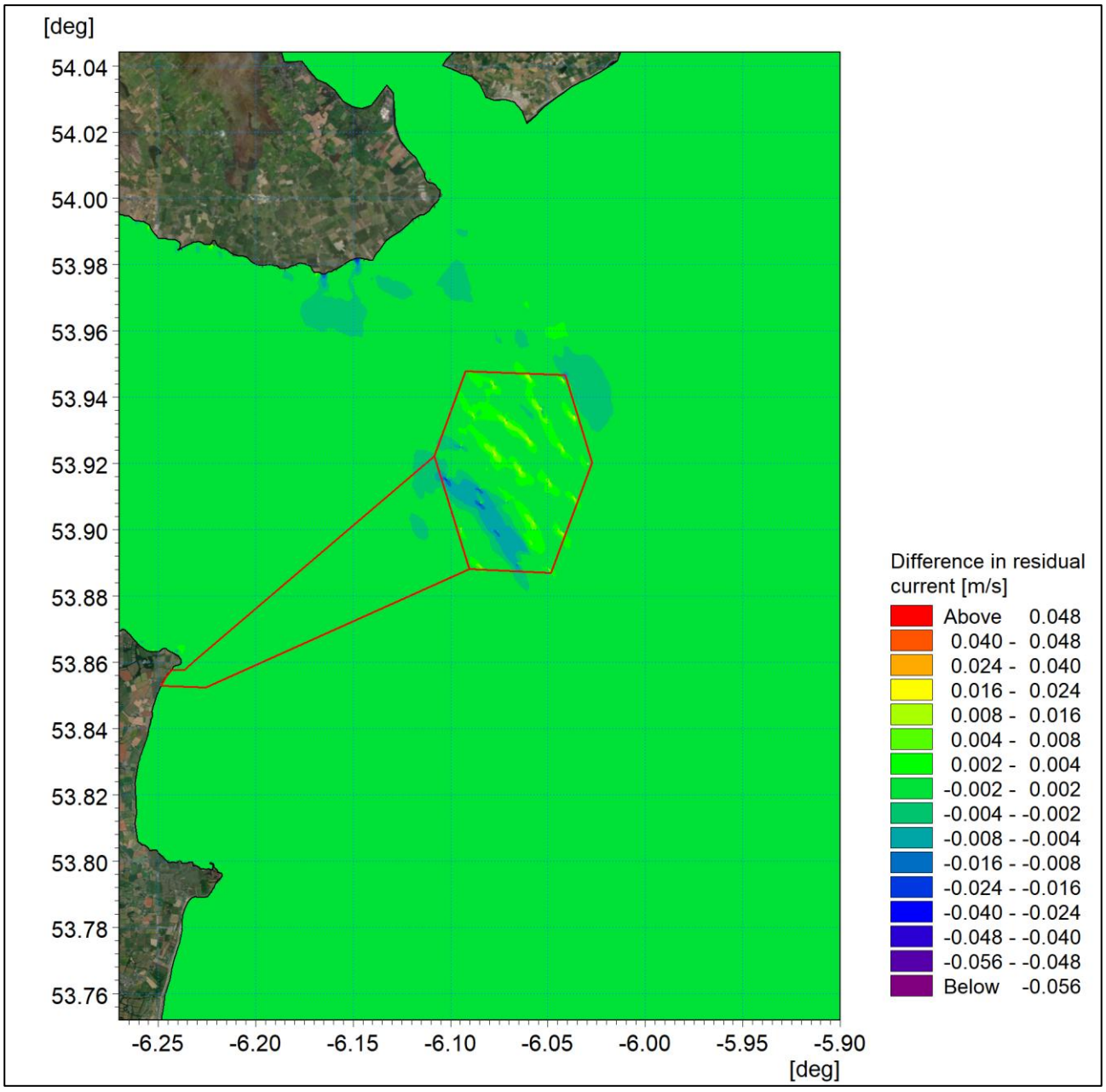

Figure 3A-52: Change in residual current 1 in 200 year storm from 165° with sea level rise - spring tide (post-construction minus baseline).

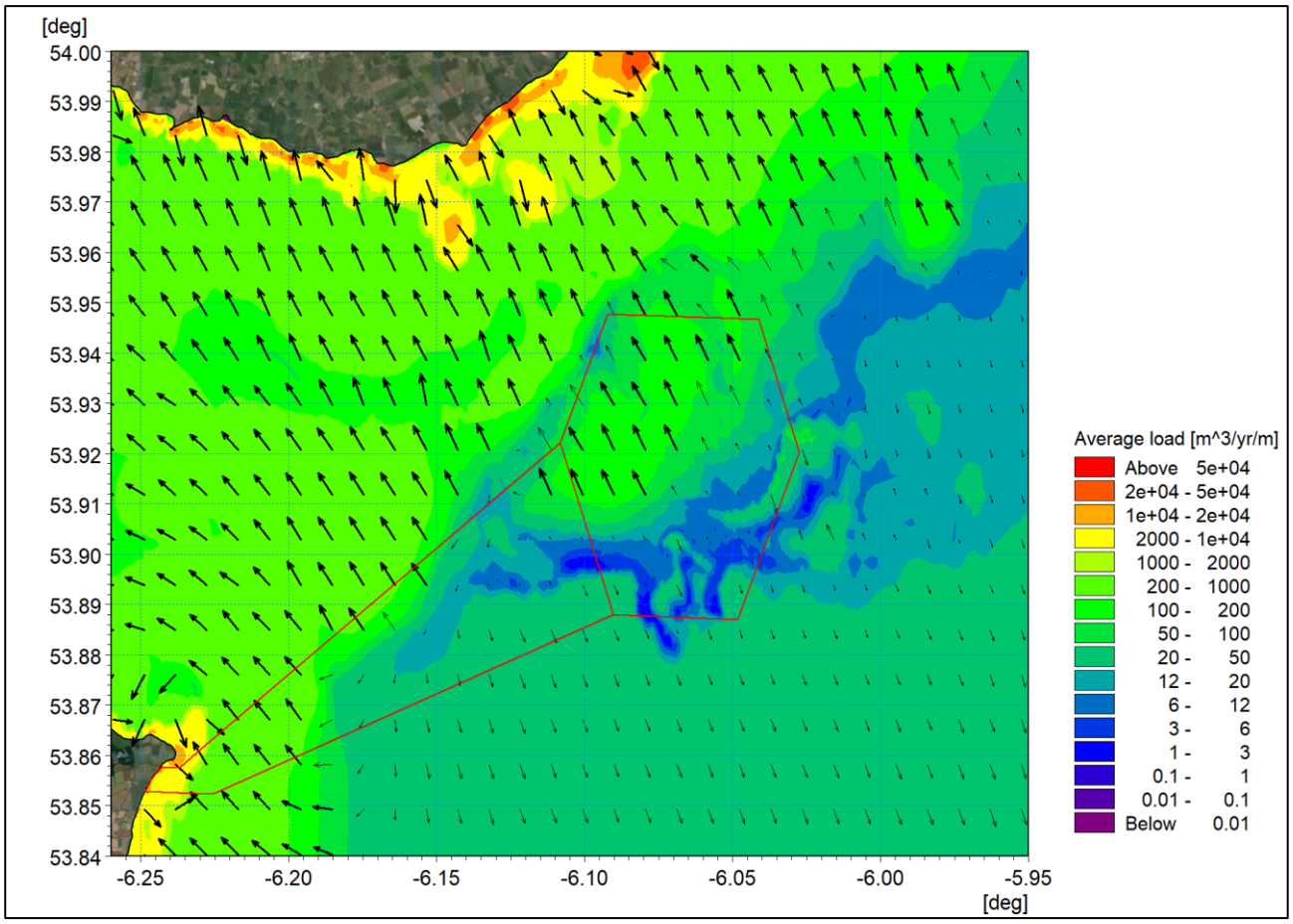

Figure 3A-53: Post-construction net sediment transport - spring tide with 1 in 200 year storm from 165° with sea level rise.

3.3 Potential changes during construction

In addition to the changes in marine processes resulting from the operational phase of the Project, the potential construction phase impacts associated with the Project design parameters were also quantified by means of numerical modelling. The principal construction elements relate to the transport and fate of sediment brought into suspension due to the installation of the structures and associated foundations and the laying of the inter-array and offshore cables.

This section provides information on suspended sediment concentrations and subsequent sedimentation relating to the Project. The parameters used in the modelling are based on the Project design parameters and described in section 2 of the NIS. This Technical Report presents the findings of:

- Drilled pile installation – across a range of hydrodynamic conditions;
- Inter-array cable installation – for a zone of sandy bed sediment; and
- Offshore cable installation – through sandy beds.

In Figure 3-54, the solid yellow line indicates the Marine Processes Study Area whilst the dashed line represents the extent of one tidal excursion. The modelled offshore cable corridor in context of the overall cable installation plan is shown in pink. This modelled offshore cable corridor traverses the offshore wind farm area passing through the range of water depths and tidal currents and will therefore provide the range of suspended sediment plumes. In this and each subsequent figure, the offshore wind farm area is outlined in red for the overview of locations and black in the modelling output to provide contrast.

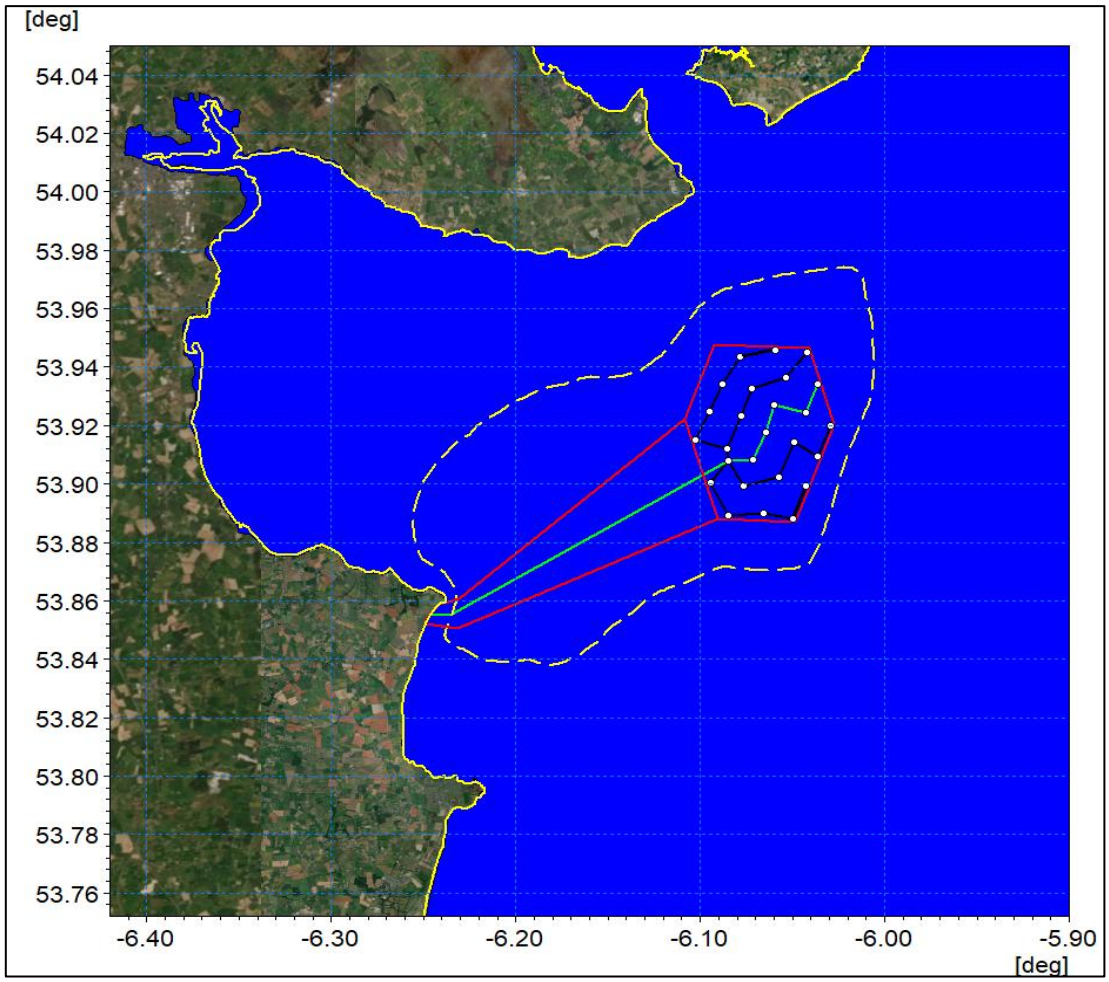

Figure 3-54: Location of the sediment source term (green line) used to model a representative installation route.

3.3.1 Foundation Installation

To assess the impact of the installation of monopiles, the structures were considered in terms of the volume of material which could potentially be released into the water column based on both a volumetric assessment of the data provided and the specified construction technique. This modelling was undertaken using the Project layout which is comprised of 25 turbines and one offshore substation (OSS) as illustrated in Figure 3-54.

Whilst piles may be driven into the seabed with minimal release of sediment material, this assessment has assumed that piles would be augured (i.e. drilled) and that material would subsequently be jetted and dispersed into the water column as a plume.

This modelling assessment assumed the following characteristics as outlined in section 2 of the NIS:

- Pile diameter 9.6 m;
- Pile depth 35 m; and
- Drilling rate 0.25 m/h and therefore a maximum drilling duration (per pile) of six days

A sample of six pile installations were selected for this assessment. These six pile locations as illustrated in Figure 3-55 were selected as they covered a range of water depth and current conditions. Furthermore, these six locations were nearest to the outer extent of the Project Wind farm area meaning that the resultant sediment plumes would represent the greatest possible dispersion characteristics.

The modelling was undertaken using the MIKE21 Mud Transport (MT) module which allows the modelling of erosion, transport and deposition of cohesive and cohesive/granular sediments. This model is suited to sediment releases in the water column as it represents sediment sources which can vary spatially and temporally. The cohesive functions were not utilised in these simulations as the material released comprising sand and drilling mud would be more widely dispersed without the inclusion of flocculation – providing the worst case scenario.

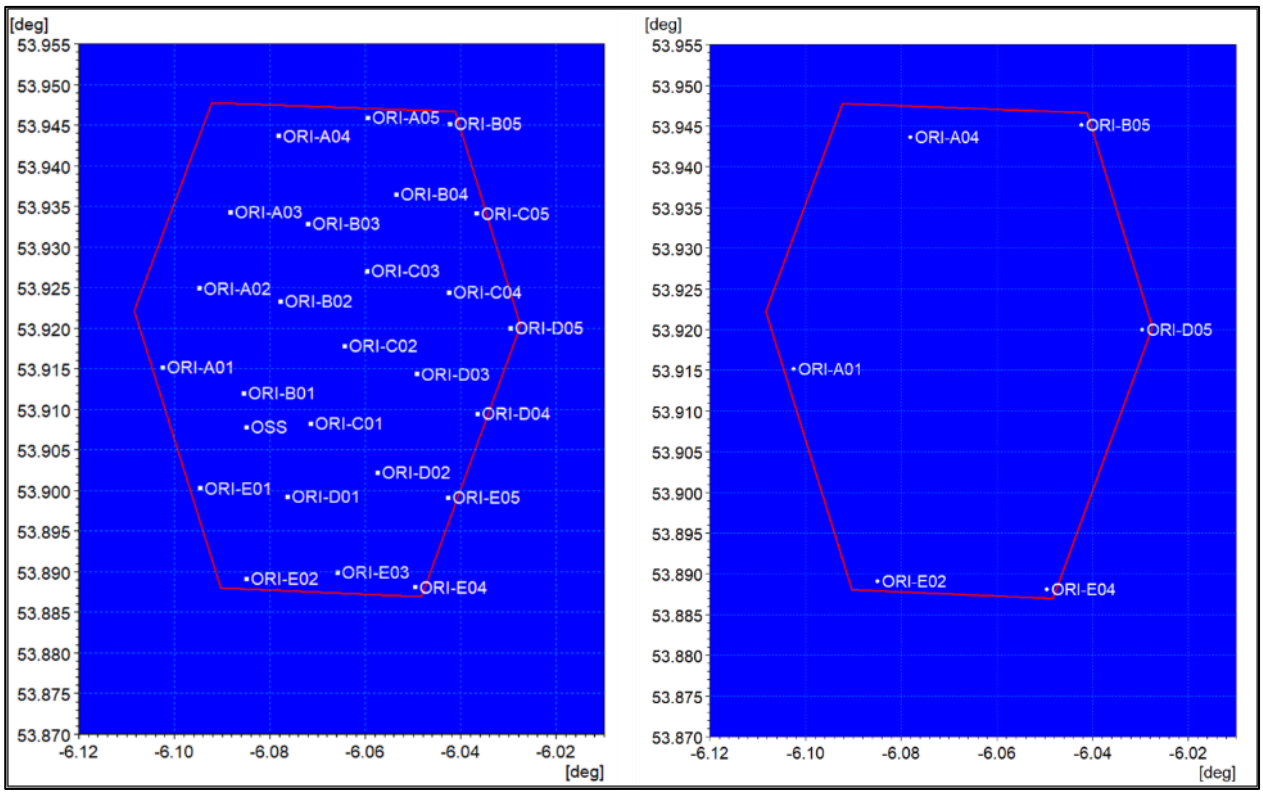

Figure 3-55: Overall wind farm layout (left) with the WTG monopiles selected to assess suspended sediments (right).

To undertake the modelling, it was necessary to define characteristics for the seabed sediment. A number of data sources were employed as previously described in section 2.3. The data collected by GSI was accessed via the EMODnet online database and used as illustrated in Figure 3-56.

The grab sample data from EMODnet was used as a basis for the sediment grading however more fine material would be released relating to bentonite used in the drilling process. The drilling was modelled as being undertaken over six days per pile which covered a period of both spring and neap tides. This represents the maximum piling duration. Should piling be undertaken with an increased drilling rate then the period over which elevated suspended sediment concentrations persist would be reduced with the reciprocal increase in instantaneous suspended sediment concentrations. The sediment plume extent and concentration would also be dependent on tidal state (with a greater extent and lower concentration for spring tide and vice versa for neap tides). For this reason the modelling was undertaken to encompass all tidal states. It was assumed that all cuttings were released into the water column with the following characteristics:

- 40% fines/bentonite 0.05 mm diameter;
- 30% sandy mud 0.1 mm diameter;
- 20% medium sand 0.5 mm diameter; and

- 10% cuttings 1 mm diameter.

It was assumed that all material would be suspended, however in practice there is likely to be a greater proportion of larger cuttings material. This material would not be widely dispersed therefore a conservative approach was taken in terms of suspended sediments and dispersion.

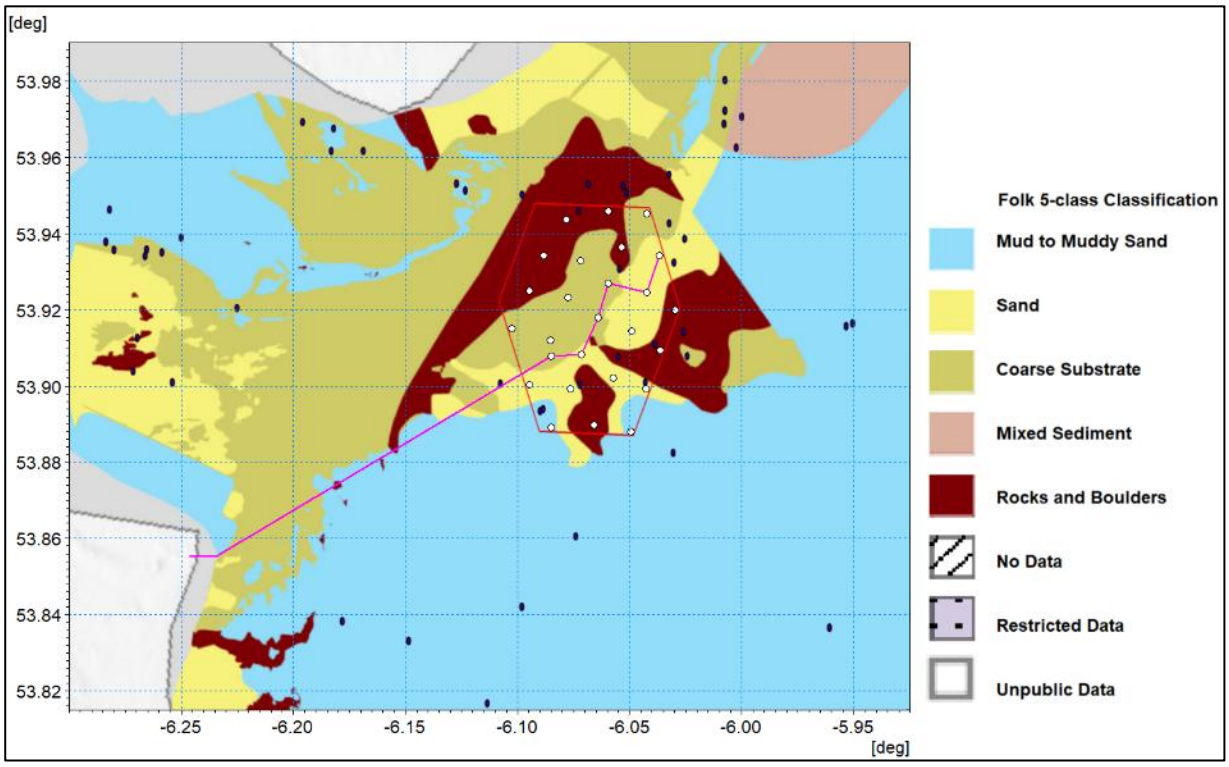

Figure 3-56: EMODnet portal data (blue dots indicate EMODnet sample locations).

For each simulation described in the sections below, a set of figures are presented, as follows:

- **Suspended sediment:** The maximum and average suspended sediment plumes are presented where the maximum shows the largest value encountered in each cell over the modelling period. These elevated values would not occur concurrently or necessarily persist for a prolonged period of time, hence the average values over the installation period are presented to provide context. Due to the variation in suspended sediment levels the plots require the use of a log scale to cover this range and provide clarity. However, all plots use the same scale for ease of comparison. It should be noted that the minimum value presented is 0.1 mg/l which would be indiscernible from background levels.

- **Sedimentation:** The second set of plots relate to sedimentation. The first figure in each set shows the sediment levels one day following the completion of the activity and therefore relates to a specific point in time. Again, the maximum plot shows the greatest amount of sedimentation experienced in each cell over the course of the operation. It should be noted that this is a statistical value and does not relate to a specific point in time. Thus, material which has settled in multiple areas on successive tides would be accounted for more than once in this figure. Therefore, average values are also provided to indicate the period of time over which the sedimentation persists. It should be noted that for the drilled piles sedimentation levels are very low. A log scale has therefore been used throughout as reducing the minimum values (0.01 mm) would be incongruous.

ORI-E04

ORI-E04 is located to the southeast of the offshore wind farm area in the deeper water where current speeds are marginally higher. Within the plume the maximum suspended sediment levels are 100 mg/l, these levels are localised and only persist for a short period. The average values are much lower, typically one tenth of peak values. The data are illustrated in Figure 3A-57 and Figure 3A-58 respectively. Following the cessation of drilling the turbidity levels reduce within a few hours. Some of the finer material associated with the drilling process is re-suspended during successive tides as it is redistributed but turbidity levels remain low.

The sedimentation plots in Figure 3A-59 and Figure 3A-60 show the sedimentation levels one day after the completion of works and maximum sedimentation respectively, whilst Figure 3A-61 presents the average value. Much of the drilled material settles in the immediate vicinity of the installation with maximum levels of 100mm, whilst at a distance of several hundred metres this is reduced to less than 0.3mm. This is due to the relatively slow drilling rate (0.25 m/hour) allowing the fines to be widely dispersed while the larger material settles at the release point due to the limited current speed. Although there is some resuspension of sediment this is very limited due to the limited current speed and generally final sediment varies little from maximum values.

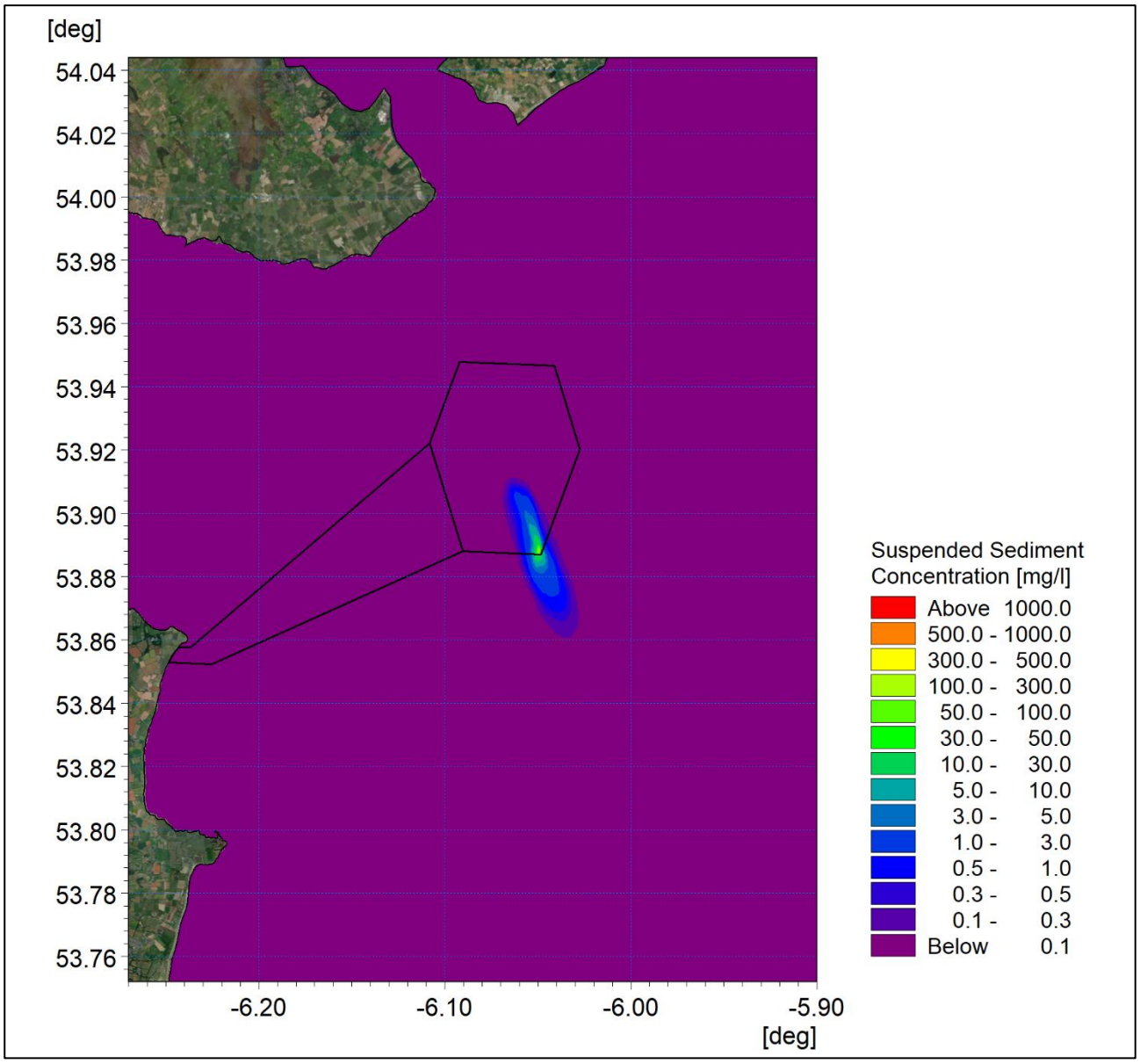

Figure 3A-57: Maximum suspended sediment concentration at ORI-E04.

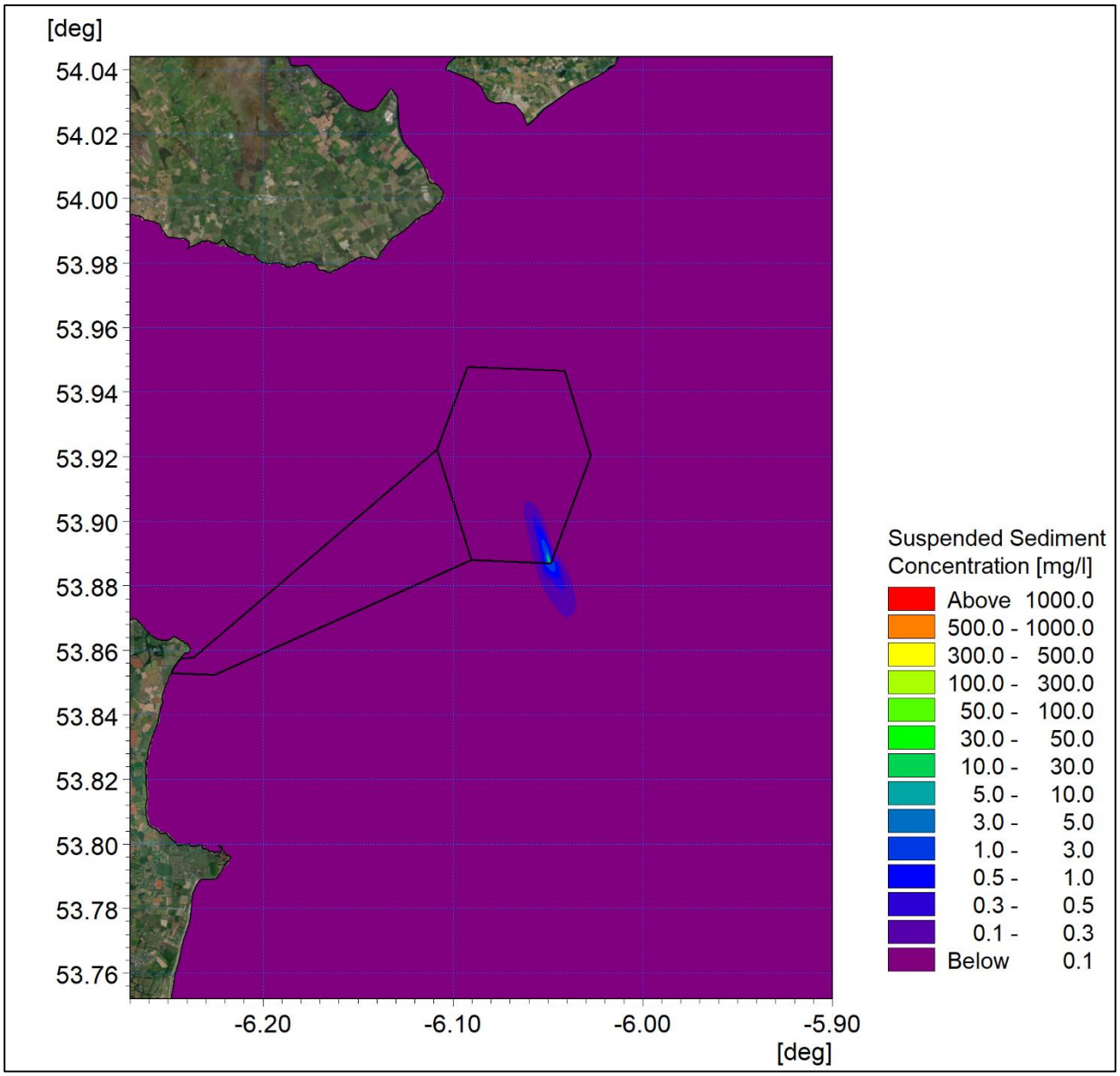

Figure 3A-58: Average suspended sediment concentration at ORI-E04.

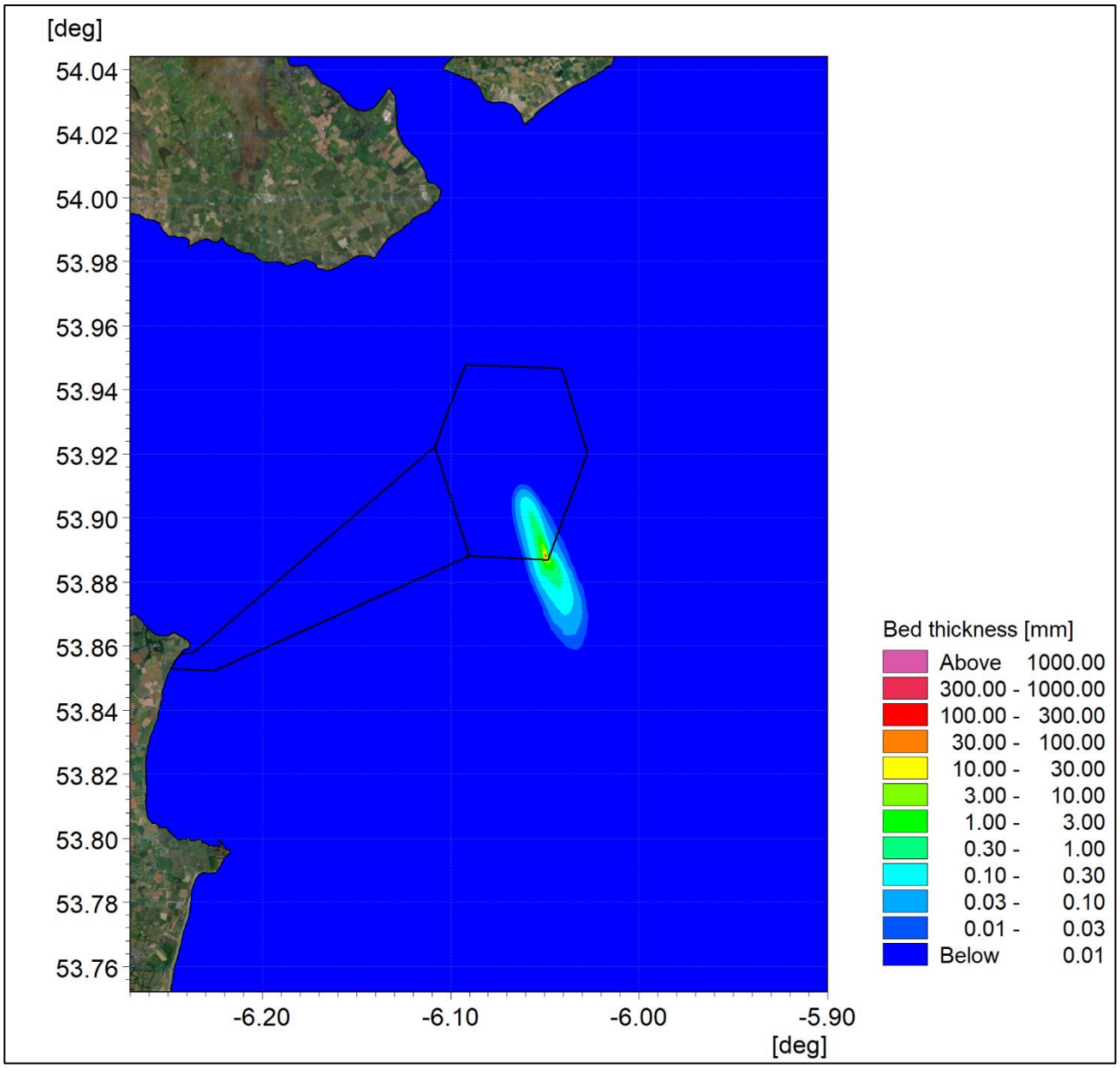

Figure 3A-59: Final sedimentation one day following installation at ORI-E04.

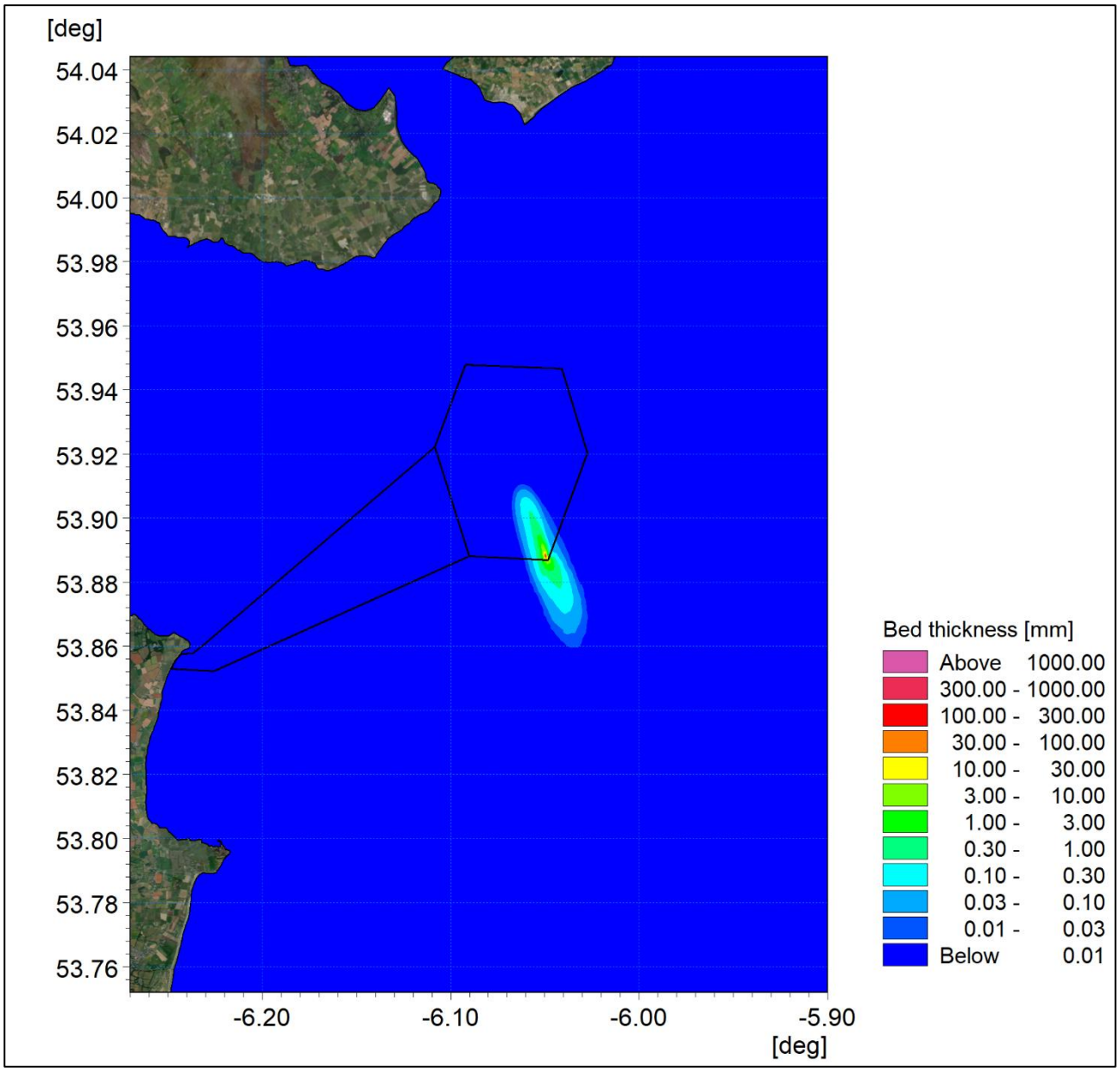

Figure 3A-60: Maximum sedimentation at ORI-E04.

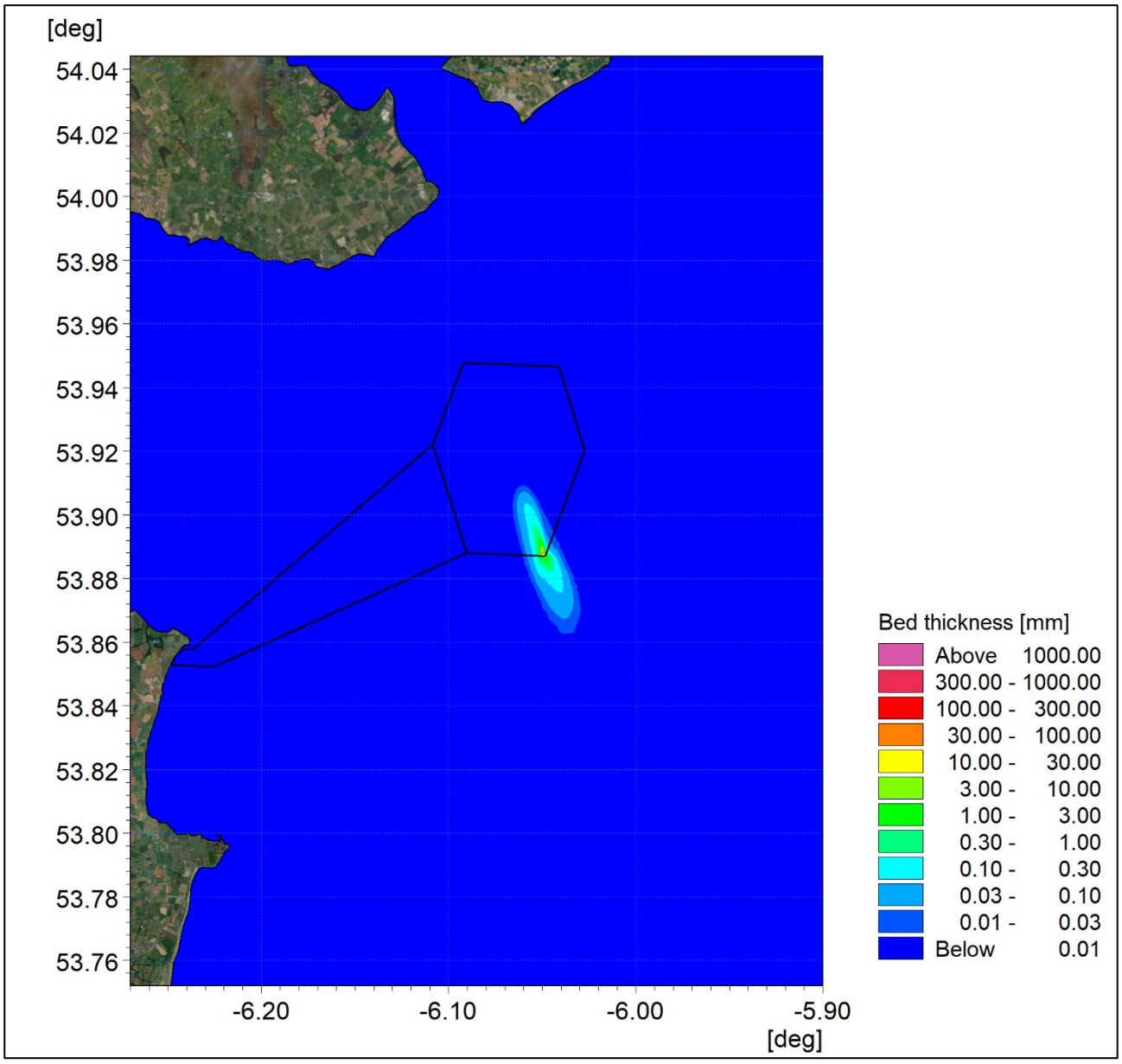

Figure 3A-61: Average sedimentation at ORI-E04.

ORI-D05

ORI-D05 is the most easterly Wind Turbine Generator (WTG) and experiences current speeds of similar magnitude to ORI-D05. The maximum and average sediment plumes presented Figure 3A-62 and Figure 3A-63 respectively are therefore of similar magnitude and spatial extent with typical average suspended sediment levels being less than 5 mg/l.

As with the previous location settlement would be imperceptible from the background activity with sedimentation depths of fractions of a millimetre beyond a few hundred meters, with the sediment footprint aligned with the bidirectional tidal flow. This is illustrated by Figure 3A-64, Figure 3A-65 and Figure 3A-66 for the final, maximum and average sedimentation results. In each case the settlement of the coarsest material at the auger site is the only notable deposit.

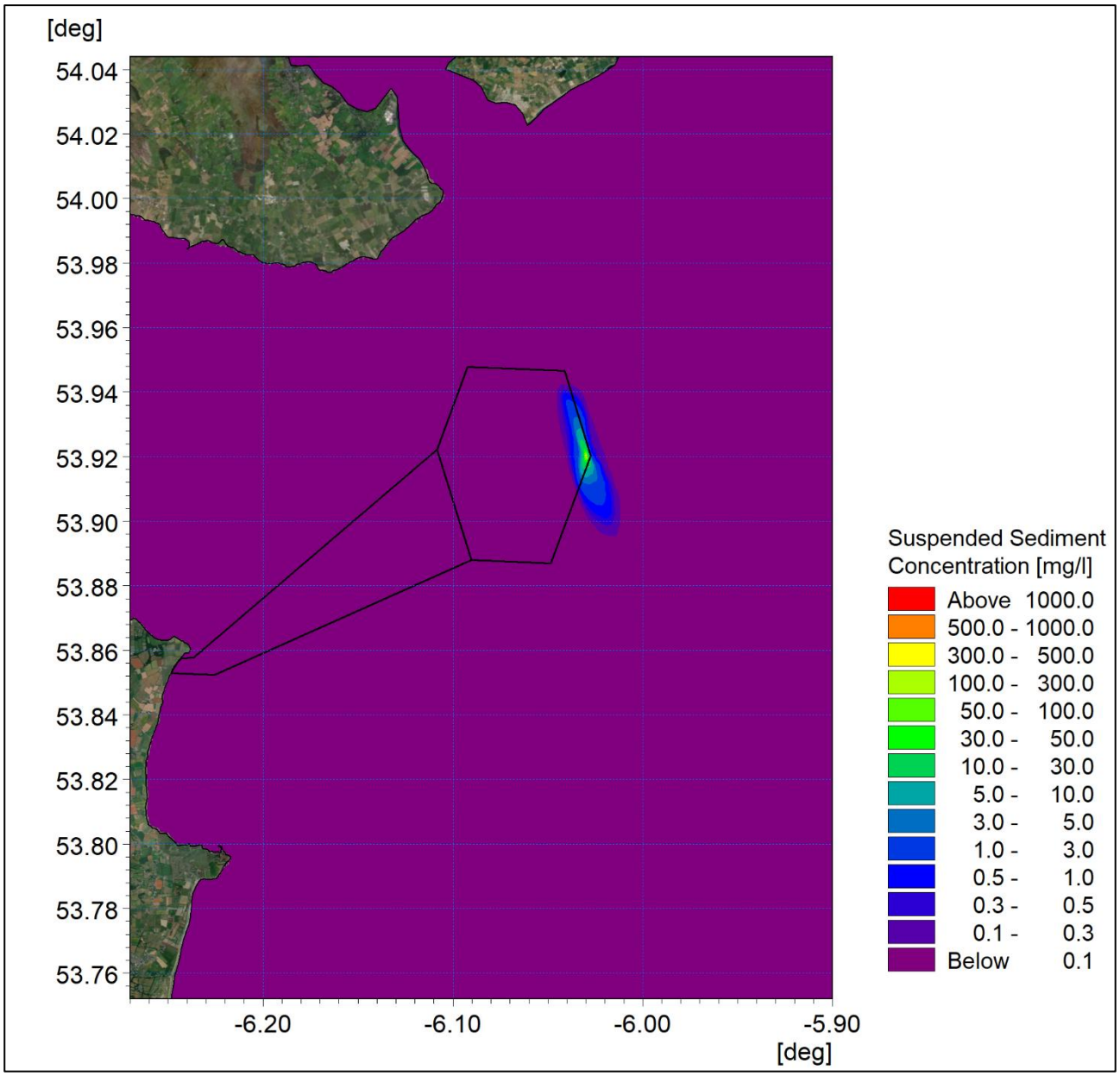

Figure 3A-62: Maximum suspended sediment concentration at ORI-D05.

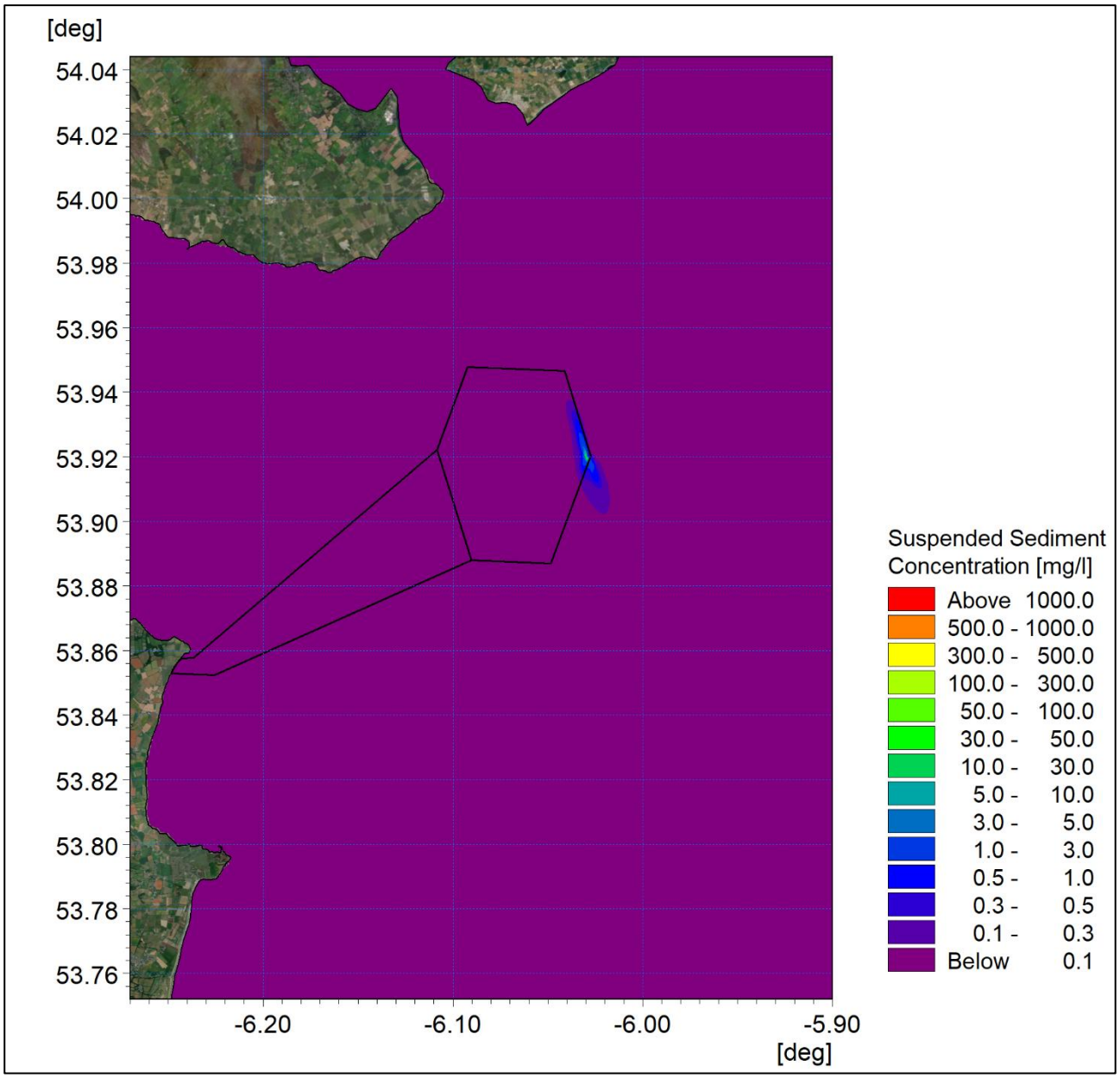

Figure 3A-63: Average suspended sediment concentration at ORI-D05.

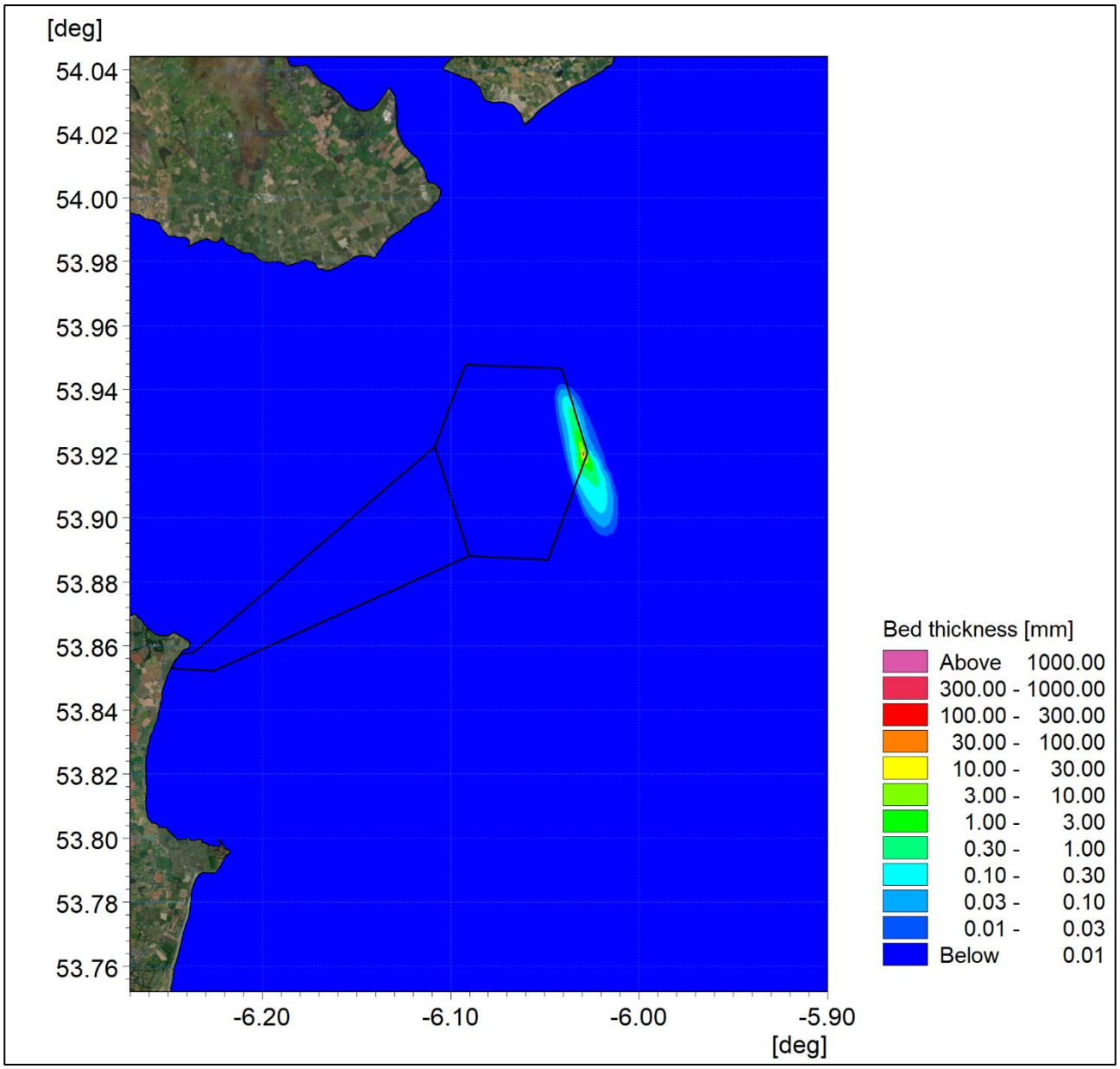

Figure 3A-64: Final sedimentation one day following installation at ORI-D05.

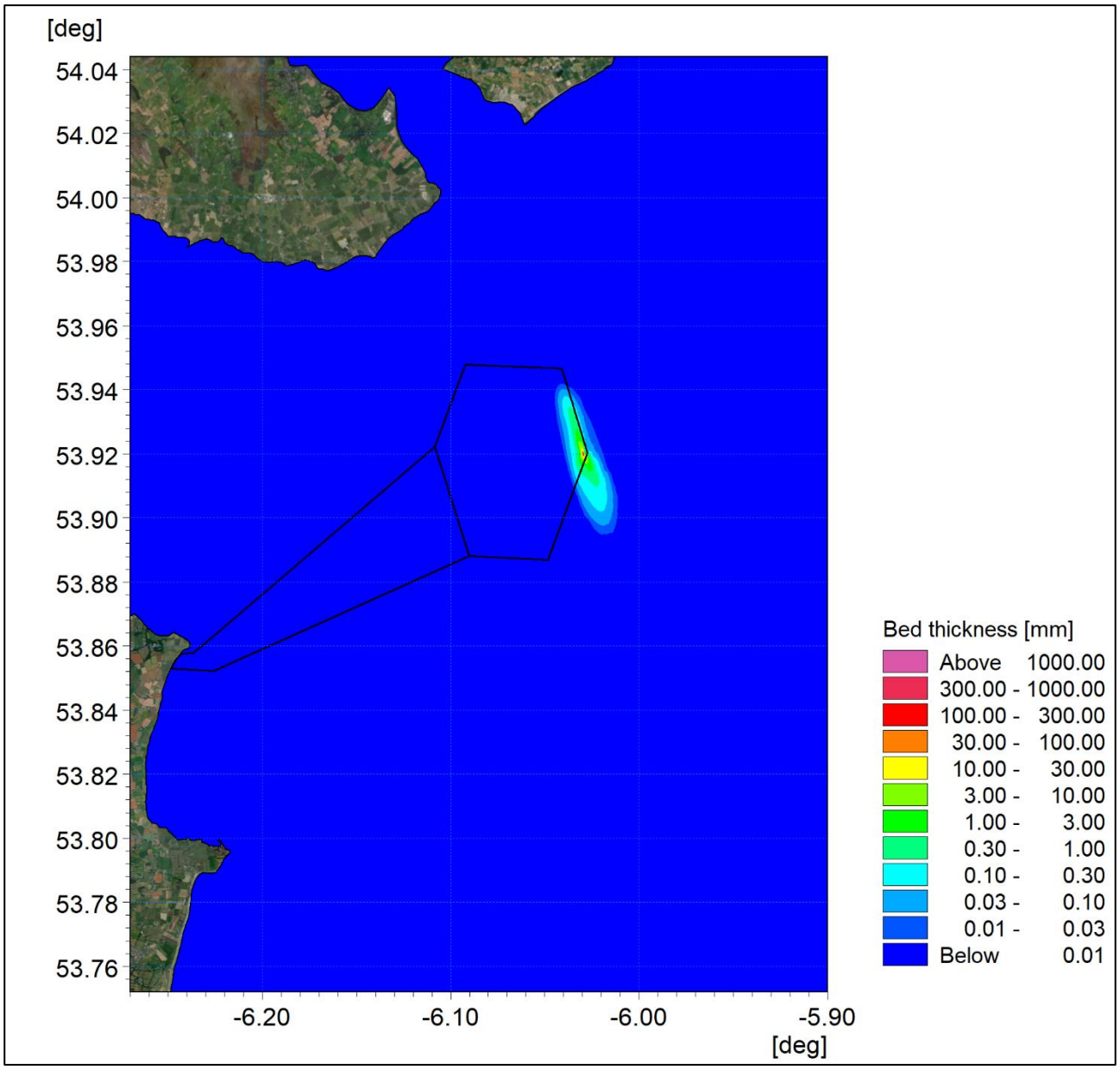

Figure 3A-65: Maximum sedimentation at ORI-D05.

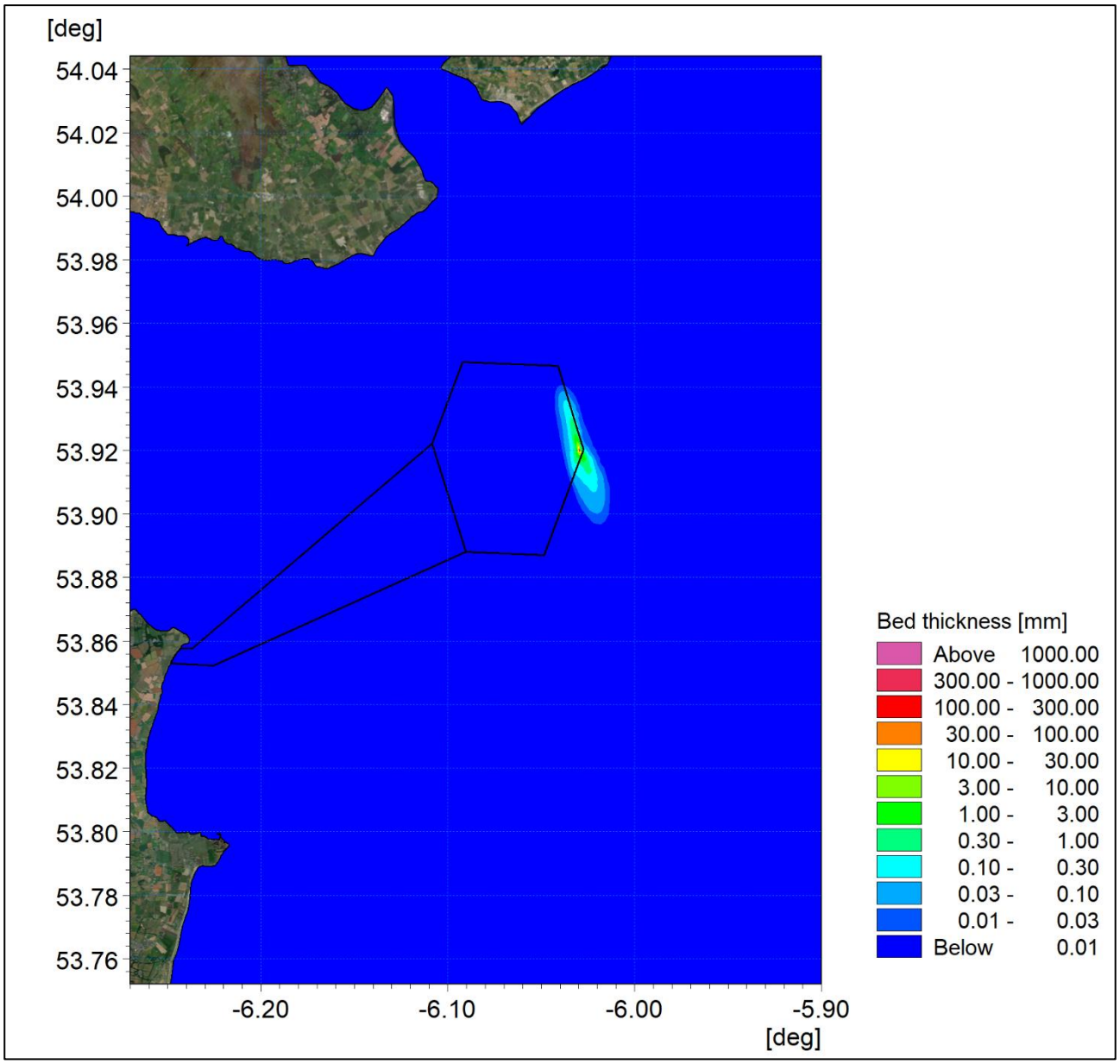

Figure 3A-66: Average sedimentation at ORI-D05.

ORI-E02

ORI-E02 is positioned in the southwest of the offshore wind farm area at a shallow location where the tidal currents are lower, therefore the initial concentrations would be larger than those for the deeper sites. Figure 3A-67 and Figure 3A-68 shows the maximum and average concentrations, with plume extents and sediment concentrations being very similar to those associated with ORI-EO4.

Common to the other sites the sedimentation levels are seen to be very limited as Figure 3A-69 to Figure 3A-71 demonstrate for the range of sediment parameters.

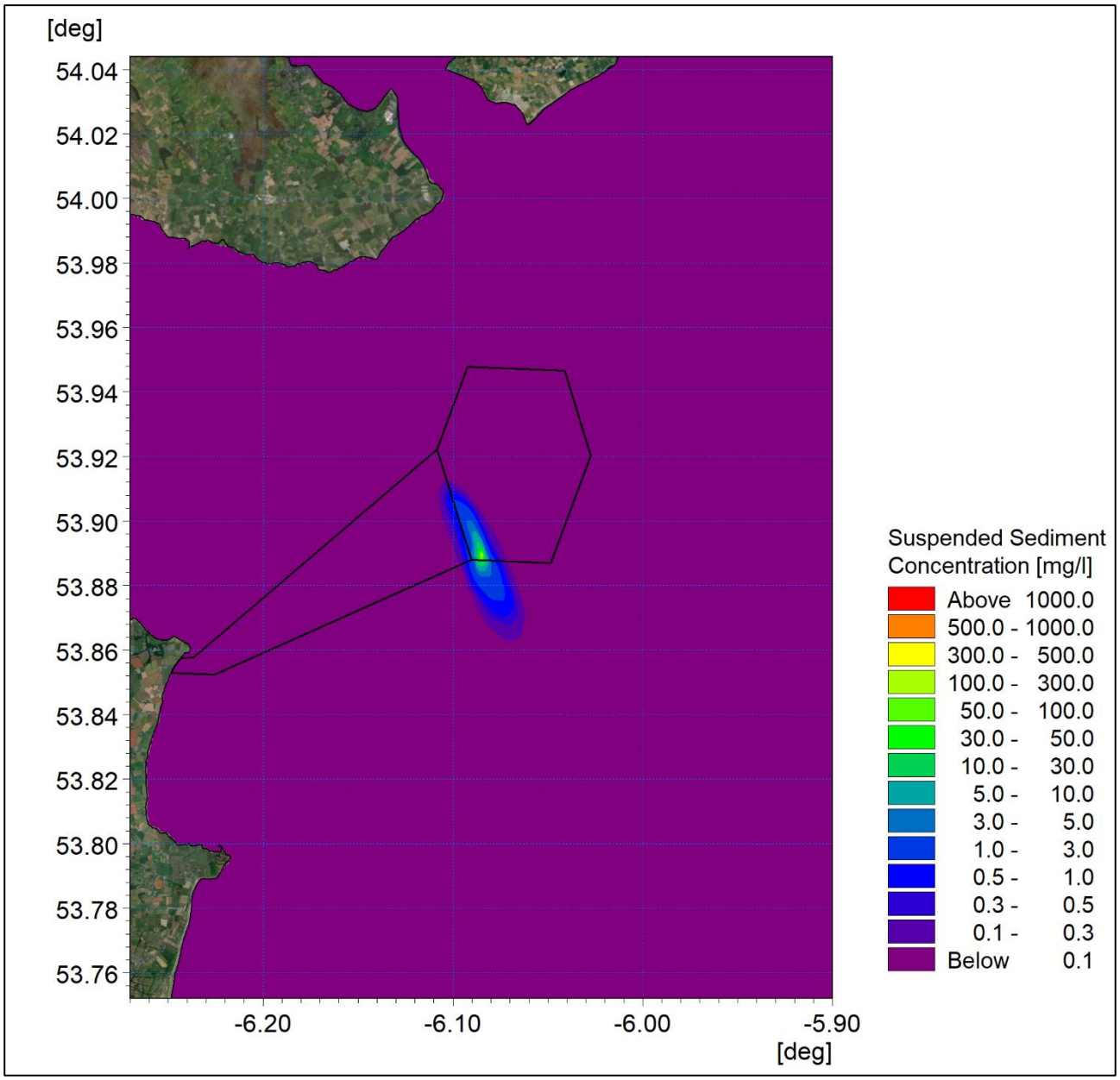

Figure 3A-67: Maximum suspended sediment concentration at ORI-E02.

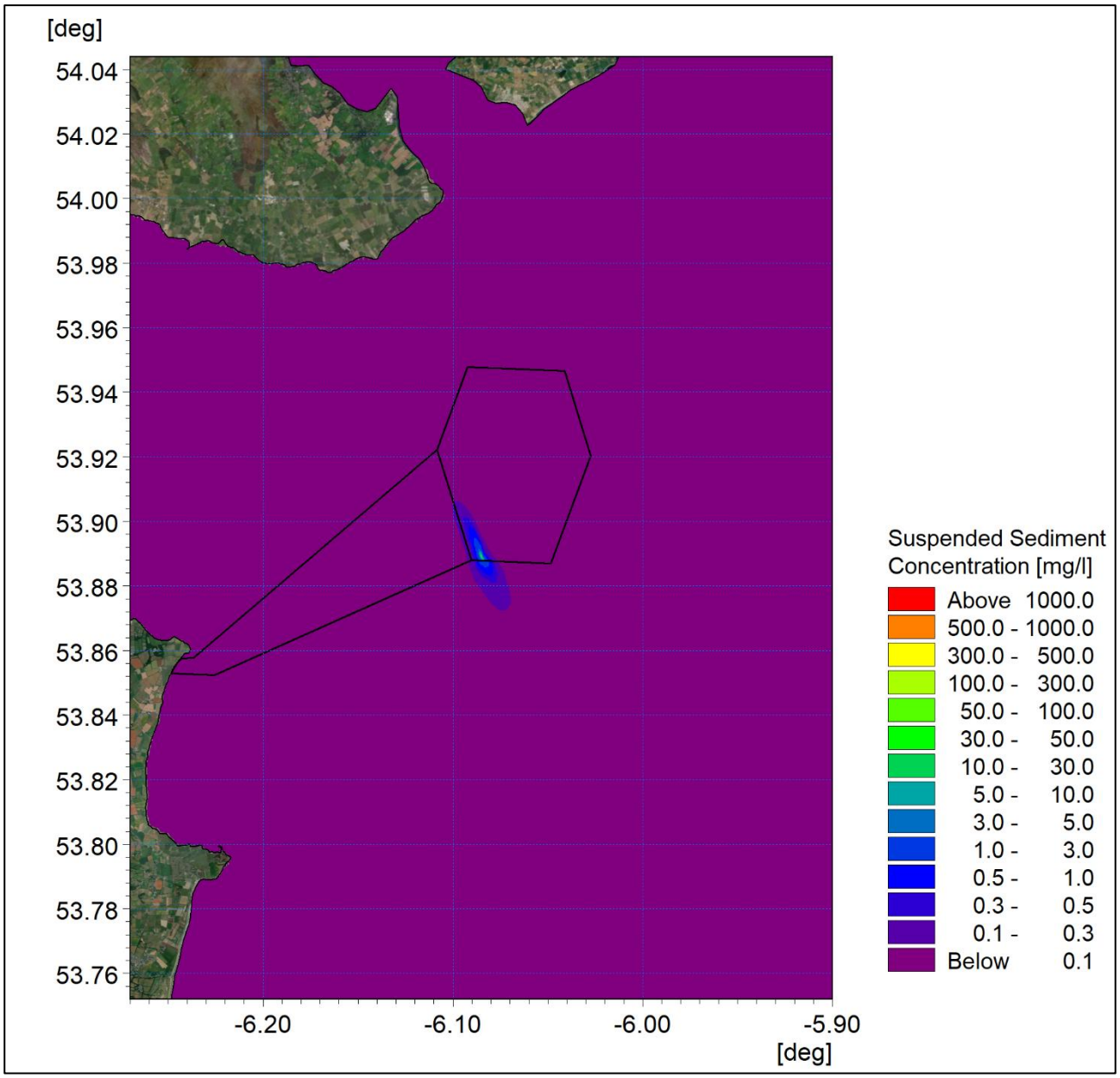

Figure 3A-68: Average suspended sediment concentration at ORI-E02.

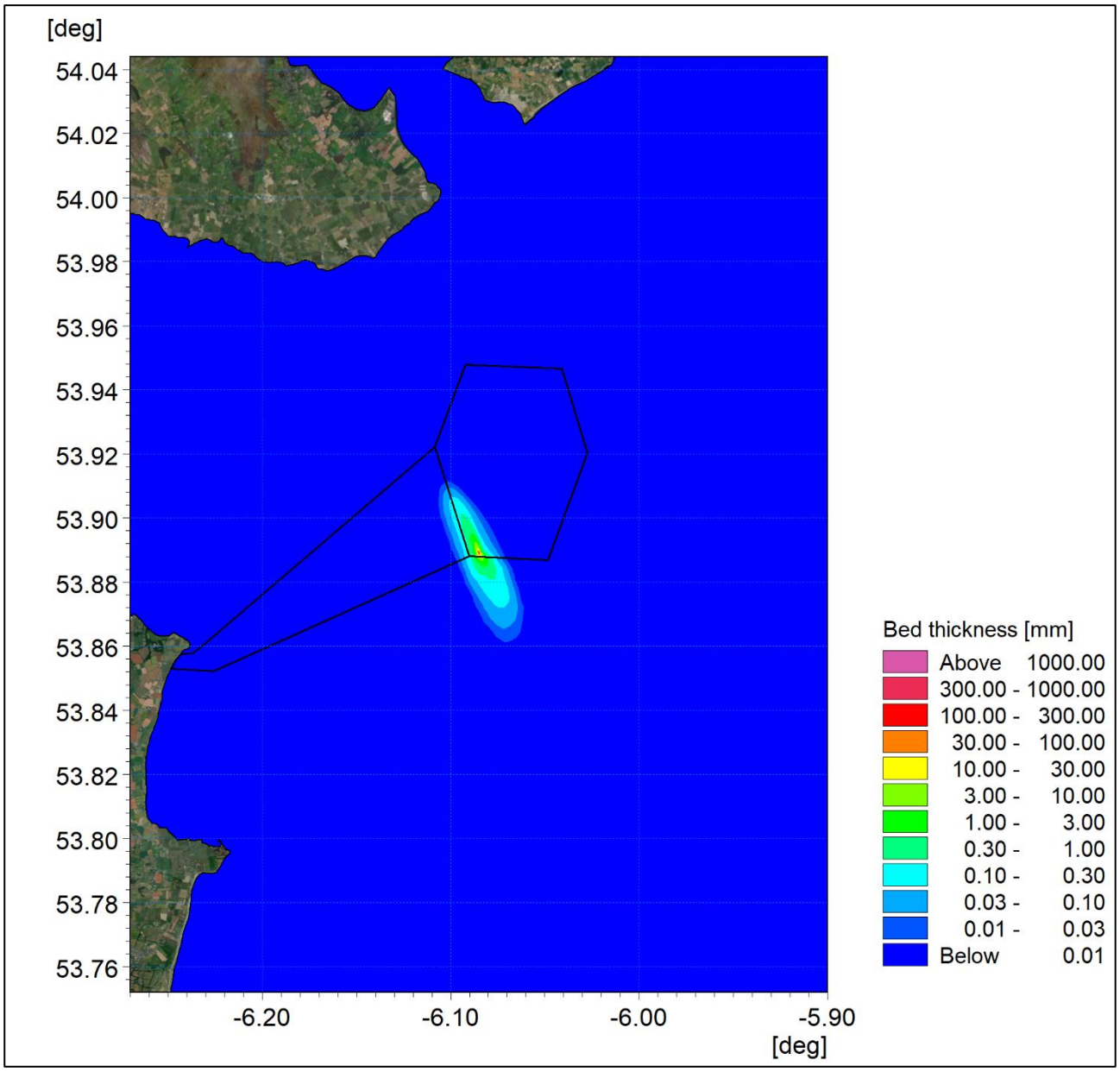

Figure 3A-69: Final sedimentation one day following installation at ORI-E02.

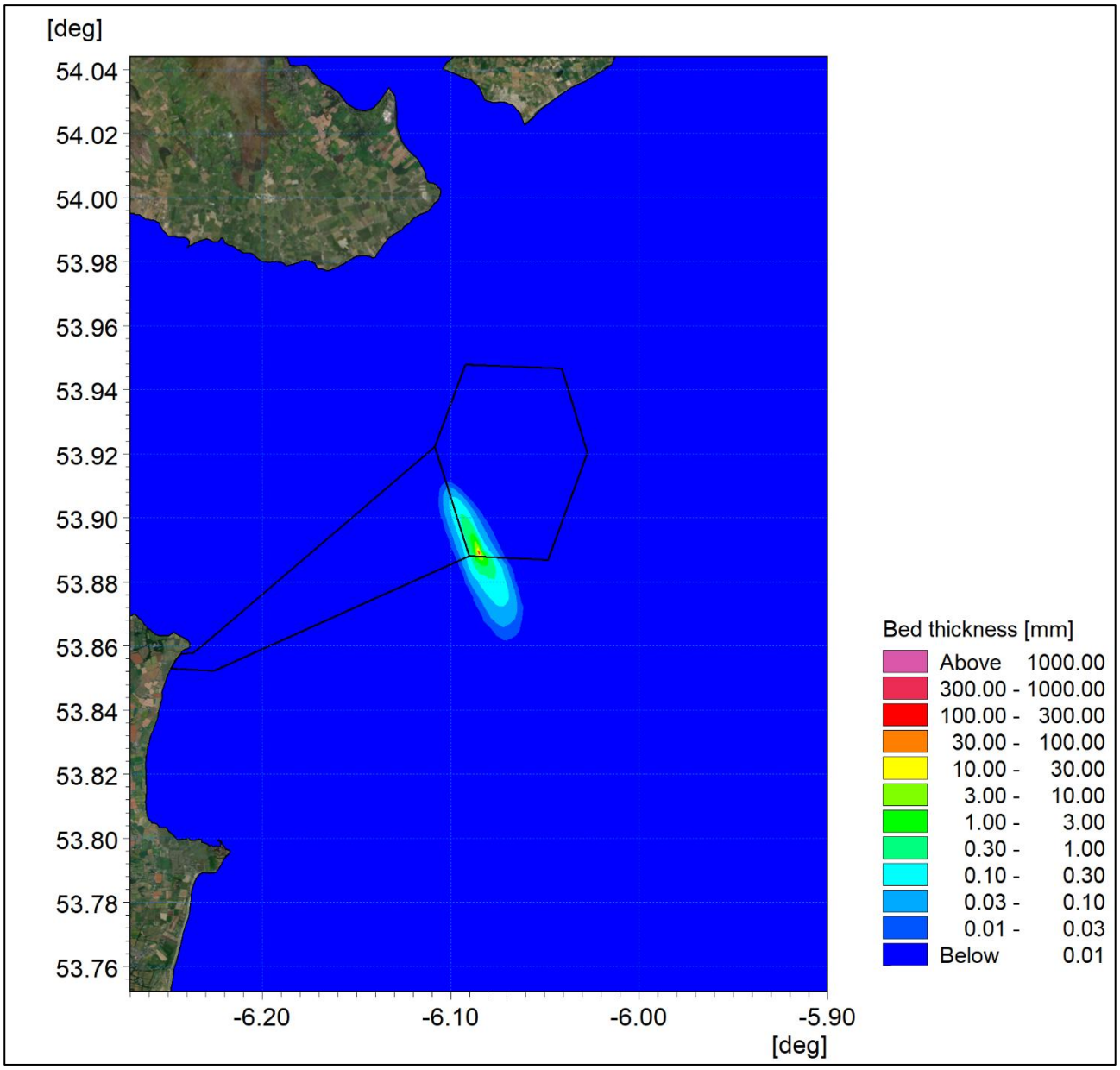

Figure 3A-70: Maximum sedimentation at ORI-E02.

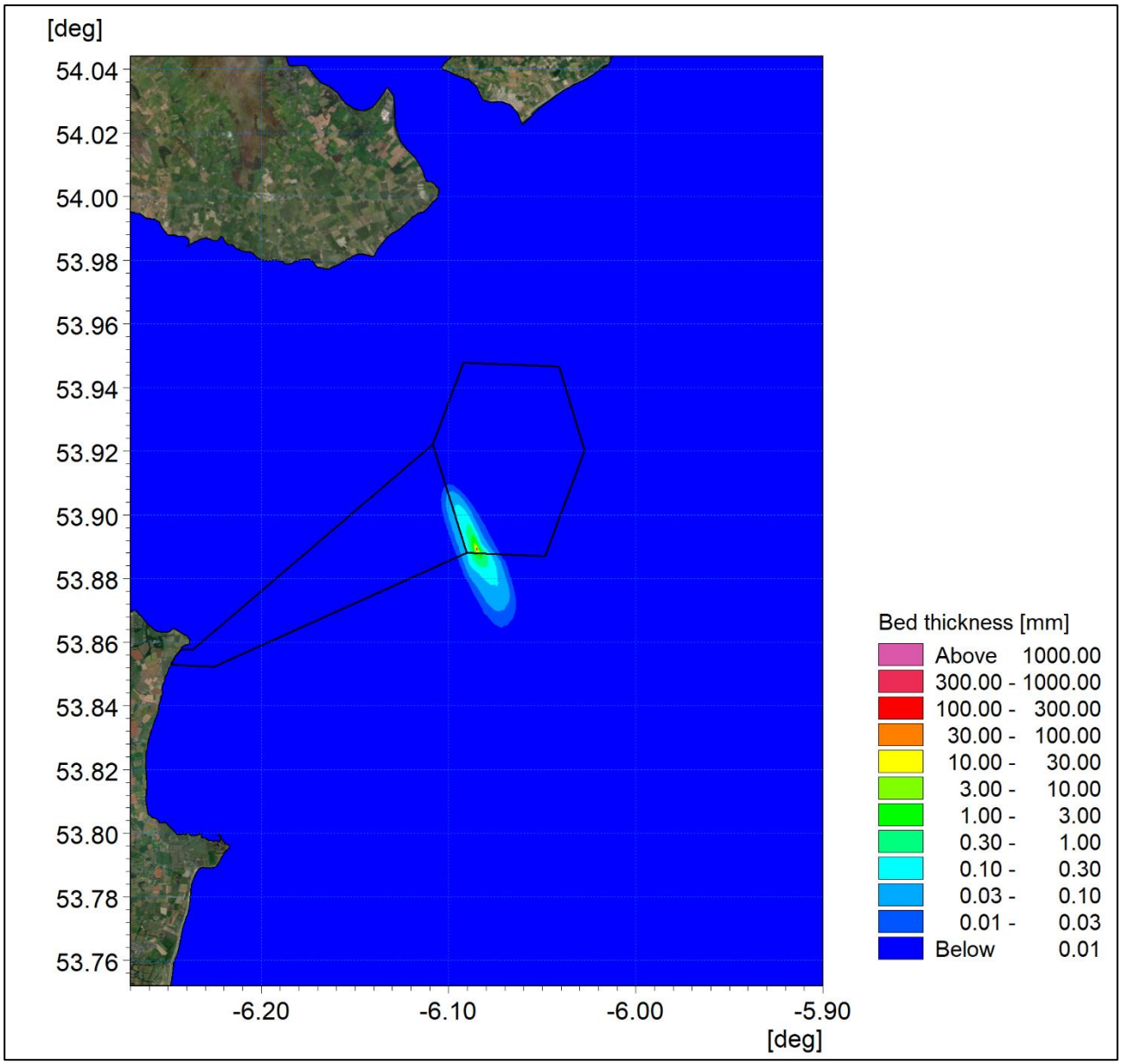

Figure 3A-71: Average sedimentation at ORI-E02.

ORI-A01

ORI-A01 is located at the shallowest location within the offshore wind farm area. Figure 3A-72 and Figure 3A-73 show the maximum and average concentrations, it can be seen that the maximum sediment concentrations are up to 300 mg/l whilst typical concentrations are 1.5 mg/l.

The sedimentation footprint at this site is more discrete due to the more limited water depth, with sedimentation depths of 1 mm extending circa 1 km in each direction along the tidal axis as shown in Figure 3A-74, again there is little variation from the maximum deposition depths in Figure 3A-75. The average depths shown in Figure 3A-76 indicates the gradual deposition over the course of the drilling operation.

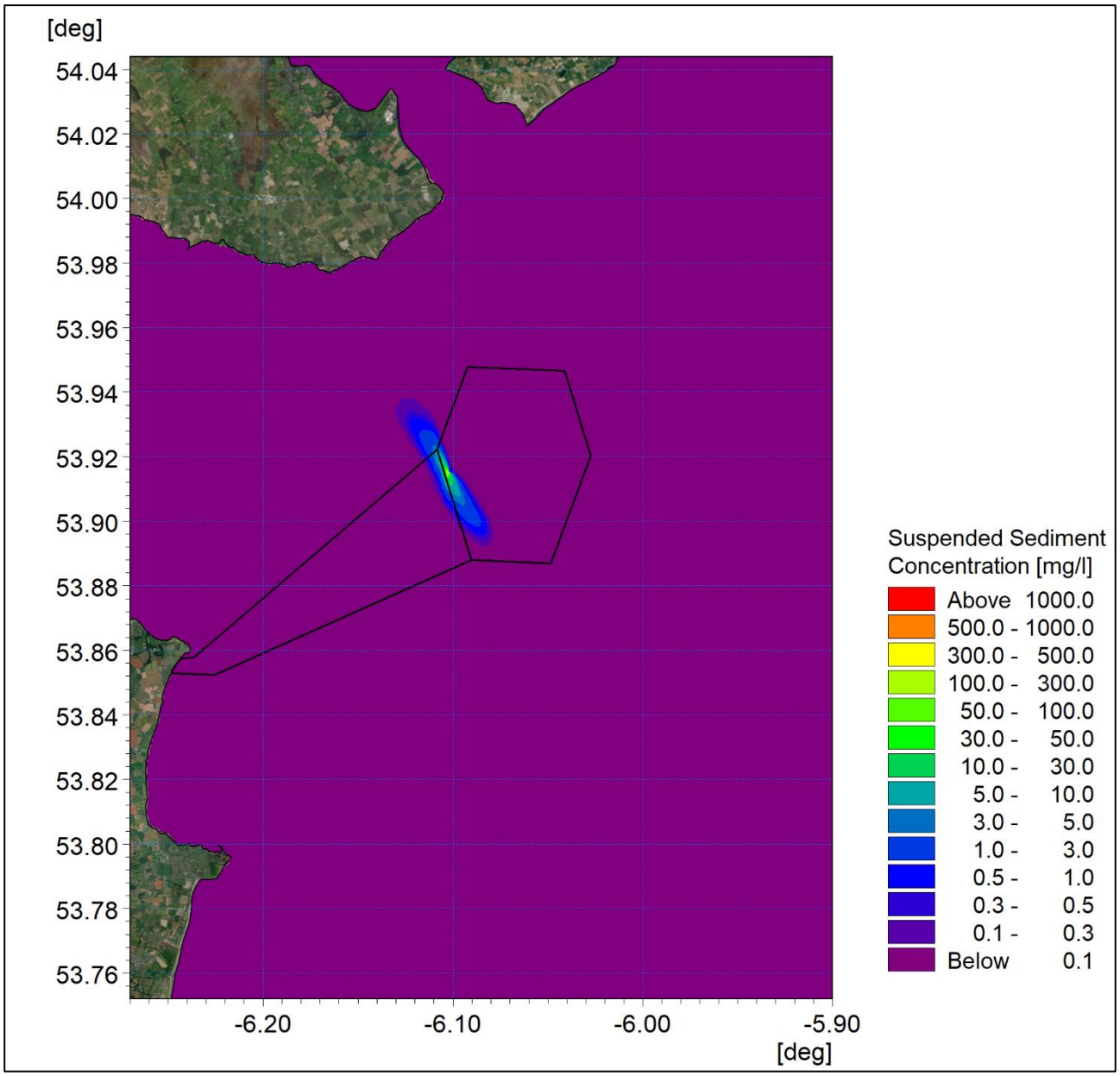

Figure 3A-72: Maximum suspended sediment concentration at ORI-A01.

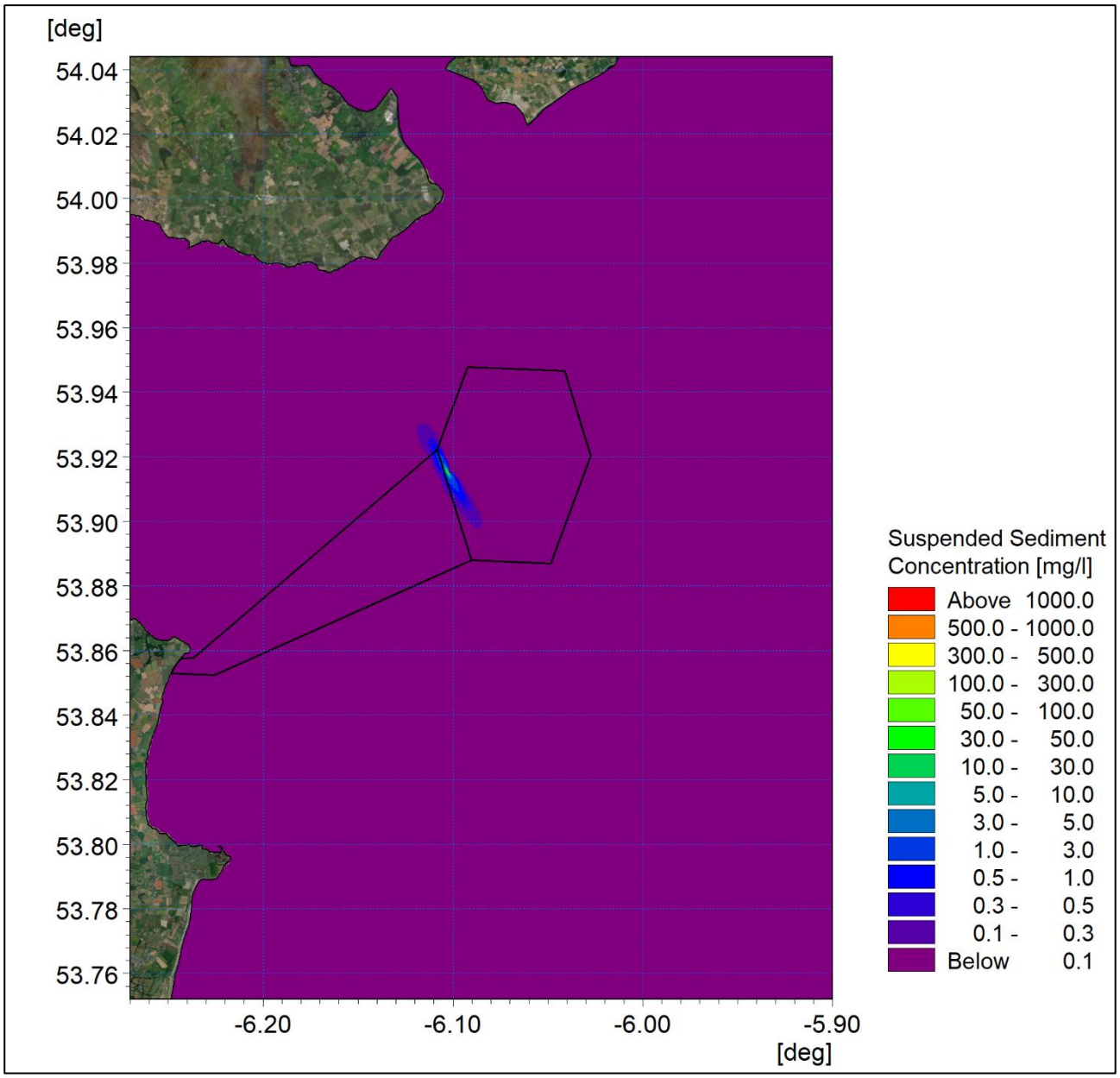

Figure 3A-73: Average suspended sediment concentration at ORI-A01.

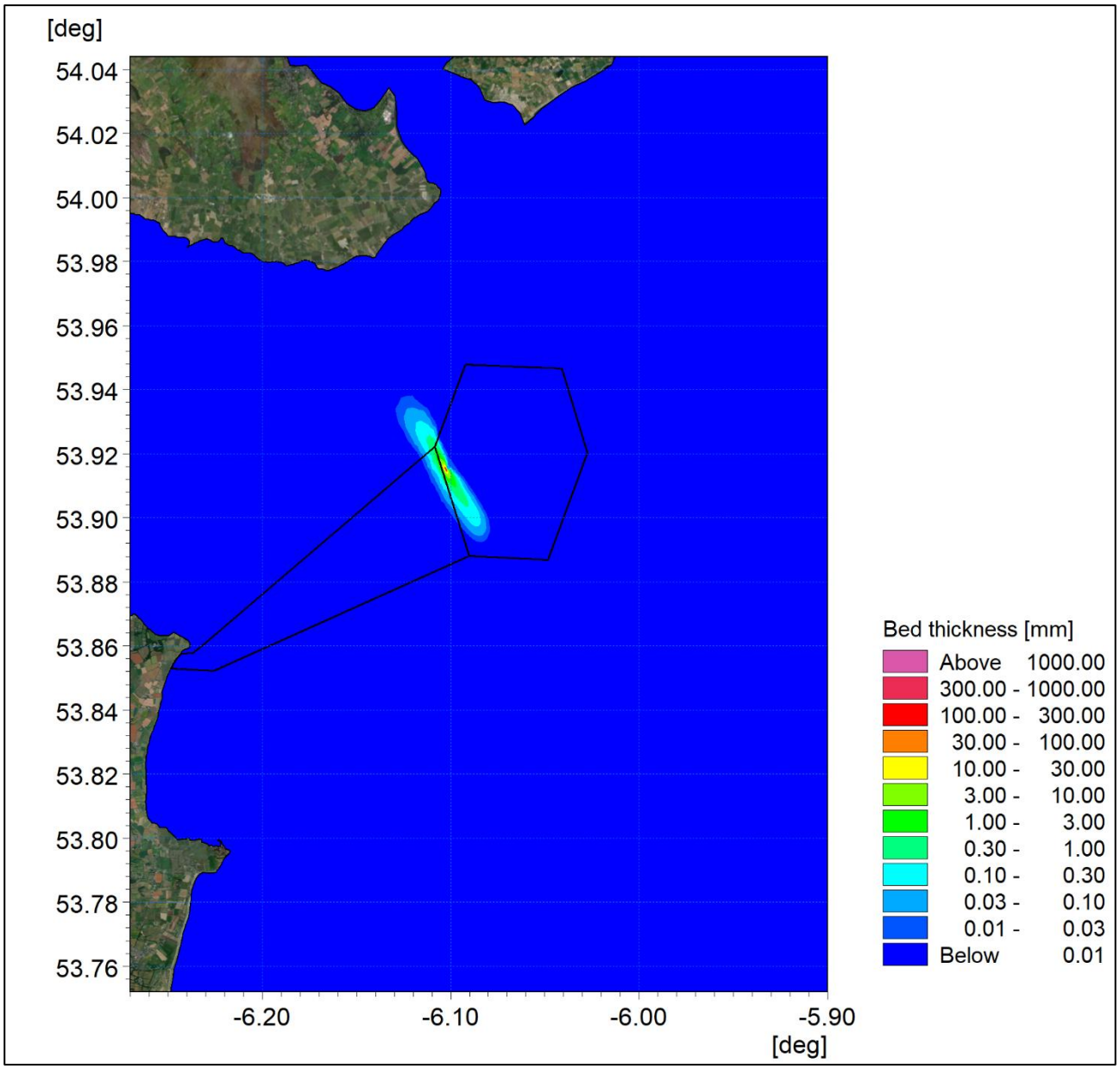

Figure 3A-74: Final sedimentation one day following installation at ORI- A01.

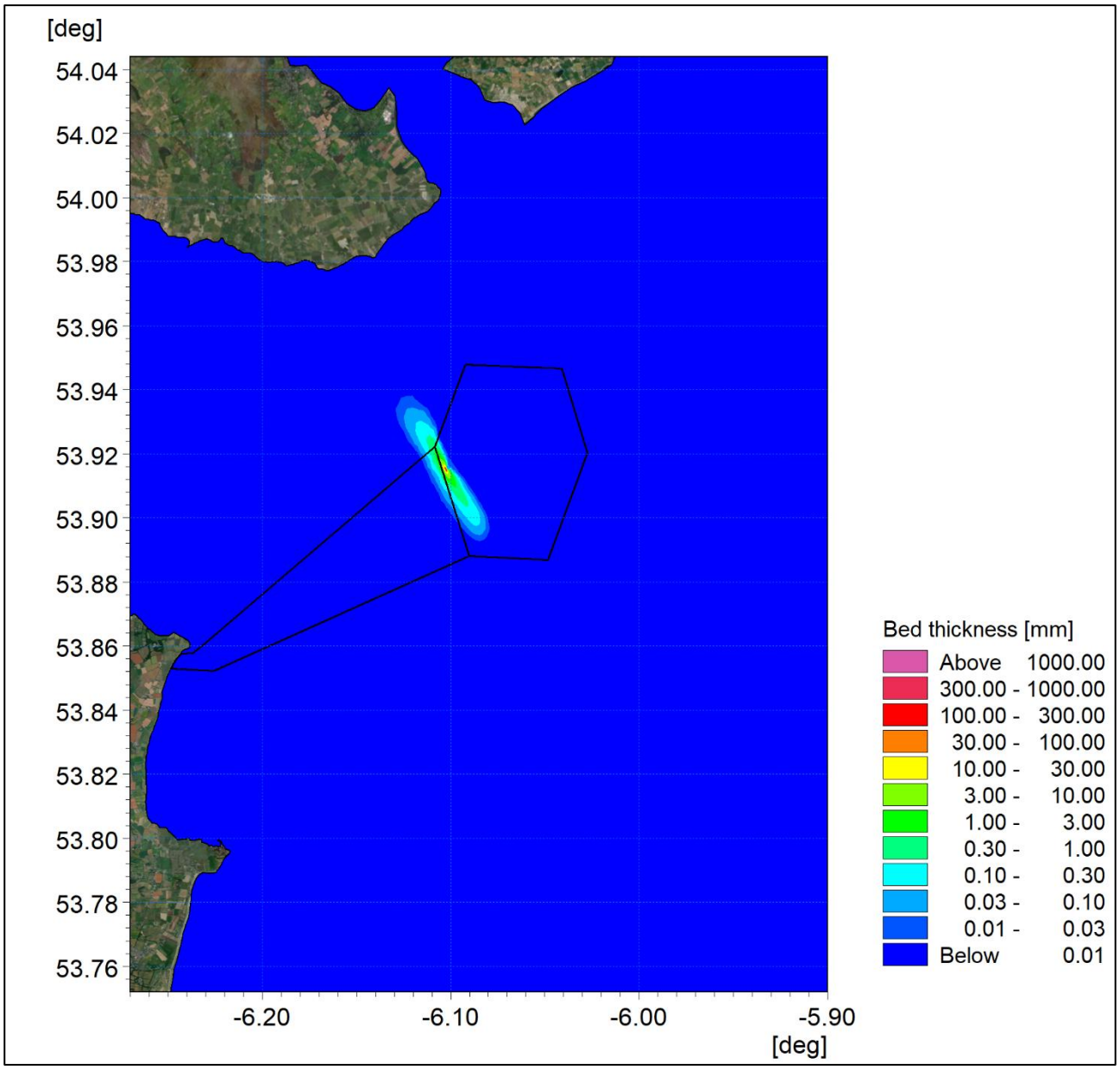

Figure 3A-75: Maximum sedimentation at ORI- A01.

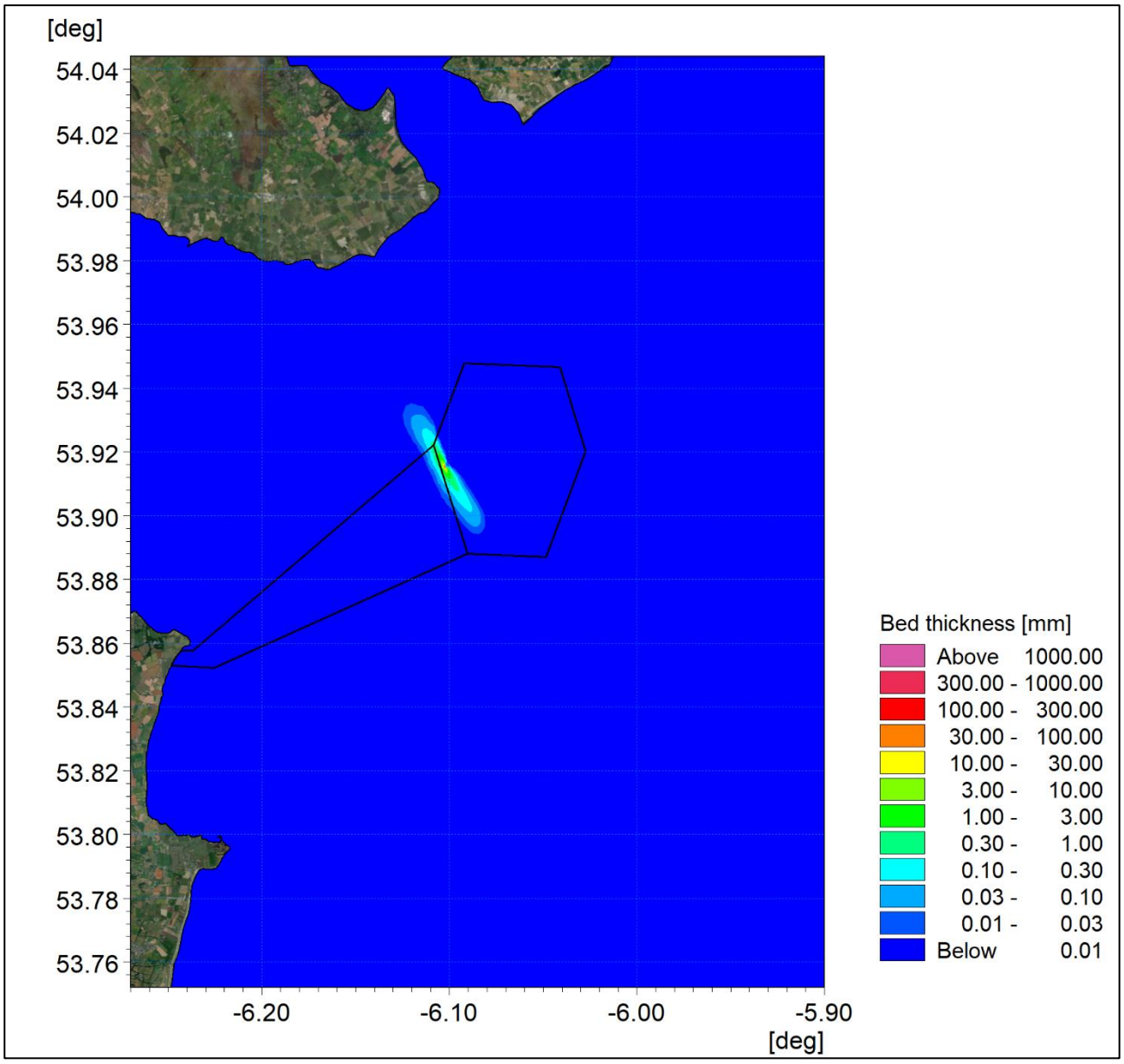

Figure 3A-76: Average sedimentation at ORI- A01.

ORI-A04

ORI-A04 is located at the northwest of the offshore wind farm area. This site presents the widest plume due to the circulatory nature of currents, this corresponds with higher levels of dispersion with peak concentrations reducing to <1mg/l at limited distance from the drilling operation, Figure 3A-77. Again, average values, shown in Figure 3A-78, are approximately an order of magnitude smaller than the maximum values.

For completeness the sedimentation data is presented in Figure 3A-79 and Figure 3A-80 for the final and maximum levels respectively, whilst Figure 3A-81 shows the average value throughout the drilling campaign. This again demonstrates that deposition depths are predicted to be fractions of a millimetre beyond the immediate vicinity of the drilling operation.

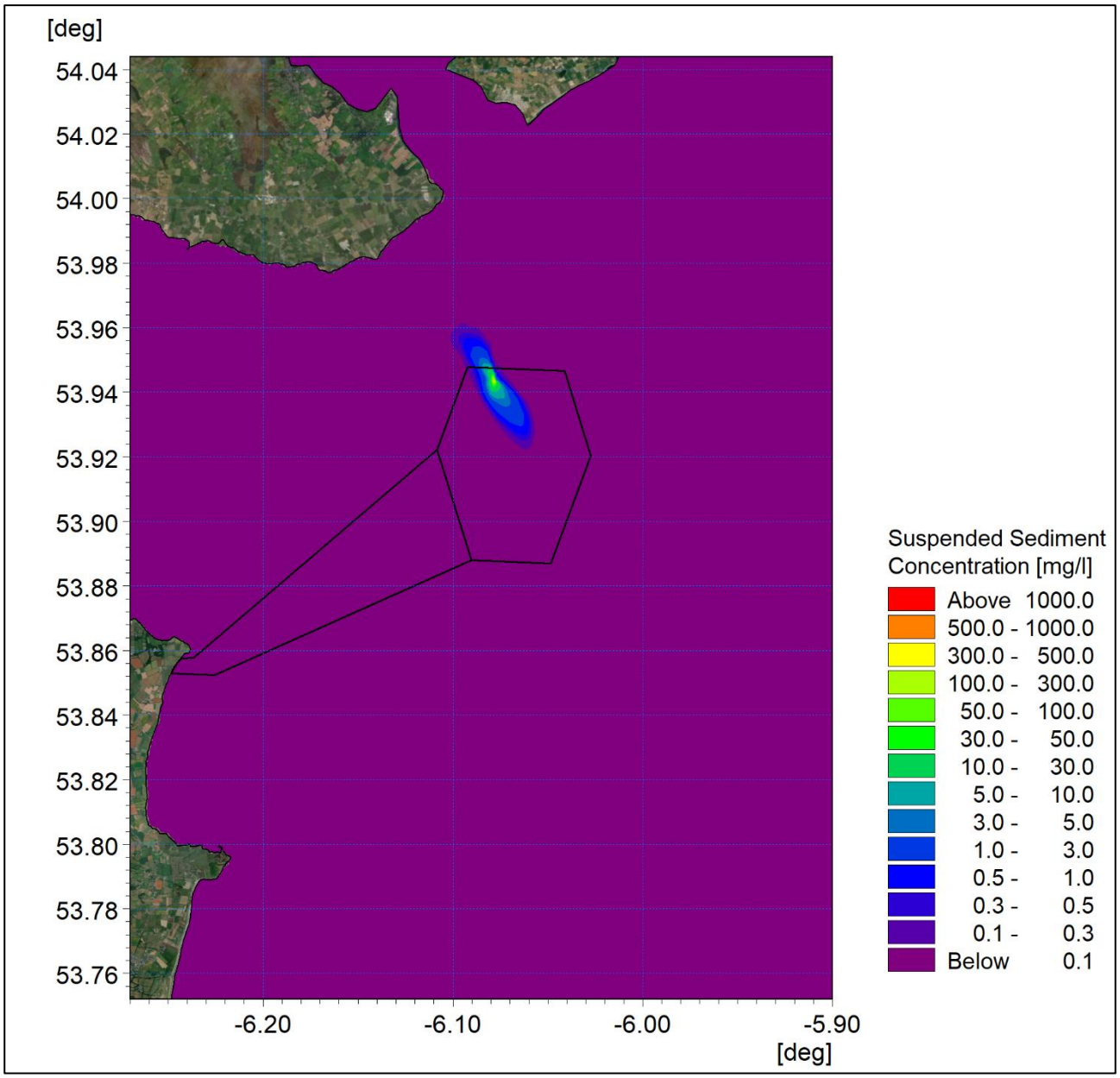

Figure 3A-77: Maximum suspended sediment concentration at ORI-A04.

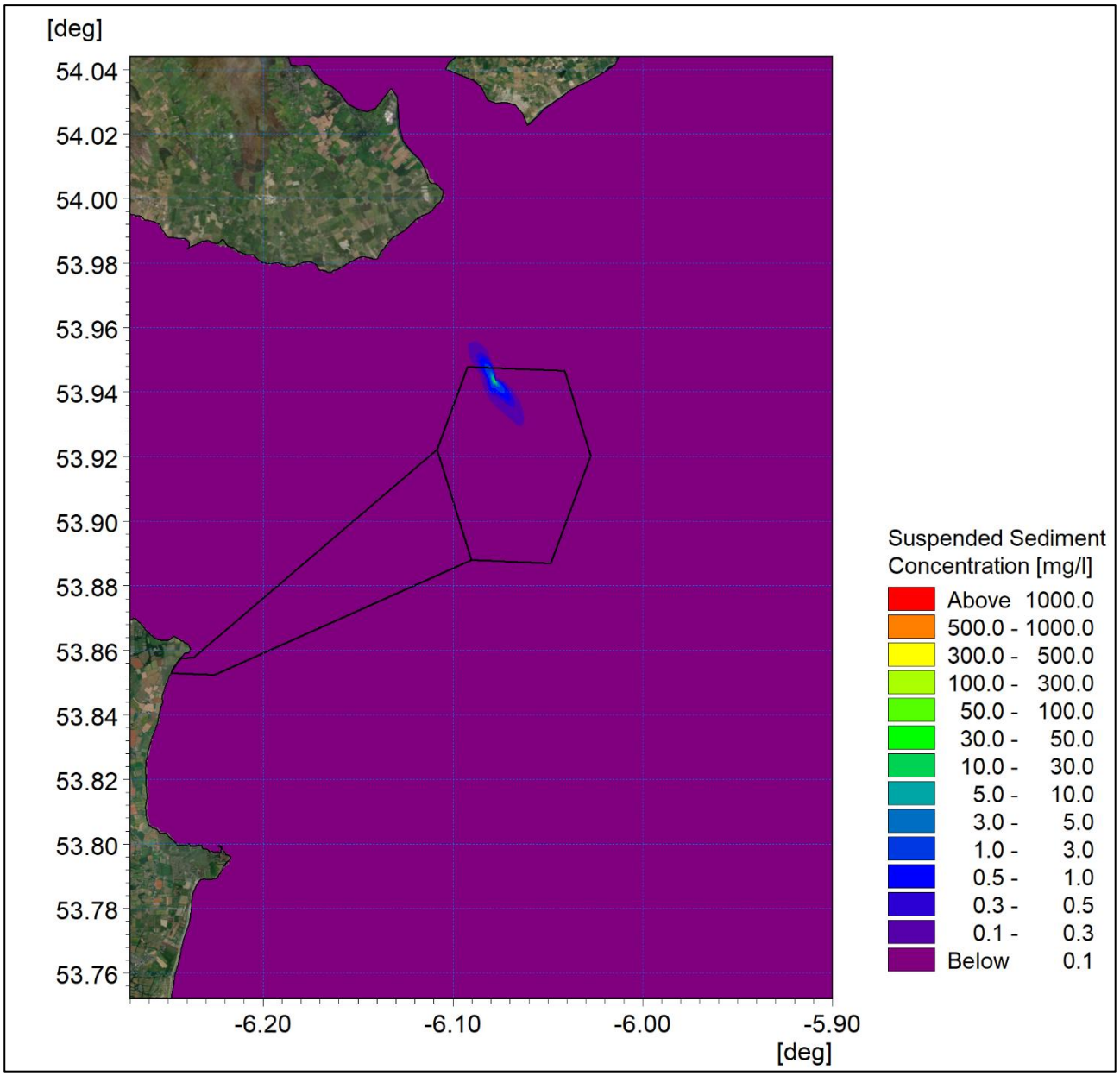

Figure 3A-78: Average suspended sediment concentration at ORI- A04.

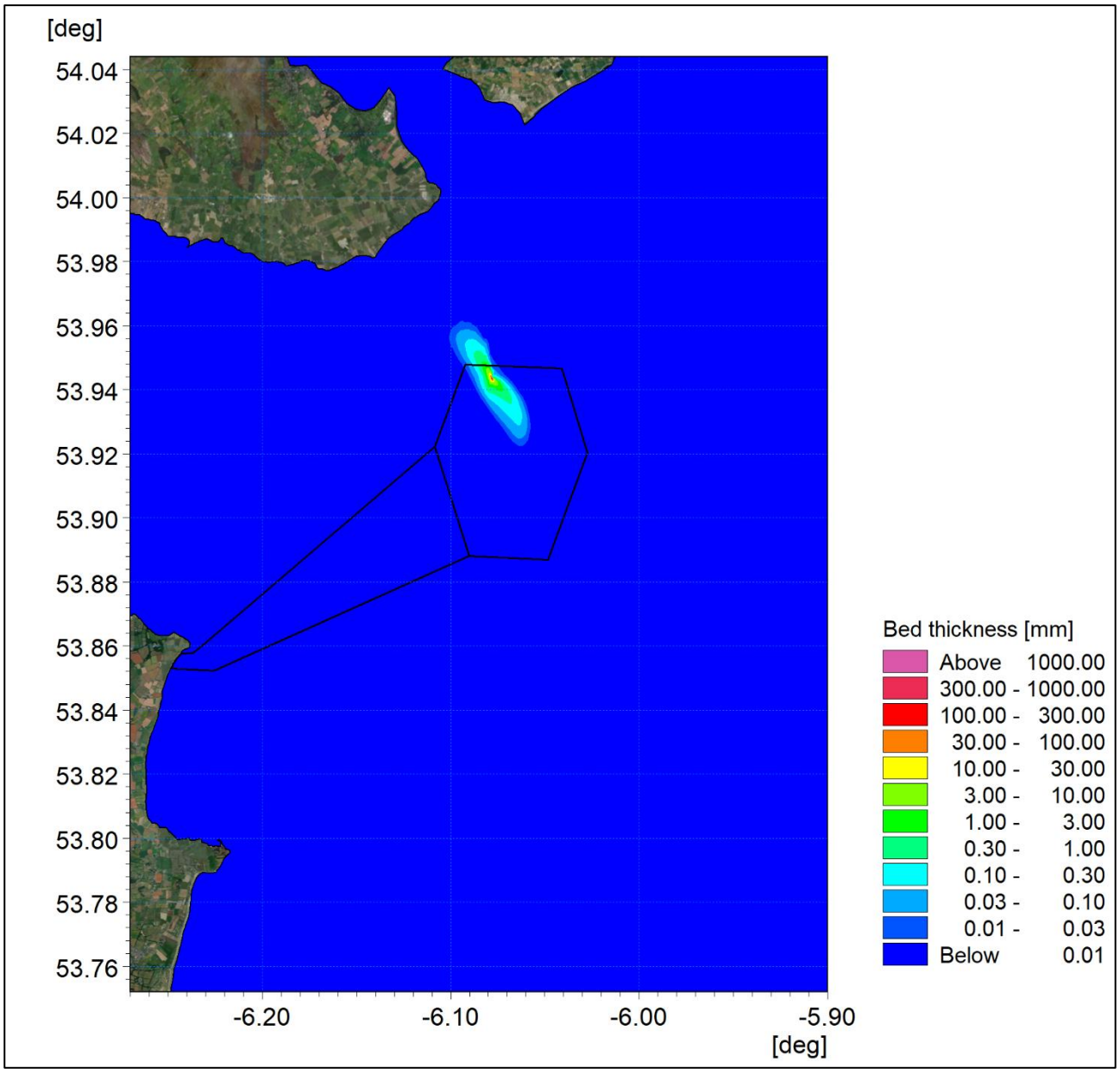

Figure 3A-79: Final sedimentation one day following installation at ORI- A04.

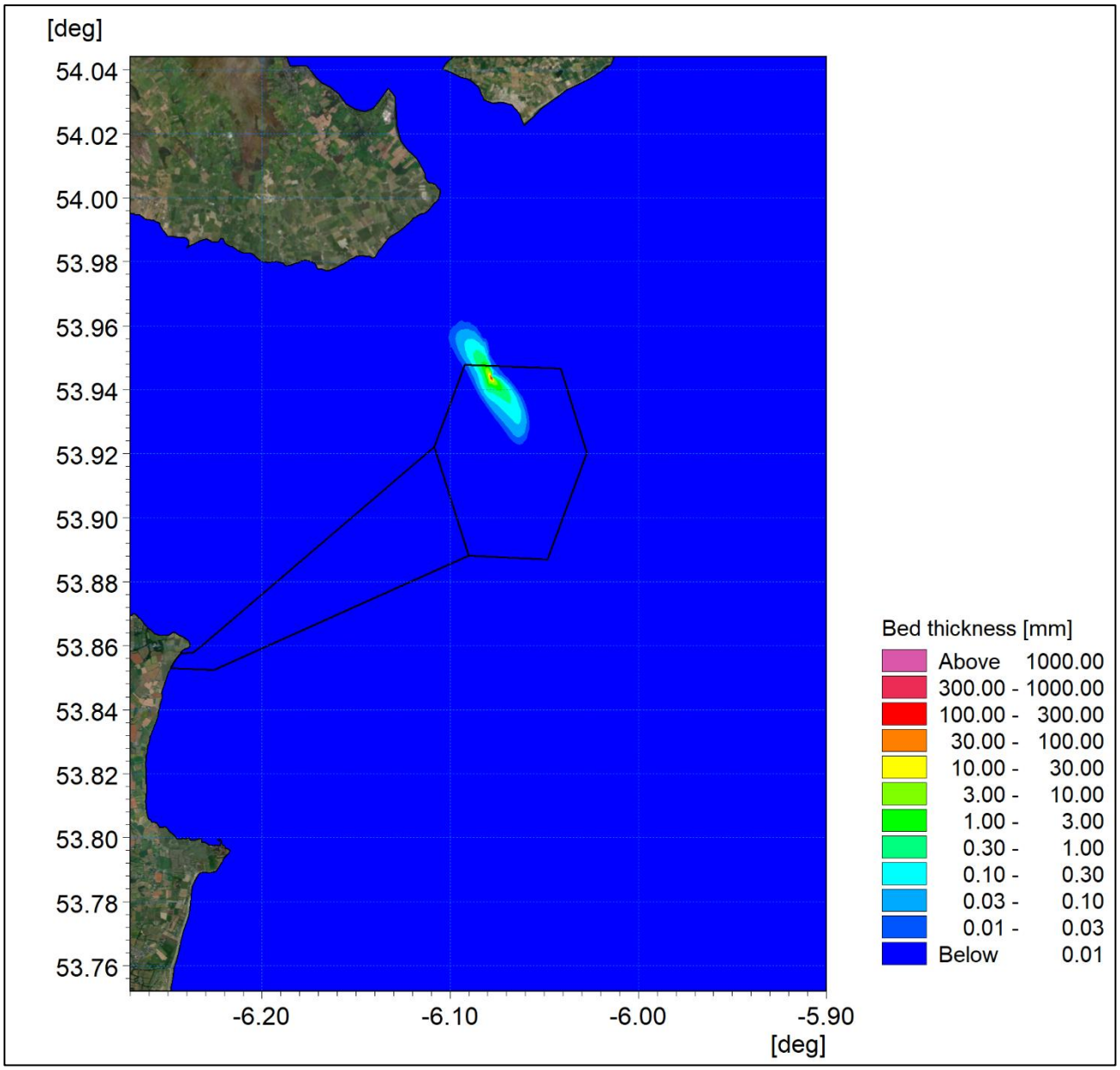

Figure 3A-80: Maximum sedimentation at ORI- A04.

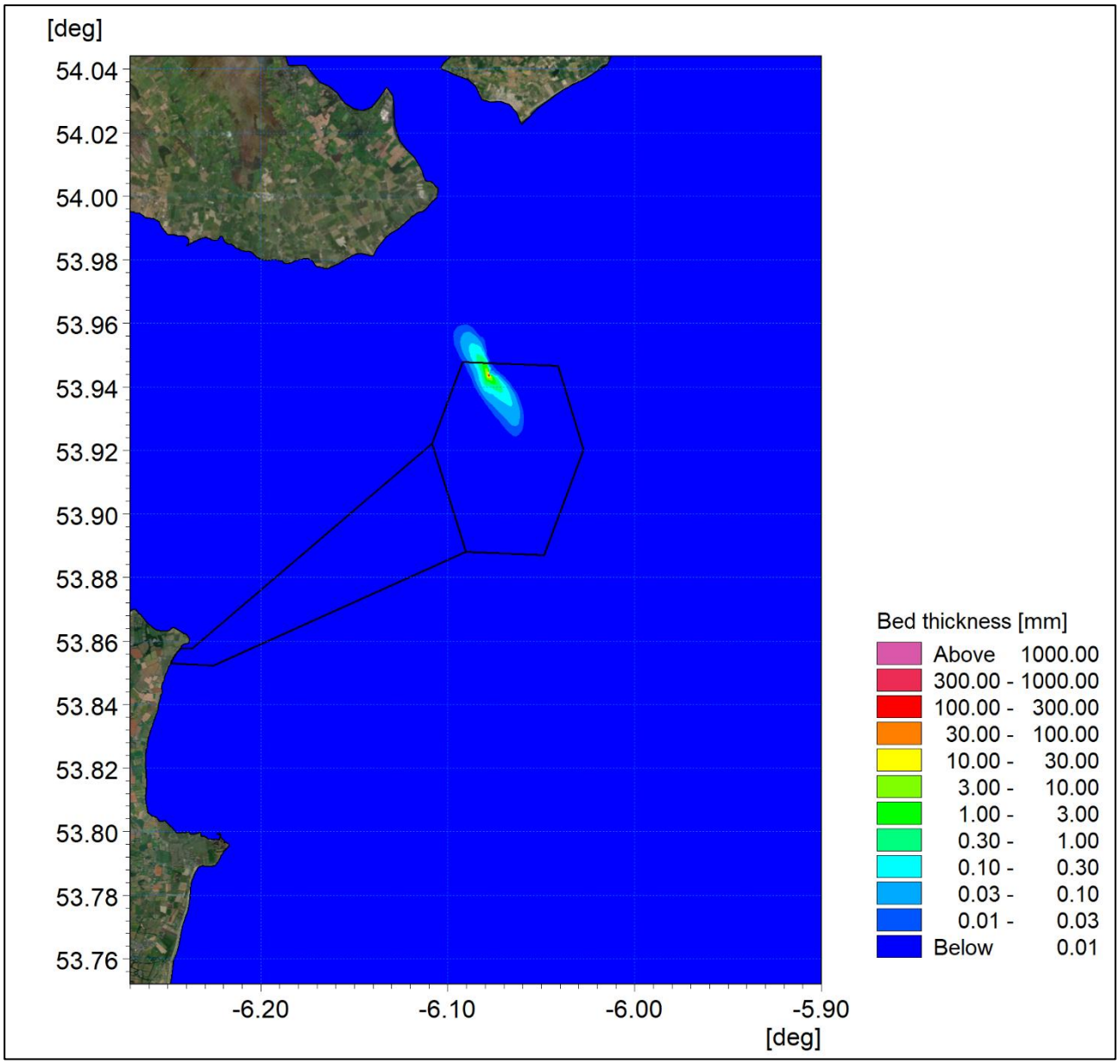

Figure 3A-81: Average sedimentation at ORI- A04.

ORI-B05

The final drill site modelled was ORI-B05 which is located at the northeast of the offshore wind farm area. As anticipated, the shape and magnitude of the concentration plumes shown in Figure 3A-82 and Figure 3A-83 lie between that experienced for the ORI-A04 and ORI-D05 sites and demonstrates the relatively homogeneous nature of the offshore wind farm area.

For completeness the sediment data is presented in Figure 3A-84 and Figure 3A-85 for the final and maximum levels respectively, whilst Figure 3A-86 shows the average value throughout the drilling campaign.

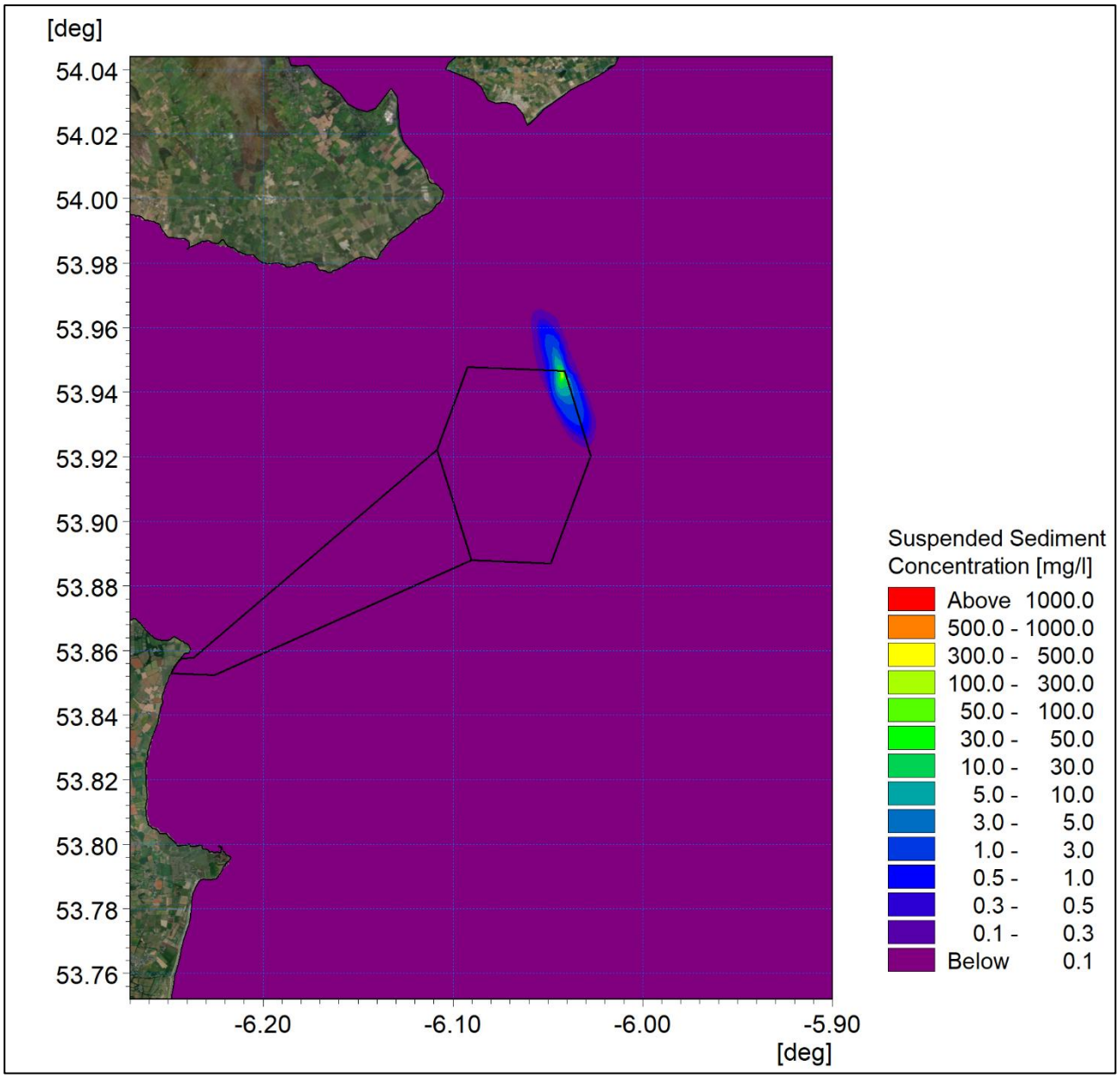

Figure 3A-82: Maximum suspended sediment concentration at ORI-B05.

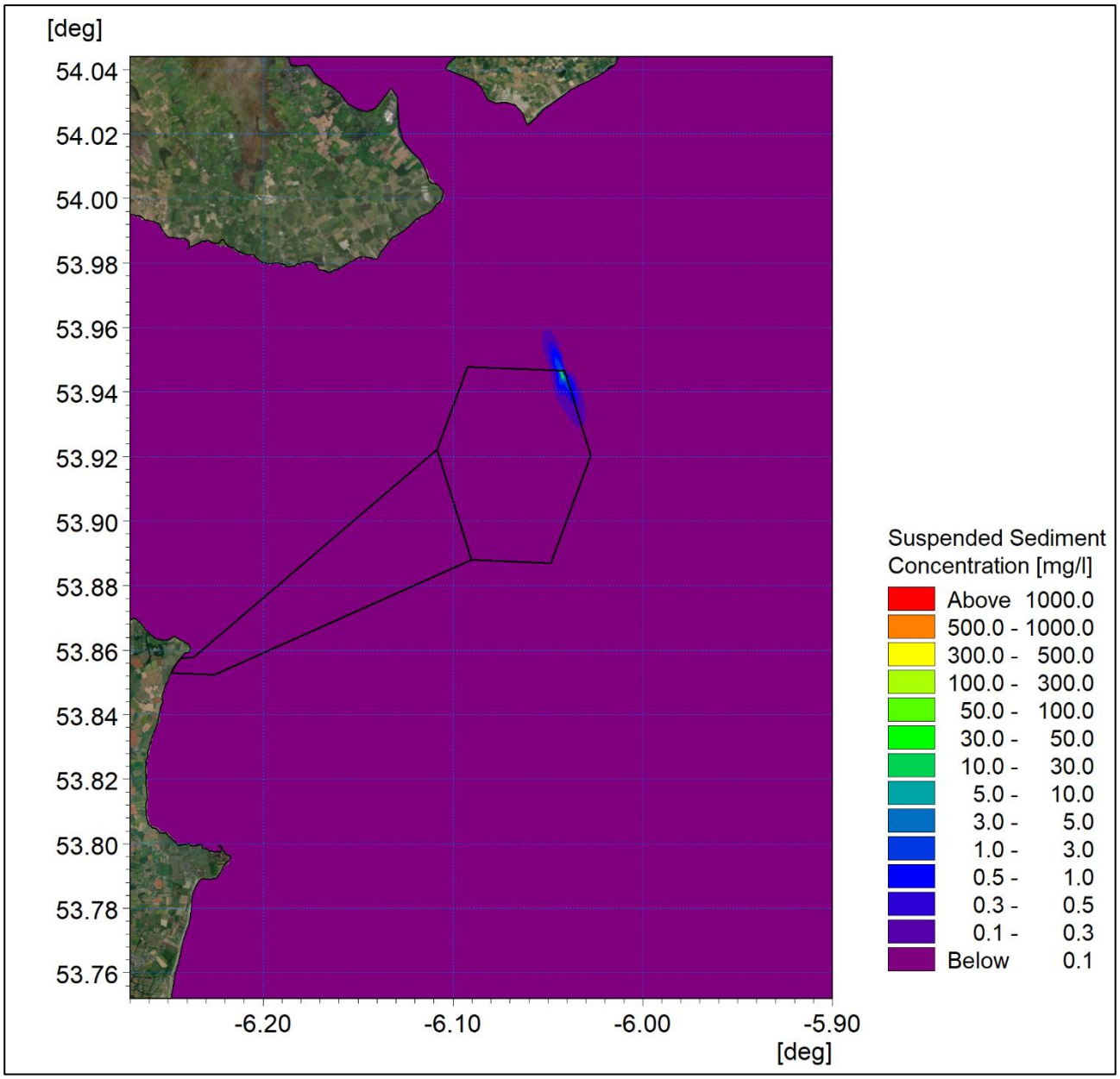

Figure 3A-83: Average suspended sediment concentration at ORI-B05.

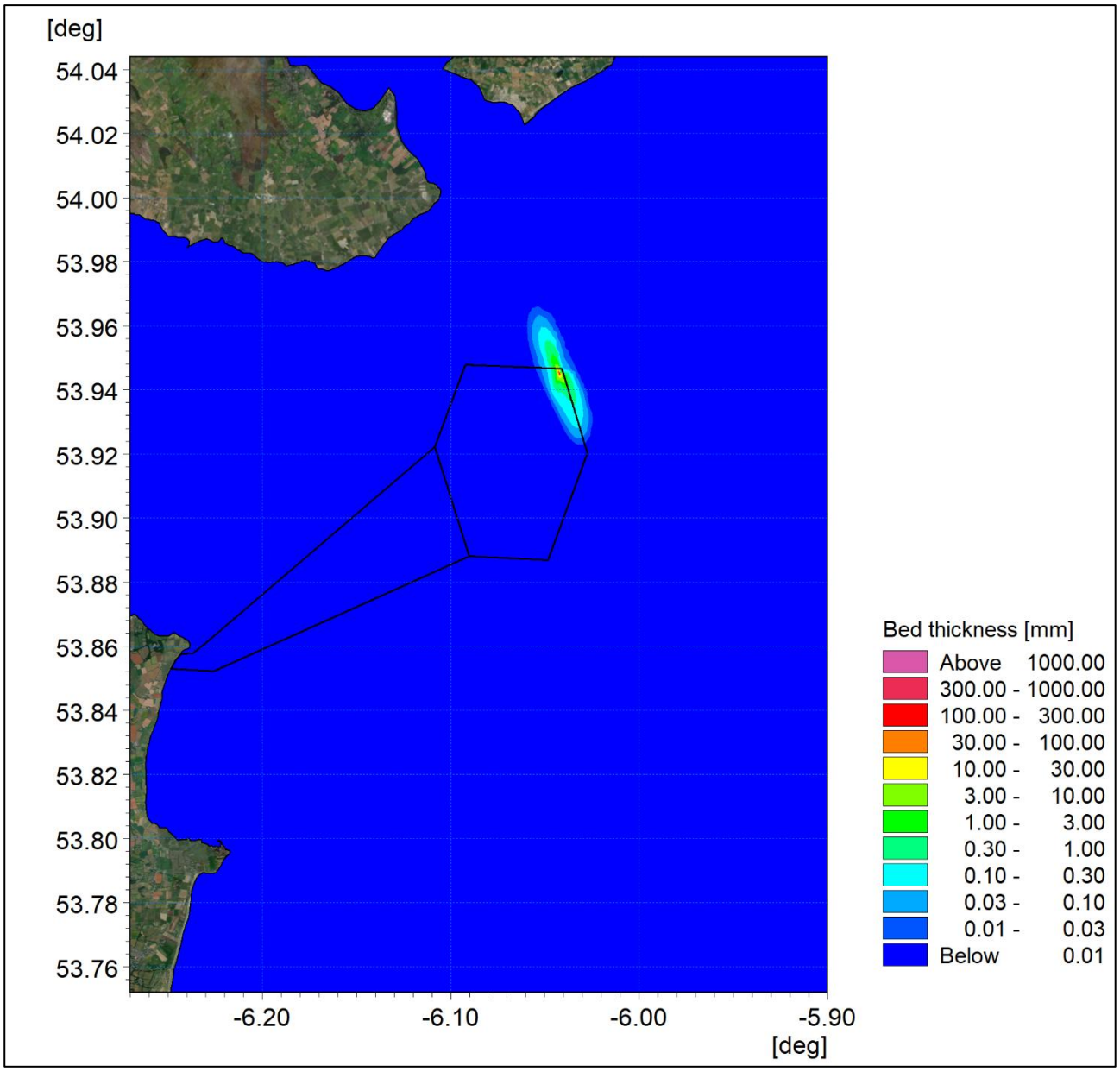

Figure 3A-84: Final sedimentation one day following installation at ORI-B05.

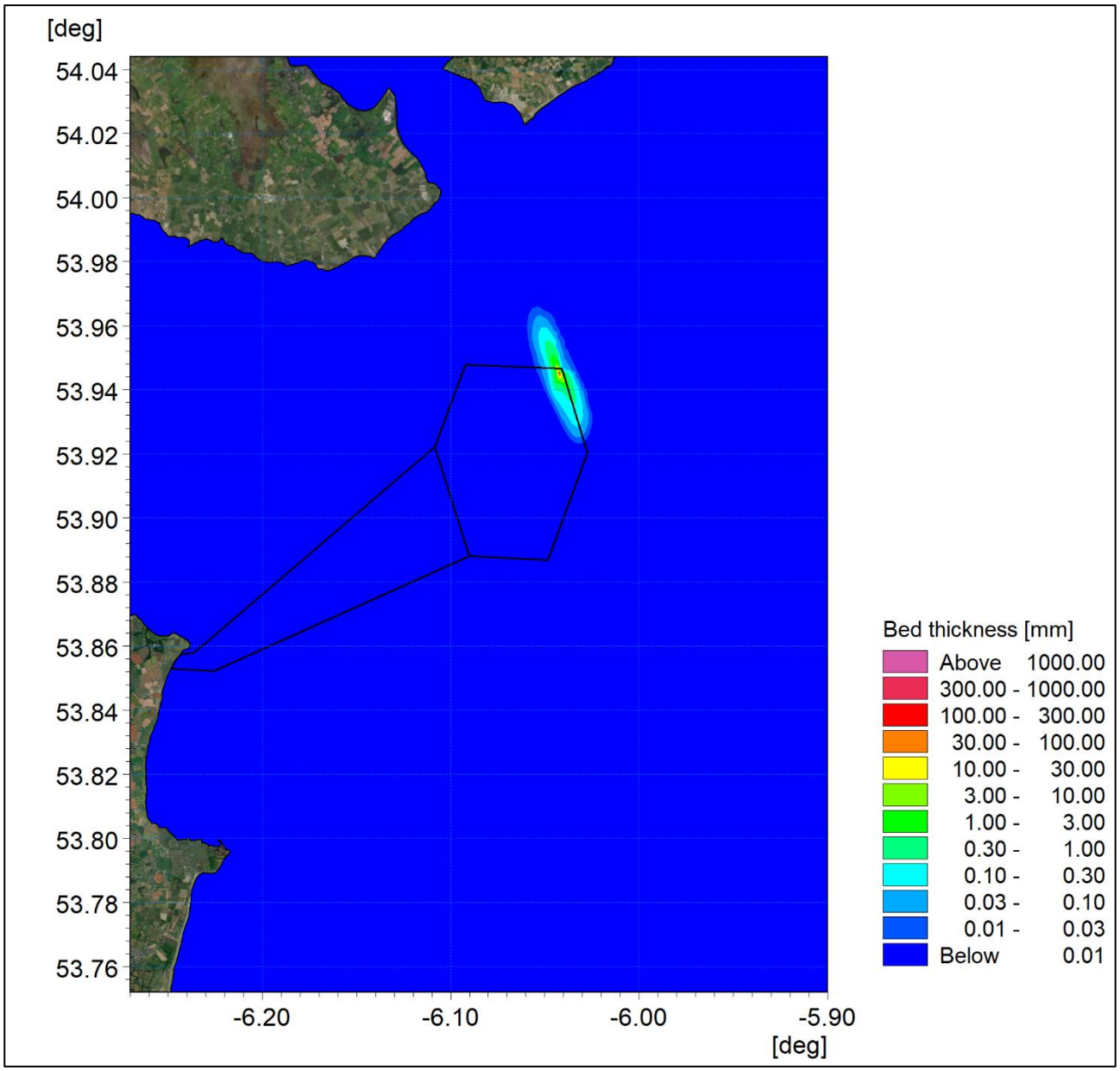

Figure 3A-85: Maximum sedimentation at ORI-B05.

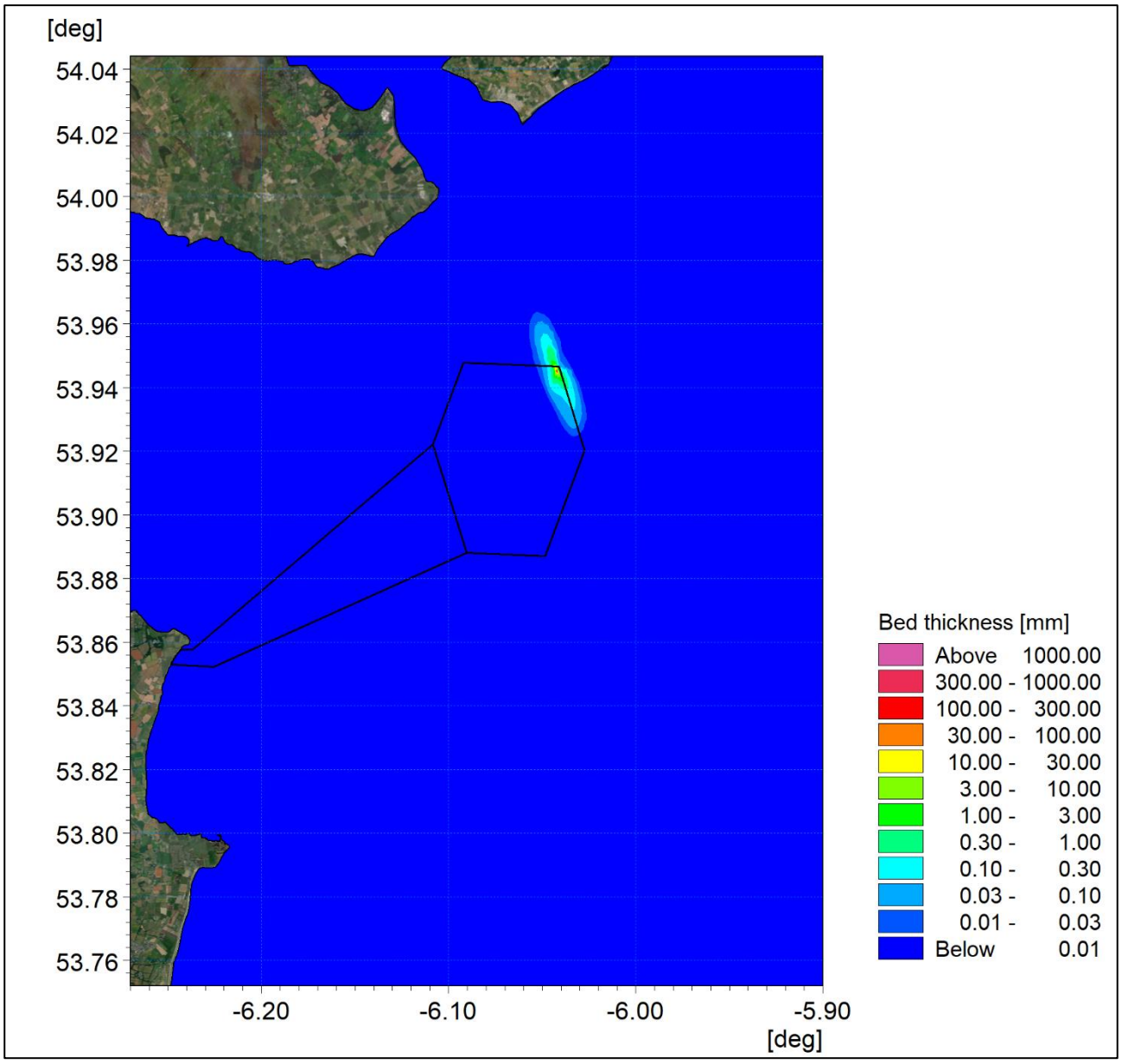

Figure 3A-86: Average sedimentation at ORI-B05.

Sensitivity of foundation installation plume dispersion

In response to RFI 6.E additional sensitivity modelling was undertaken to examine the influence of flocculation on the sediment dispersion and subsequent deposition. The modelling of drilling piled foundations at the six locations presented in the previous section was repeated with the inclusion of flocculation within the MIKE Mud Transport modelling parameters. The drilling of foundations constitutes the construction operation most likely to be influenced by flocculation as the material released includes bed material, with a fine sand fraction, and also bentonite mud associated with the drilling activity.

For flocculation to occur a critical suspended sediment concentration of the finest particles is required. The simulations included data derived from the seabed grab sampling and drilling mud however due to the volume of material being mobilised, the relatively low rate of the drilling (hence diminutive release rate), coupled with the nature of tidal currents, flocculation was very limited. Although flocculation occurred to some degree the resulting sediment plume extents and concentrations were only marginally altered. Sedimentation depths in the immediate vicinity of the drilling were increased fractionally, however these changes were not significant enough to alter the outcome of the assessment.

For completeness the model output has been provided in the following figures. Tabulated links are provided for ease of navigation in Table 3A-1. As changes due to flocculation are indiscernible from the scenario for which flocculation has been excluded a detailed commentary has not been provided.

Table 3A-1: Summary of results for foundation installation with flocculation enabled.

Drill Location	Maximum SSC	Average SSC	Final Sedimentation	Maximum Sedimentation	Average Sedimentation
ORI-E04	Figure 3A-87	Figure 3A-88	Figure 3A-89	Figure 3A-90	Figure 3A-91
ORI-D05	Figure 3A-92	Figure 3A-93	Figure 3A-94	Figure 3A-95	Figure 3A-96
ORI-E02	Figure 3A-97	Figure 3A-98	Figure 3A-99	Figure 3A-100	Figure 3A-101
ORI-A01	Figure 3A-102	Figure 3A-103	Figure 3A-104	Figure 3A-105	Figure 3A-106
ORI-A04	Figure 3A-107	Figure 3A-108	Figure 3A-109	Figure 3A-110	Figure 3A-111
ORI-B05	Figure 3A-112	Figure 3A-113	Figure 3A-114	Figure 3A-115	Figure 3A-116

ORI-E04

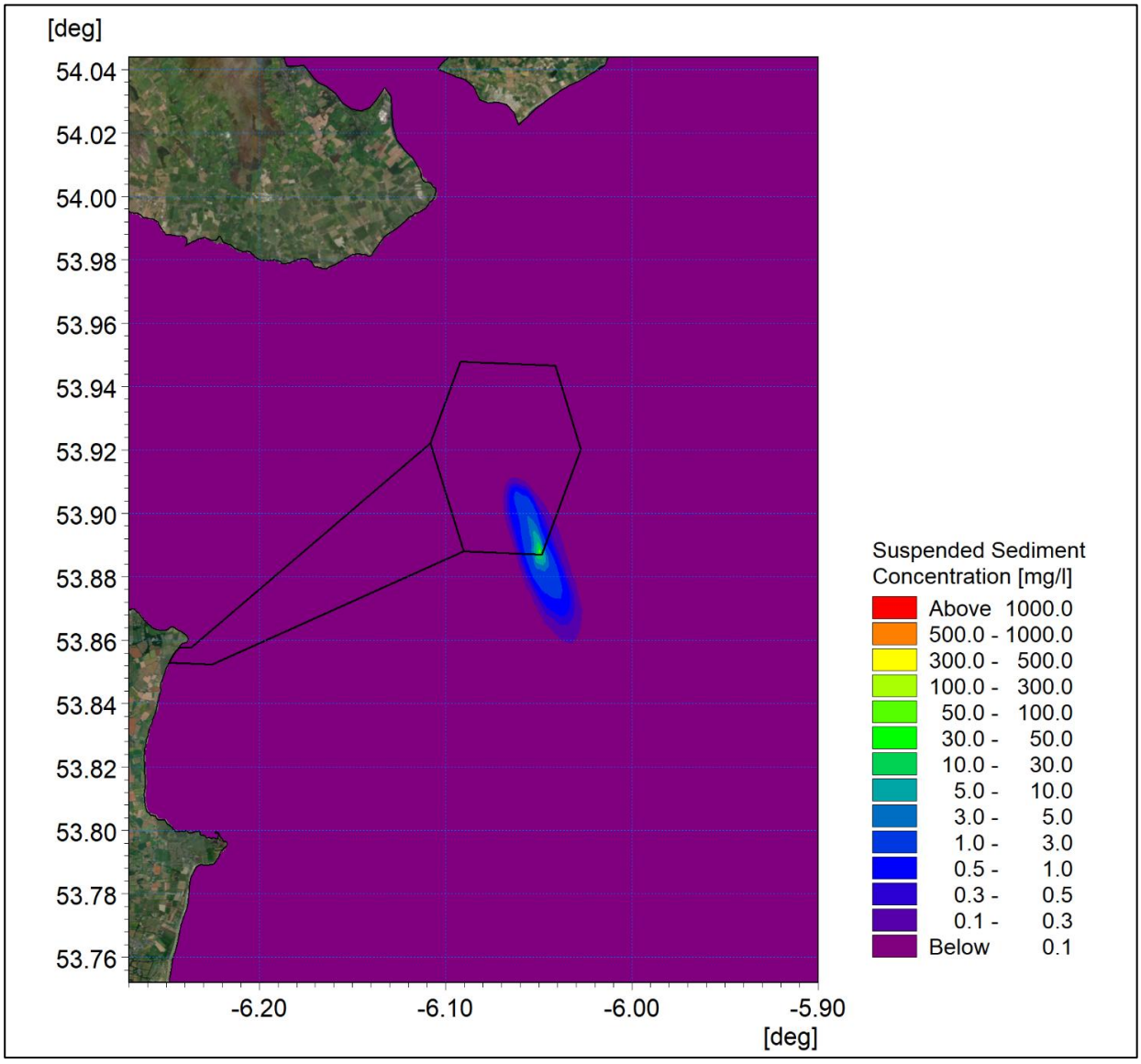

Figure 3A-87: Maximum suspended sediment concentration at ORI-E04 with flocculation.

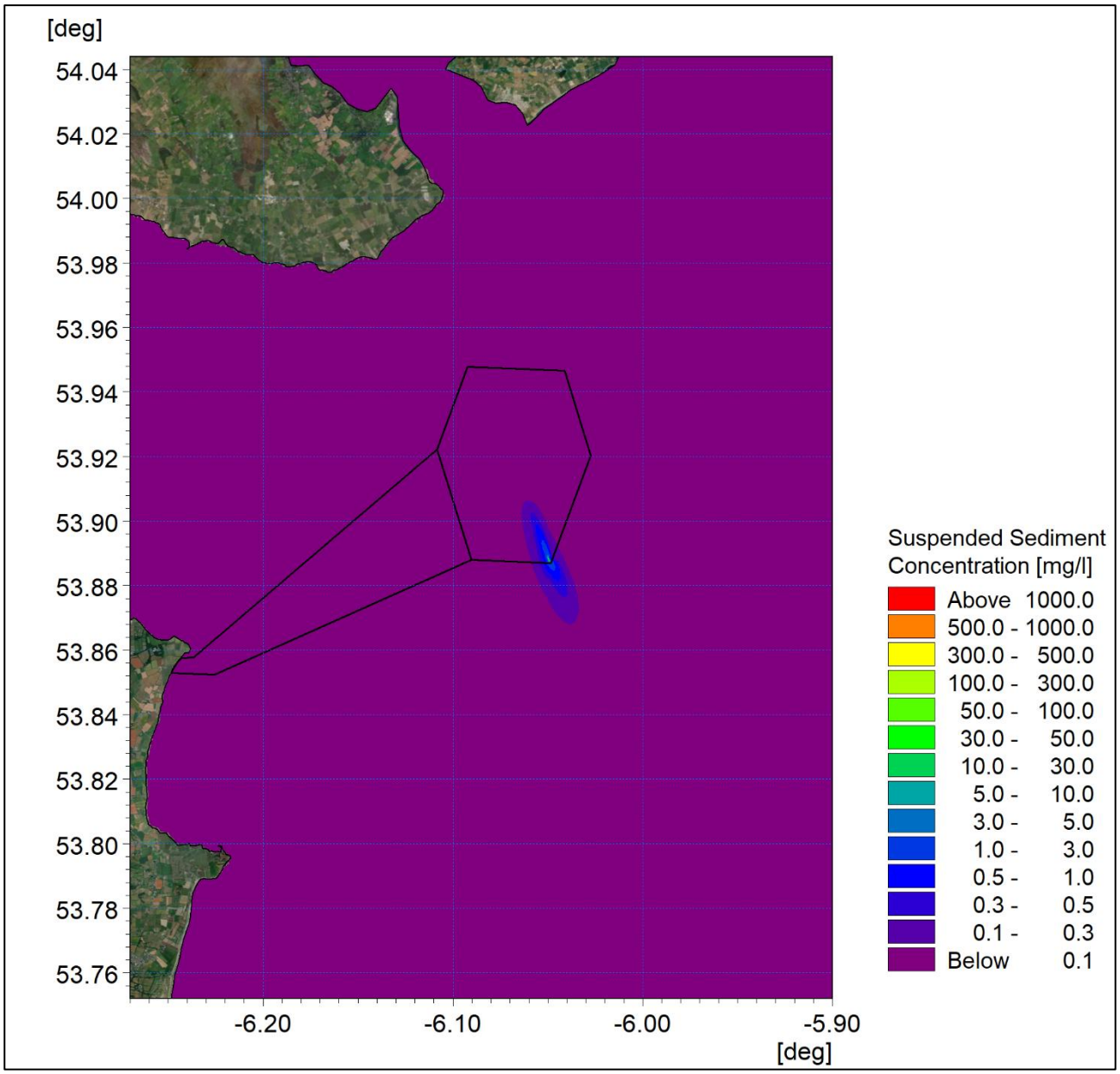

Figure 3A-88: Average suspended sediment concentration at ORI-E04 with flocculation.

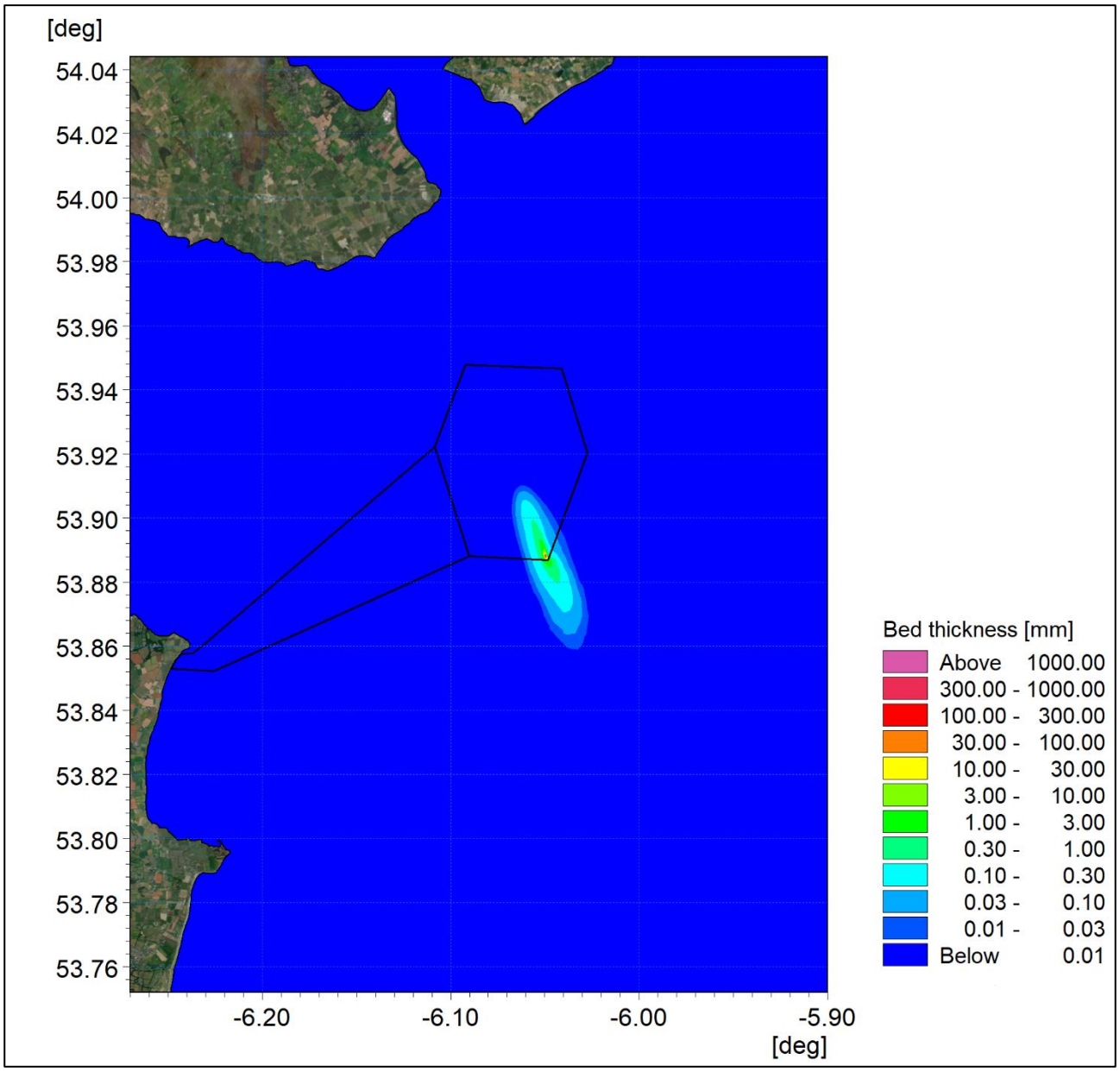

Figure 3A-89: Final sedimentation one day following installation at ORI-E04 with flocculation.

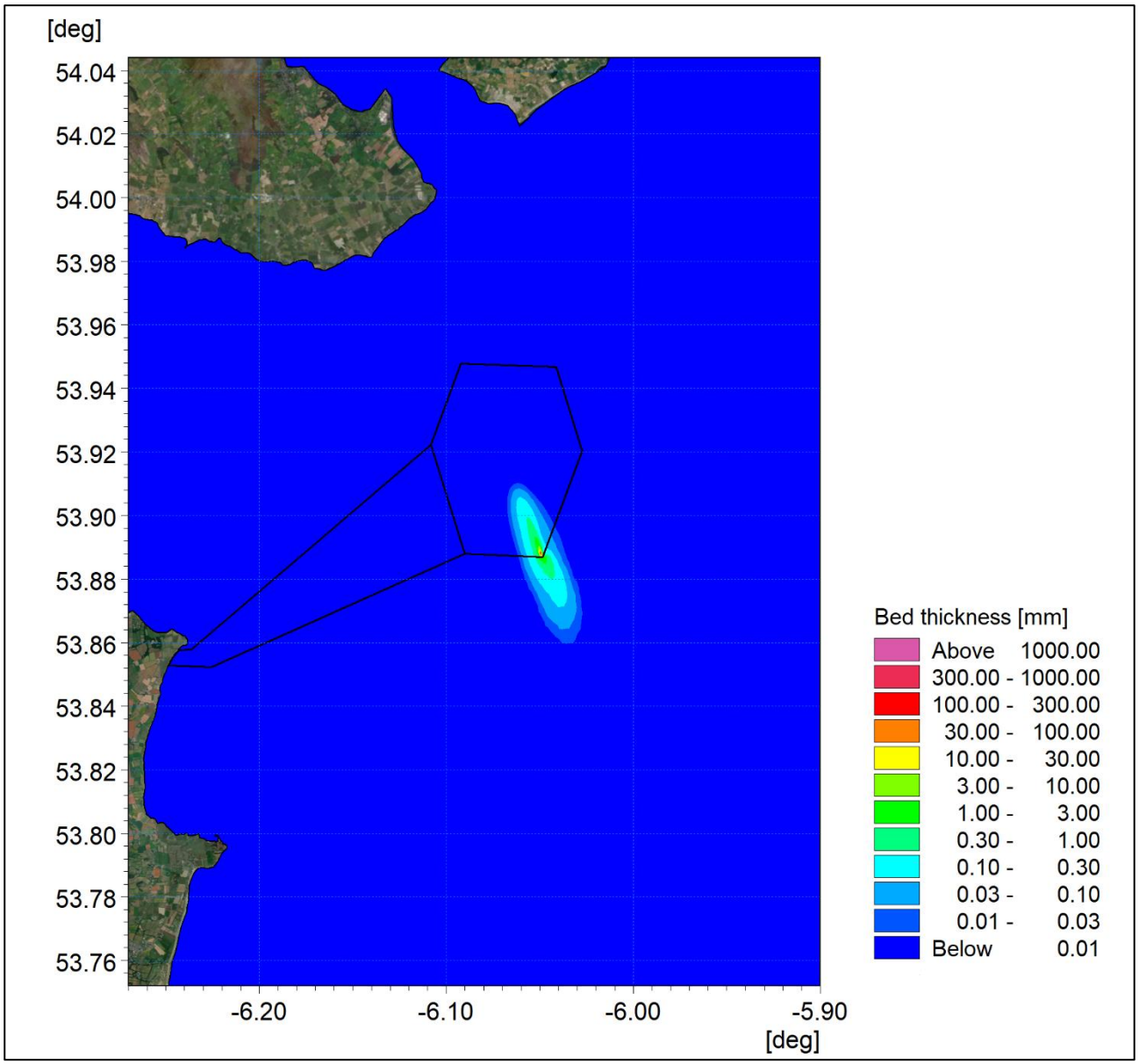

Figure 3A-90: Maximum sedimentation at ORI-E04 with flocculation.

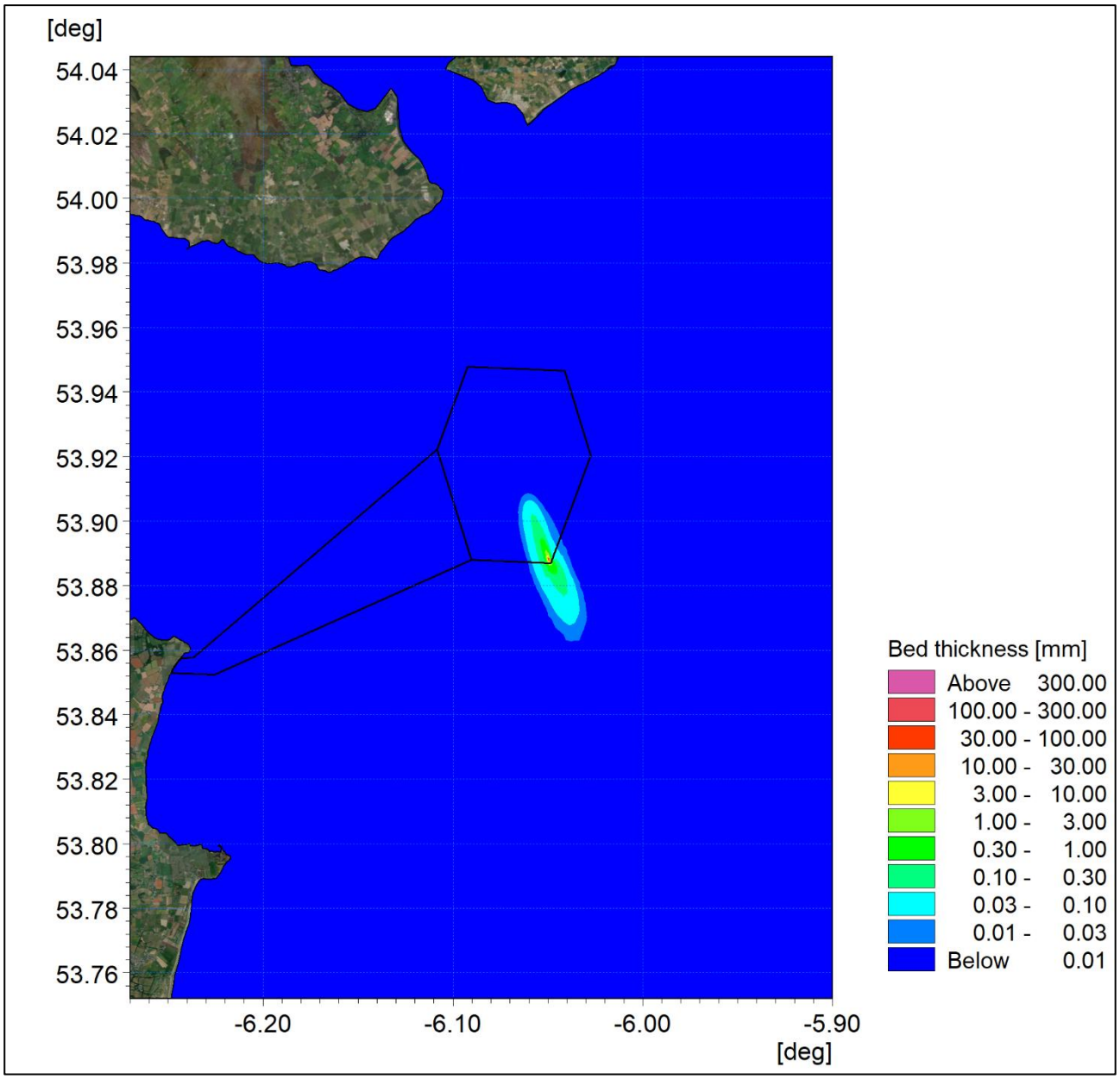

Figure 3A-91: Average sedimentation at ORI-E04 with flocculation.

ORI-D05

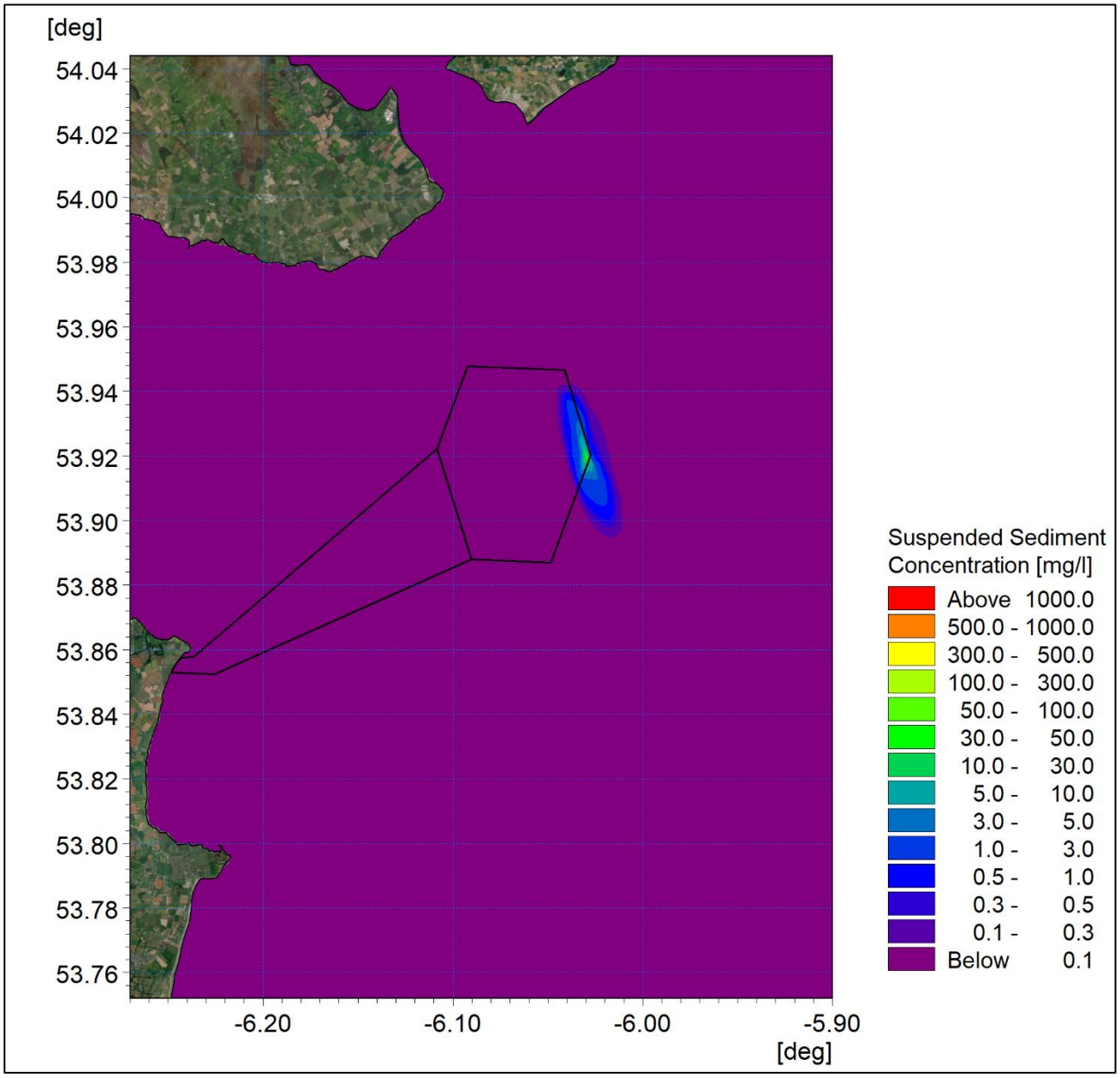

Figure 3A-92: Maximum suspended sediment concentration at ORI-D05 with flocculation.

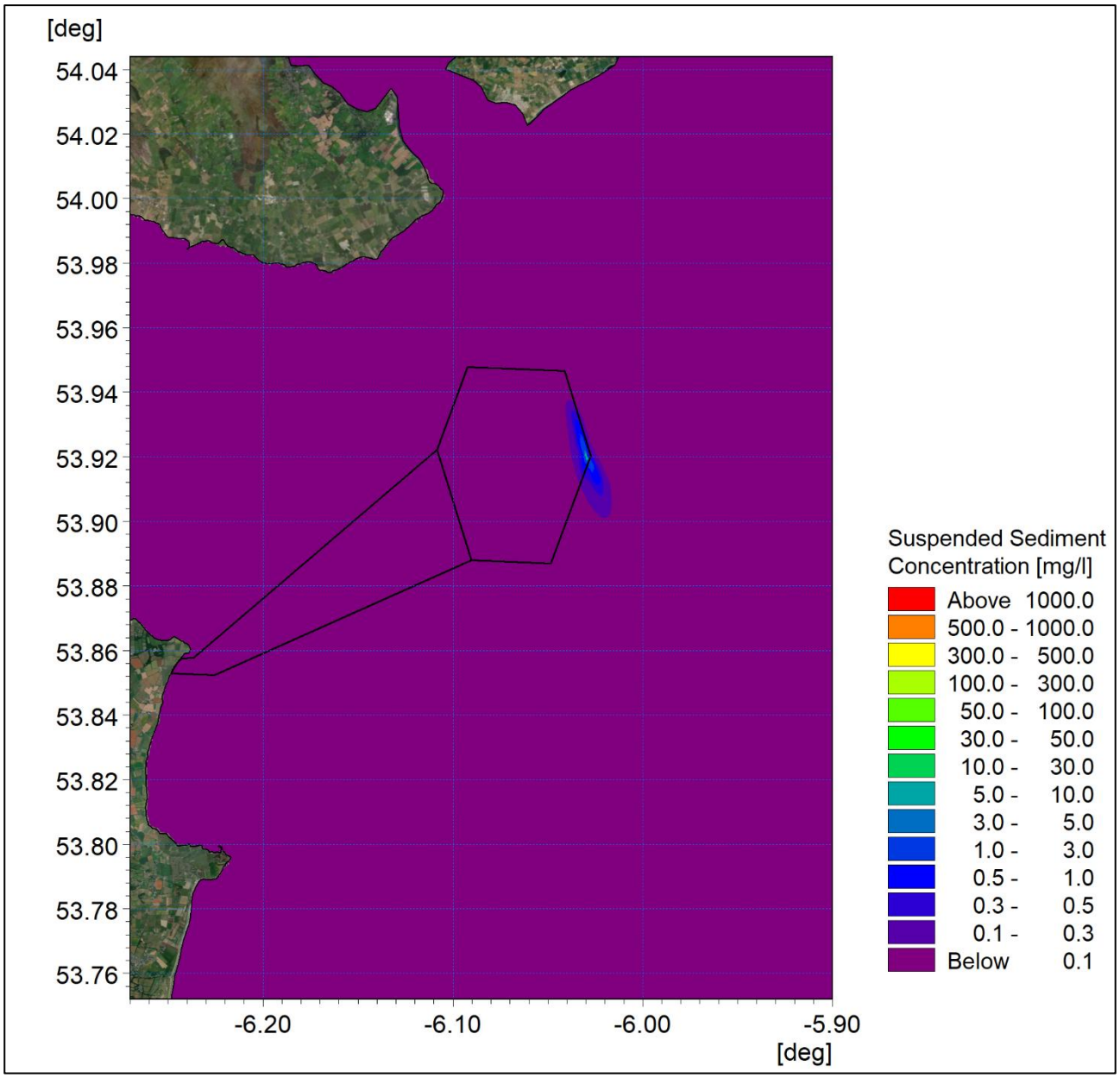

Figure 3A-93: Average suspended sediment concentration at ORI-D05 with flocculation.

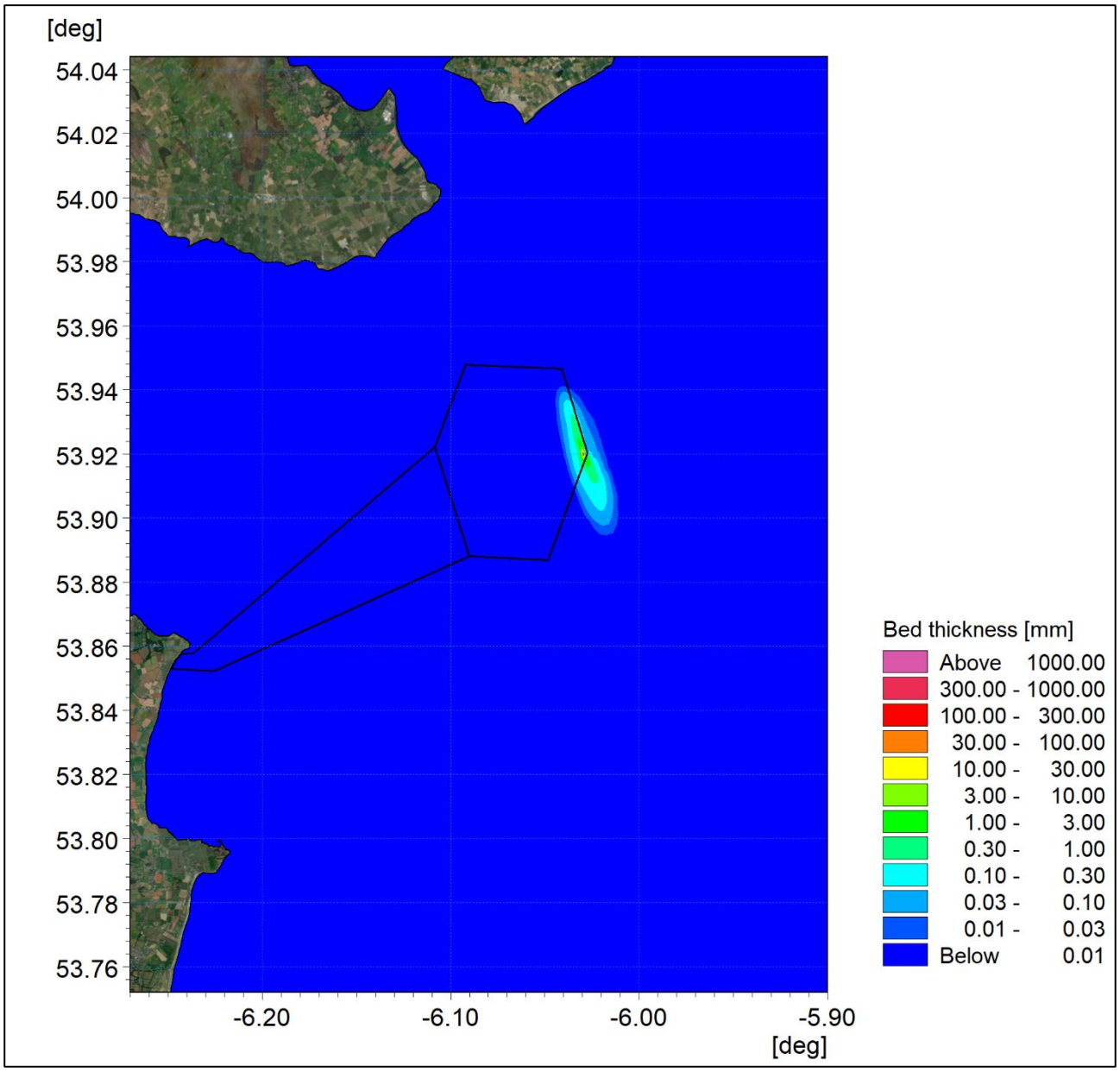

Figure 3A-94: Final sedimentation one day following installation at ORI-D05 with flocculation.

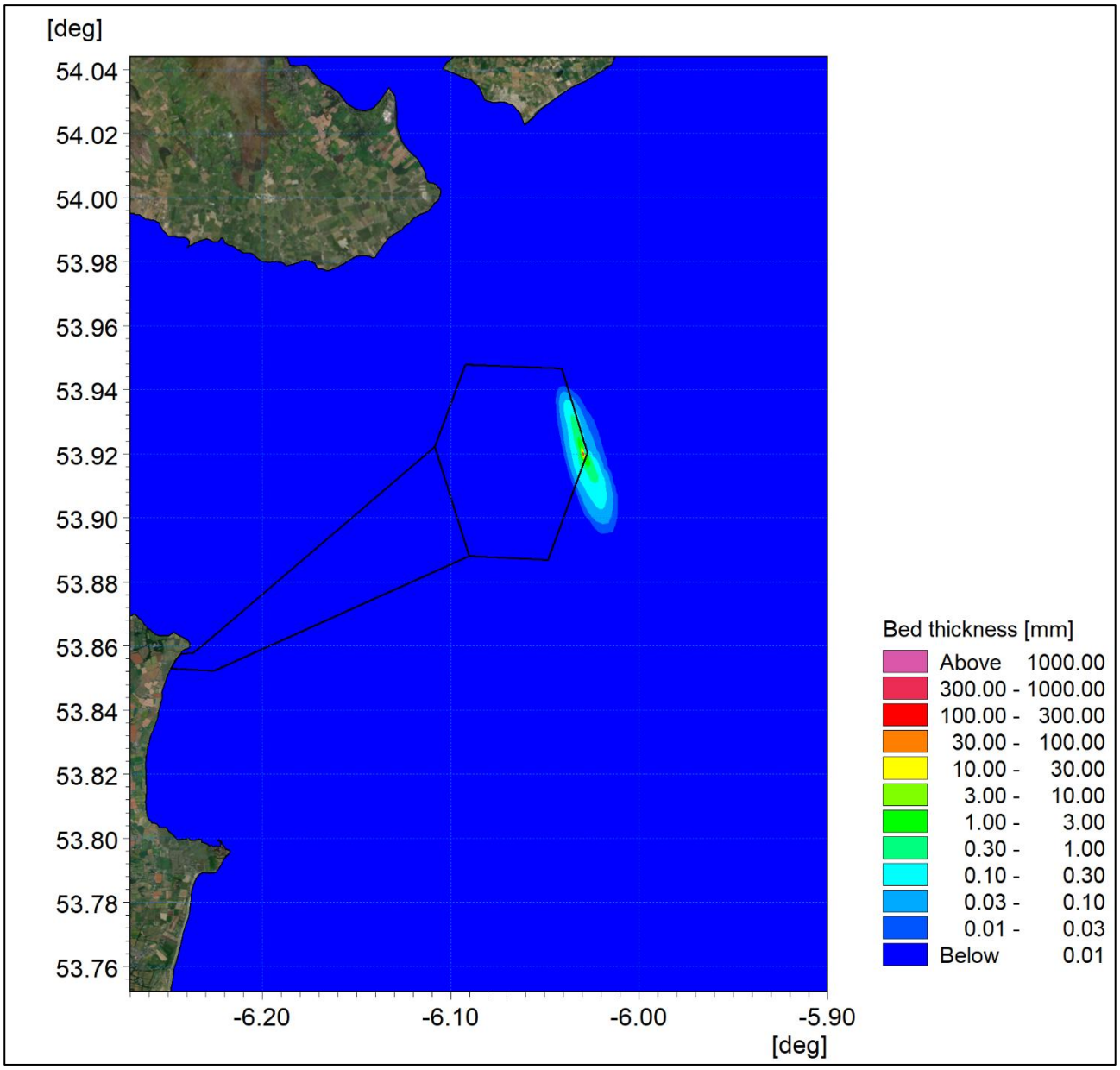

Figure 3A-95: Maximum sedimentation at ORI-D05 with flocculation.

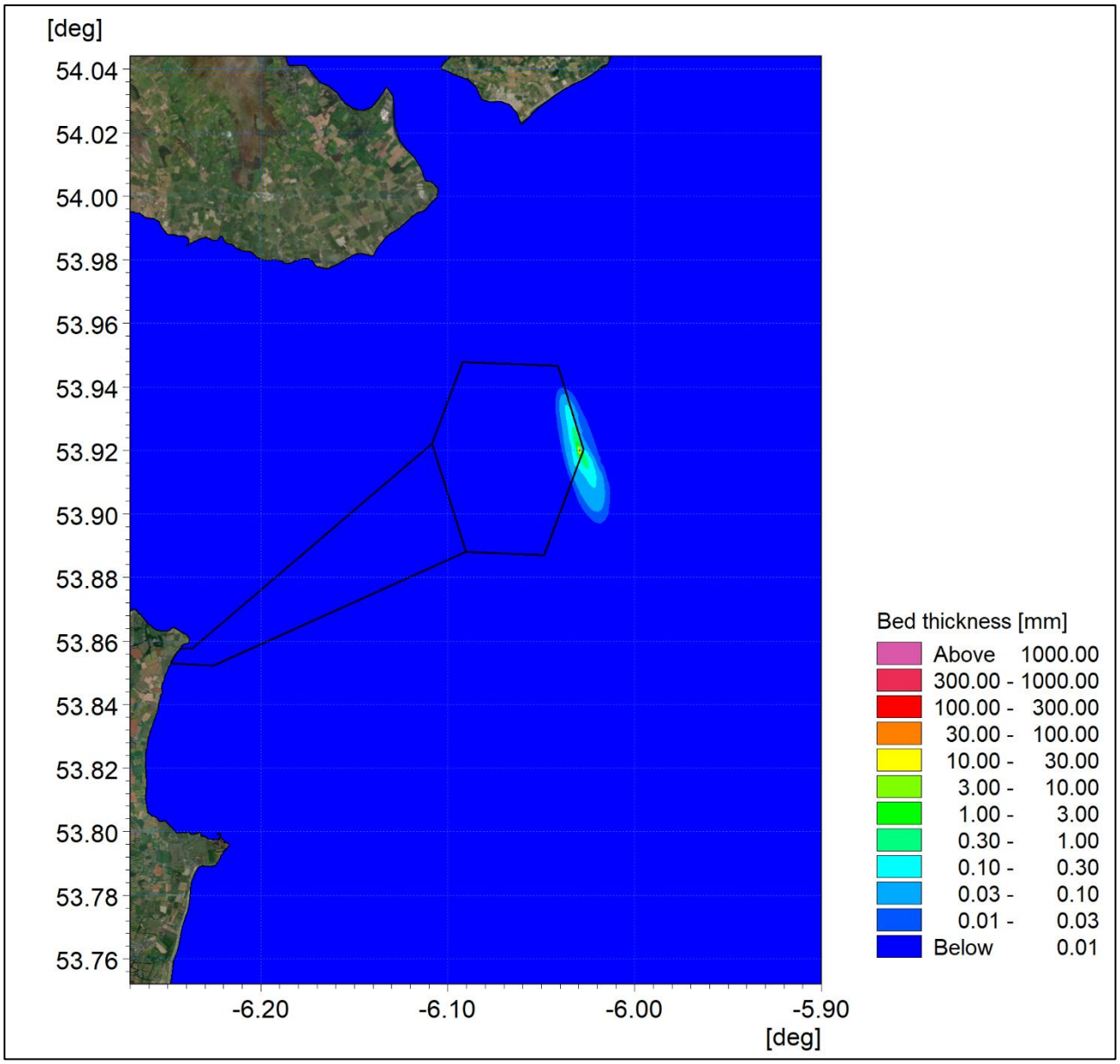

Figure 3A-96: Average sedimentation at ORI-D05 with flocculation.

ORI-E02

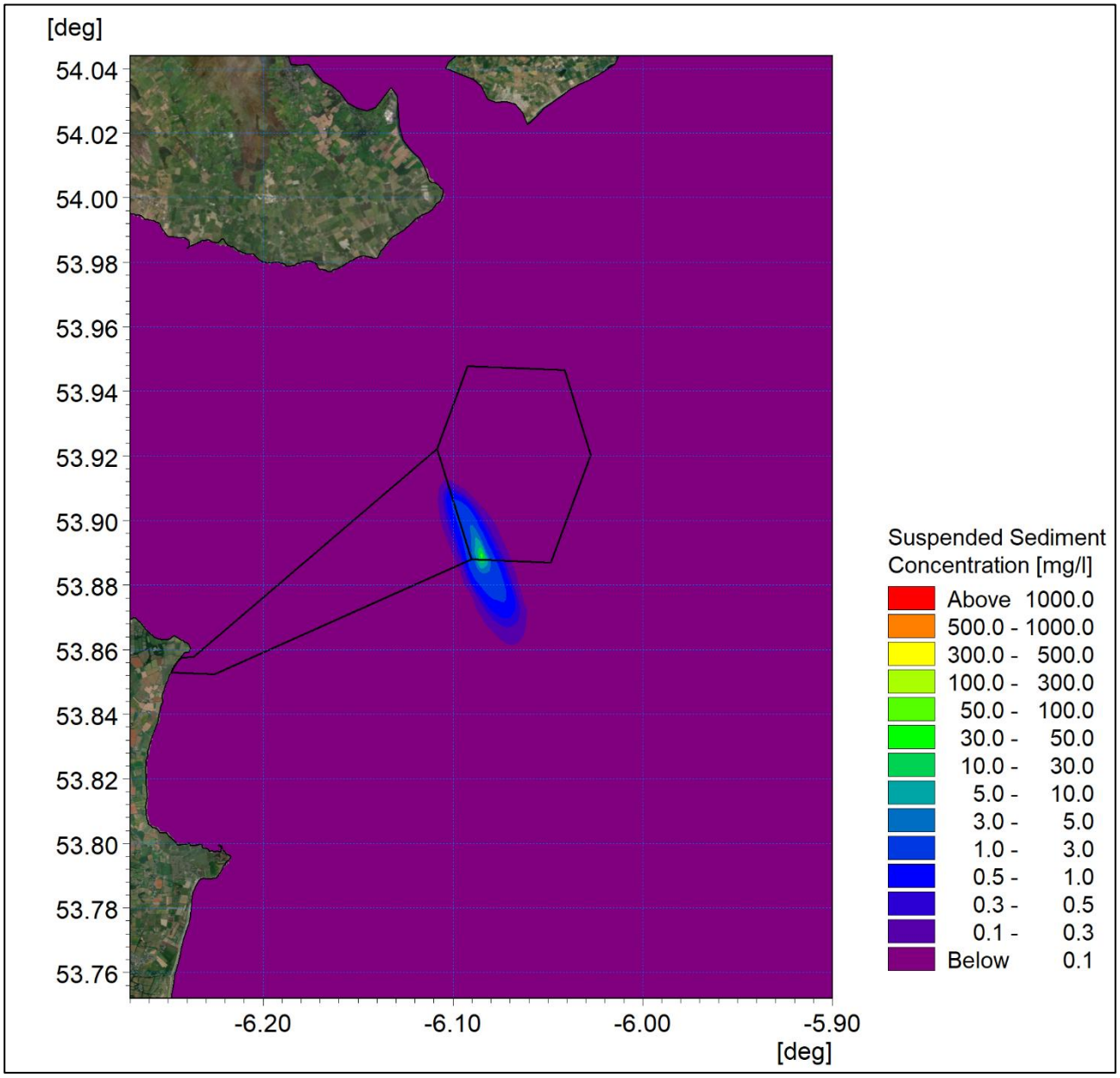

Figure 3A-97: Maximum suspended sediment concentration at ORI-E02 with flocculation.

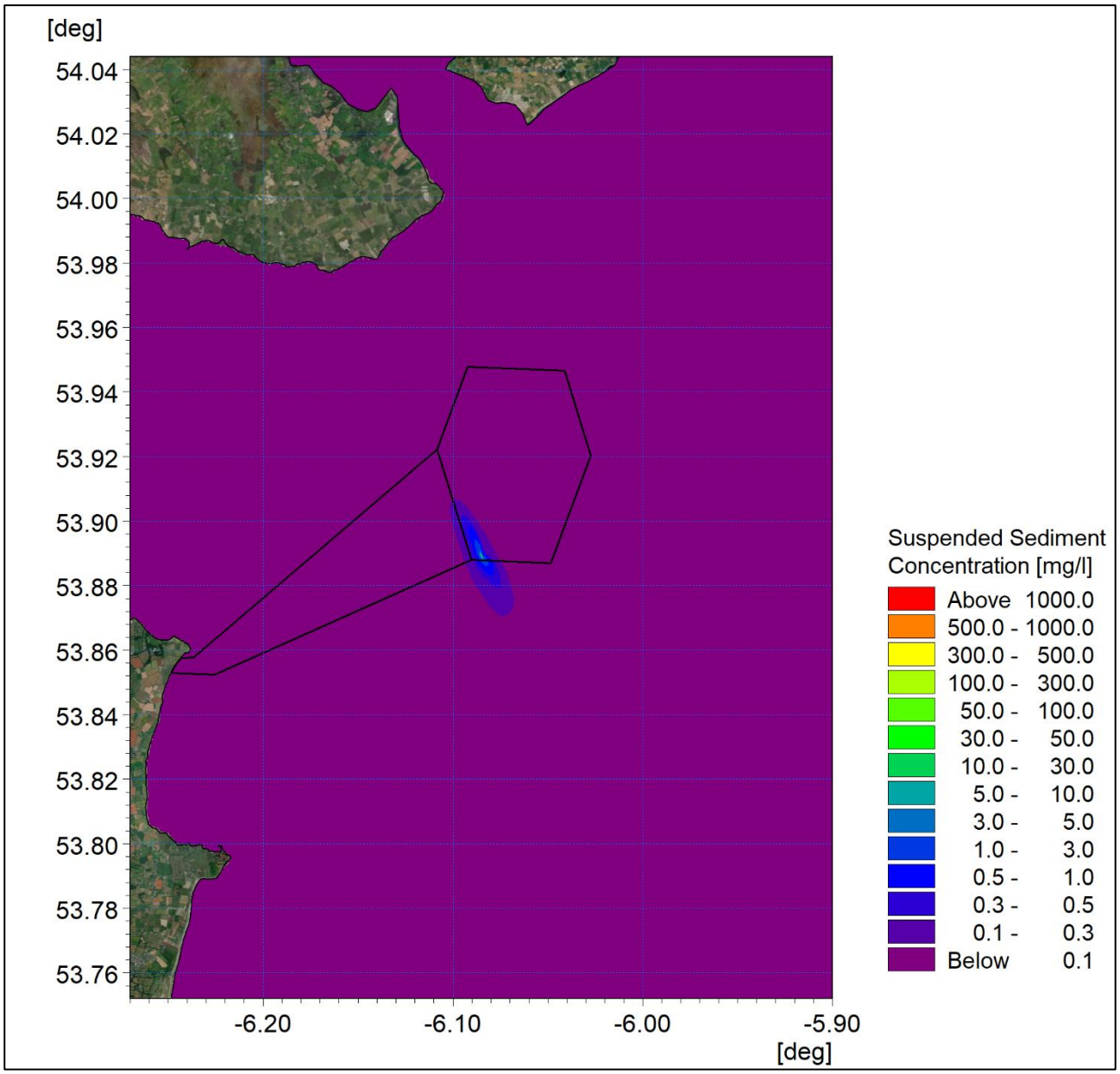

Figure 3A-98: Average suspended sediment concentration at ORI-E02 with flocculation.

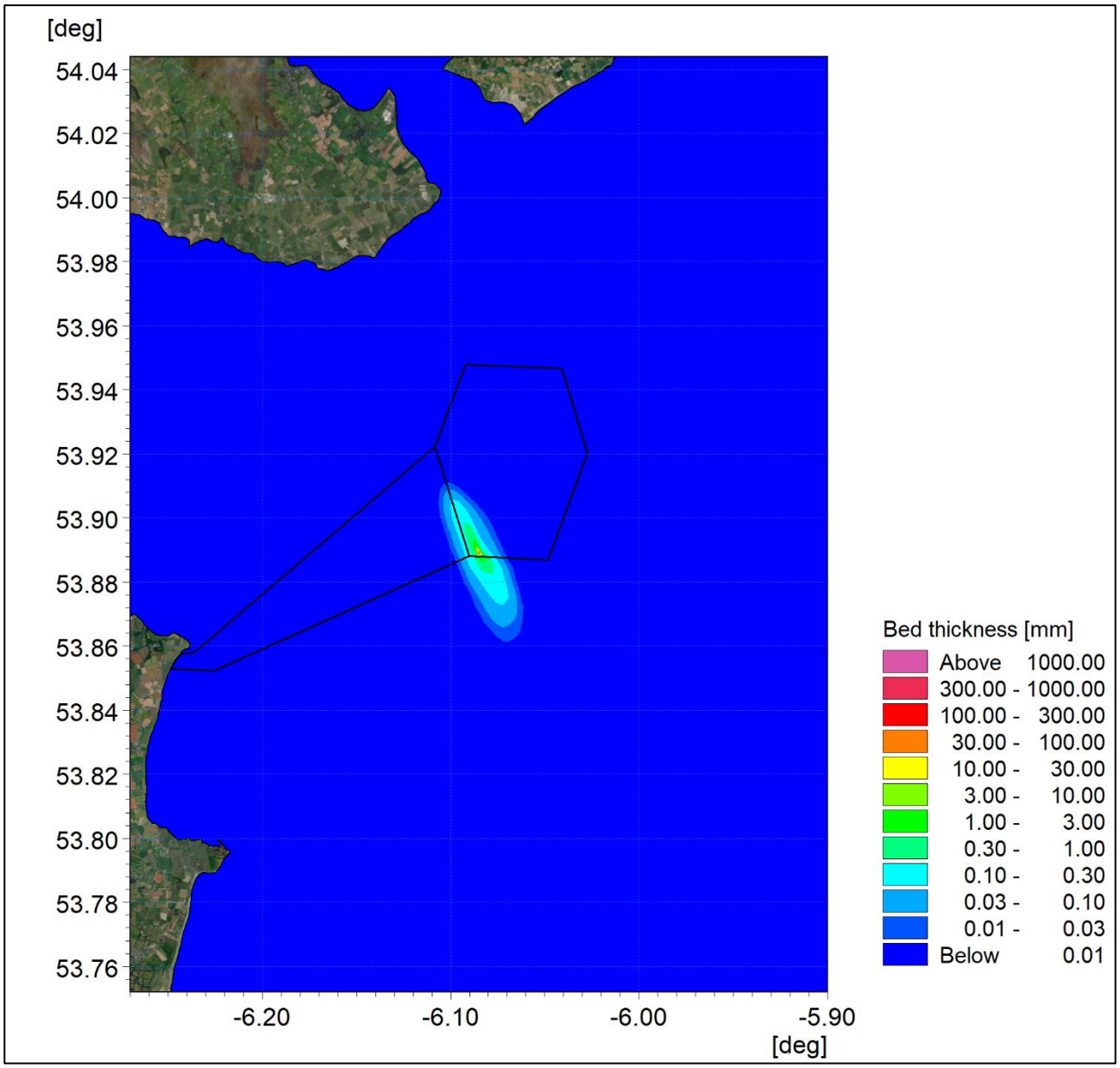

Figure 3A-99: Final sedimentation one day following installation at ORI-E02 with flocculation.

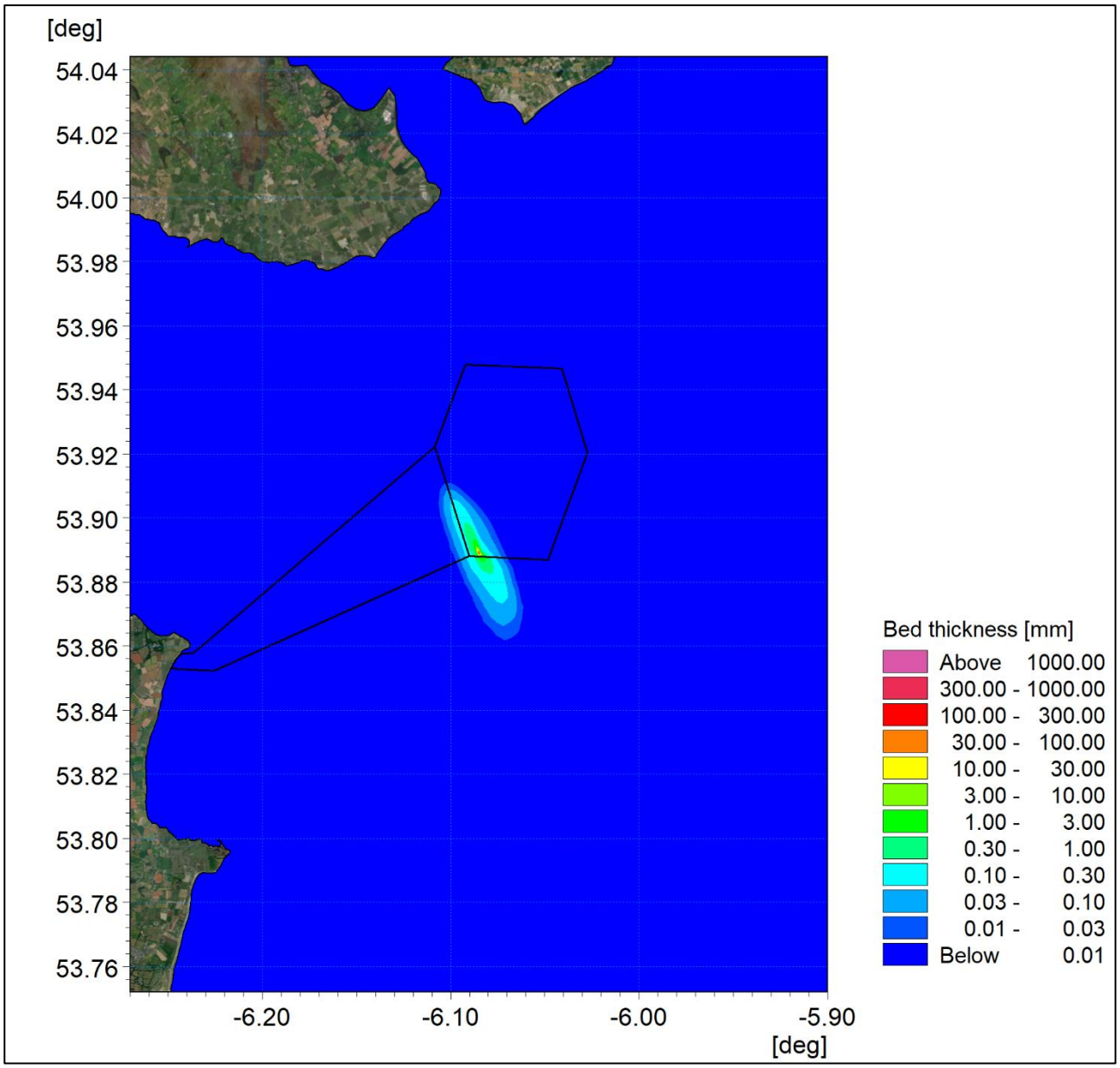

Figure 3A-100: Maximum sedimentation at ORI-E02 with flocculation.

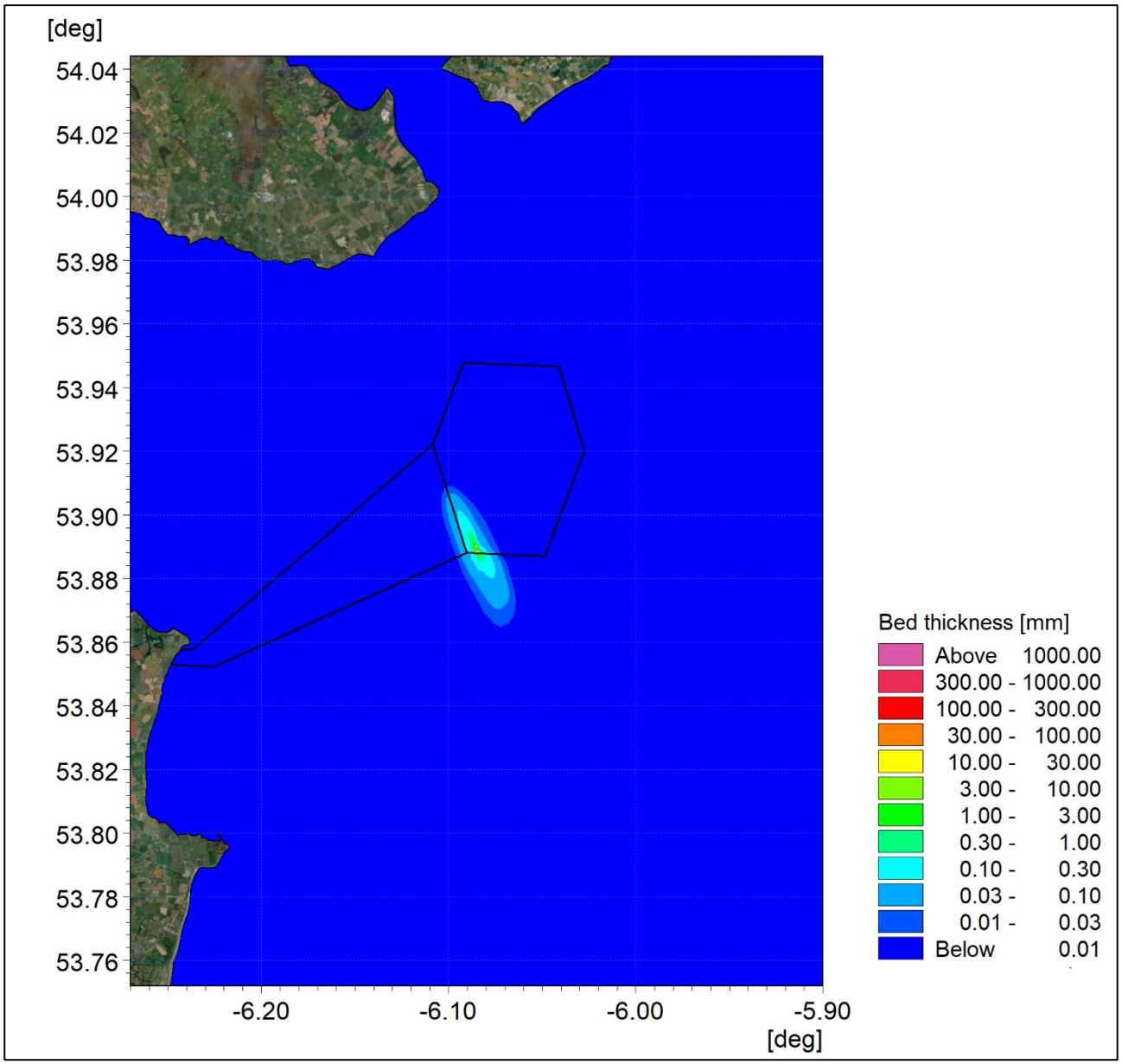

Figure 3A-101: Average sedimentation at ORI-E02 with flocculation.

ORI-A01

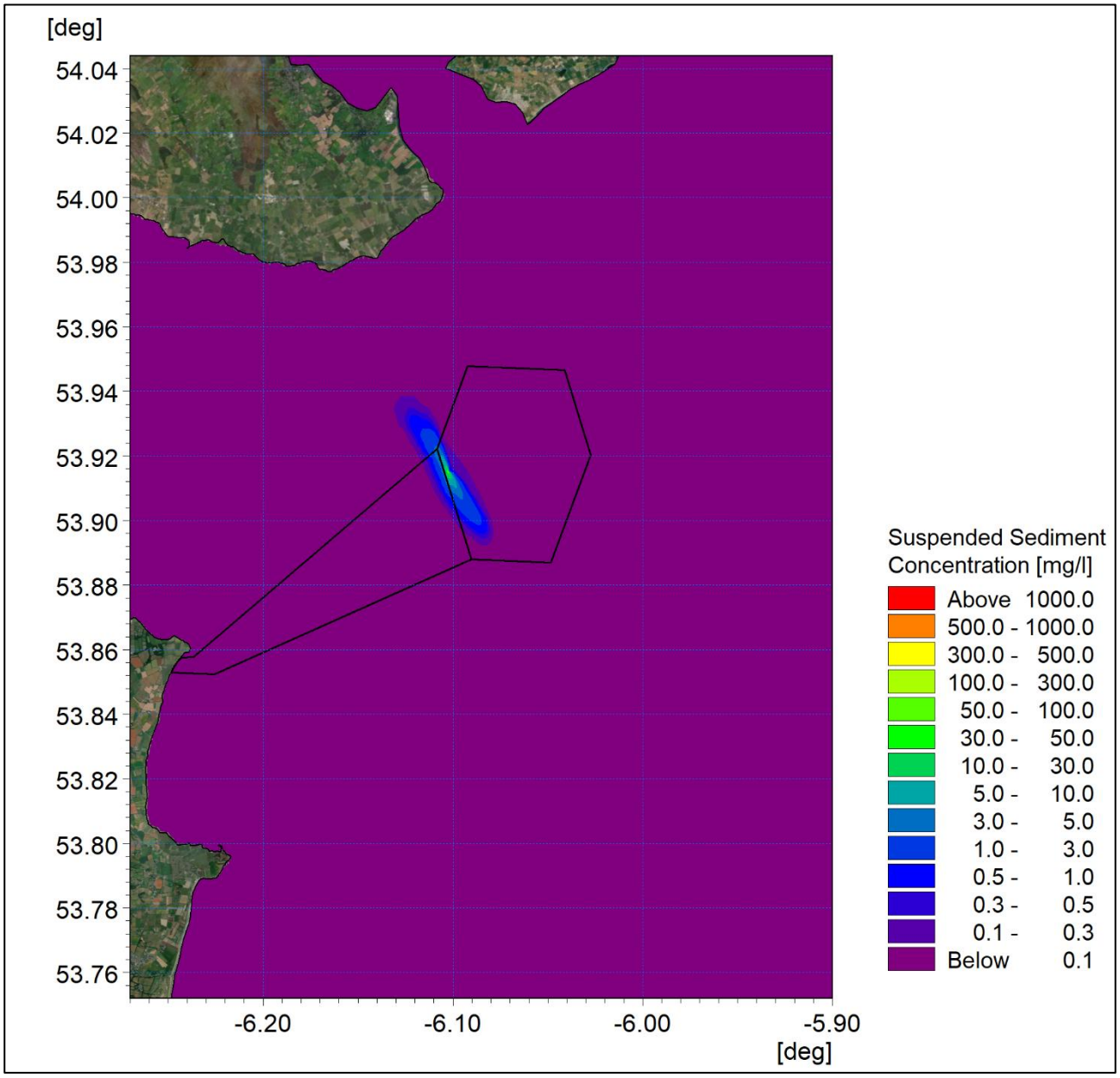

Figure 3A-102: Maximum suspended sediment concentration at ORI-A01 with flocculation.

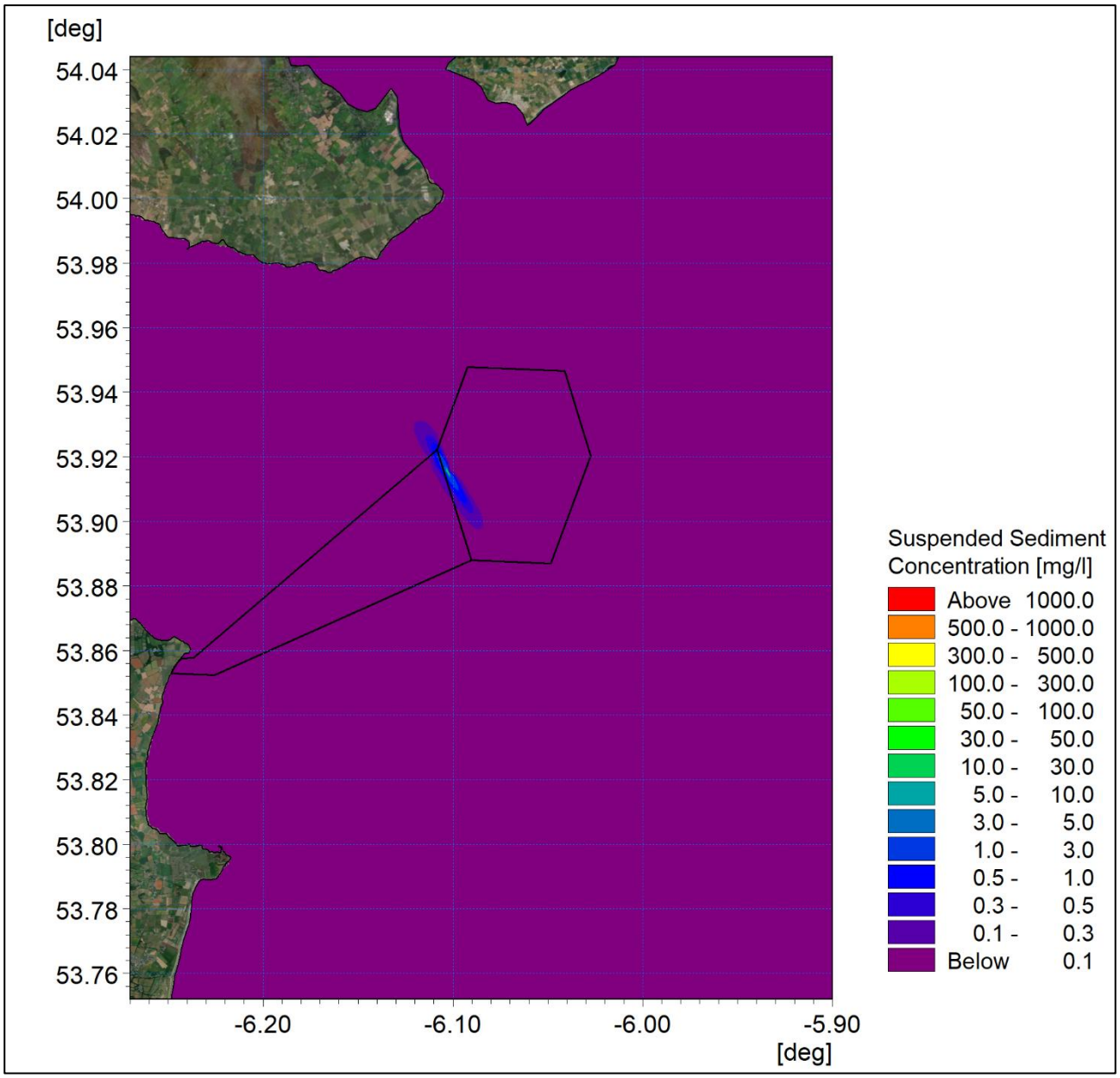

Figure 3A-103: Average suspended sediment concentration at ORI-A01 with flocculation.

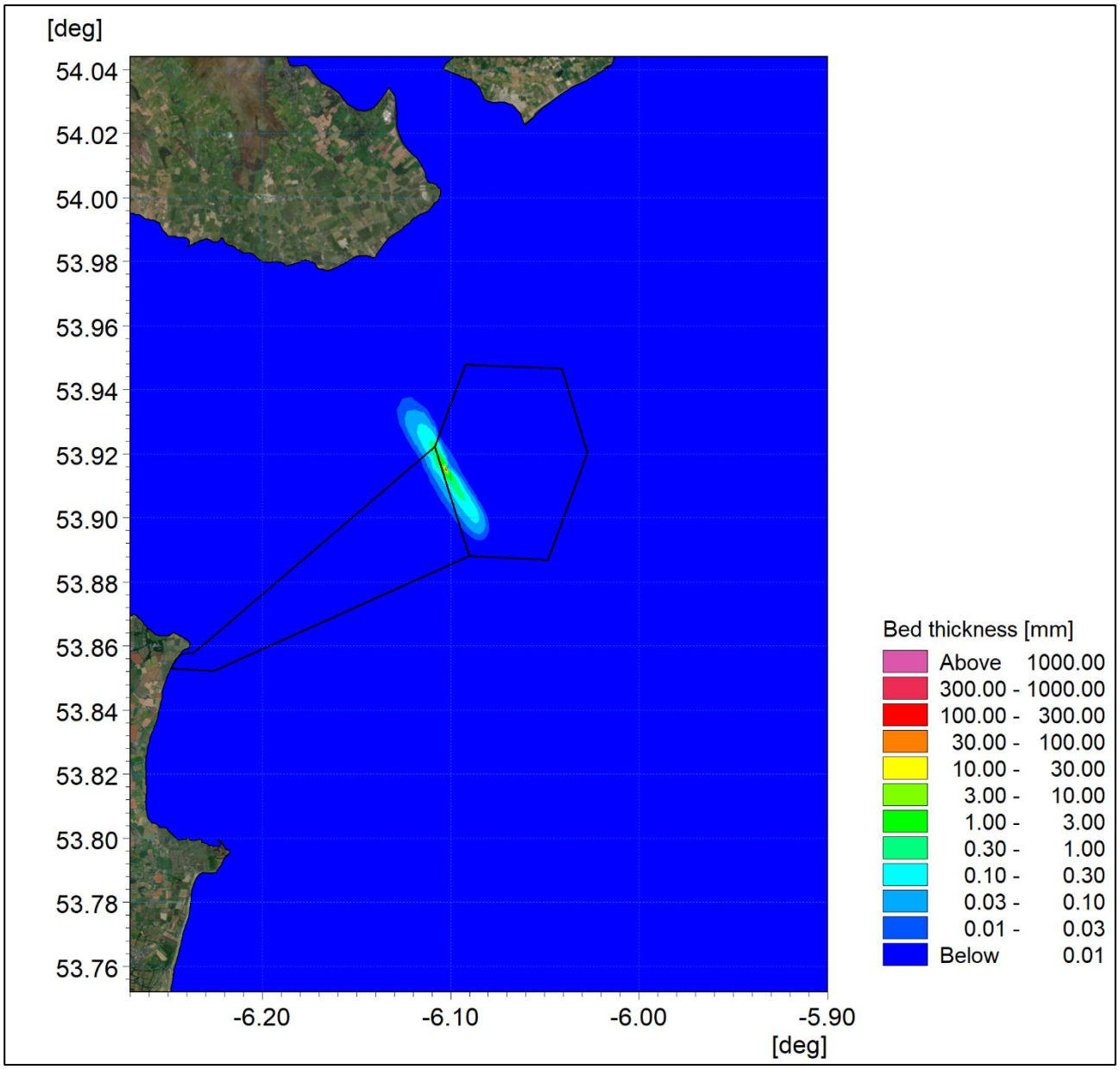

Figure 3A-104: Final sedimentation one day following installation at ORI- A01 with flocculation.

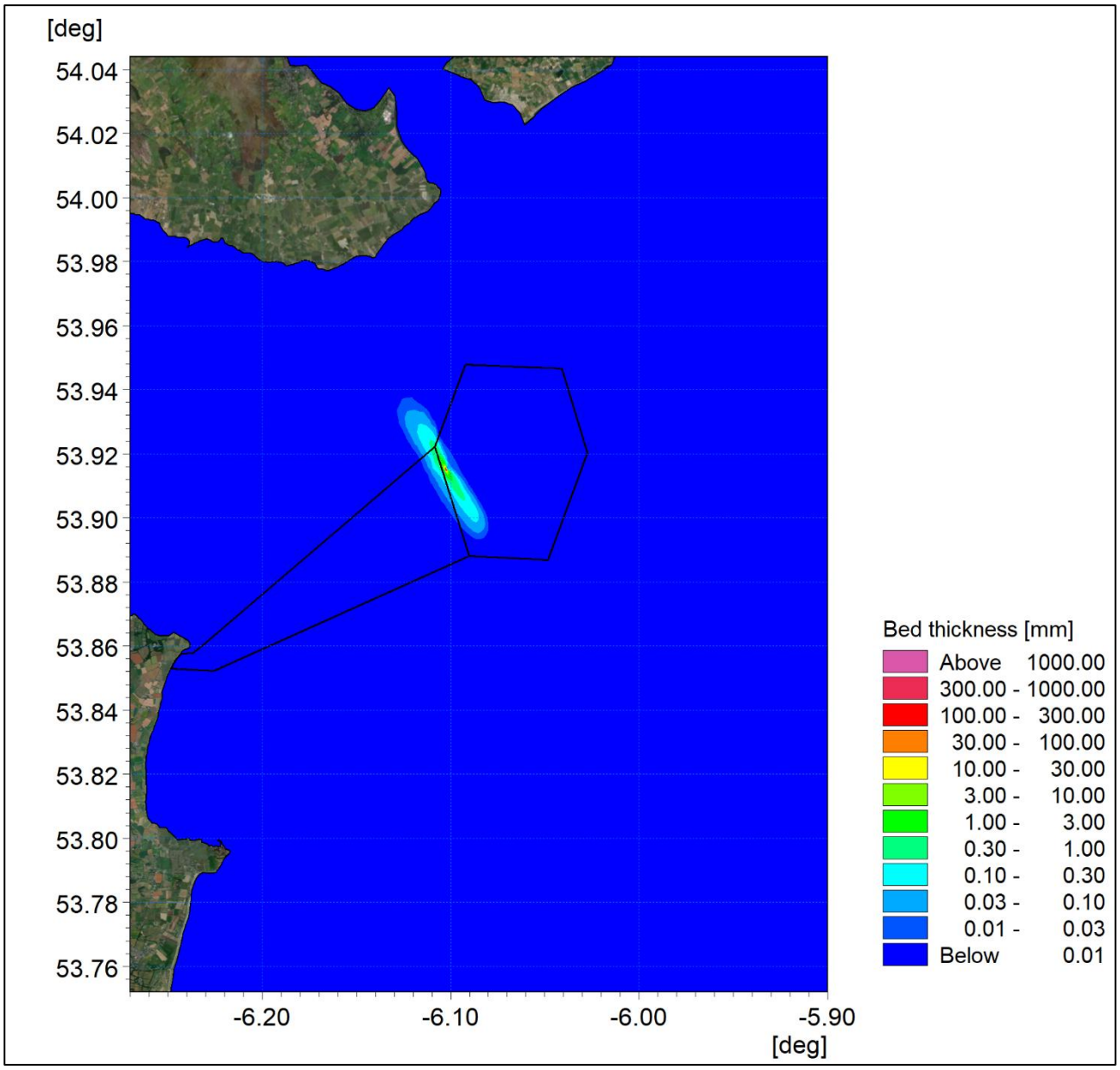

Figure 3A-105: Maximum sedimentation at ORI- A01 with flocculation.

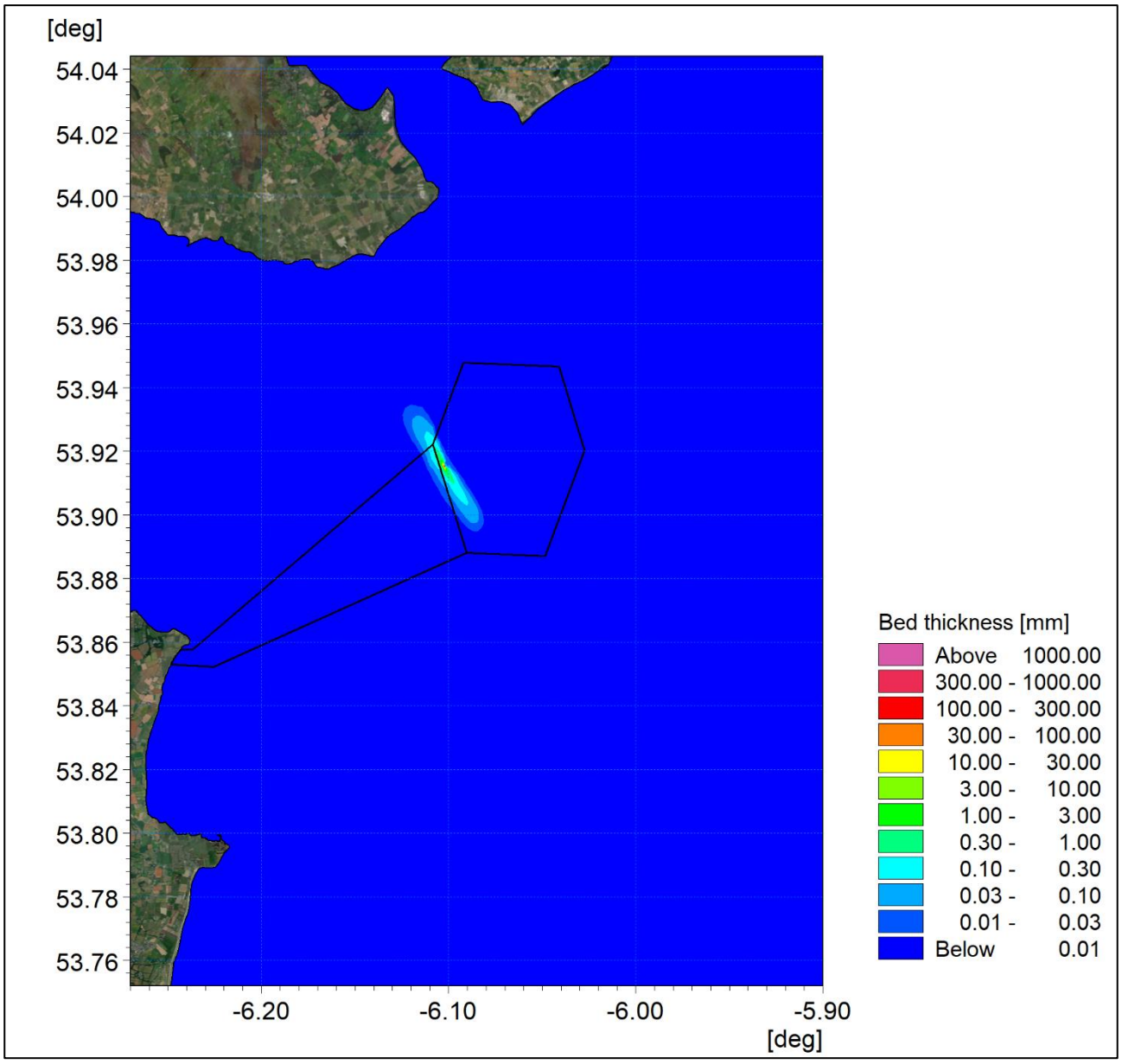

Figure 3A-106: Average sedimentation at ORI- A01 with flocculation.

ORI-A04

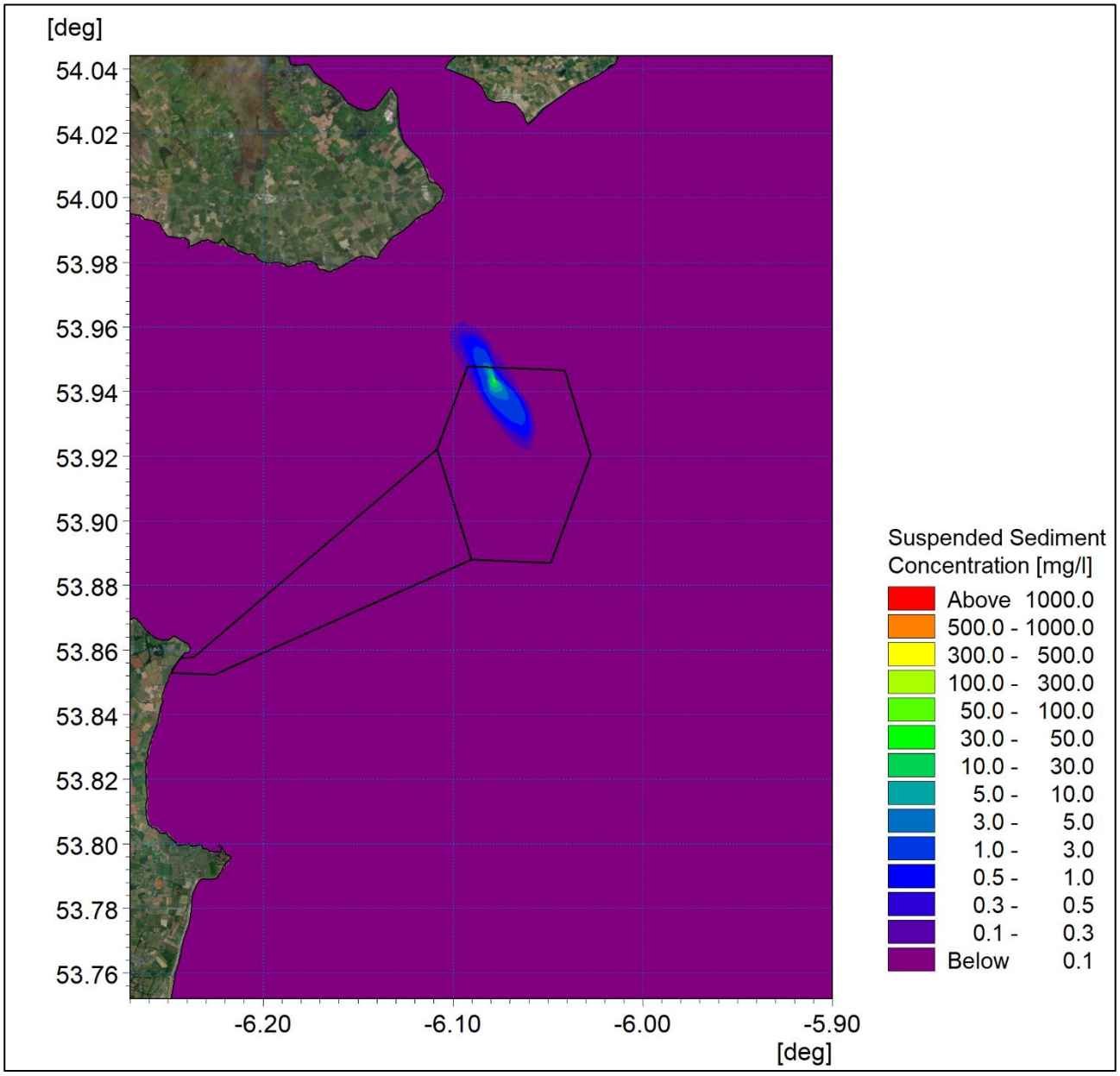

Figure 3A-107: Maximum suspended sediment concentration at ORI-A04 with flocculation.

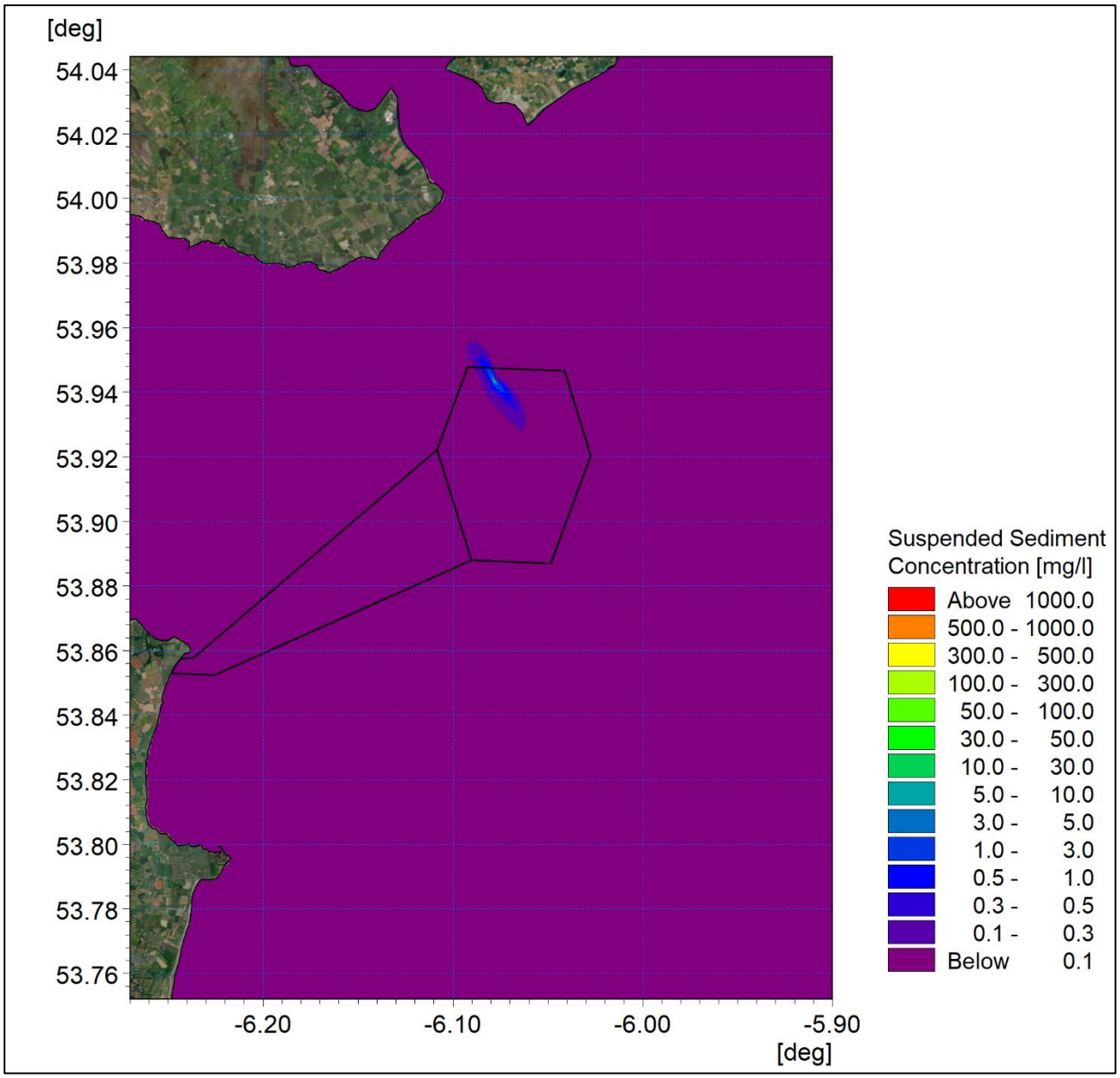

Figure 3A-108: Average suspended sediment concentration at ORI- A04 with flocculation.

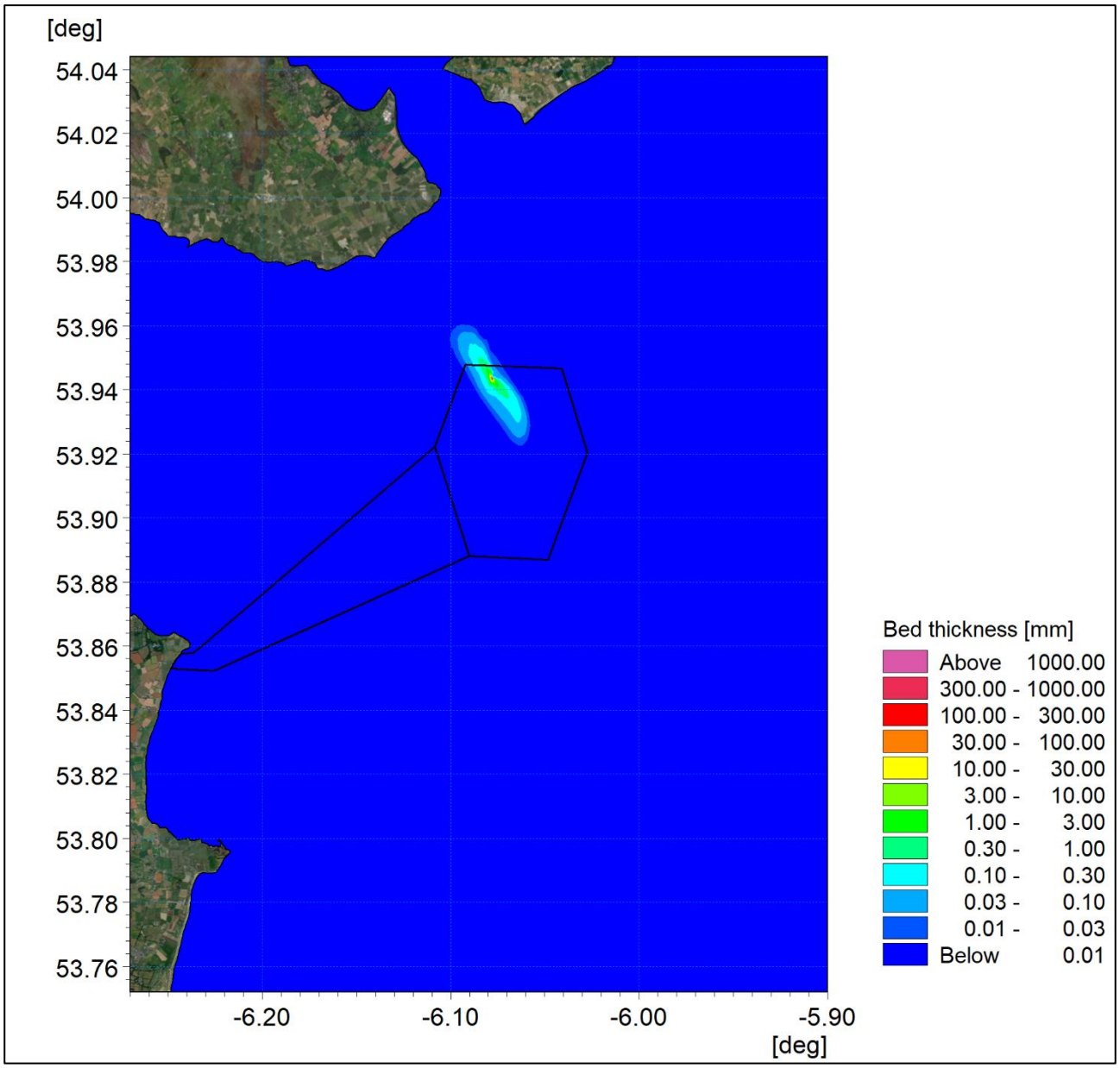

Figure 3A-109: Final sedimentation one day following installation at ORI- A04 with flocculation.

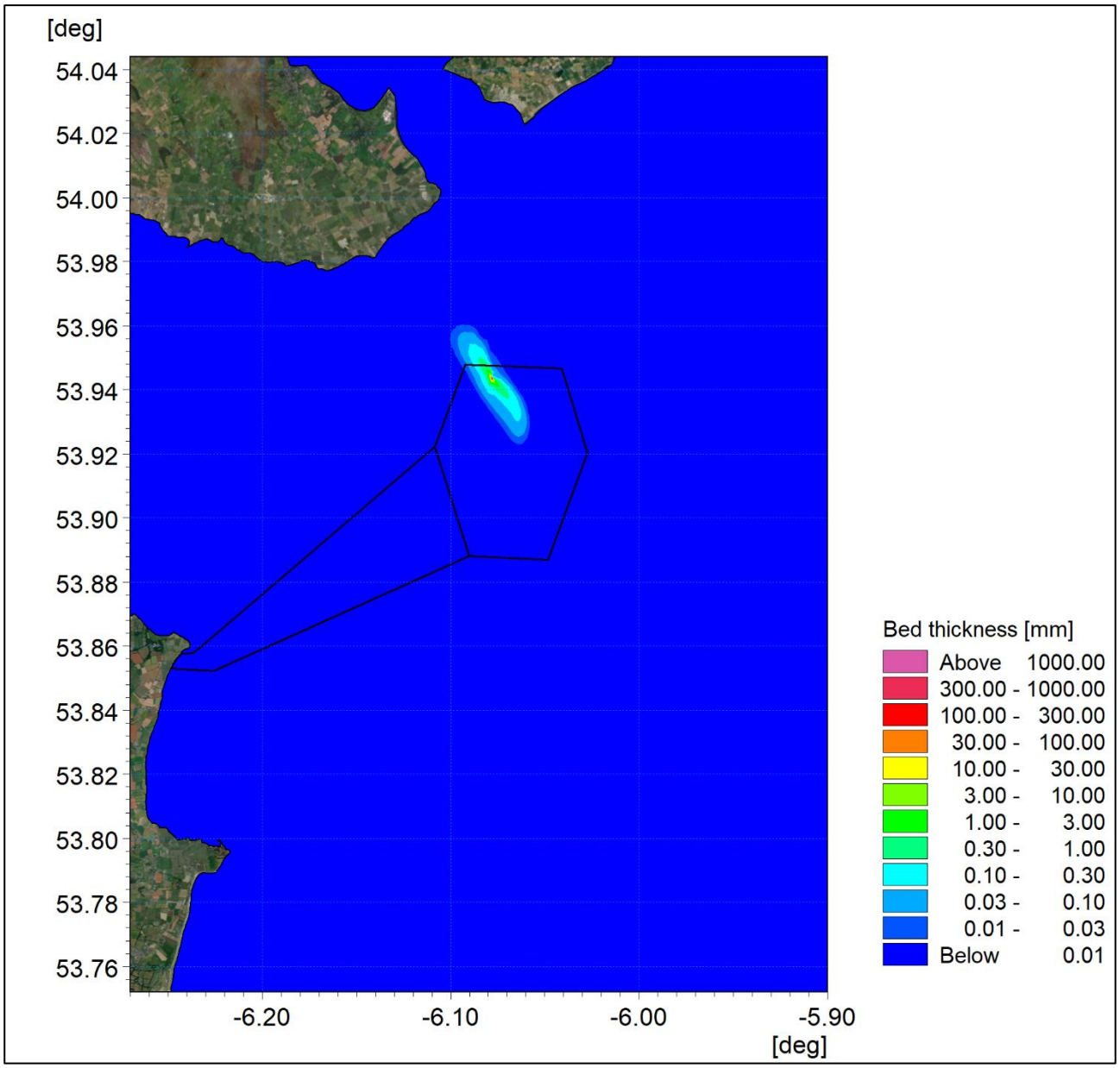

Figure 3A-110: Maximum sedimentation at ORI- A04 with flocculation.

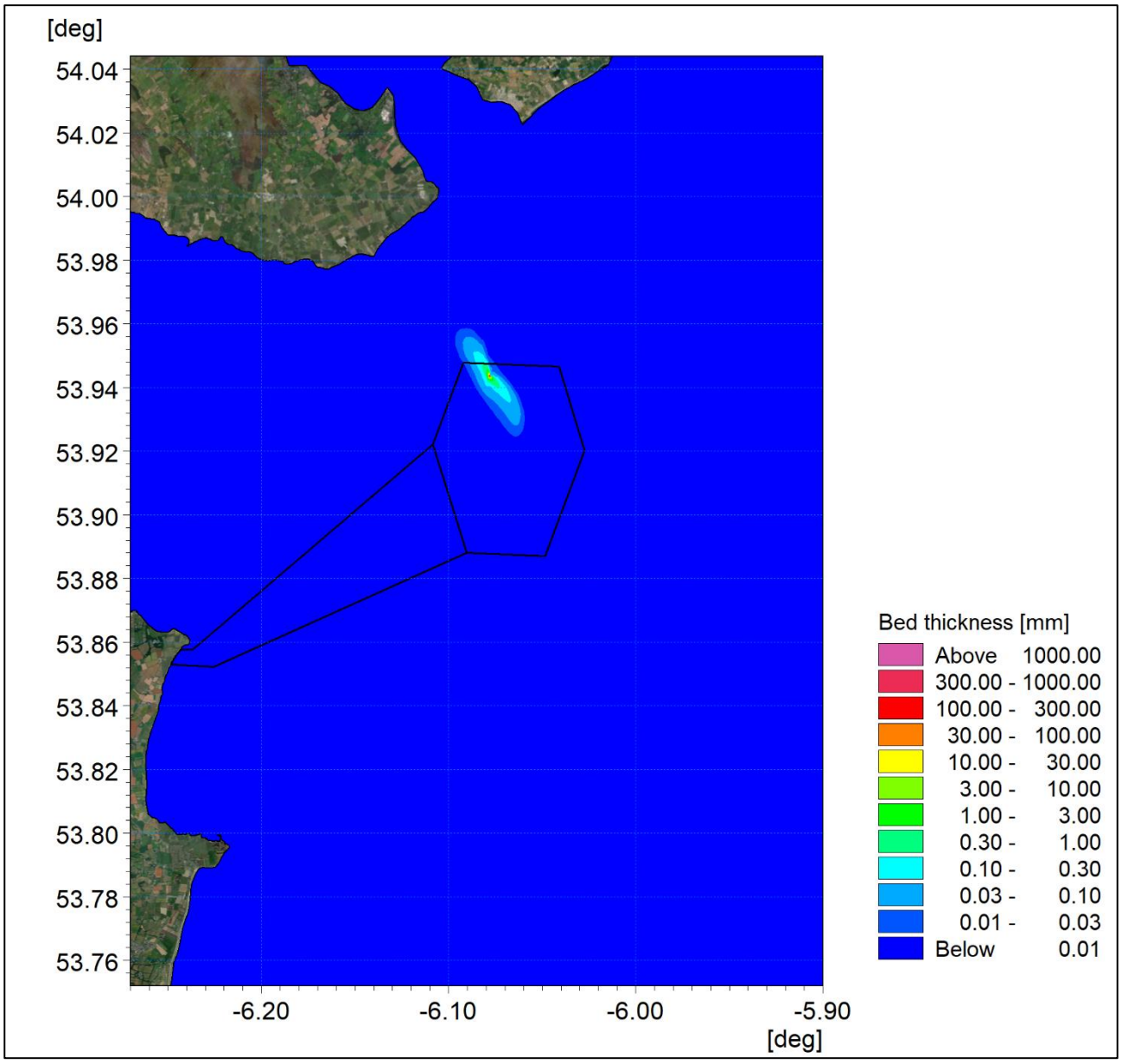

Figure 3A-111: Average sedimentation at ORI- A04 with flocculation.

ORI-B05

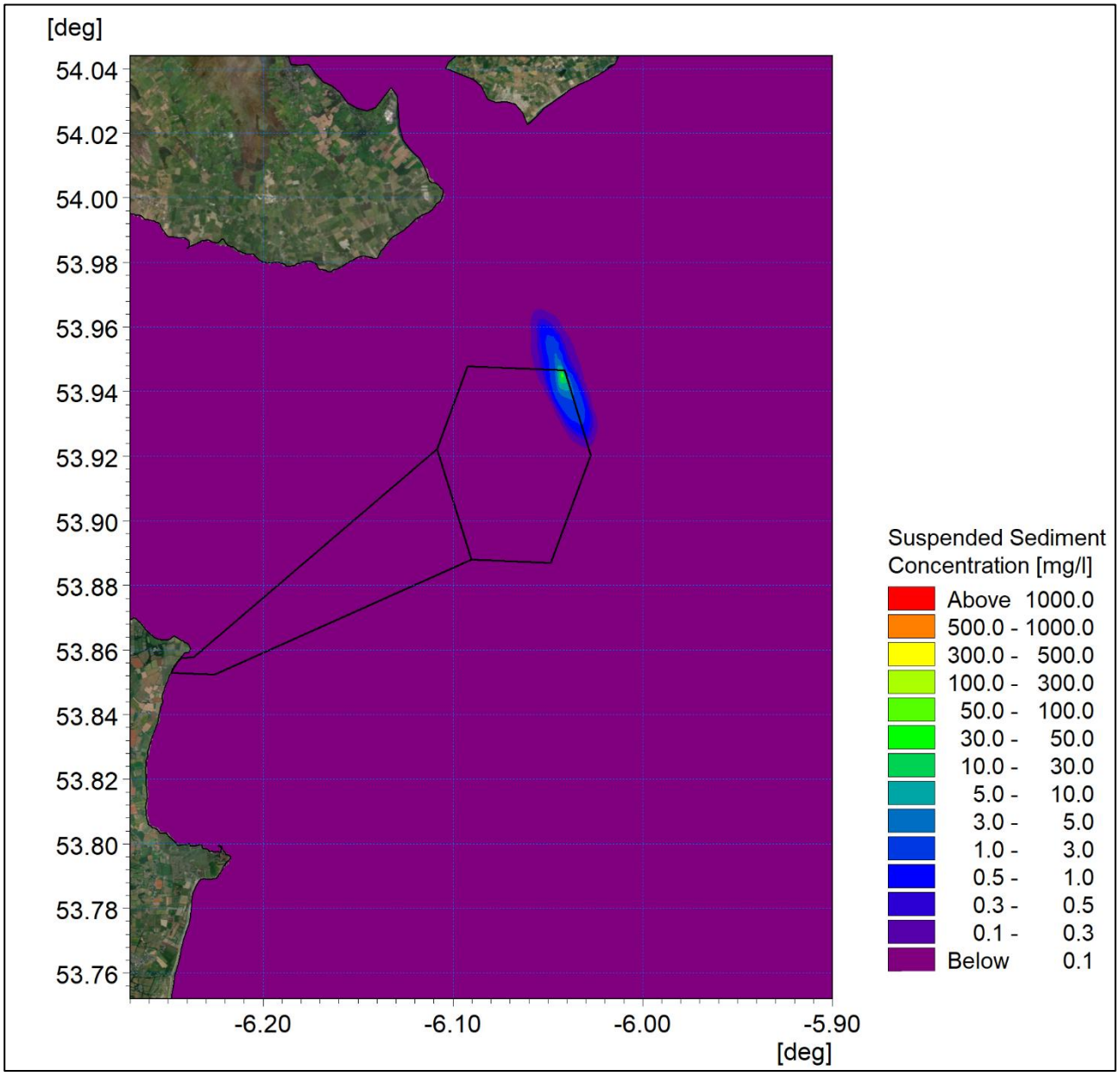

Figure 3A-112: Maximum suspended sediment concentration at ORI-B05 with flocculation.

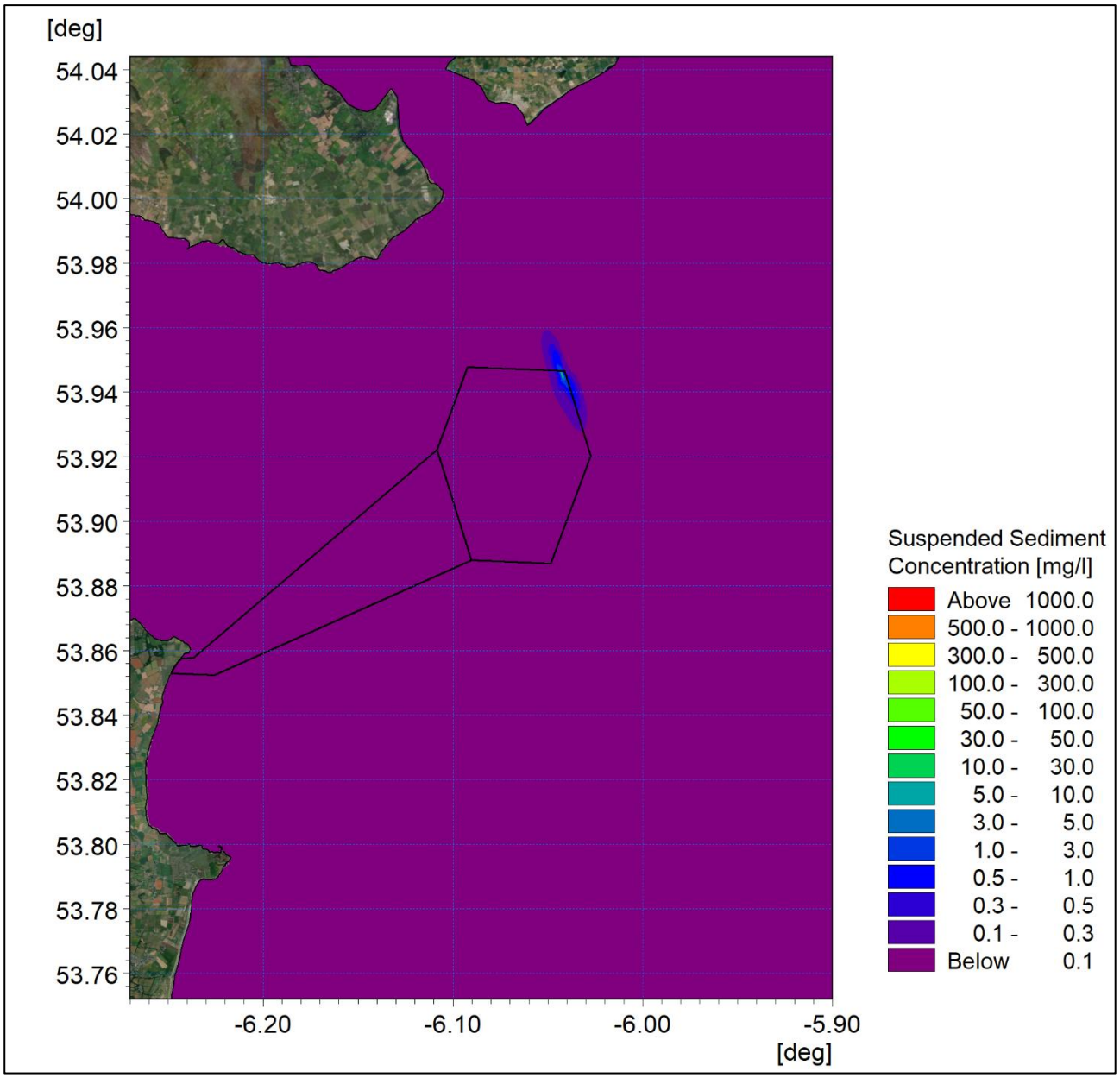

Figure 3A-113: Average suspended sediment concentration at ORI-B05 with flocculation.

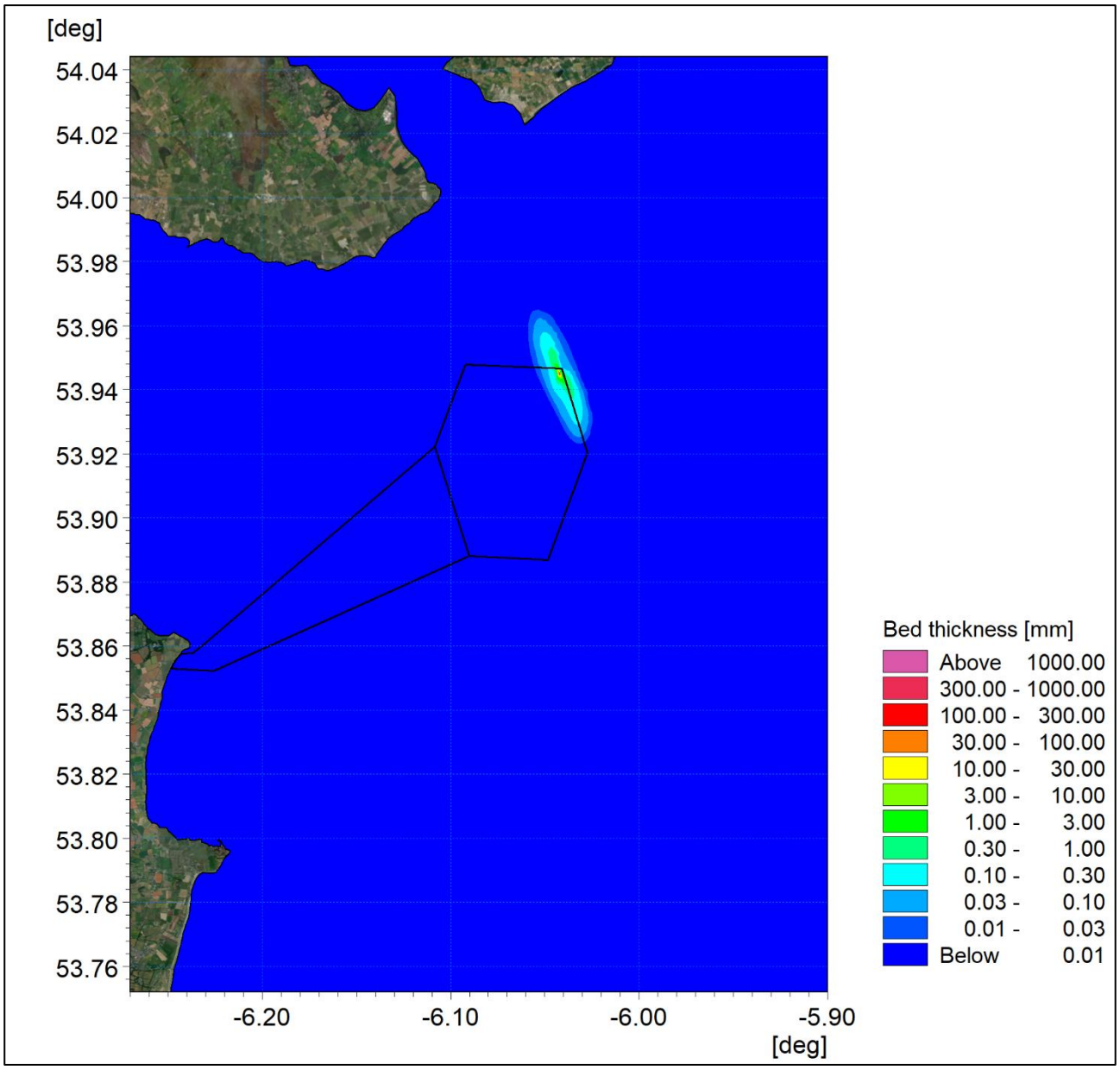

Figure 3A-114: Final sedimentation one day following installation at ORI-B05 with flocculation.

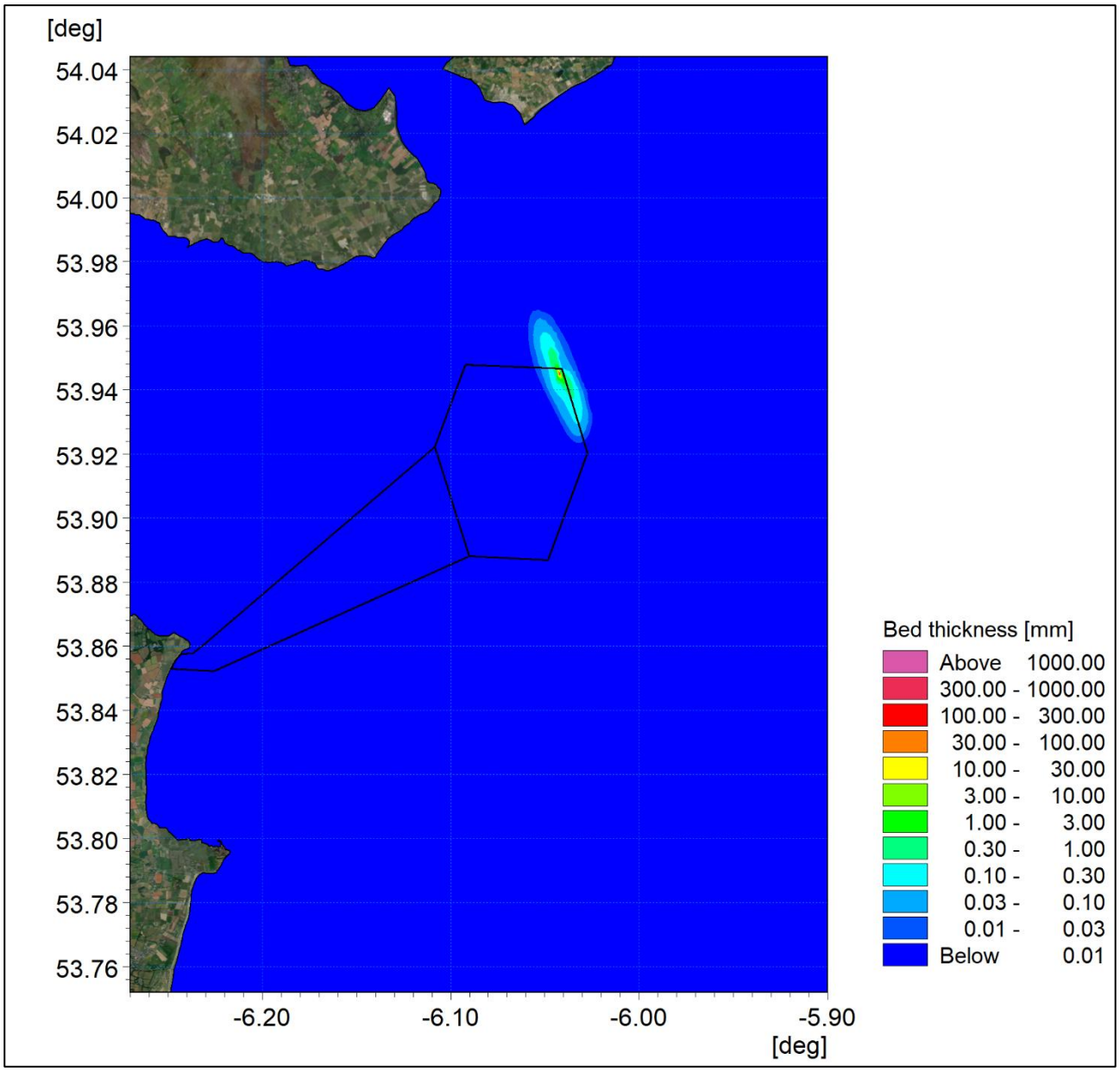

Figure 3A-115: Maximum sedimentation at ORI-B05 with flocculation.

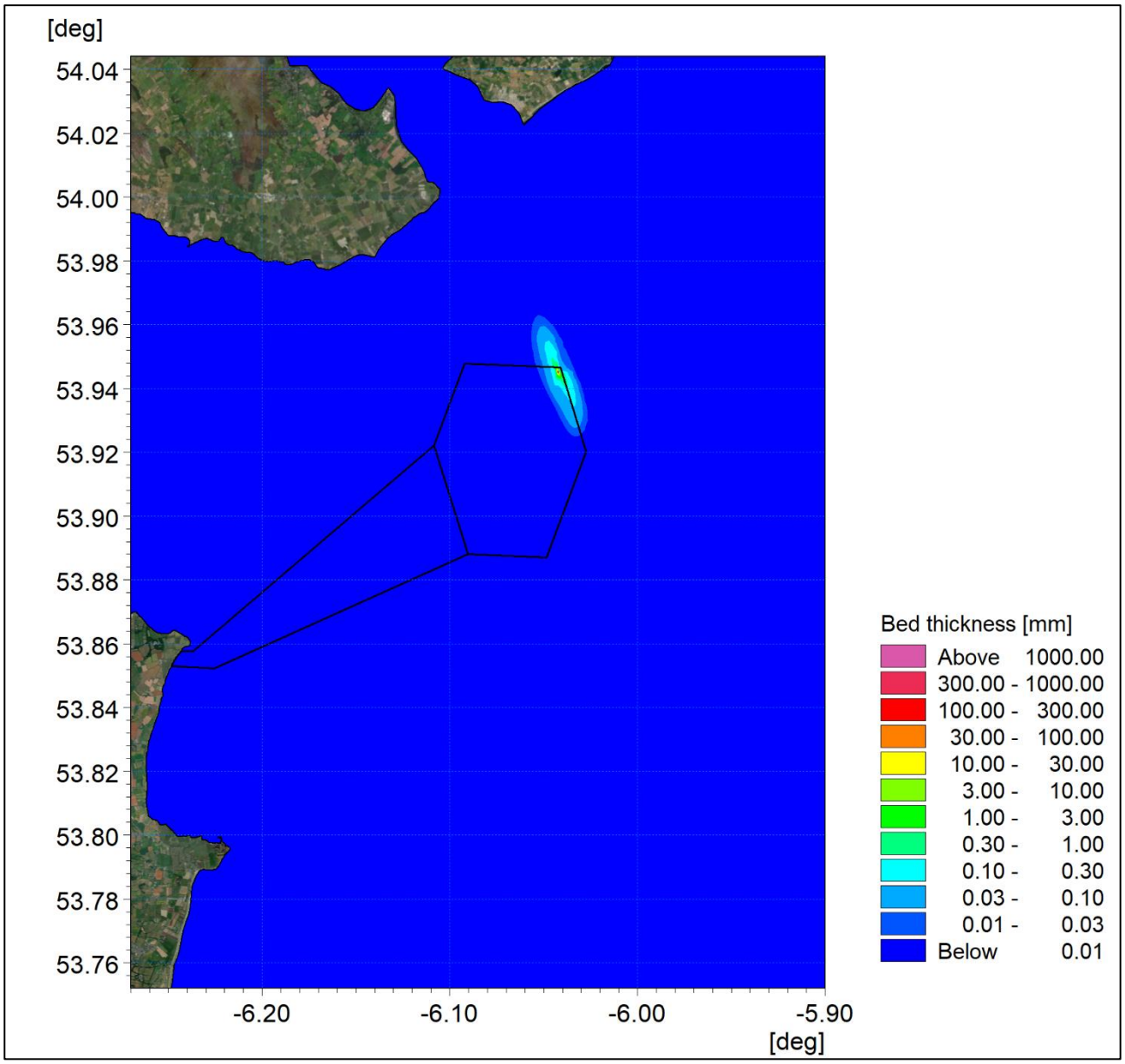

Figure 3A-116: Average sedimentation at ORI-B05 with flocculation.

3.3.2 Cable Installation

Section 2 of the NIS presents the installation parameters for the inter-array cables and the offshore cable. Both cable types are to be installed to a depth of 3 m in an excavation 1 m wide for inter-array cables and 3 m wide for offshore cables; although cable laying equipment may disturb a surface width of 10 m.

Cables will be installed into the seabed via jetting or ploughing methods where feasible. Jetting modifies the seabed with high-speed water jets so that the pre-laid cables sink by their own weight to a pre-determined depth. In the case of ploughing, a subsea plough is towed by the cable installation vessel to bury the cables simultaneously with the laying process. The plough lifts a wedge of soil and places the cable at the base of the trench before the wedge of soil backfills over the cable due to gravity. The amount of sediment mobilised will vary depending on both the installation technique and how it is implemented. In some cases cable jetting may simply liquify the seabed whereby relatively small amounts of material are mobilised into the water column. For the purposes of this modelling assessment as a worst case scenario, it was assumed that a wedge of material (i.e. represented by the maximum width of 3 m at the surface and able to accommodate the maximum external cable diameter of 0.25 m and 0.35 m at the base for inter-array and offshore cables respectively) was mobilised into the lower water column as a result of the burial process in line with the guidelines (BERR, 2008).

Similarly, to pile installation, the model simulations used the sediment grading determined from sediment sampling. However, in this instance, the modelling was undertaken using the MIKE21 Particle Tracking (PT) module. This module was considered more applicable as sediment could be released at discrete points in the water column as opposed to being introduced on a depth averaged basis. In this way the dispersion would not be over-estimated, or the corresponding sedimentation underestimated by the application of a current profile through the water column.

Installation rates can vary widely depending on the seabed material and equipment used; typically, rates are between 25 m/h and 780 m/h. For the simulation a relatively low rate of 120 m/hour was used ensuring that material was released at all tidal states over a number of tides whilst not so low that release rates and initial concentrations were underestimated.

Inter-array cables

A consecutive section of cabling from the offshore substation (OSS) and between ORI-C01 and ORI-C05 as illustrated in Figure 3-117 was modelled for this assessment. This route was chosen as the sediment along this corridor has the greatest potential for mobilisation and thus dispersion. As noted above the Project design parameters includes for a trench of 3 m depth and 1 m in width at the seabed. The modelling assumed that a wedge of material was displaced and reintroduced at 1 m above the seabed, in line with the installation process.

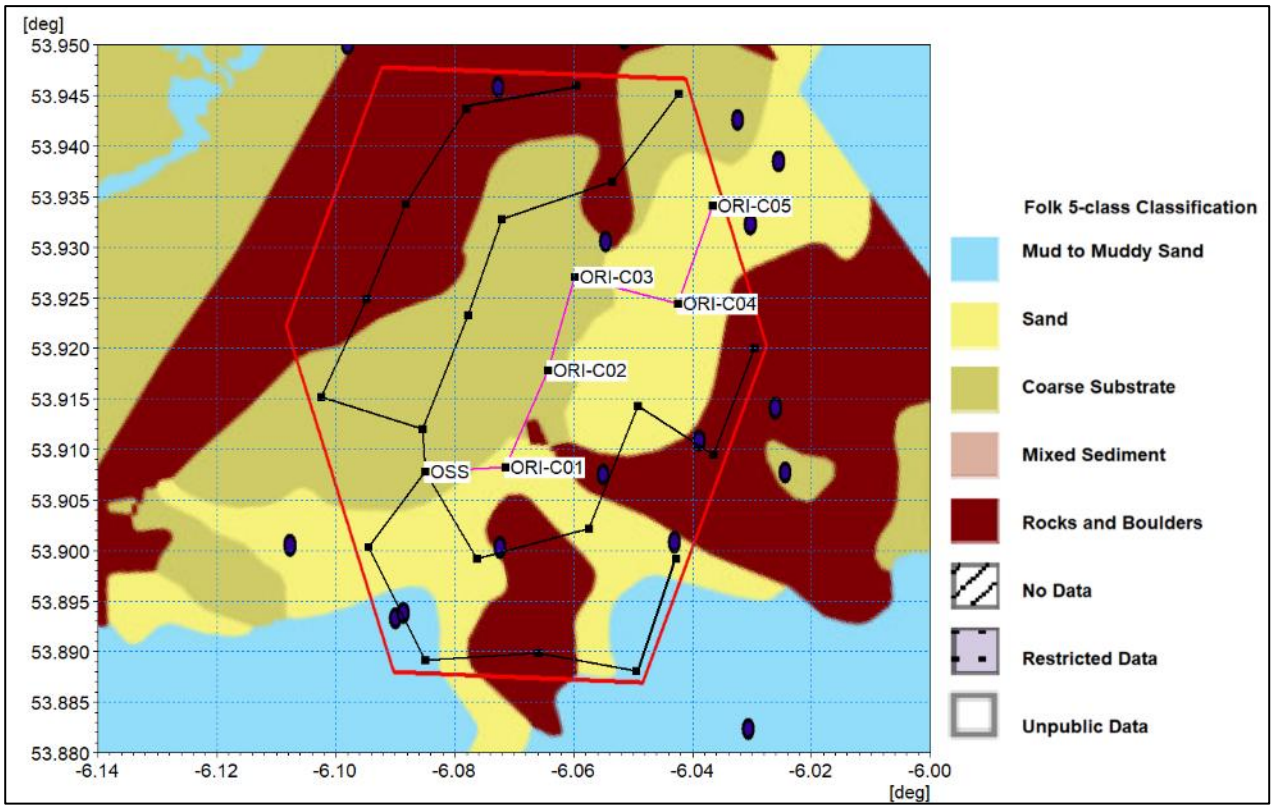

Figure 3-117: Location of the sediment source term (pink line) used to model a representative dredging route for the inter-array cables.

The GSI sampling data indicated the following sediment characteristics:

- 45% silt/clay 0.05 mm diameter;
- 15% sandy mud 0.1 mm diameter; and
- 40% medium sand 0.5 mm diameter.

The model results presented follow the same format as those for foundation installation described in the previous section. It should be noted that the maximum and average suspended sediment contour palette in has been accentuated using a log scale for clarity. The average values presented in Figure 3A-118 are typically one tenth of the maximum value in Figure 3A-119. The sediment plumes are much smaller than those seen for the auger pile installation. The reason for this is twofold, firstly there is no fine bentonite material associated with the cable installation activities which was utilised in the foundation drilling process; and secondly the material is mobilised at the seabed where current speeds are significantly lower.

Maximum plume concentrations are around 2,000 mg/l but these values are not sustained, as average values are less than 3 mg/l which is comparable to background levels. The sediment plume will only persist for a maximum period of *c.* three hours in any location as the installation moves on and the tide turns. Following the completion of the works the turbidity levels return to background within several of tidal cycles. It would however be anticipated that spring tides following the works may mobilise and redistribute unconsolidated material which would then re-settle at later stages of the construction phase.

Figure 3A-120 shows the final sedimentation levels one day after completion whilst the maximum values are shown in Figure 3A-121. Figure 3A-122 illustrates the average sedimentation. If these three plots are considered together it can be determined that the native seabed material settles close to where it is mobilised and remains *in situ* as these results are very similar. This would be expected as the baseline modelling indicated that sediment transport potential is limited across the offshore wind farm area.

The sedimentation is seen to be concentrated along the installation route as material effectively returns to the site from where it is disturbed. Beyond 50 m the sedimentation levels are in the order of 1 mm and at the offshore wind farm area boundary <1 mm and therefore indiscernible from the existing seabed sediment.

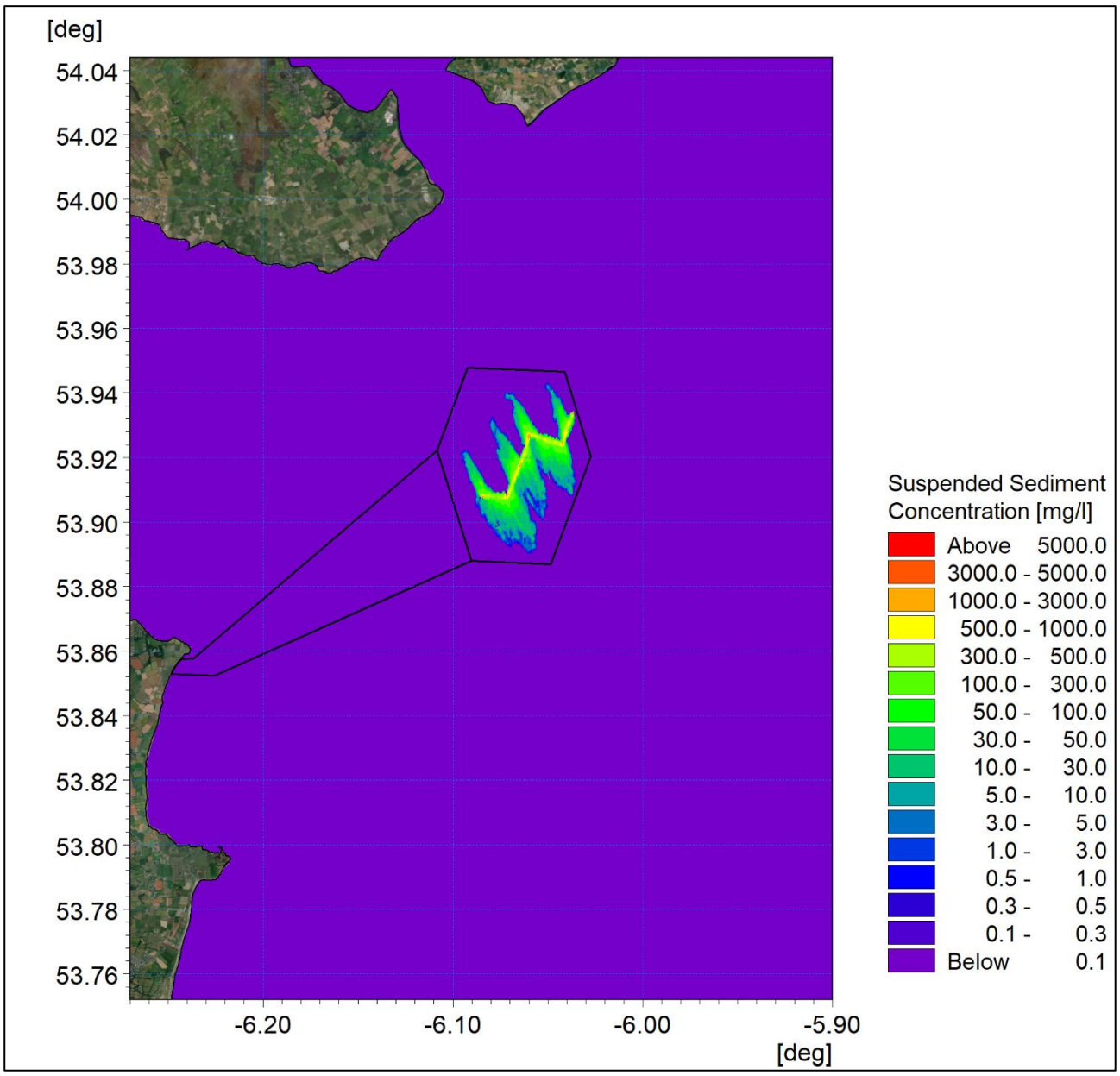

Figure 3A-118: Maximum suspended sediment concentration for inter-array cable trench.

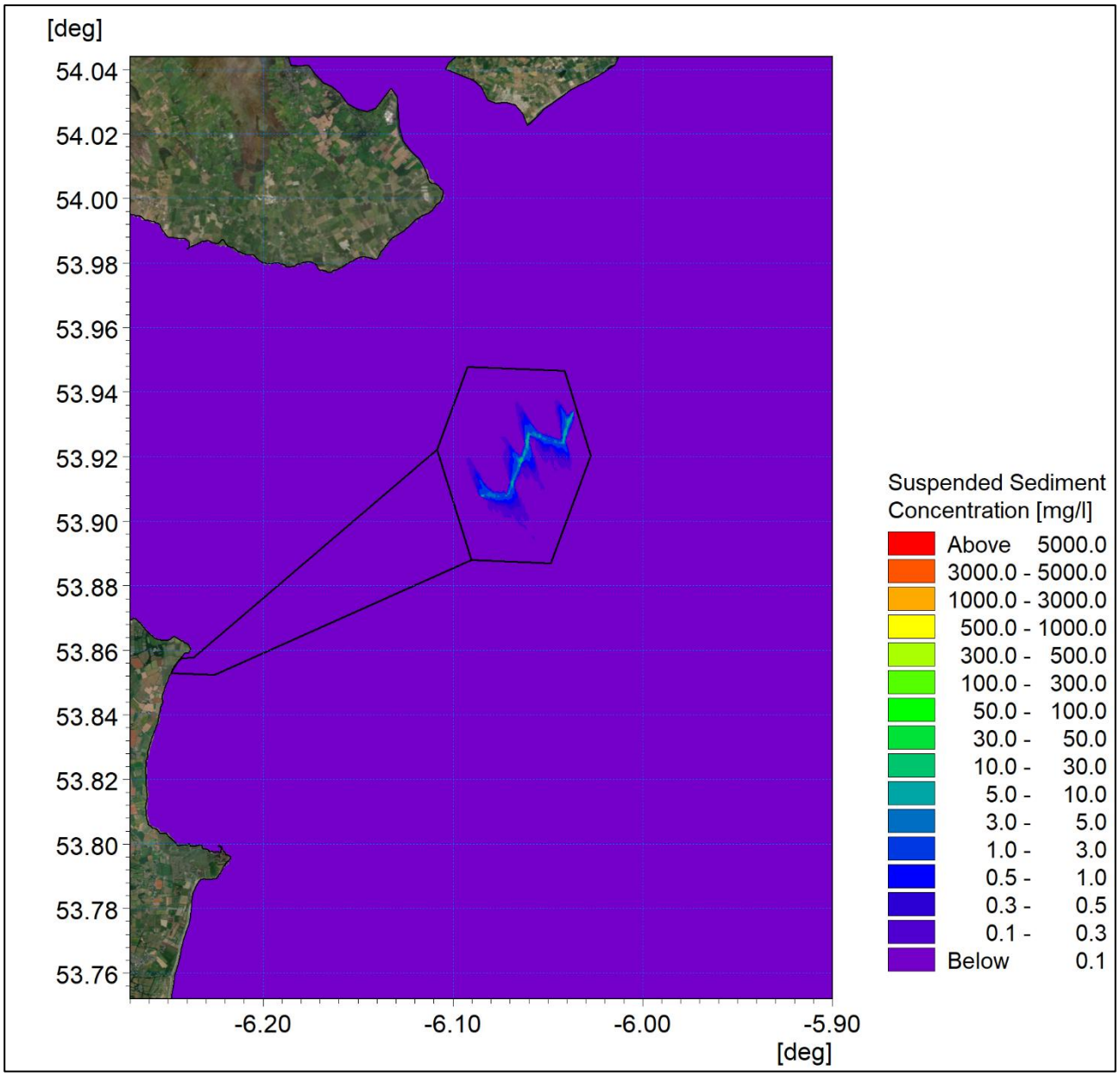

Figure 3A-119: Average suspended sediment concentration for inter-array cable trench.

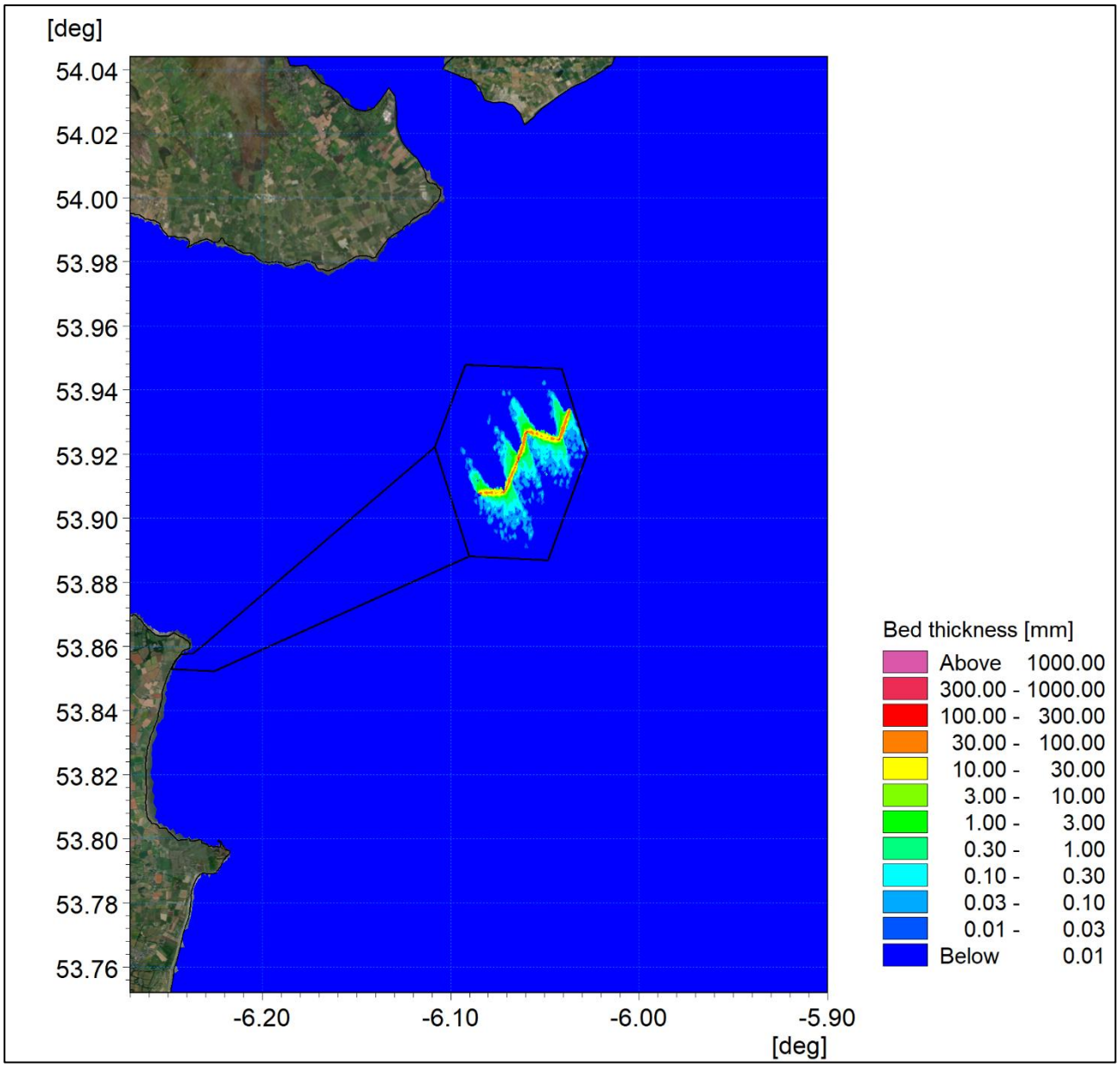

Figure 3A-120: Final sedimentation one day after installation for inter-array cable trenching.

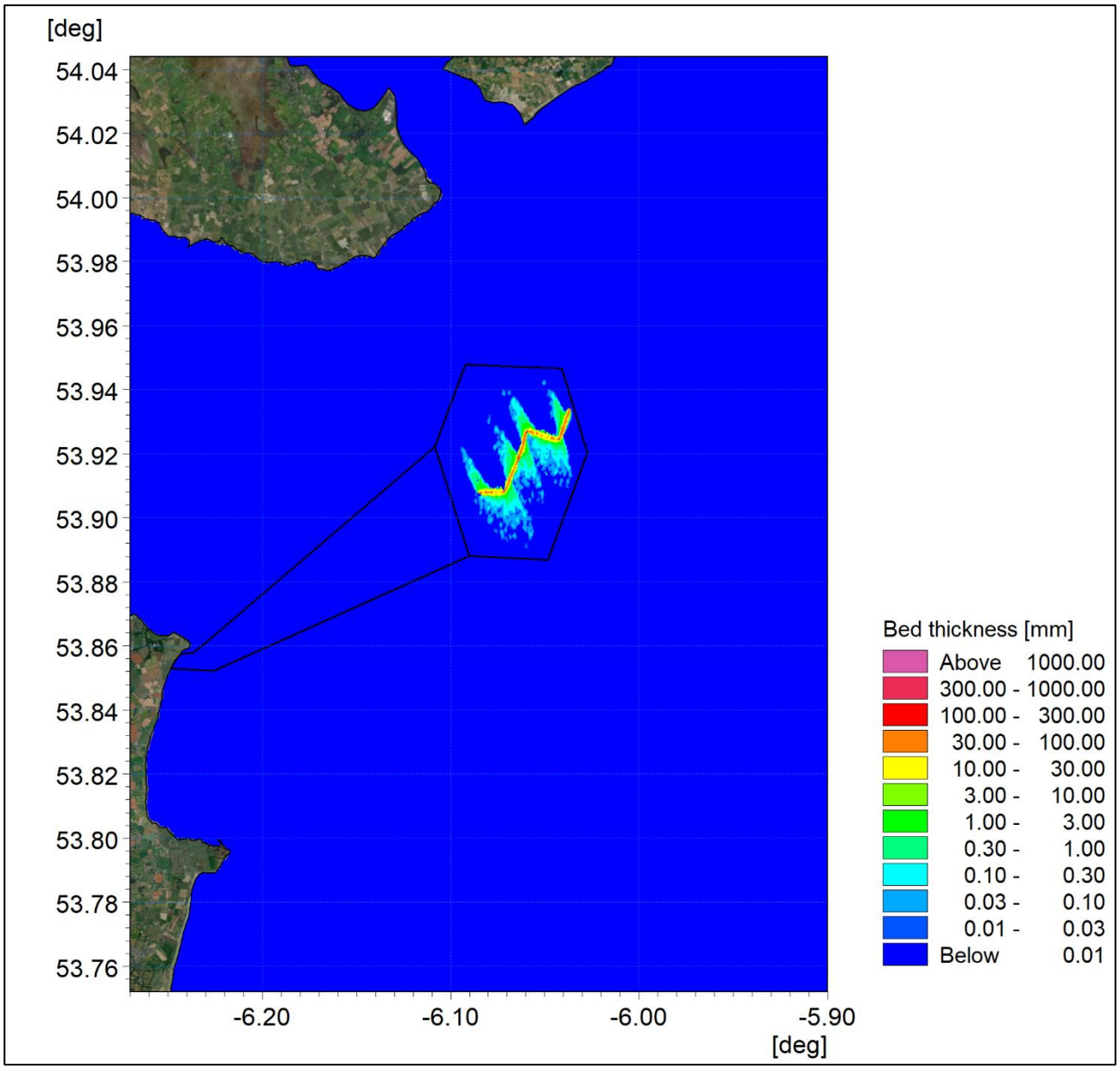

Figure 3A-121: Maximum sedimentation for inter-array cable trenching.

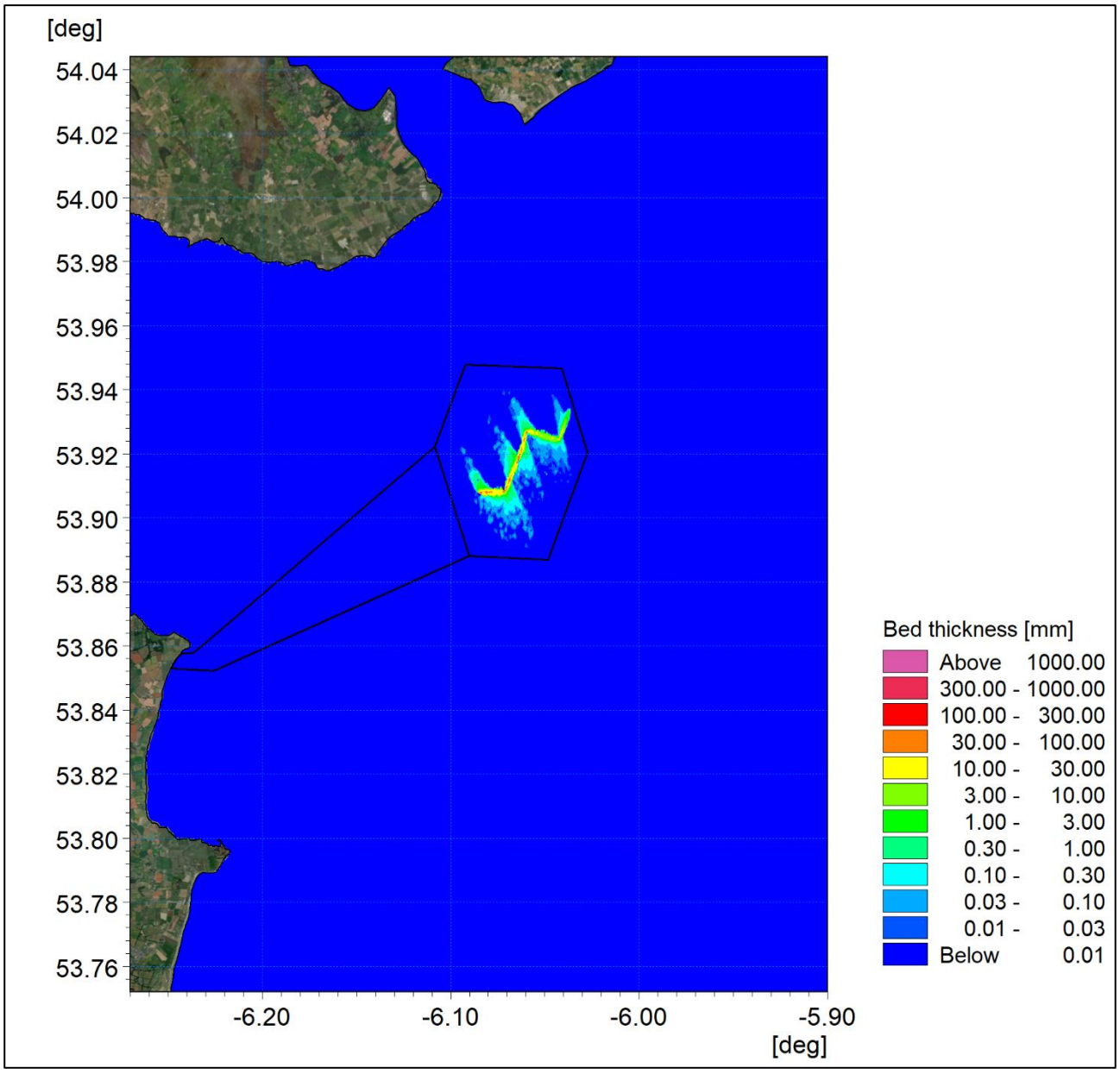

Figure 3A-122: Average sedimentation for inter-array cable trenching.

Offshore Cable

Modelling was undertaken of the installation of the offshore cable between the OSS and the landfall location as indicated by the pink trace in Figure 3-123. As for inter-array cables, the Project design parameters include for a trench of 3 m depth and 3 m in width at the seabed. This was represented by a wedge of material being released into the lower water column as described in the previous section.

The modelling was undertaken with the sediment released along the full length of the offshore cable corridor, running offshore to inshore. The release continued through the intertidal zone to the High Water Mark, to represent the installation of the intertidal section of the cable by open trenching. The modelling assumed that this volume of material was displaced and reintroduced at 1 m above the seabed, in line with the installation process. The simulation assumed the same trenching rate as with the inter-array cables.

The GSI sampling data indicated the following sediment characteristics:

- 45% silt/clay 0.05 mm;
- 15% sandy mud 0.1 mm; and
- 40% medium sand 0.5 mm.

Figure 3A-124 and Figure 3A-125 show the suspended sediment plumes with a log scale to accentuate result for the maximum and average values respectively. Nearshore tidal currents are stronger than those in the offshore locations and water depths are limited, therefore much higher suspended sediment levels would be expected in these areas. The sediment plume is seen to extend both north and south of the offshore cable corridor as it is dispersed by tidal flows.

Generally, peak values are around 300 mg/l which is akin to turbidity levels experienced during storm conditions. Towards the landfall these peaks increase due to the limited depth into which the material is dispersed. However, these areas are localised, and average concentrations are less than 50 mg/l. As with the inter-array cable scenario the plume does not remain stationary, and these elevated levels do not persist for more than three to four hours as material settles and the tide turns. Following completion of the work material would be re-suspended on successive tides and be drawn into the existing transport regime in nearshore regions.

Figure 3-123: Location of modelled offshore cable corridor.

The plot in Figure 3A-126 shows the sediment thickness one day after completion of the cable installation. It demonstrates the influence of the eddy south of Dunany Head and how material will be incorporated into the existing transport patterns. The maximum values are shown in Figure 3A-127, however, care must be taken when interpreting this data as material which is repeatedly settled on slack water and re-suspended may be double counted. Figure 3A-128 shows the average sedimentation over the course of the cable installation.

The distribution of the sediment which is released during the operation is typically less than 20 mm in depth. Most material settles in the vicinity of the offshore cable corridor, within 200 m either side of the works, with final settled depth being less than 5 mm outside the offshore cable corridor. It should be noted that installation is continued through the intertidal zone and under calm conditions.

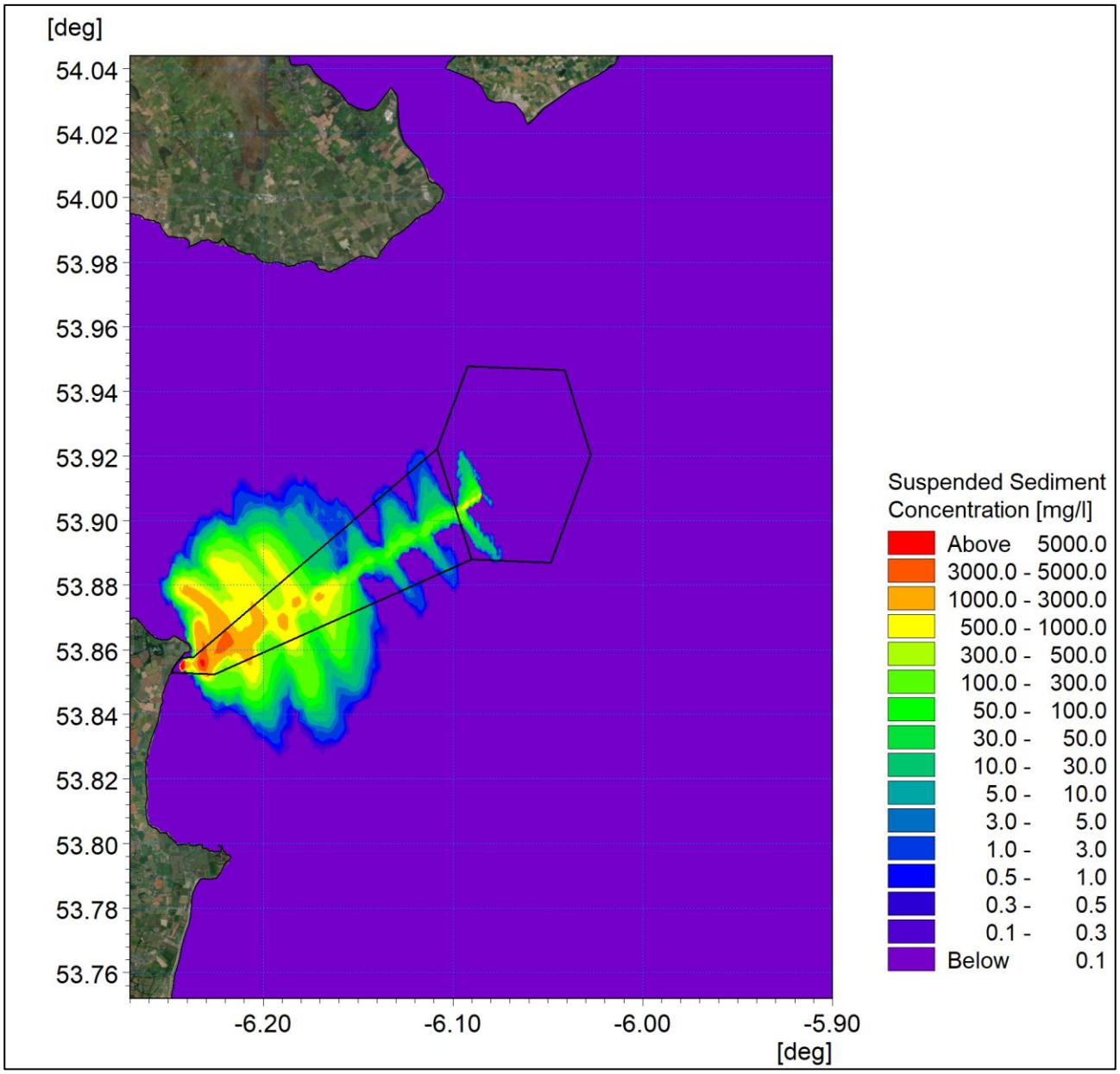

Figure 3A-124: Maximum suspended sediment concentration for offshore cable trenching.

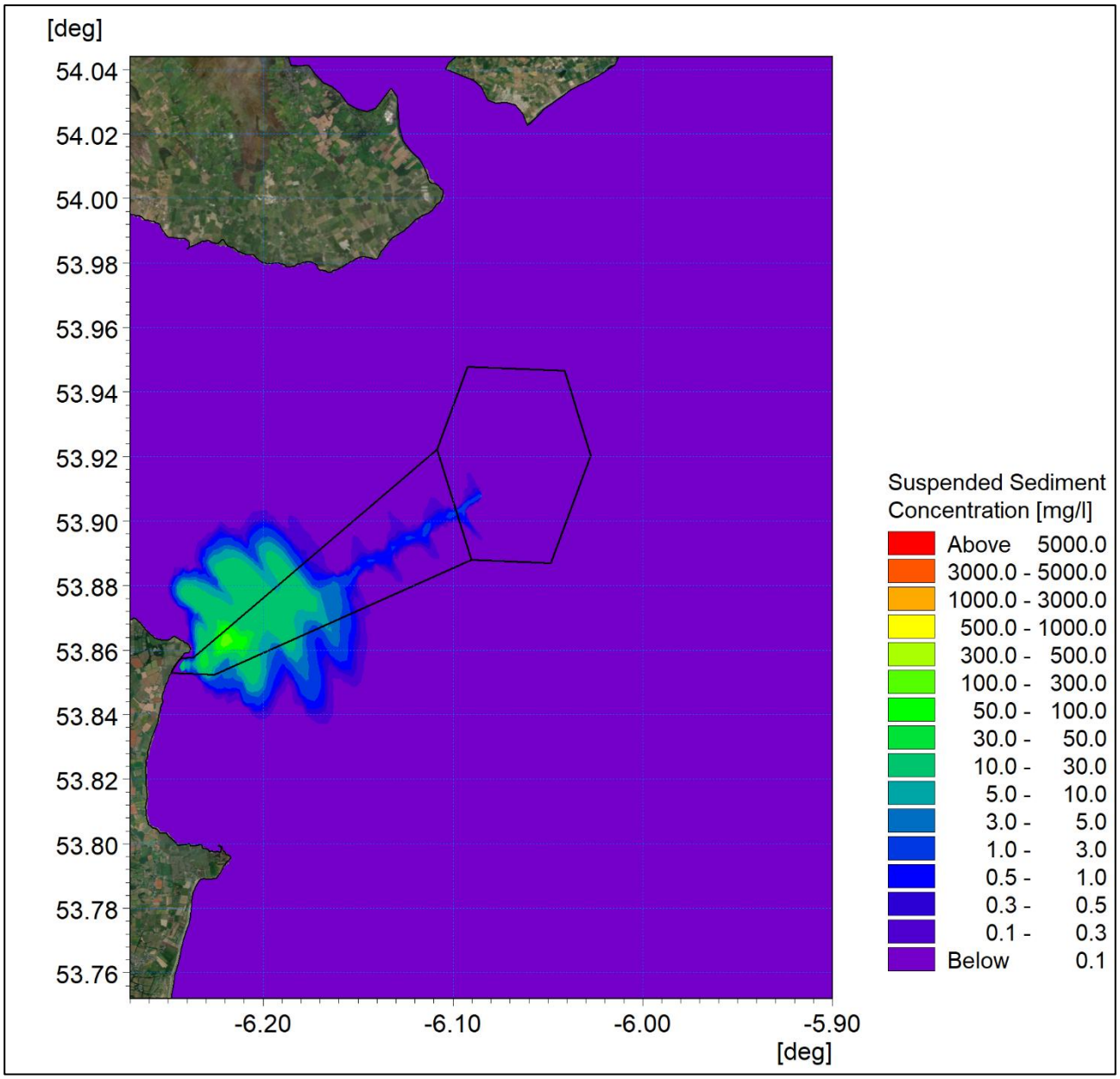

Figure 3A-125: Average suspended sediment concentration for offshore cable trenching.

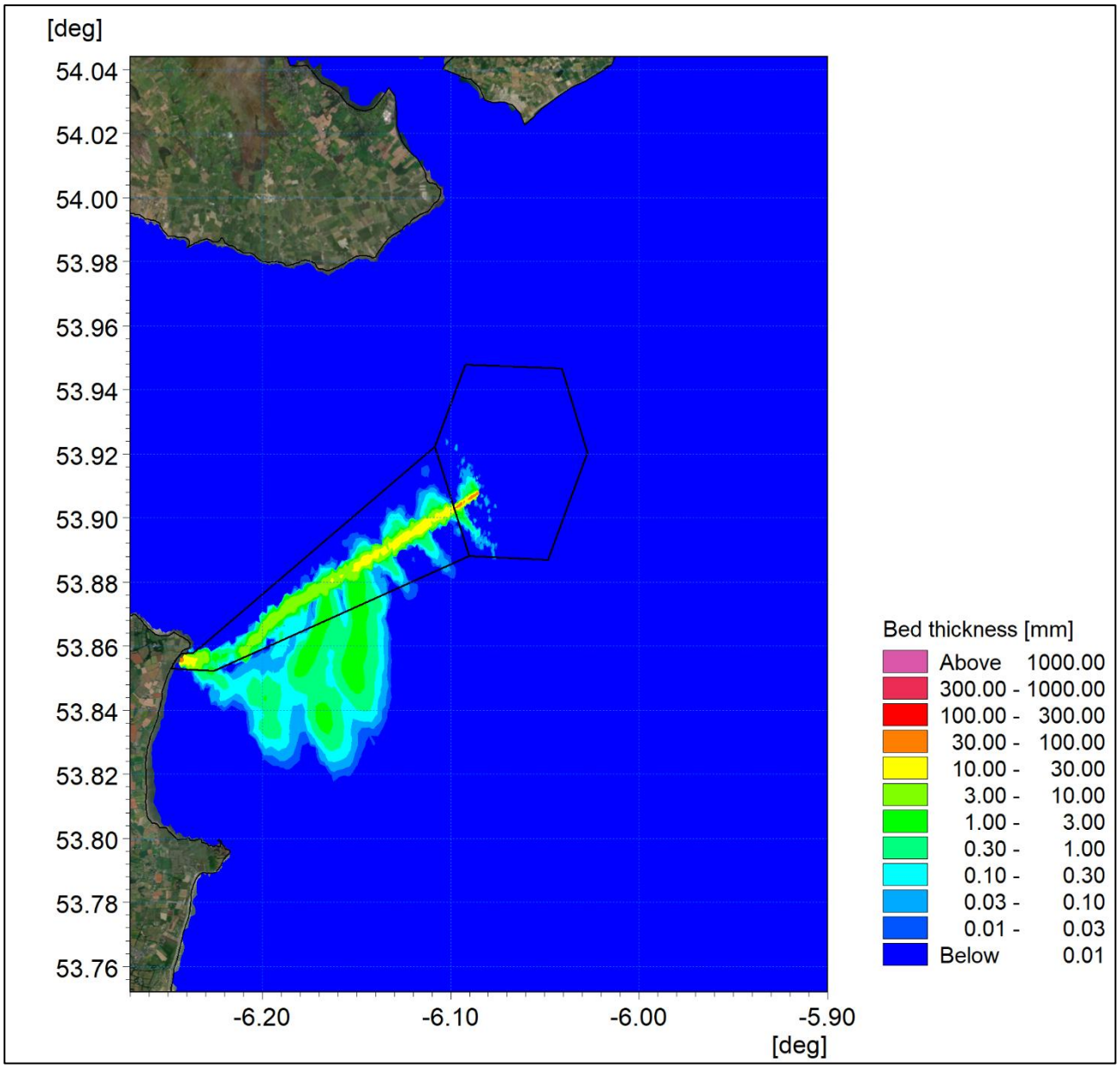

Figure 3A-126: Final sedimentation one day following installation for offshore cable trenching.

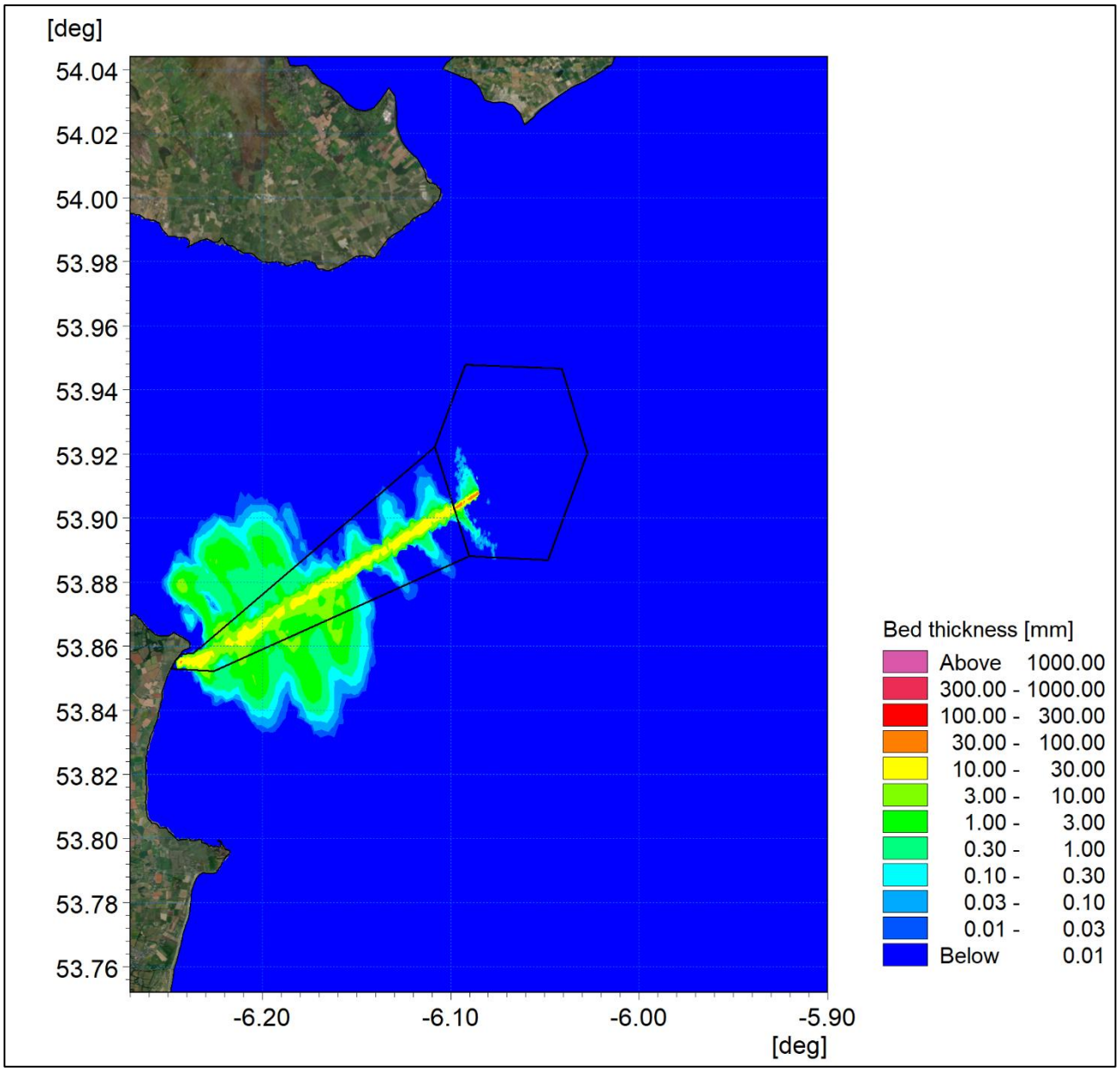

Figure 3A-127: Maximum sedimentation for offshore cable trenching.

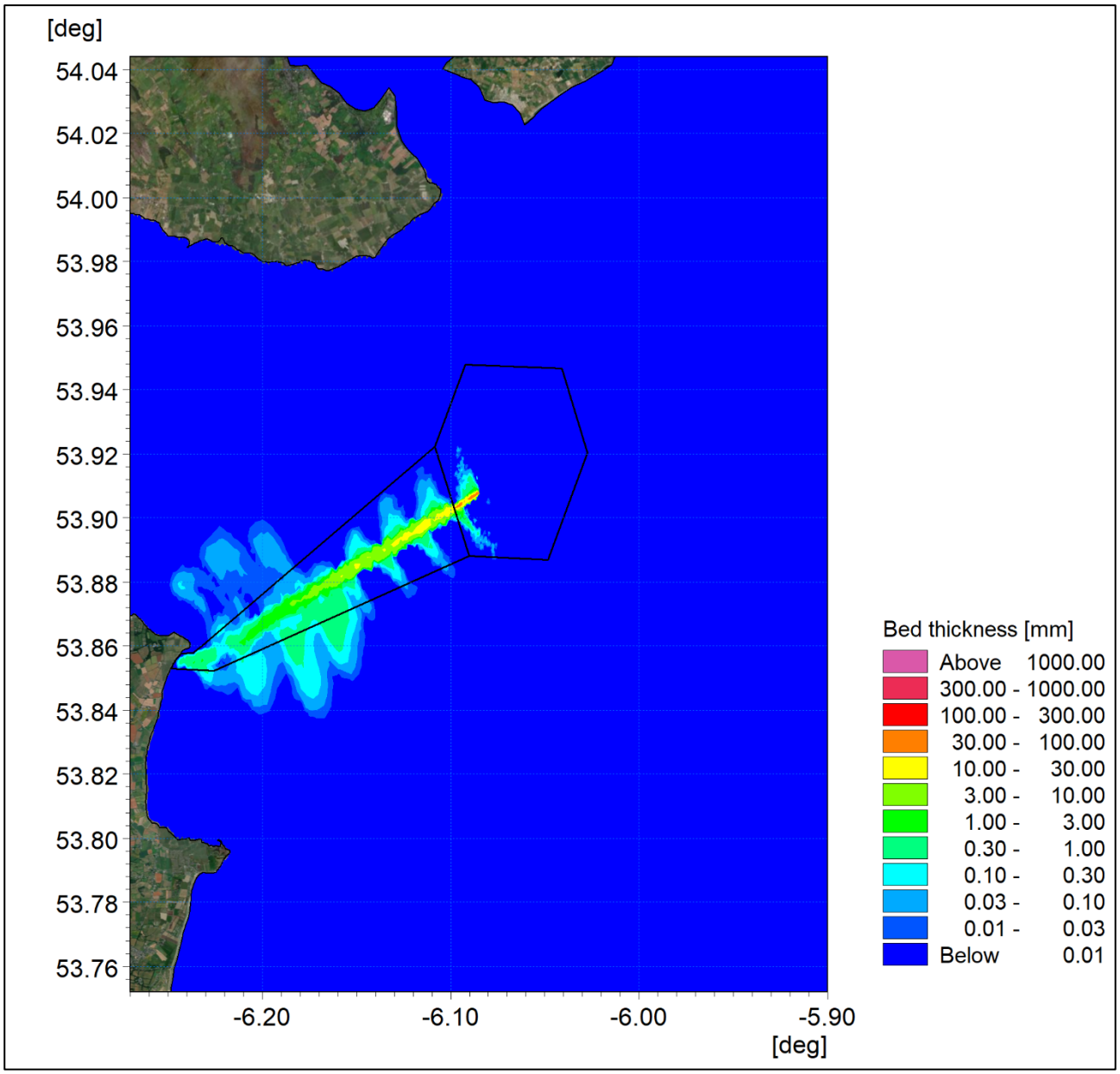

Figure 3A-128: Average sedimentation for offshore cable trenching.

Sensitivity of cable installation plume dispersion

Akin to the foundation installation (section 3.3.1), in response RFI 6.E additional sensitivity modelling was undertaken to examine the influence of flocculation on the sediment dispersion and subsequent deposition. The modelling of offshore cable installation was used for the sensitivity test as it included trenching in both nearshore areas and those offshore which are similar to the inter-array trenching conditions. The previous simulation was repeated with the inclusion of flocculation within the MIKE Particle Tracking modelling parameters. The trenching scenario releases proportionally less fine material than the drilling (as drilling mud it not used) however the sediment volumes mobilised are greater and as they are released closer to the seabed, the critical concentration for flocculation may be achieved.

Figure 3A-129 and Figure 3A-130 present the maximum and average suspended sediment concentration for the trenching scenario with the inclusion of flocculation. When compared with the non-flocculation counterparts, Figure 3A-124 and Figure 3A-125, it is evident that flocculation has occurred. The maximum concentrations are increased along the trenching route and, although the plume extent has only been slightly

reduced, the sediment concentrations beyond the immediate vicinity of the trench are reduced. Figure 3A-131, Figure 3A-132 and Figure 3A-133 illustrated the sedimentation depths following completion, maximum values and average values respectively. These are comparable with Figure 3A-126, Figure 3A-127 and Figure 3A-128 for the simulation without flocculation enabled. As one would expect, the resulting sedimentation footprint has been reduced and a lesser degree of resuspension has occurred. With the application of flocculation within the model a larger percentage of the dredged material has settled at the site of the trenching and, in terms of NIS assessment, this represents a lesser impact than the worst case scenario taken forward into the assessment.

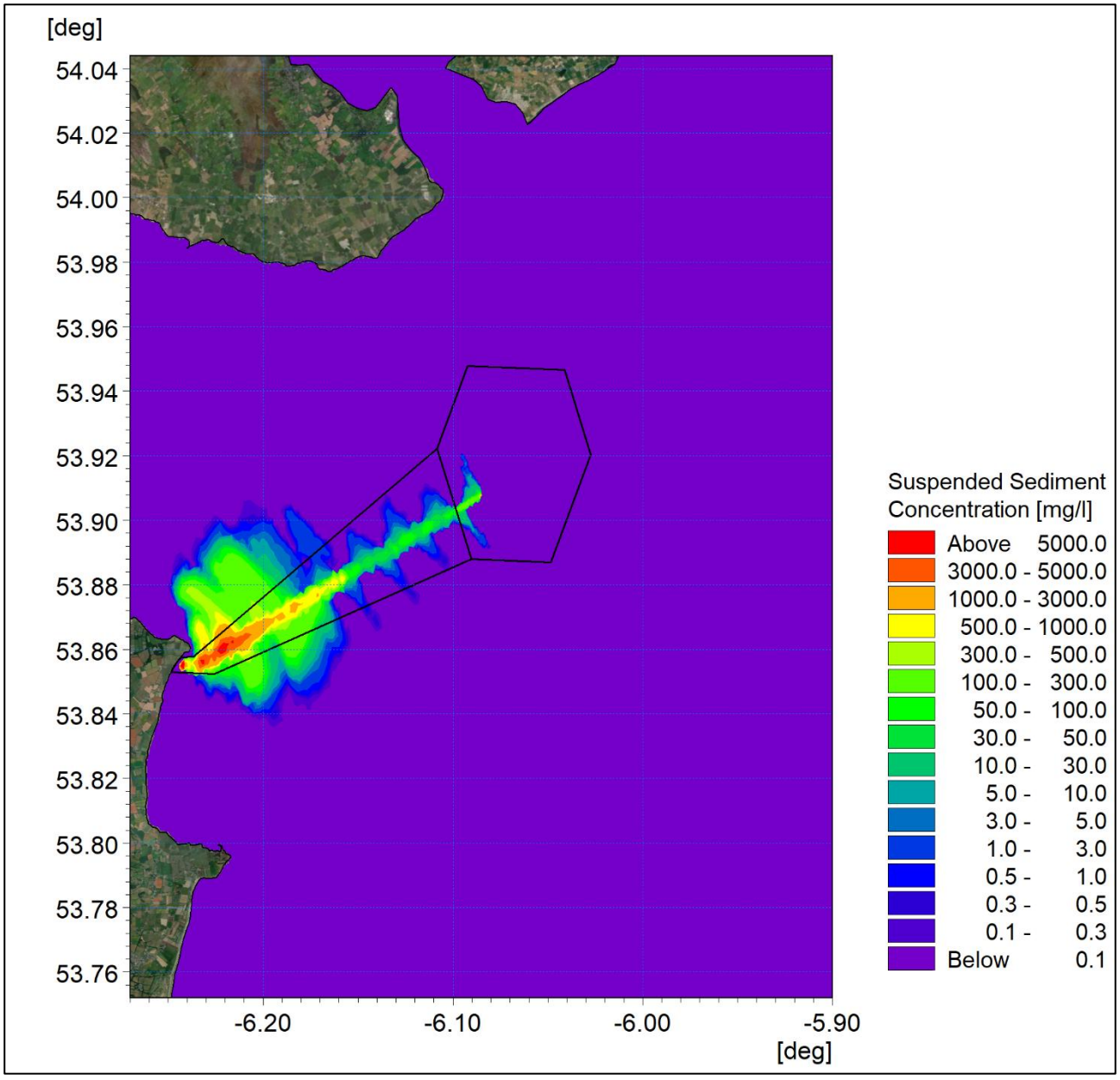

Figure 3A-129: Maximum suspended sediment concentration for offshore cable trenching with flocculation.

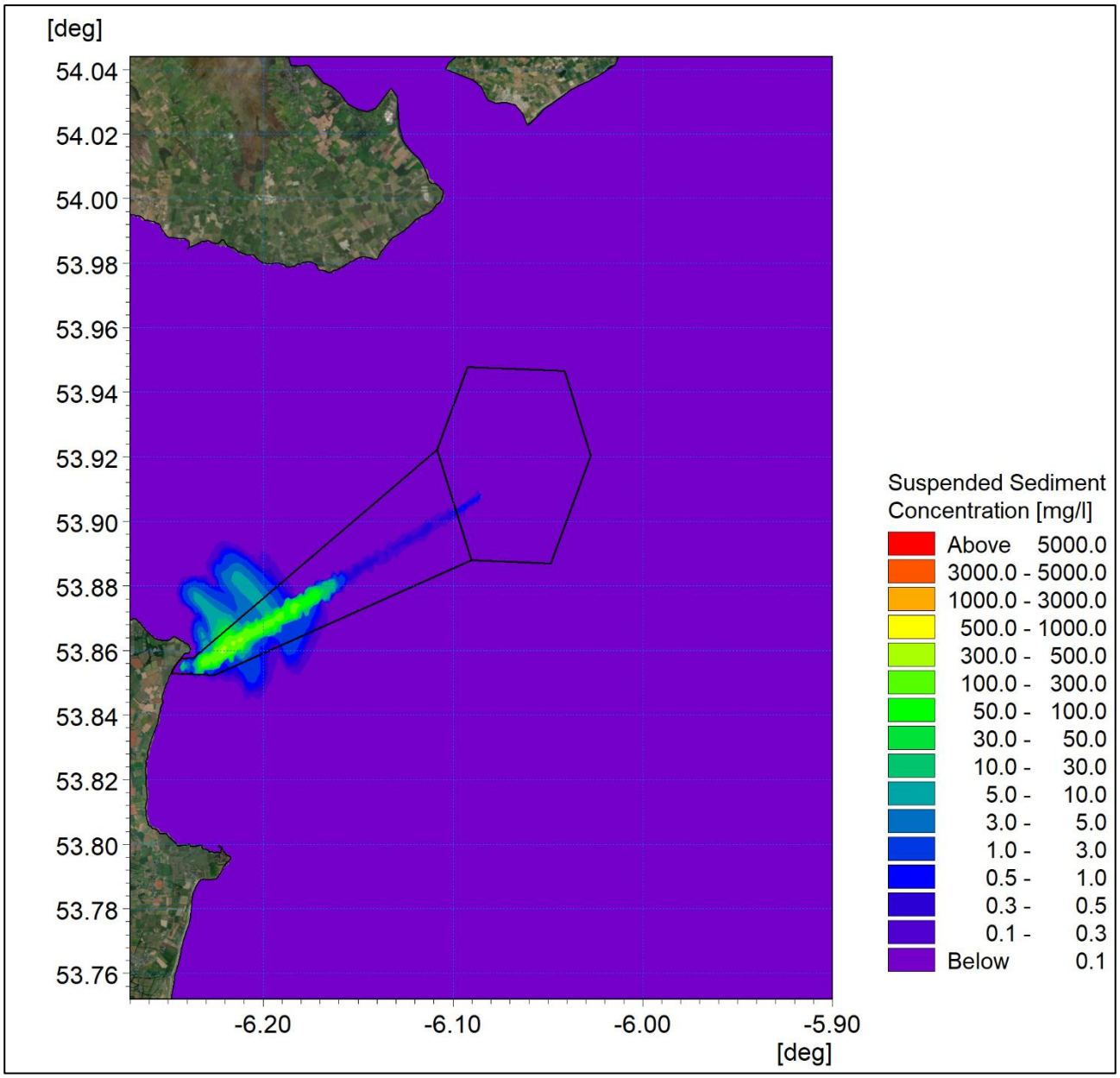

Figure 3A-130: Average suspended sediment concentration for offshore cable trenching with flocculation.

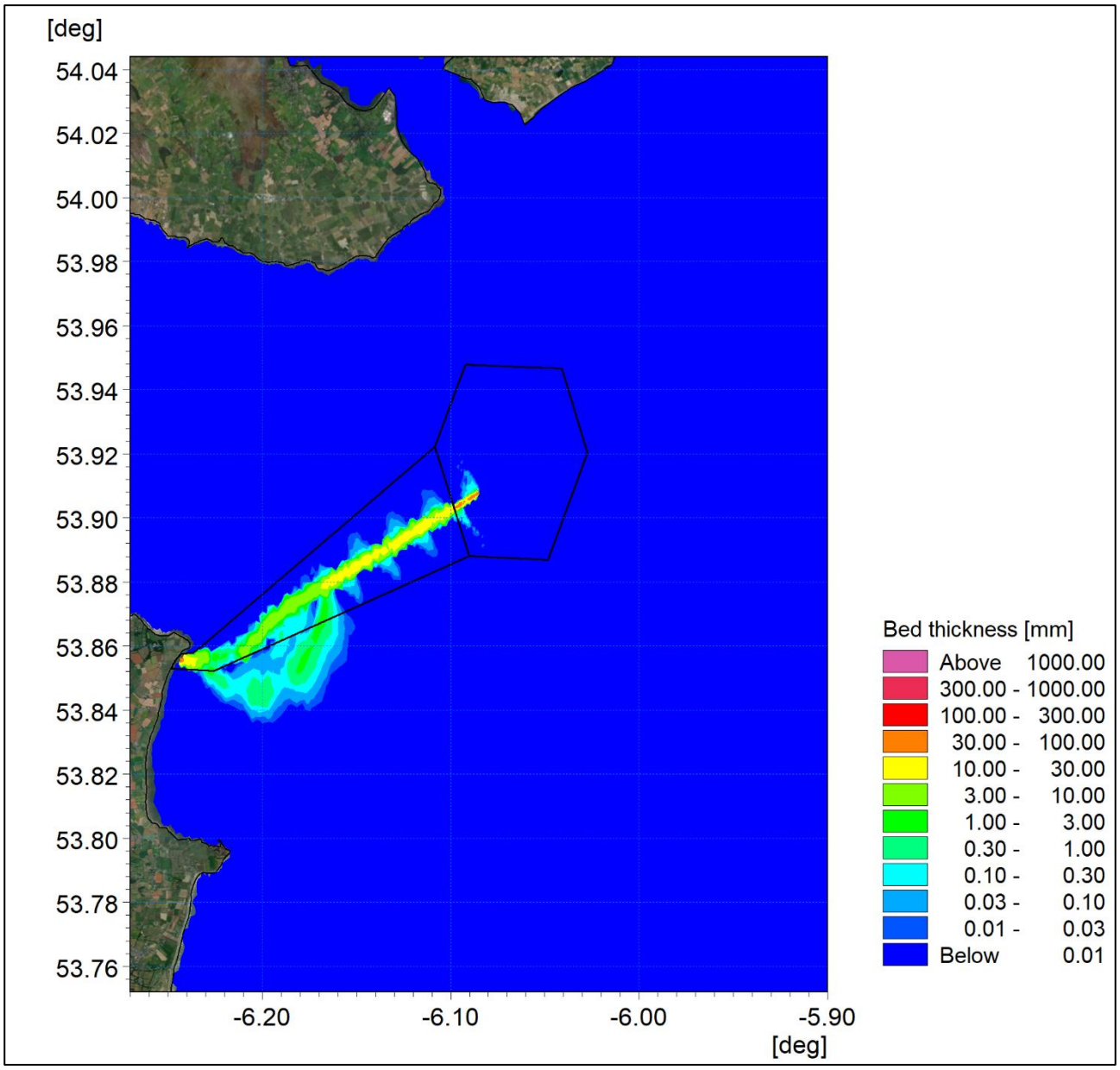

Figure 3A-131: Final sedimentation one day following installation for offshore cable trenching with flocculation.

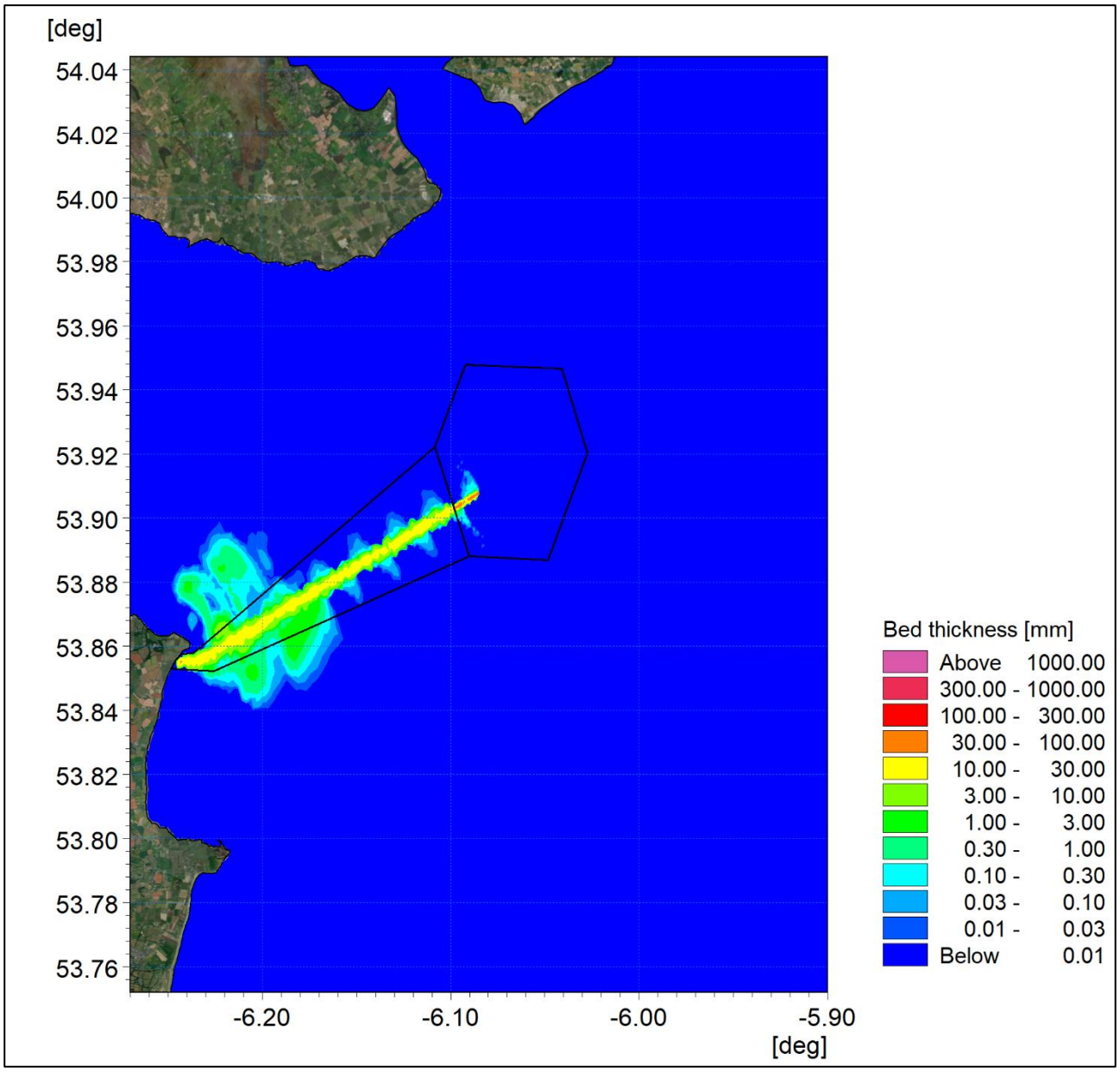

Figure 3A-132: Maximum sedimentation for offshore cable trenching with flocculation.

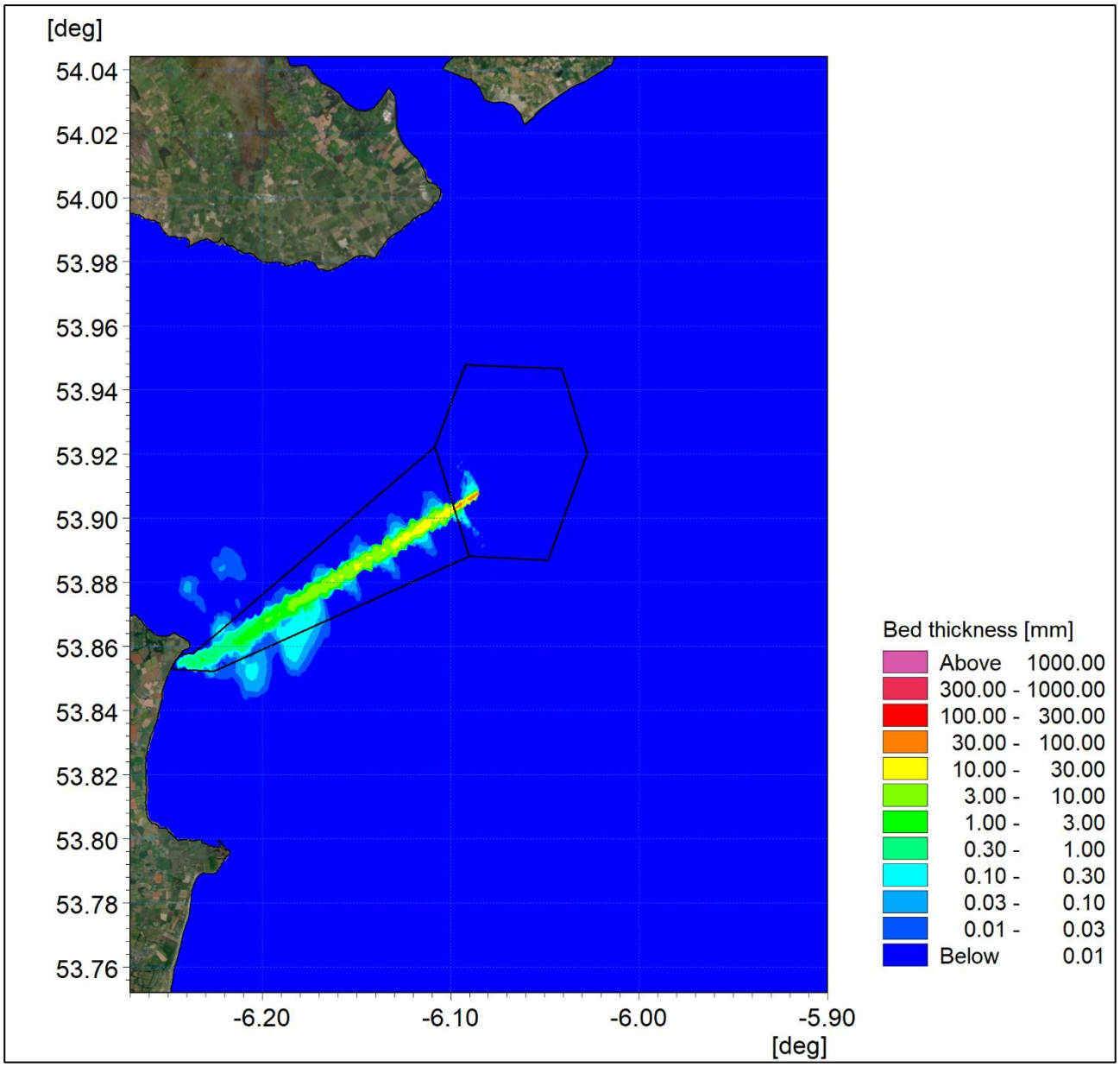

Figure 3A-133: Average sedimentation for offshore cable trenching with flocculation.

4 MODEL VERIFICATION

The numerical models used to undertake the marine processes modelling outlined in the previous sections of this document were verified across a range of parameters, namely:

- Water level;
- Current regime; and
- Wave climate.

The data used to undertake calibration and validation were obtained from a range of sources in addition to project specific field data, including:

- Office of Public Works (OPW);
- Marine Institute (MI); and
- British Oceanographic Data Centre (BODC).

This section of the Technical Report presents an overview of the model calibration and verification. The locations of the datasets detailed are presented in Figure 4A-1. Overall the models were found to be within the acceptable margins of accuracy and were determined ‘fit for purpose’ for use in the modelling study to provide supporting information for the NIS of the Project.

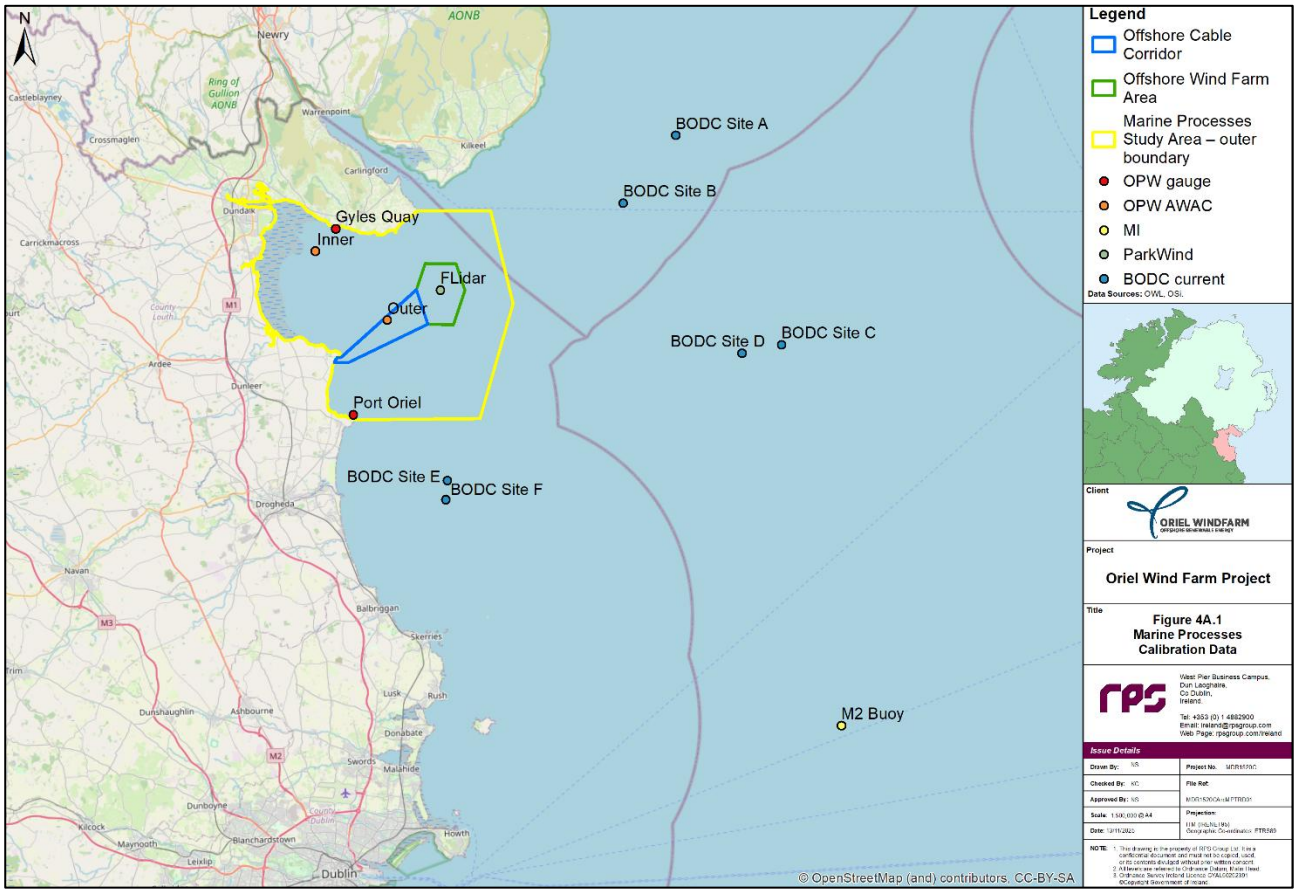

Figure 4A-1: Marine processes calibration data.

4.1 Modelling standard

The Time Series Comparator tool provided within MIKE was used to undertake statistical analysis of water level, depth averaged vector components and wave height data from the modelled and measured datasets. This tool provides several performance measures and statistics including the Index of Agreement which is also known as d_2 or model skill. Model performance may be assessed using two main types of metrics: those related to absolute values such as the mean absolute error (MAE) or the root-mean-square error (RMSE) and those which are normalised such as the model skill (d_2) or the Coefficient of efficiency.

The MIKE analysis provides three normalised parameters directly:

- Coefficient of determination R^2 being the square of the Pearson's product-moment correlation coefficient. It ranges from 0 to 1 with larger values indicating a better fit.
- Coefficient of efficiency or Nash-Sutcliffe coefficient E (Nash and Sutcliffe, 1970). It ranges from minus infinity to 1 with larger values indicating a better fit.
- Index of agreement d_2 (Willmott *et al.,* 1985). It ranges from 0 to 1 with large values indicating a better fit.

Having developed a value relating to goodness-of-fit between measured and modelled data it is necessary to determine if the model is fit for the purpose of undertaking modelling and assessment. Classification is a useful tool in this respect. The simplest form of classification, shown in Table 4A-1, may be applied to those metrics whose values range from zero to unity.

Table 4A-1: Coefficient of determination interpretation.

Coefficient of Determination (R^2)	Interpretation
0	The model does not predict the outcome
Between 0 and 1	The model partially predicts the outcome
1	The model perfectly predicts the outcome

On the other end of the scale more complex classifications have been developed, such as that proposed by Ladson for application of the coefficient of efficiency in stream flow modelling (Ladson, 2008). This is a dual system in which a reduced level of fit is accepted as satisfactory for the validation phase compared with that from the calibration phase parameters, Table 4A-2.

Table 4A-2: Coefficient of efficiency interpretation.

Classification	Coefficient of Efficiency Calibration	Coefficient of Efficiency Validation
Excellent	$E \geq 0.93$	$E \geq 0.93$
Good	$0.8 \leq E < 0.93$	$0.8 \leq E < 0.93$
Satisfactory	$0.7 \leq E < 0.8$	$0.6 \leq E < 0.8$
Passable	$0.6 \leq E < 0.7$	$0.3 \leq E < 0.6$
Poor	$E < 0.6$	$E < 0.3$

For the purposes of verification of the marine processes modelling the coefficient of efficiency was applied. The purpose of the modelling study was to undertake a comparative study, i.e. determine the change in baseline conditions due to the Project, therefore a satisfactory standard was applied. For calibration a value of the coefficient of efficiency is ideally greater than 0.7 and 0.6 for verification to satisfy these criteria.

4.2 Water level

Water level verification was undertaken by calibration of the model using the Port Oriel tides gauge and verification by examining the Gyles Quay gauge for the same period from the same simulation, i.e. with model parameters unchanged.

4.2.1 Water level calibration

A model simulation was undertaken for a period of one month to encompass the range of tidal conditions experienced within the marine processes study area. The selected period included periods of meteorological conditions, and the model included wind and pressure data from the ECMWF operational forecast model. The comparison of surface elevation measured at the Port Oriel gauge (red trace) and the model with meteorological forcing at the same location (black trace) is presented in Figure 4A-2. These datasets were analysed using the Time Series comparator and the coefficient of efficiency was found to be 0.97, as illustrated in Figure 4A-3. Although the goodness of fit is within acceptable limits it was noted that the modelled range was seen to be somewhat smaller than the measured value therefore further modelling was undertaken to determine if this arises due to harmonic or meteorological factors.

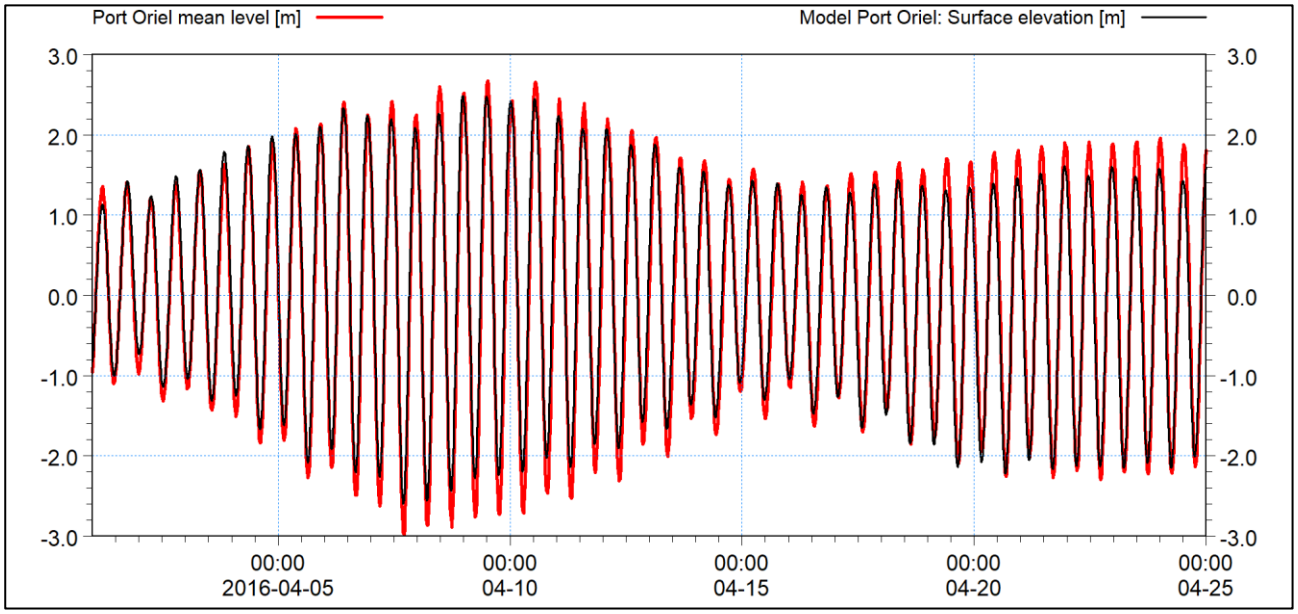

Figure 4A-2: Measured and modelled water level Port Oriel.

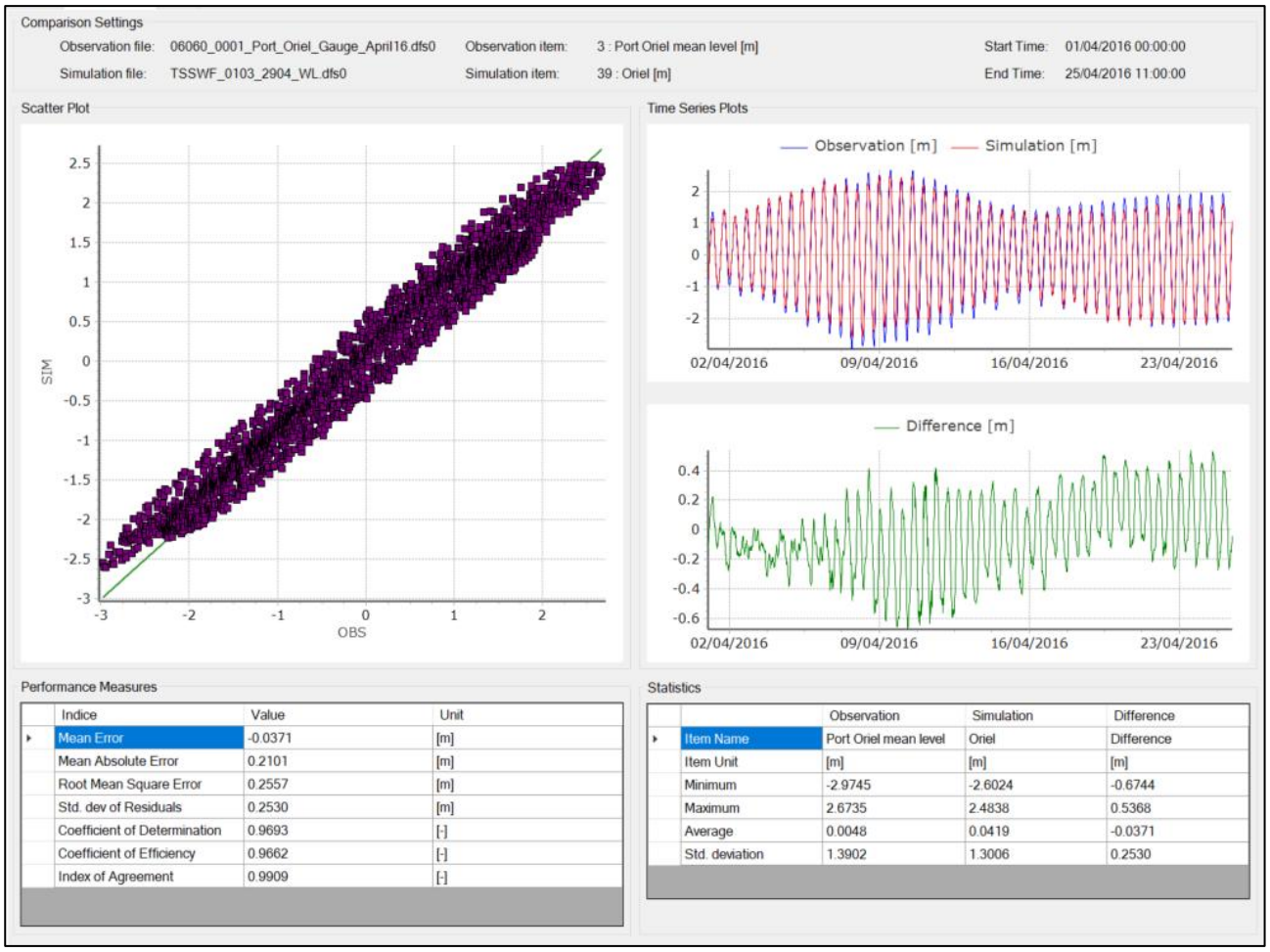

Indice	Value	Unit
Mean Error	-0.0371	[m]
Mean Absolute Error	0.2101	[m]
Root Mean Square Error	0.2557	[m]
Std. dev of Residuals	0.2530	[m]
Coefficient of Determination	0.9693	[-]
Coefficient of Efficiency	0.9662	[-]
Index of Agreement	0.9909	[-]

	Observation	Simulation	Difference
Item Name	Port Oriel mean level	Oriel	Difference
Item Unit	[m]	[m]	[m]
Minimum	-2.9745	-2.6024	-0.6744
Maximum	2.6735	2.4838	0.5368
Average	0.0048	0.0419	-0.0371
Std. deviation	1.3902	1.3006	0.2530

Figure 4A-3: Evaluation of water level modelling Port Oriel.

A second period was selected for analysis noting that no model parameters, such as turbulence, viscosity or bed roughness values, were altered from the previous scenario. During this second period the meteorological conditions were more settled, and the model was run under a condition of pure tidal forcing. Figure 4A-4 and Figure 4A-5 present the comparison of the datasets and analysis at Port Oriel respectively. The correlation is seen to be improved with a coefficient of efficiency of 0.99 for the modelled period of one month. This is therefore well within the acceptable range for model calibration.

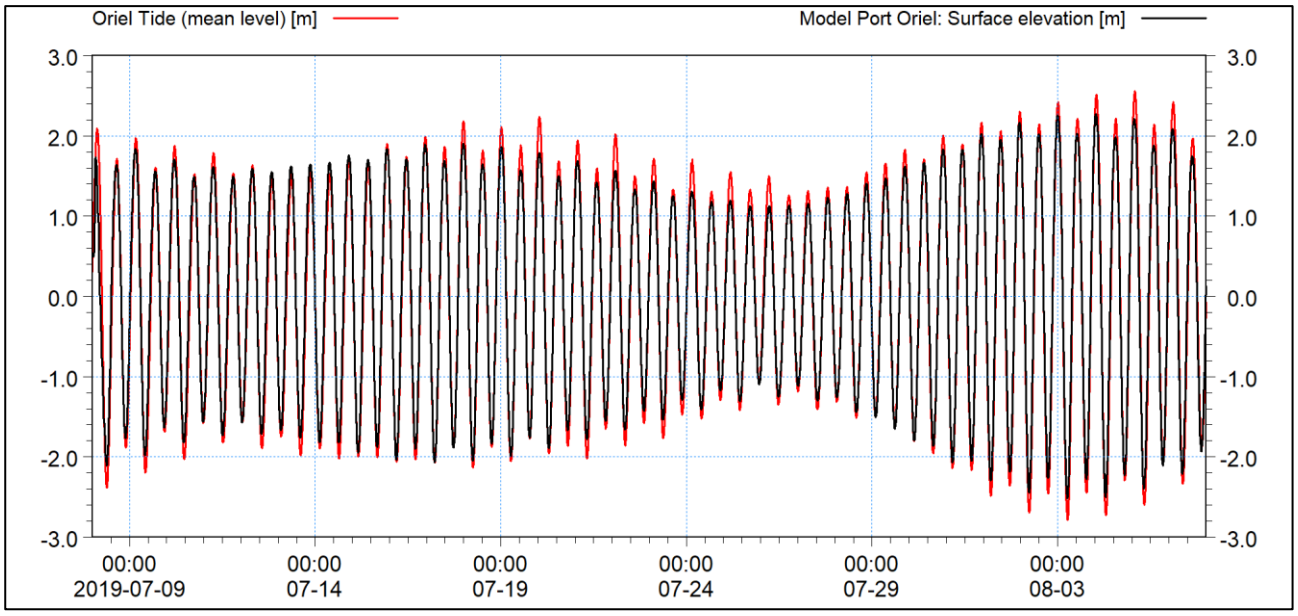

Figure 4A-4: Measured and modelled water level Port Oriel - calm.

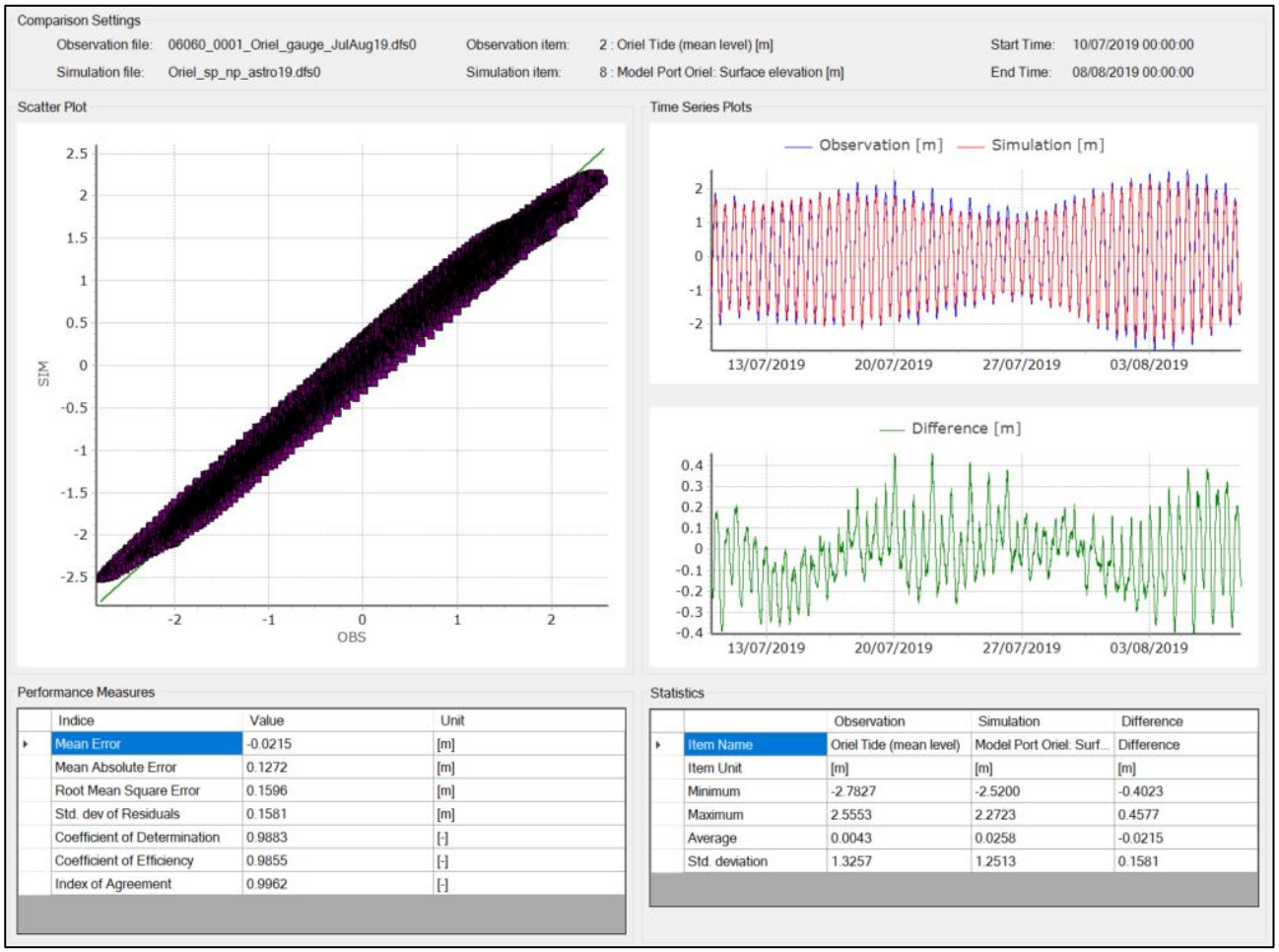

Figure 4A-5: Evaluation of water level modelling Port Oriel - calm.

4.2.2 Water level validation

A second set of tide gauge data was used to verify water level. The Gyles Quay tide gauge was found to be somewhat more unstable than Port Oriel and is prone to drying out approaching low water during spring tides. Figure 4A-6 shows the comparison of the measured gauge data (blue trace) and modelled data (green trace) during the period with meteorological conditions. The modelled data extraction point was located slightly further offshore to avoid drying, however even with this disparity, when the analysis is applied the coefficient of efficiency is 0.9. This is illustrated in Figure 4A-7.

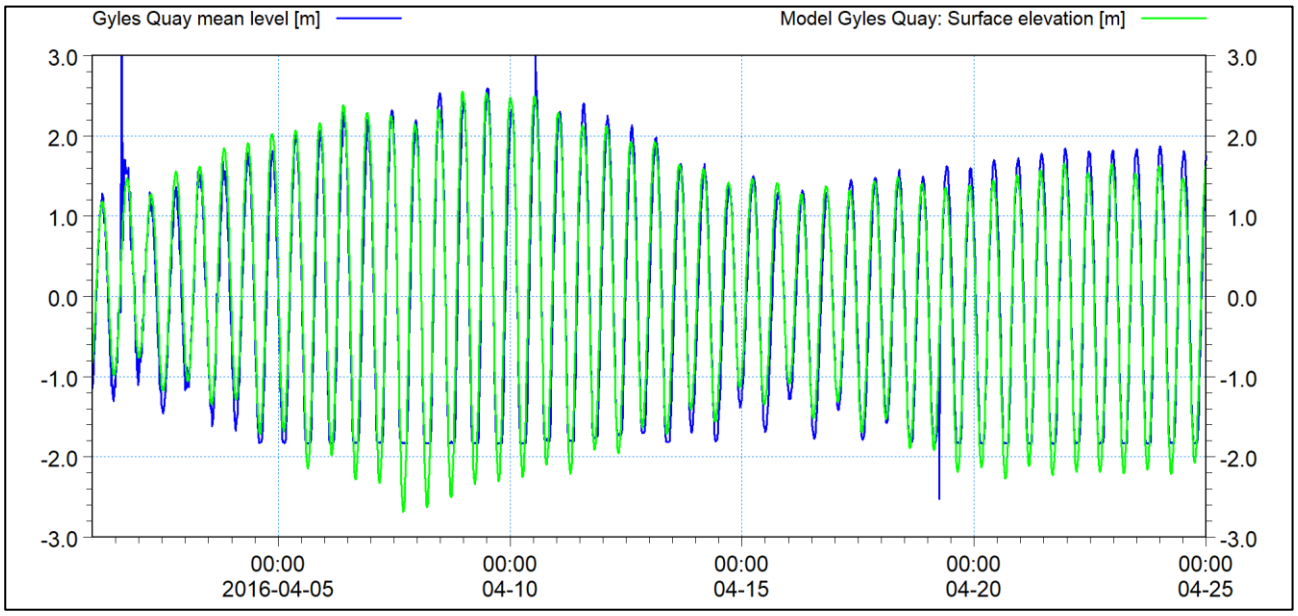

Figure 4A-6: Measured and modelled water level Gyles Quay.

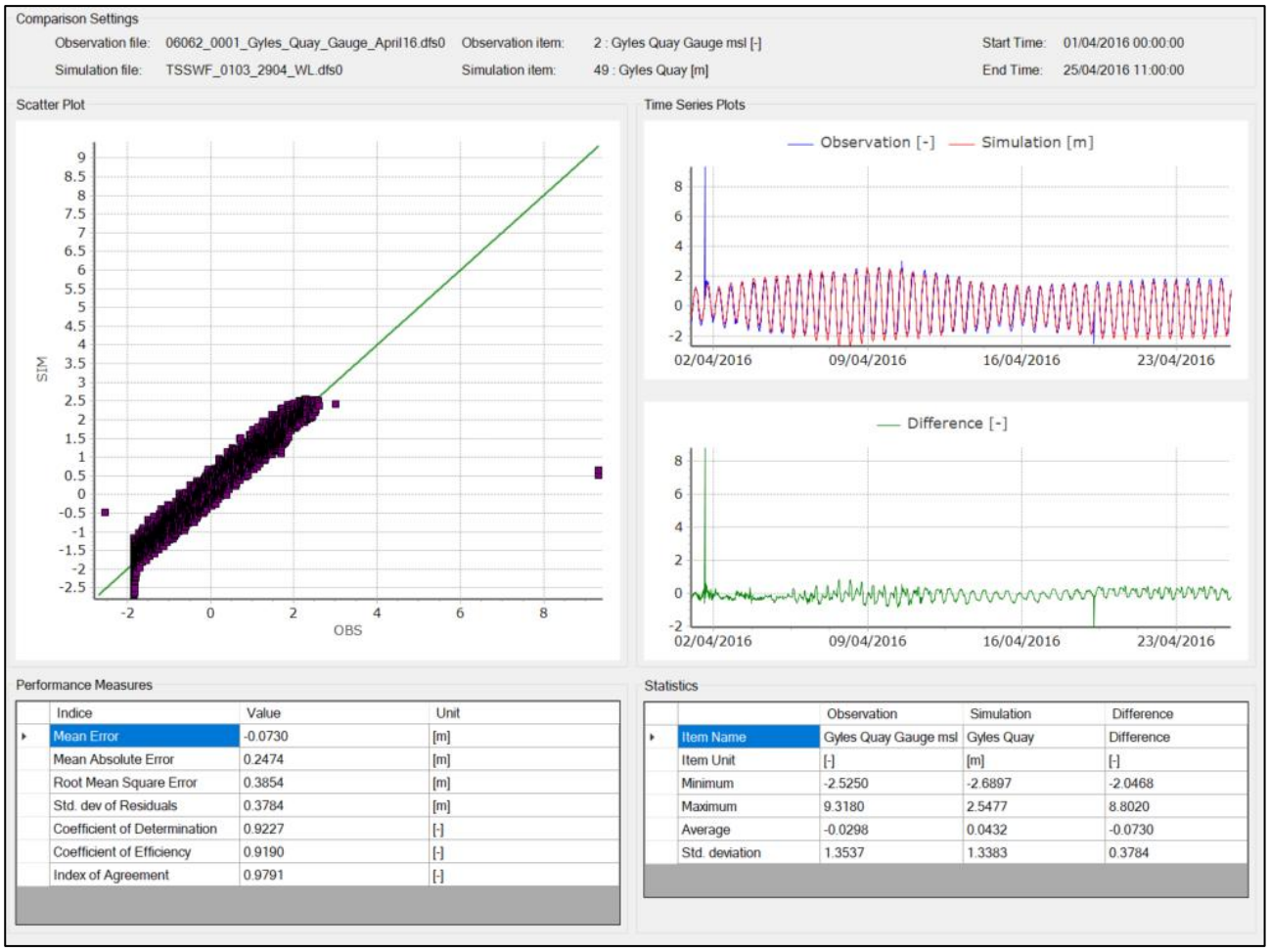

Figure 4A-7: Evaluation of water level modelling Gyles Quay.

Finally, the second calm period was examined at the Gyles Quay gauge – with the model extraction location moved further inshore. Figure 4A-8 show the comparisons of the two datasets and illustrates that, although the model dries out slightly earlier that the tidal phasing and range are well represented within the model.

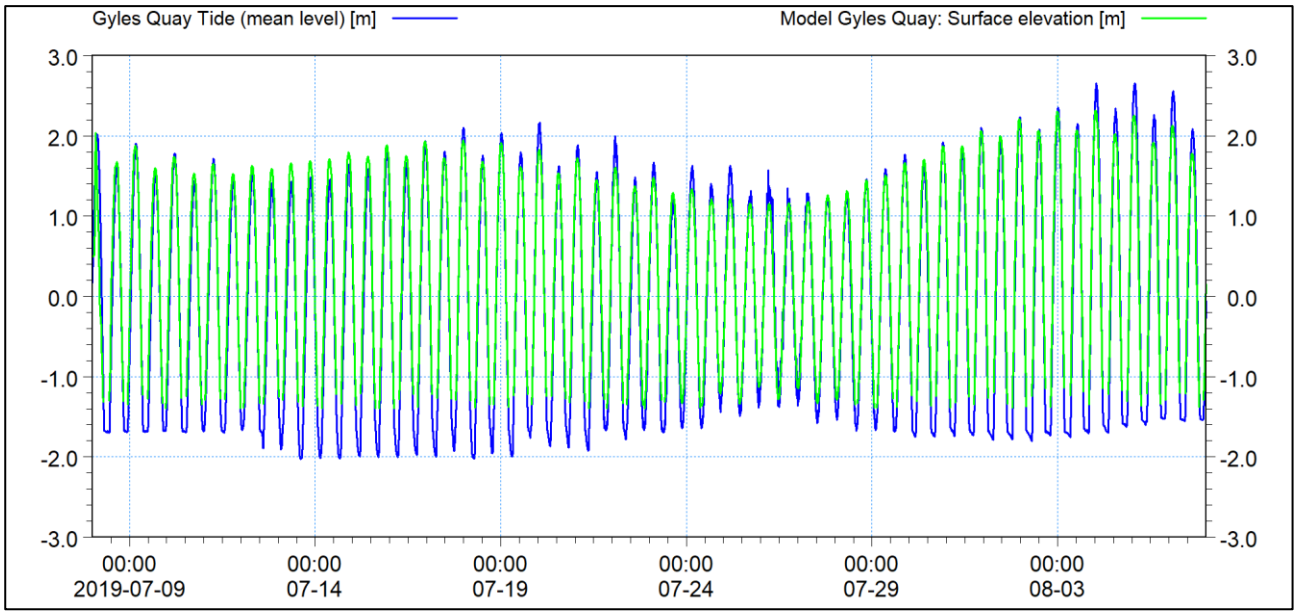

Figure 4A-8: Measured and modelled water level Gyles Quay - calm.

4.3 Tidal current

The verification of tidal currents was undertaken in concert with the water level verification. The simulation period and applied meteorological conditions related to the deployment of two AWAC units by OPW in Dundalk Bay in 2016. These provide a combined current profiler and wave directional system in one unit which measured the current speed and direction in 1 m thick layers from the bottom to the surface. The deployment within the offshore cable corridor was used for calibration and is labelled 'Outer', whilst the 'Inner' site located within the Bay was used for verification.

In common across the plots presented within this section of the report are that the values associated with the parameter noted in the key relates to the distance from the bed to the bin bottom, e.g. Speed#3(3.5m) relates to the current speed measured in bin three which is located between 3 and 4 m from the bed. It was also noted that all bins were recorded including those within the range of tidal oscillation. For example, the Outer deployment was sited at a location -19.8m msl, with depths ranging from *circa* 18 to 22m and where 20 bins were recorded. Where a depth averaged monitored value is presented this has been evaluated from all records and, for the purposes of undertaking the analysis, the top two bins have been omitted to ensure a more representative comparison is made. Throughout this section it has been endeavoured to maintain figure axes of the same magnitude where possible to allow visual comparison between parameters.

4.3.1 Tidal current calibration

For visual comparison and to aid understanding of the flow regime the measured and modelled current speed and directions are presented. Figure 4A-9 shows the current speed in the upper plot whilst the current direction is shown in the lower plot. Similarly Figure 4A-10 shows the same information for neap tides. Visual comparison shows a good level of agreement, with modelled values falling within the range of the measured data.

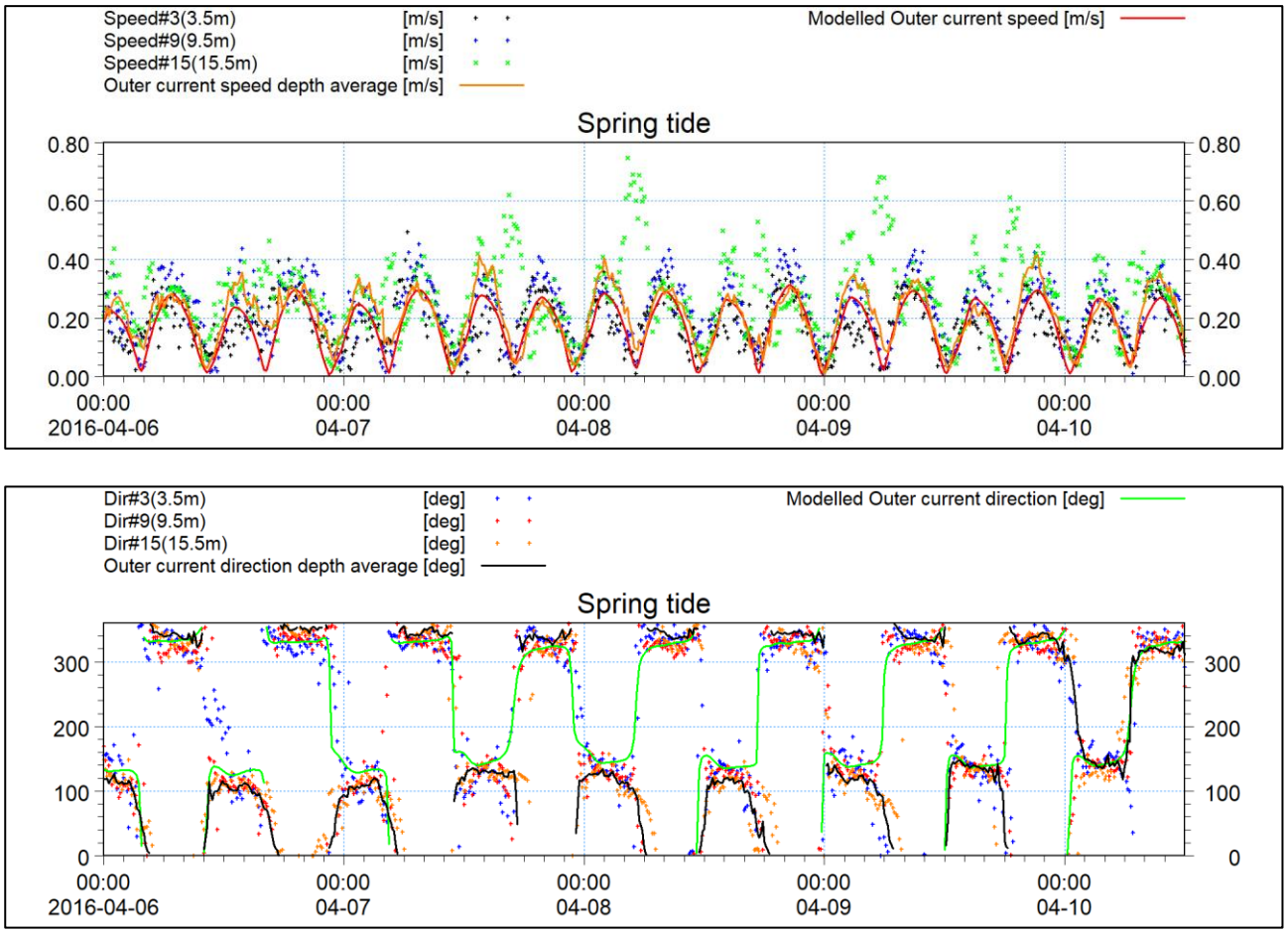

Figure 4A-9: Measured and modelled Outer current speed (upper) and direction (lower) – spring tide.

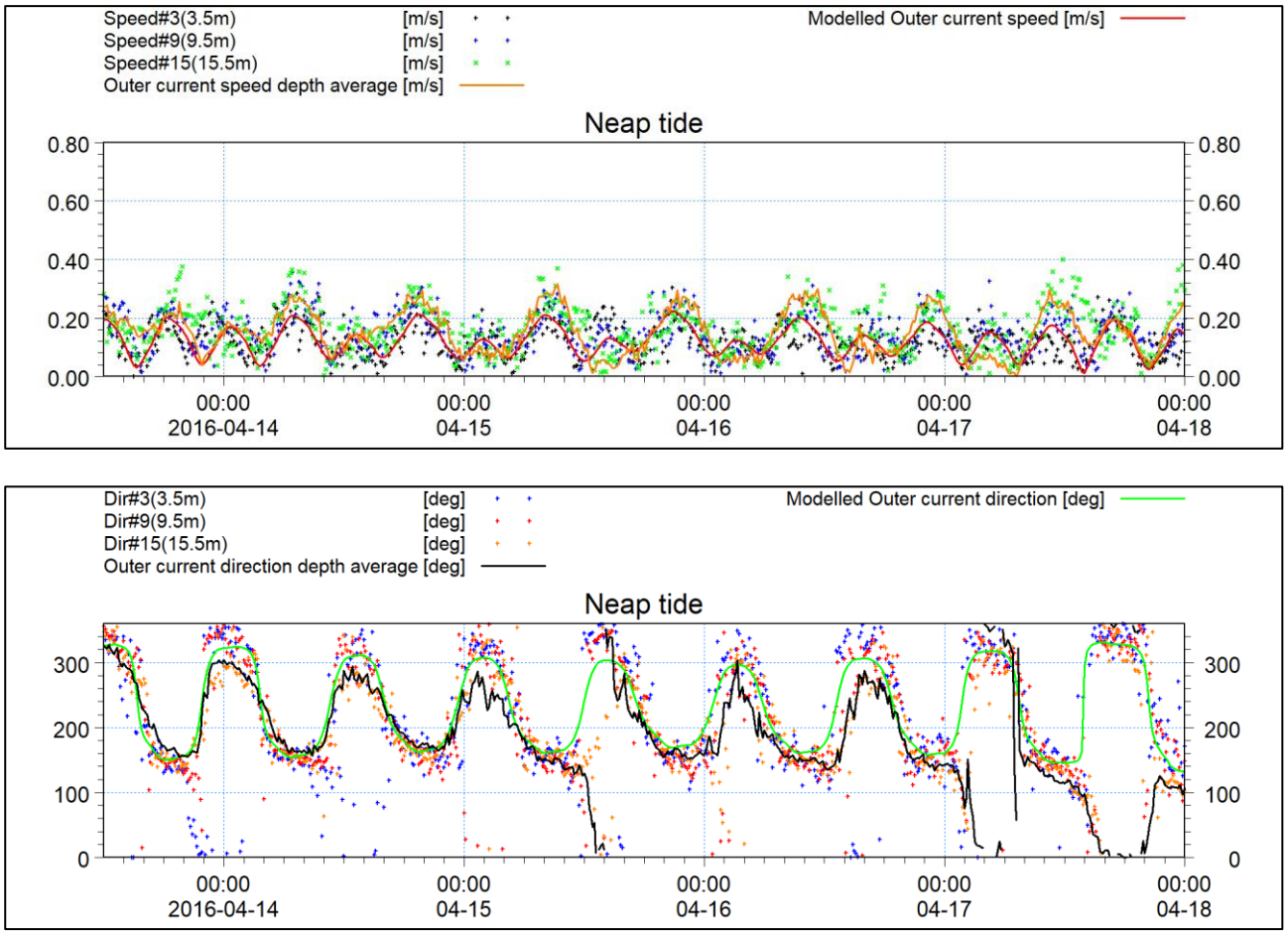

Figure 4A-10: Measured and modelled Outer current speed (upper) and direction (lower) – neap tide.

In order to undertake the analysis of goodness of fit the U and V velocity components are required, as current speed does not account for differences in directionality. Figure 4A-11 and Figure 4A-12 illustrate the comparison of the vector components U and V in a similar format as the previous plots. These figures clearly indicate that the upper bin data is influenced by surface wind during the spring period. The U and V depth average velocity components were analysed over the period of one month and had a coefficient of efficiency of 0.76 and 0.92 respectively, as illustrated in Figure 4A-13 and Figure 4A-14. This is well within the acceptable criteria.

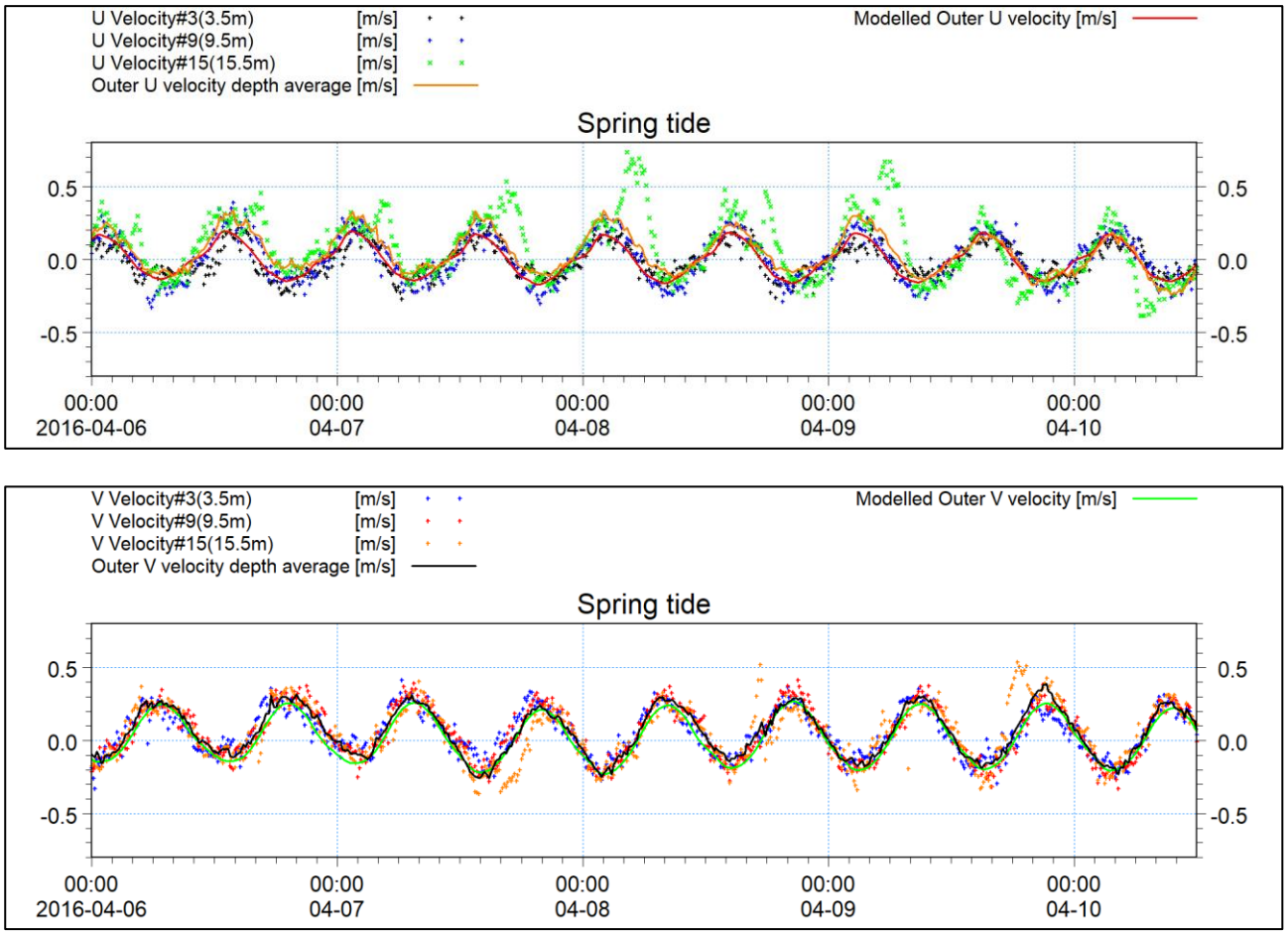

Figure 4A-11: Measured and modelled Outer U-velocity (upper) and V-velocity (lower) – spring tide.

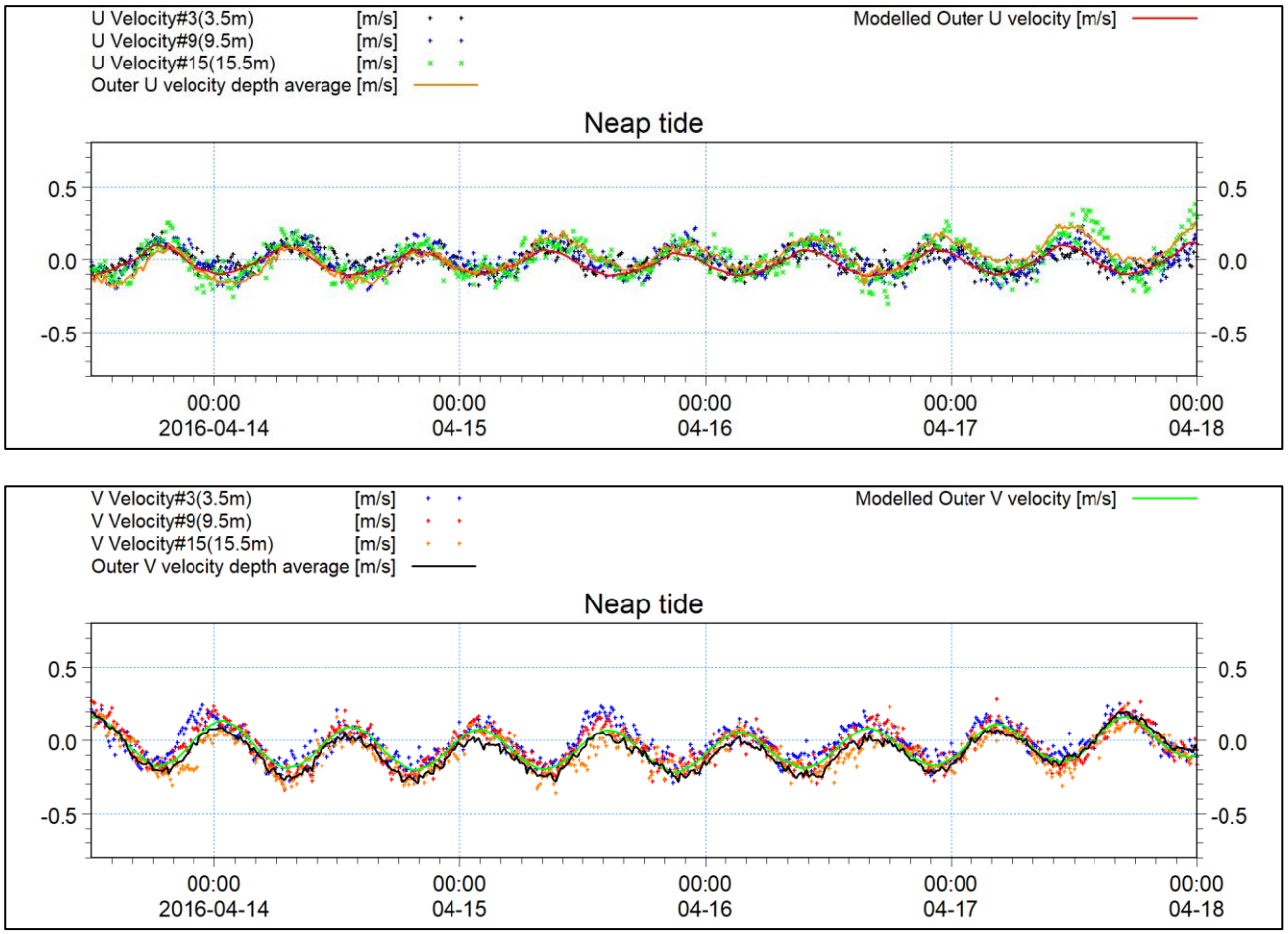

Figure 4A-12: Measured and modelled Outer U-velocity (upper) and V-velocity (lower) – neap tide.

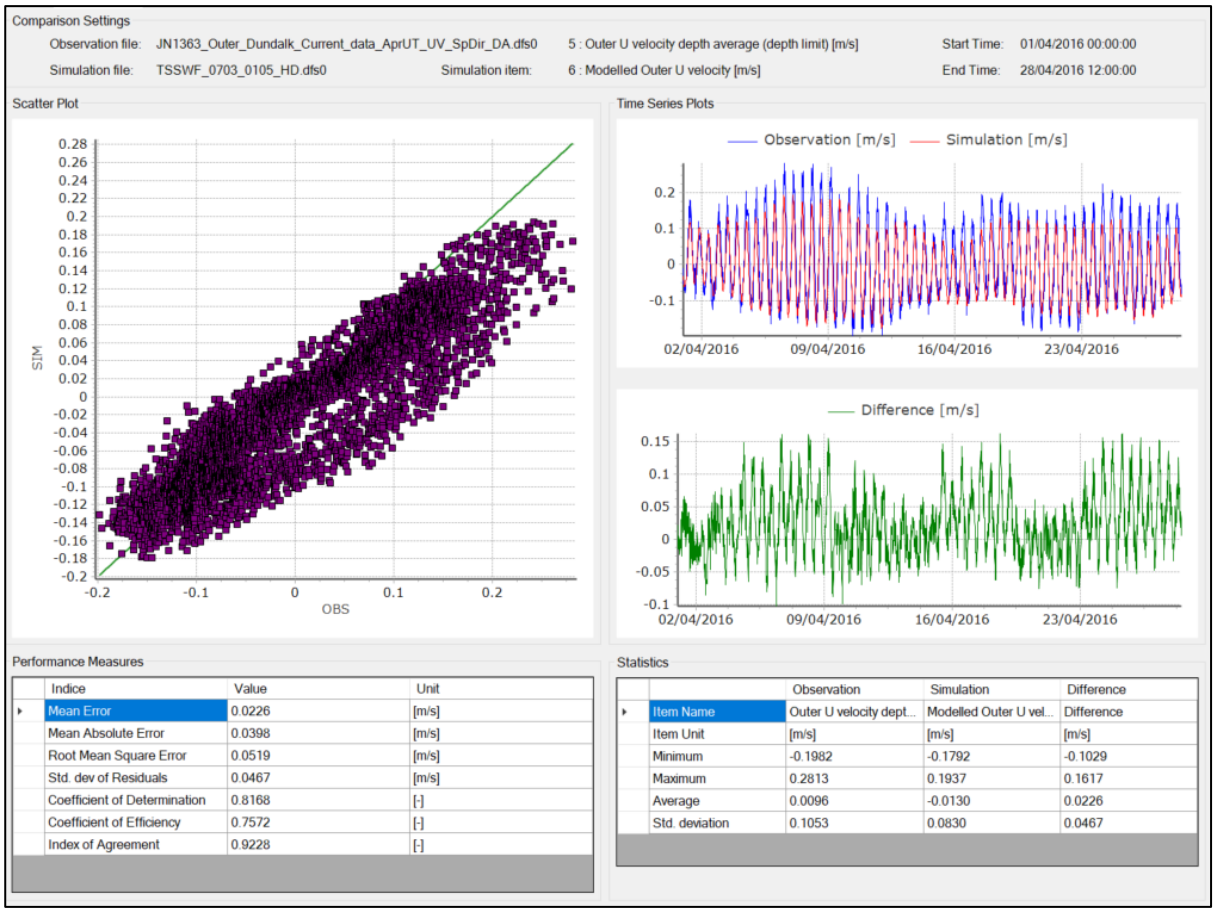

Figure 4A-13: Evaluation of Outer U-velocity.

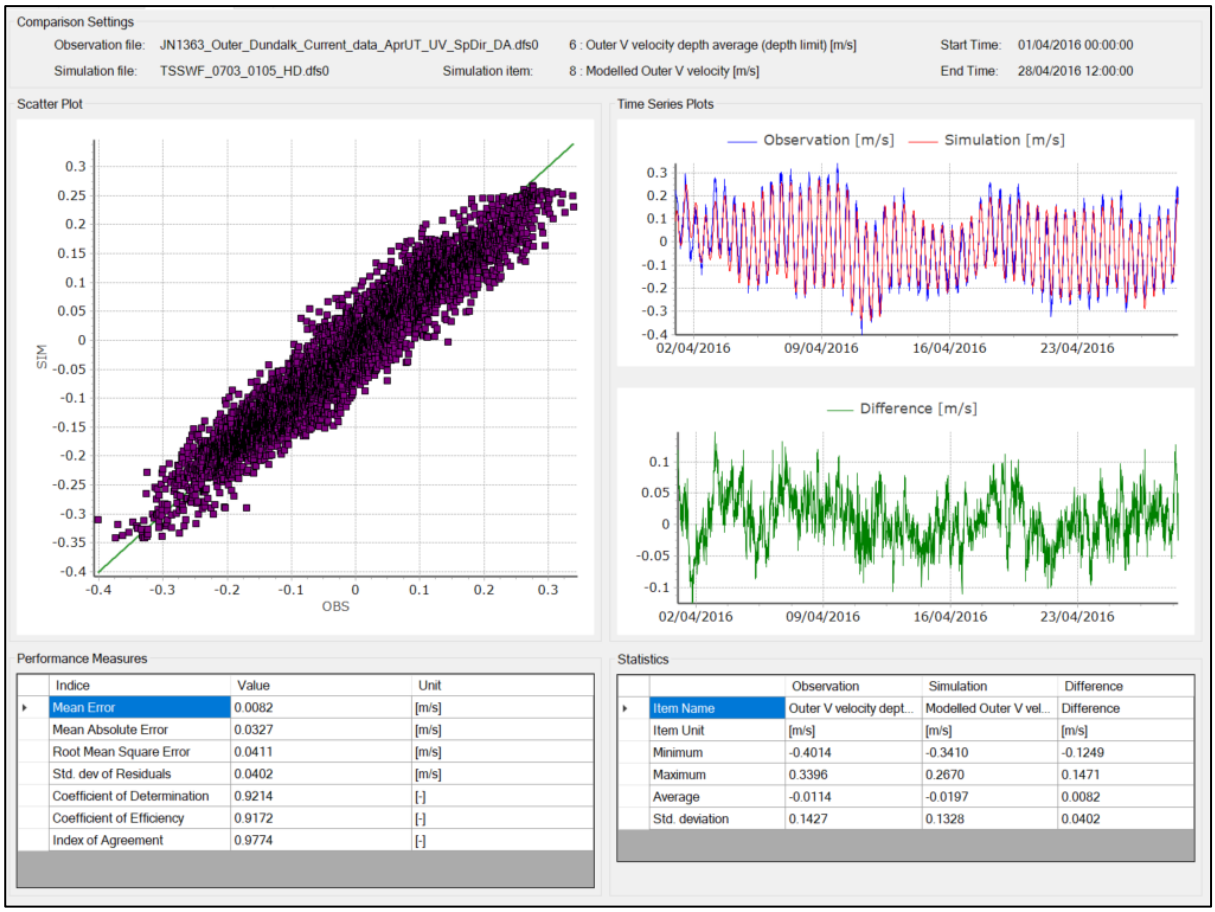

Figure 4A-14: Evaluation of Outer V-velocity.

4.3.2 Tidal current validation

By way of verification the analysis was undertaken for the Inner location, noting that no model parameters had been altered to optimise the model at this location. Figure 4A-15 and Figure 4A-16 present the spring and neap current speed and direction data respectively. It is noted that this site is located in shallow water and therefore has greater sensitivity to weather and wind induced surface currents. This is evident during spring and neap tidal conditions where both surface current speeds and directions differ from the sub-surface layers.

Figure 4A-17 and Figure 4A-18 show the vectors components of the current regime at the Inner site. When the U and V components were analysed over the full month the coefficient of efficiency was determined to be 0.84 and 0.56 respectively. The V component falls slightly below the desirable value of 0.6 for validation however it is noted that the principle flow direction is north-south and this is well within the acceptable margin. The analysis for U and V depth average values for the Inner site is presented in Figure 4A-19 and Figure 4A-20 respectively.

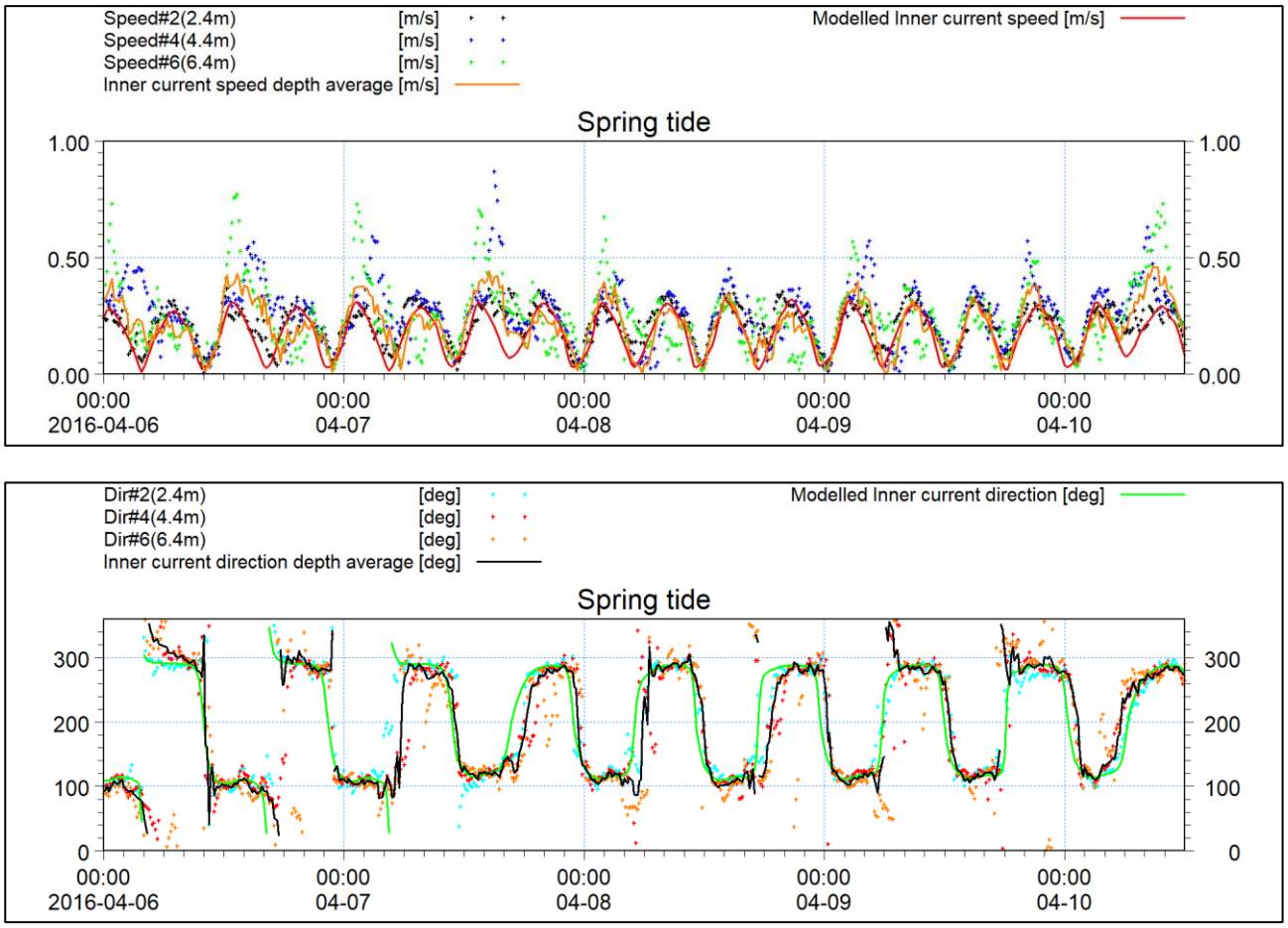

Figure 4A-15: Measured and modelled Inner current speed (upper) and direction (lower) – spring tide.

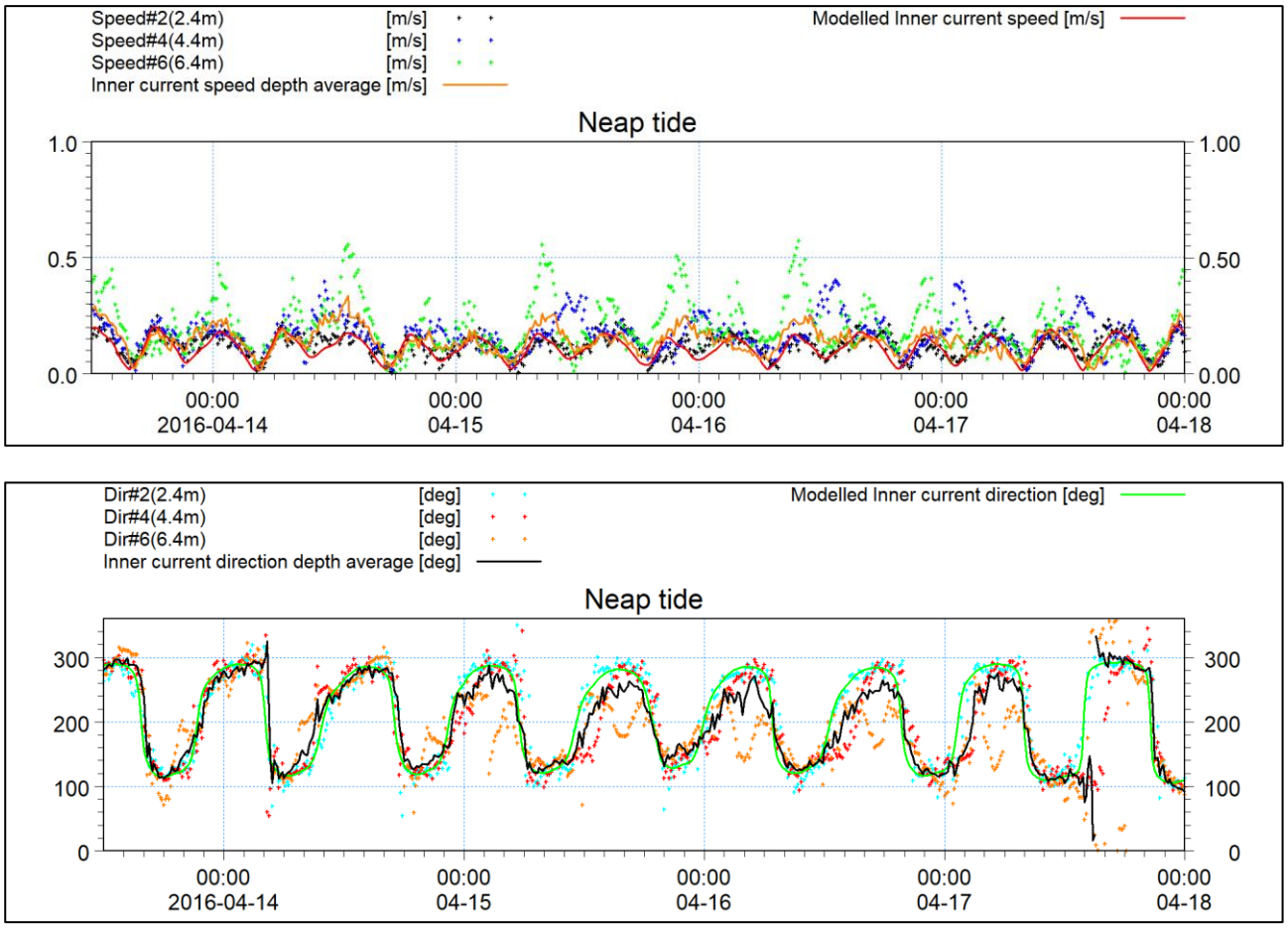

Figure 4A-16: Measured and modelled Inner current speed (upper) and direction (lower) – neap tide.

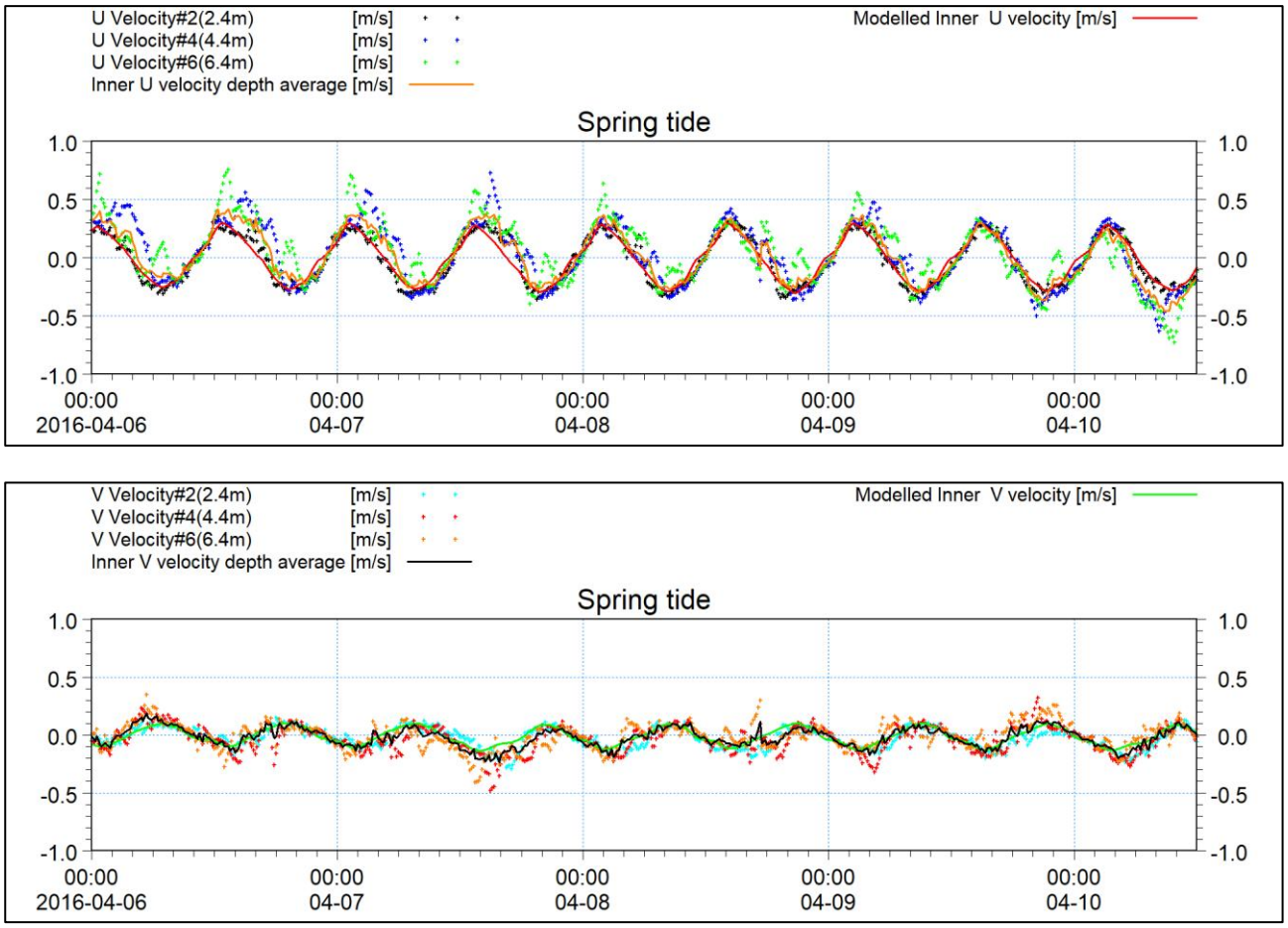

Figure 4A-17: Measured and modelled Outer U-velocity (upper) and V-velocity (lower) – spring tide.

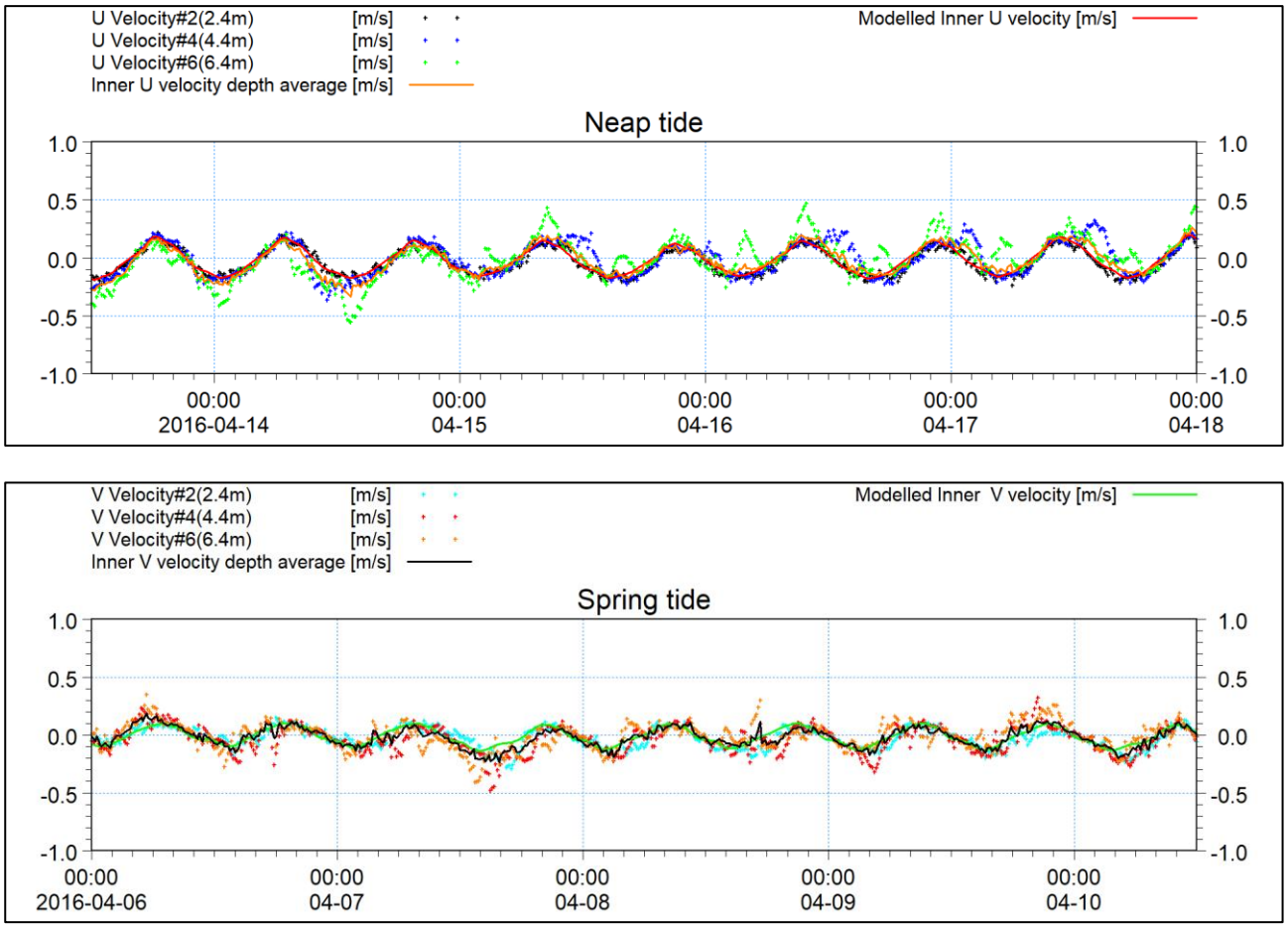

Figure 4A-18: Measured and modelled Outer U-velocity (upper) and V-velocity (lower) – neap tide.

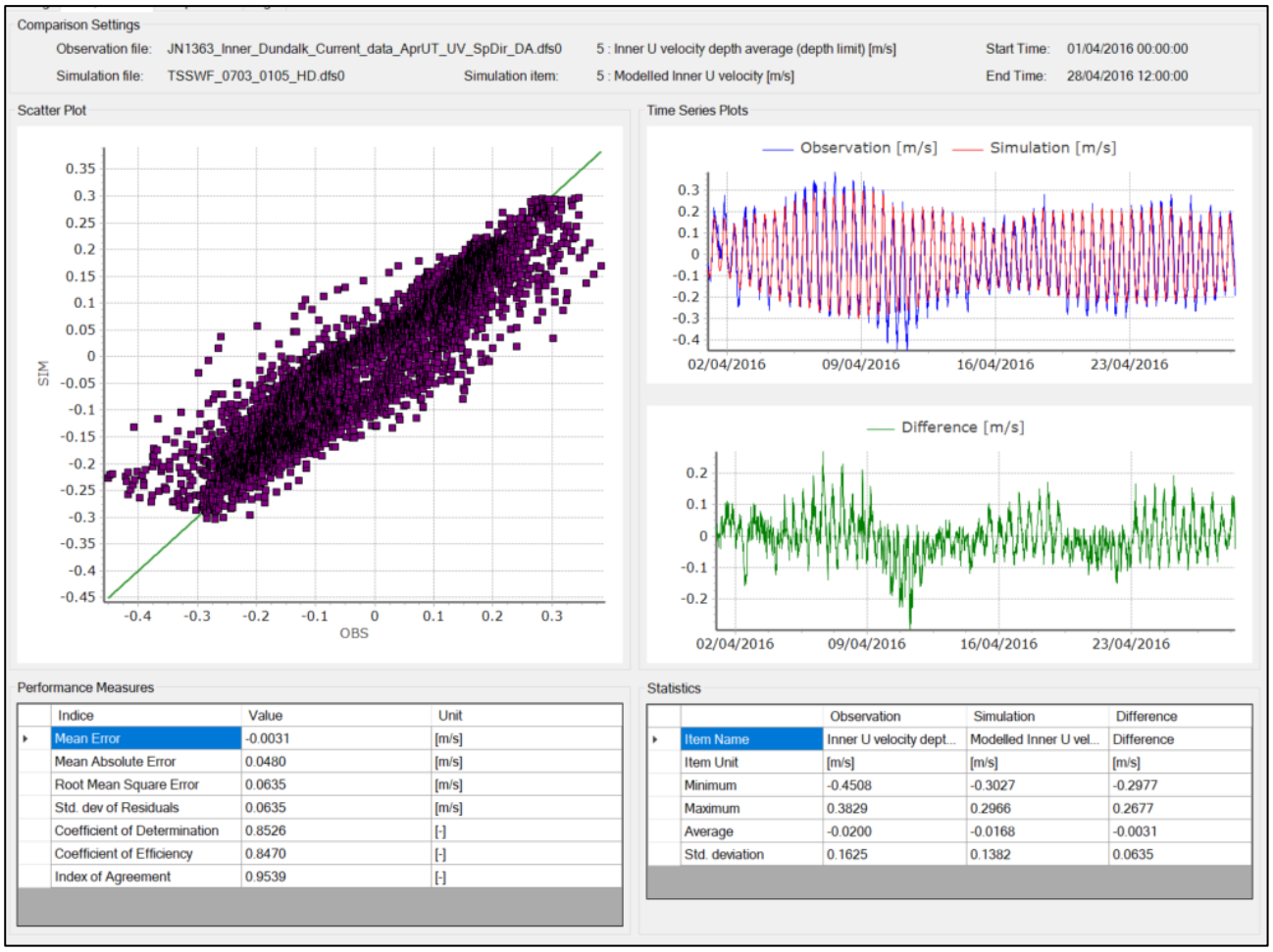

Figure 4A-19: Evaluation of Inner U-velocity.

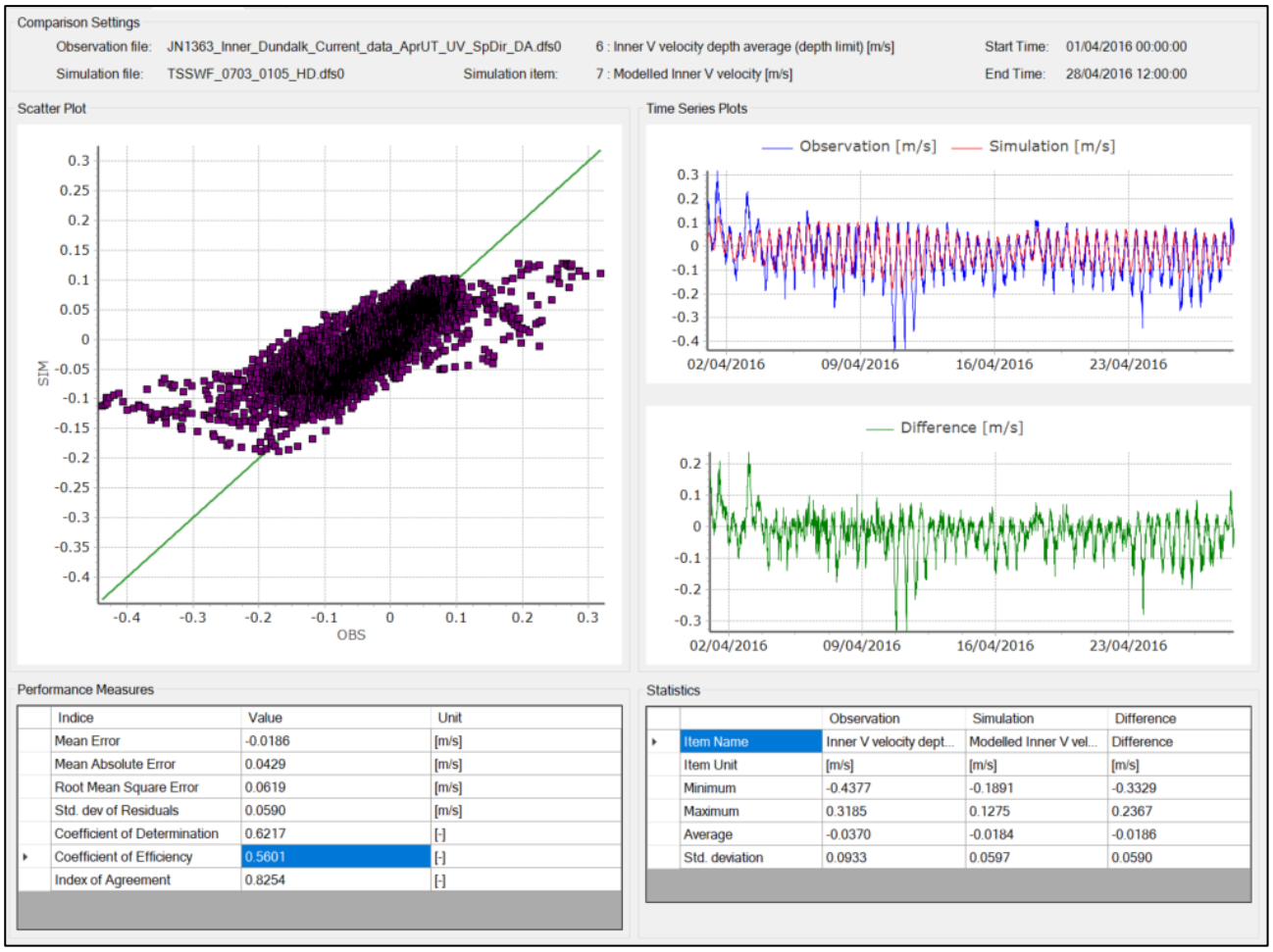

Figure 4A-20: Evaluation of Inner V-velocity.

4.4 Wave climate

4.4.1 Wave climate calibration

In a similar manner to the tidal data the wave data for the Outer site was used for model calibration. A period of one moth was selected for simulation to include a number of events with a range of wave heights and durations. The wave climate model utilised the meteorological data from the ECMWF i.e. the same datasets used for the Irish sea tide and surge operational forecast for the same period as the data collection.

Figure 4A-21 shows the datasets for modelled (blue trace) and measured (black discrete points) significant wave height. The analysis of significant wave height over the period of a month, illustrated in Figure 4A-22, gave a coefficient of efficiency value of 0.78, being above the desired benchmark or 0.7 for model calibration.

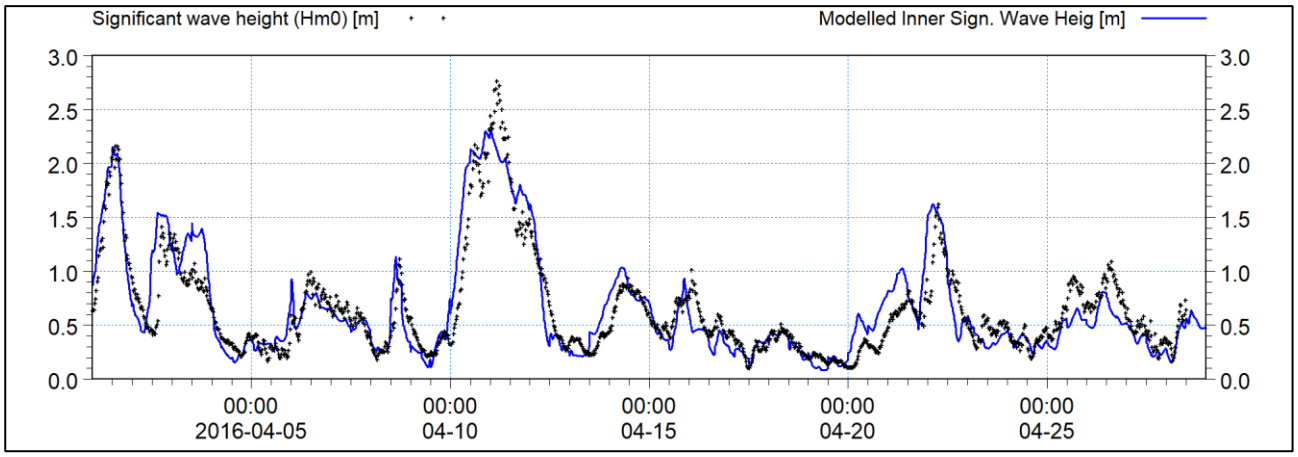

Figure 4A-21: Measured and modelled Outer wave height.

Figure 4A-22: Evaluation of Outer wave height.

4.4.2 Wave climate validation

The model data at the Inner site was examined for verification. As previously noted, no parameters were altered to optimise for model calibration at this location. Figure 4A-23 shows the visual comparison between modelled and measured significant wave height, whilst Figure 4A-24 presents the data analysis. The coefficient of efficiency value was determined to be 0.8 and therefore also within the desirable margin.

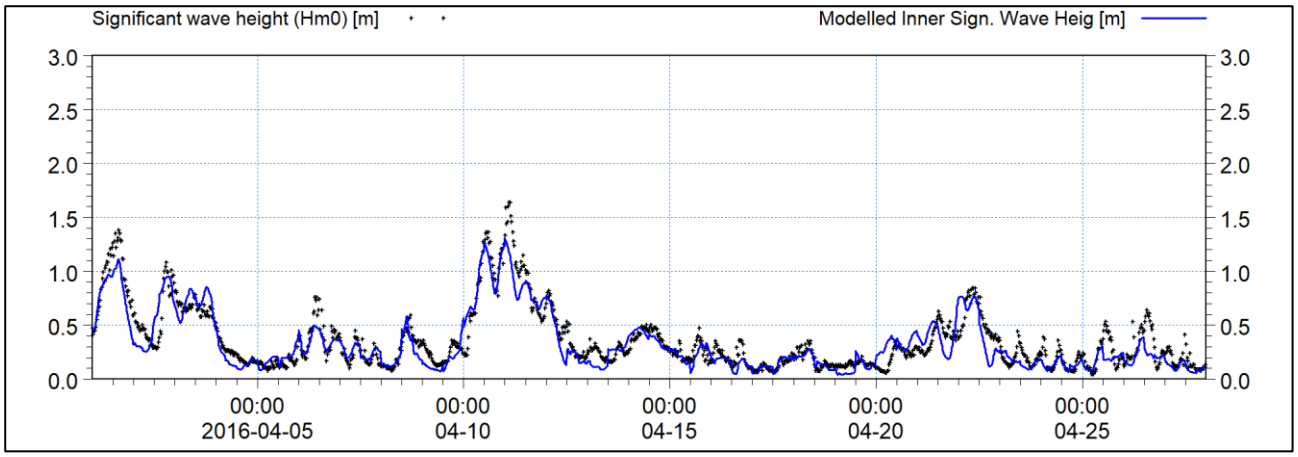

Figure 4A-23: Measured and modelled Inner wave height.

Figure 4A-24: Evaluation of Inner wave height.

The OPW Inner and Outer Dundalk Bay datasets indicated that the model was suitable for undertaking the wave climate modelling to provide supporting information for the NIS for the Project. However it is always prudent to cross check the model with as many data sources as available. For this reason a validation check was undertaken using data from the M2 buoy located further offshore. A period covering a range of events was examined, as illustrated in Figure 4A-25. It provided a coefficient of efficiency 0.74, indicating that the model was also suitably accurate further offshore in the wider domain.

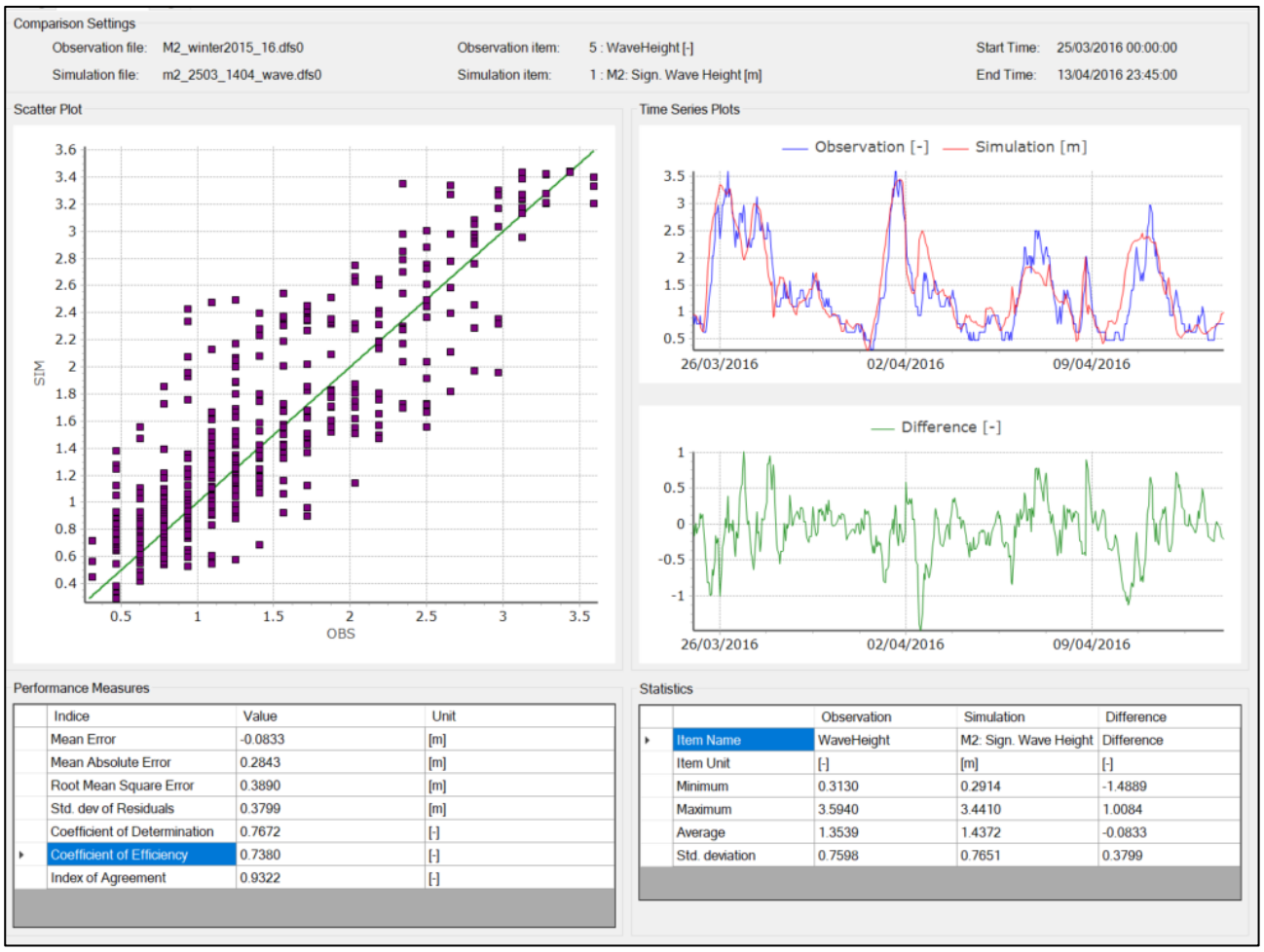

Indice	Value	Unit
Mean Error	-0.0833	[m]
Mean Absolute Error	0.2843	[m]
Root Mean Square Error	0.3890	[m]
Std. dev of Residuals	0.3799	[m]
Coefficient of Determination	0.7672	[-]
Coefficient of Efficiency	0.7380	[-]
Index of Agreement	0.9322	[-]

	Observation	Simulation	Difference
Item Name	WaveHeight	M2: Sign. Wave Height	Difference
Item Unit	[-]	[m]	[-]
Minimum	0.3130	0.2914	-1.4889
Maximum	3.5940	3.4410	1.0084
Average	1.3539	1.4372	-0.0833
Std. deviation	0.7598	0.7651	0.3799

Figure 4A-25: Evaluation of M2 buoy wave height.

4.5 Project data

Following model development, calibration and validation project specific data was made available. Monitoring was undertaken for an extended period to include wind, wave and current. However it was noted that there were issues with the equipment. Within the dataset there were periods where wave climate records were absent and there were instabilities within the current monitoring data. For completeness the datasets were examined to provide further model validation where appropriate.

4.5.1 Floating LiDAR (Fidar)

The Floating Light Detection and Ranging (Fidar) data was supplied at an interval of one hour. A period of two weeks was selected from the record of wave climate, at a time when a couple of events were seen to occur and the data appeared to be reliable. The wave model was then re-run using the same parameters and applying the meteorological forcing from the ECMWF operational dataset for consistency. Figure 4A-26 shows the comparison been the monitored and modelled significant wave height for this period. The two week dataset was analysed and the coefficient of efficiency was determined to be 0.83, as illustrated in Figure 4A-27, demonstrating that the model within the desired level of accuracy.

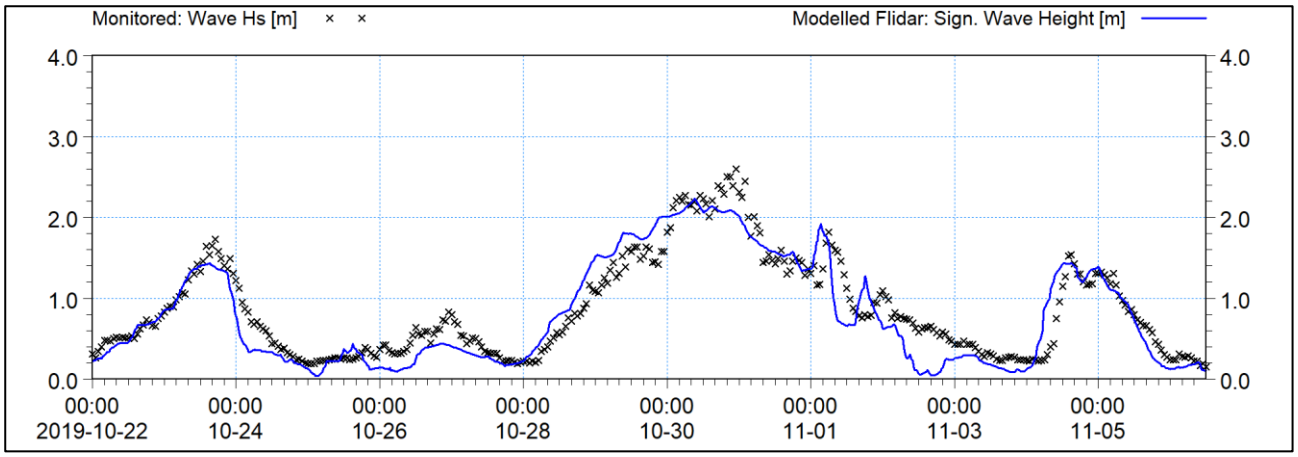

Figure 4A-26: Measured and modelled Fidar deployment wave height.

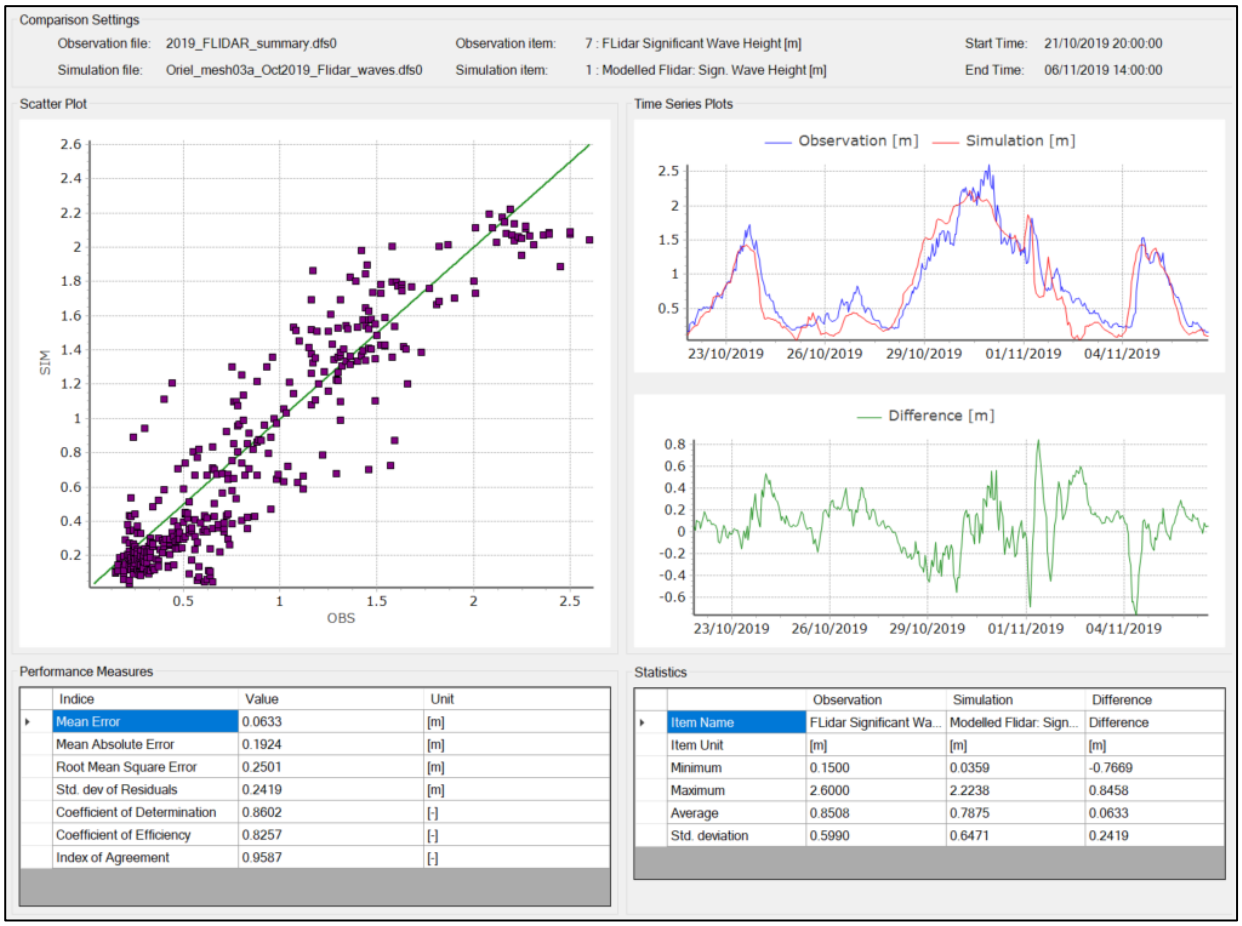

Figure 4A-27: Evaluation of Flidar deployment wave height.

Current data was also collected by the Flidar unit. As the name suggests, the floating unit recorded current speeds in relative to the surface. Figure 4A-28 shows current speed (upper plot) and current direction (lower plot) within a range of measurement zones or bins across the water column (values accompanying Speed# indicate depth from surface). It is apparent that the signal is very noisy and there is no consistency in the data. Values in adjacent bins and timesteps vary radically in a manner which would not be experienced in reality; the surface elevation has been included to indicate the tidal state over this period. The tidal currents were resolved into U and V components and depth averaged. These are presented in Figure 4A-29. The resulting trace does not demonstrate the tidal variation which would be anticipated at this location particularly given the proximity to the OPW Outer monitoring location. This indicates issues with equipment or the setup of the equipment which is not unusual with recording low current speeds with this type of equipment. This dataset was not utilised further with regards to model validation.

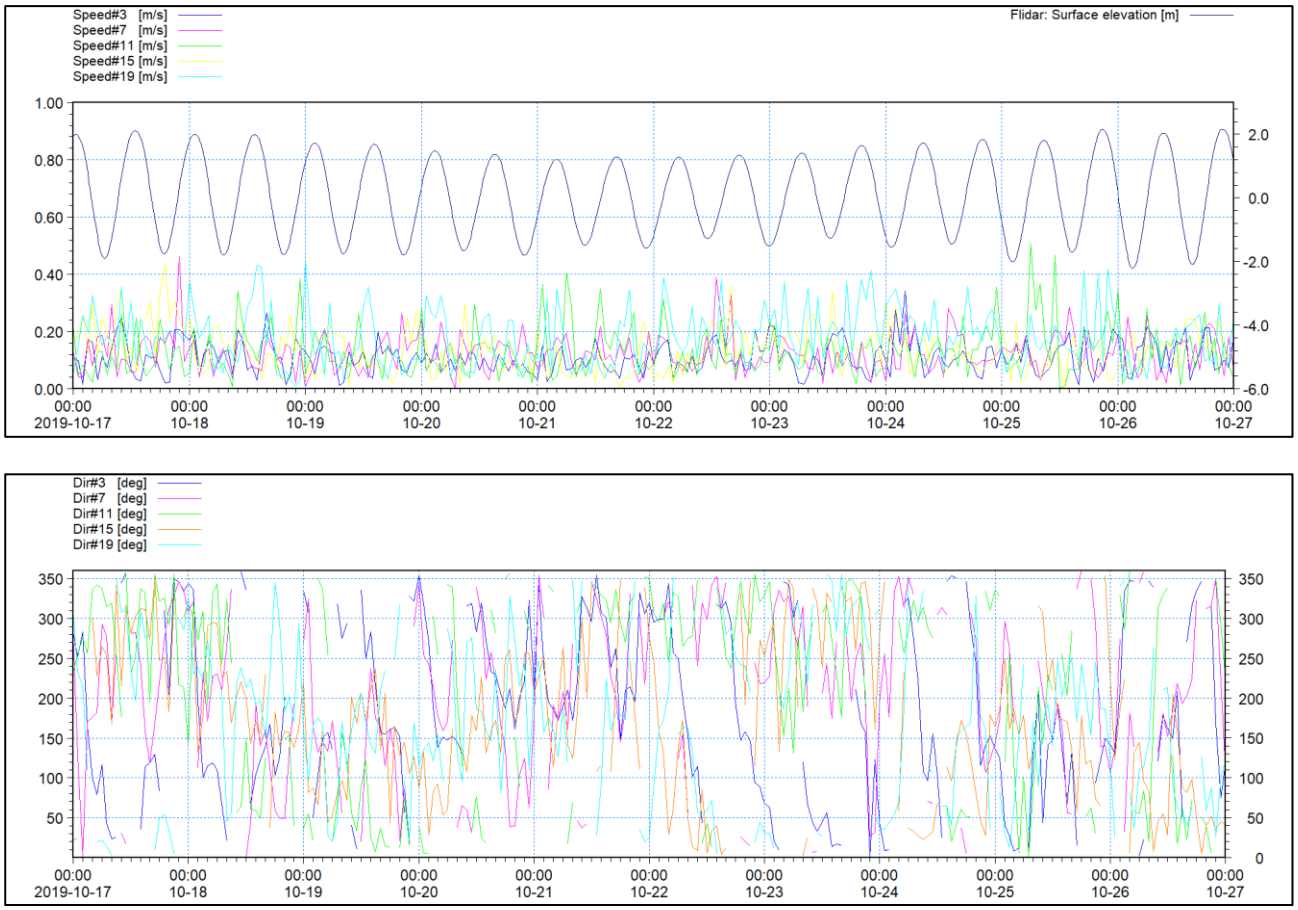

Figure 4A-28: Measured Flidar current speed (upper) and direction (lower).

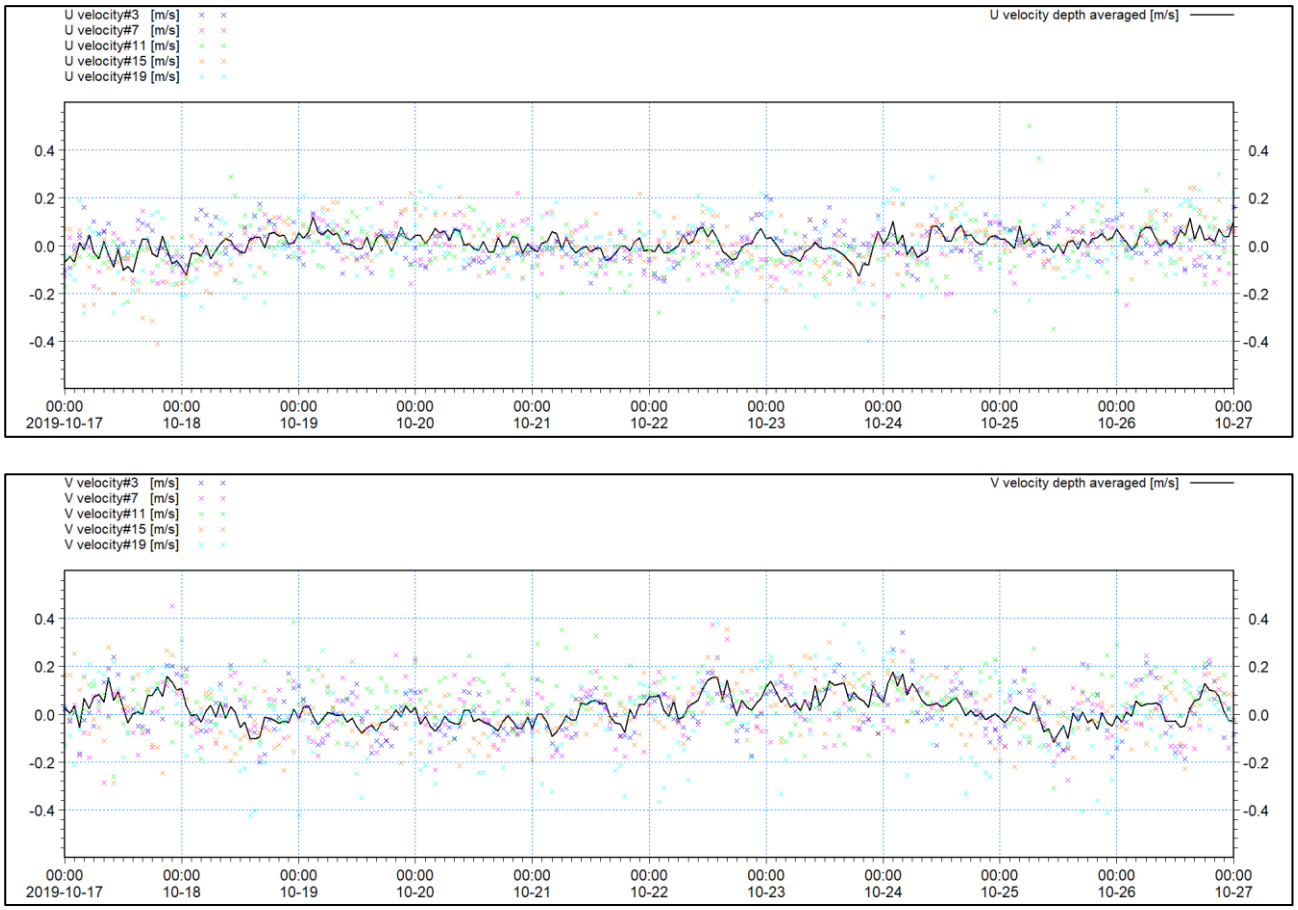

Figure 4A-29: Measured and depth average Flidar U-velocity (upper) and V-velocity (lower).

4.6 Additional data

When developing models is it always beneficial to use all available data to validate models. This is particularly useful in the wider domain where detailed calibration is not essential but ensuring that larger scale flow regimes are simulated is important. The model boundaries were driven using 'flather' datasets whereby both water levels and current speeds are prescribed. These boundaries were extracted from the Irish Seas Storm Surge Model, an operational forecast model currently run by Met Eireann, which was developed as part of Phase 2 of the Irish Coastal Protection Strategy Study (ICPSS) and has been thoroughly verified.

Within the model domain there are several potential sources of data such as Admiralty tidal streams published on navigational charts which provide an indicative set of hourly data. Additionally, data from the BODC archive is also available; the latter of which was utilised in model verification and are presented here.

4.6.1 BODC current data

The BODC archive provides an historical collection of hydrographic data from around the UK and Irish waters. The data includes deployments of different monitoring devices and periods dating back to the 1960's and, although not generally homogenous enough for detailed model calibration, can form a useful tool in verification. Six locations around the periphery of the marine processes study area were examined, as illustrated in Figure 4A-1. In each case the baseline simulated month used within the environmental assessment was used as a basis for comparison.

Tidal prediction was used to generate the tidal elevations at the monitored location for the period of the dataset. This was compared with the tidal elevations from the simulated month and the data was overlayed for a period of similar tidal phase and amplitude. So, although the model data would not account for any

meteorological effects, it would indicate if the underlying tidal flow patterns are represented in more general terms. In the Irish Sea tidal currents are strongly bi-directional. Within the recorded data, instabilities and noise are likely indicators of when meteorological events are taking place. Ideally, the depth average model current speed should be of the same order of magnitude and lie within the range of the monitored values.

In each figure presented the current speed is shown on the left axis whilst the direction is shown on the right axis. The recorded data is plotted using light traces with the associated monitoring depth indicated in the legend. The depth average model traces are shown with a heavier trace, dark blue for current speed and dark green for current direction.

The BODC Site A data is presented in Figure 4A-30 and was collected during November 1968 using an impeller current meter. Data was collected at depths of 14m, 20m and 21m at a location with a total water depth of 38m. The modelled current speed is of the same order of magnitude and principle current directions are largely aligned. However it is noted that, at times, the current speeds are underestimated however the dataset is quite noisy and given the timing (in November) there is likely meteorological activity.

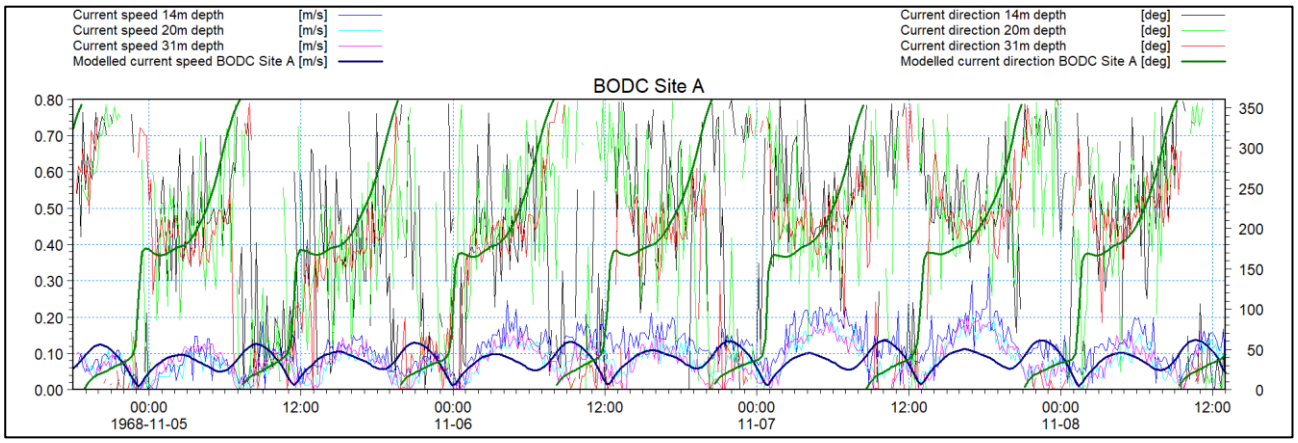

Figure 4A-30: Measured and modelled current speed (left axis) and direction (right axis) BODC Site A.

The BODC Site B data is presented in Figure 4A-31 and was collected during March 1984 using a Savonius rotor current meter. Data was collected at depths of 21m, 28m and 35m at a location with a total water depth of 43m. The modelled current speed largely lies within the range of that monitored with principle current directions largely aligned. As with the previous dataset, at times the current speeds are underestimated and the dataset is noisy indicating there is likely meteorological activity.

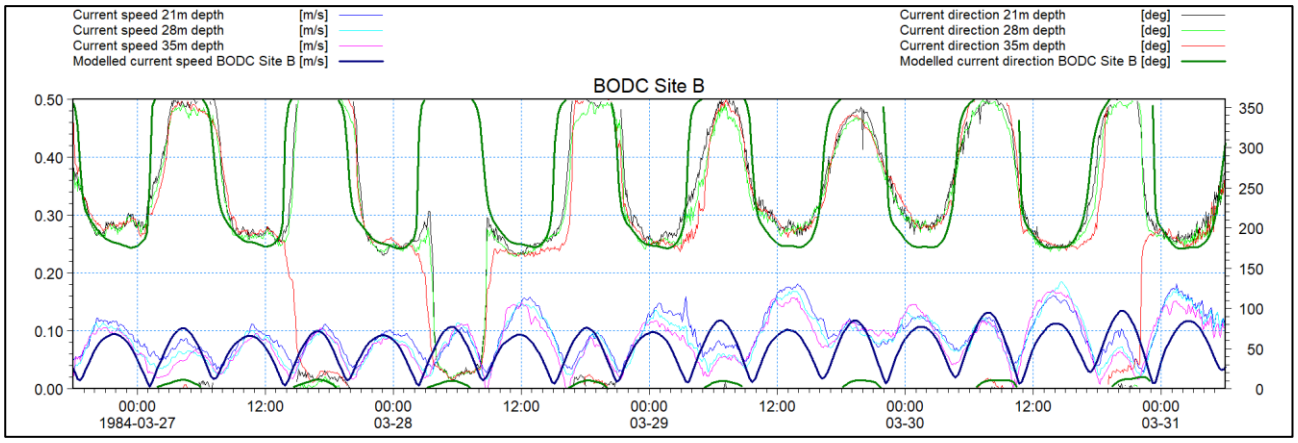

Figure 4A-31: Measured and modelled current speed (left axis) and direction (right axis) BODC Site B.

The BODC Site C data is presented in Figure 4A-32 and was collected during July 1981 using a Savonius rotor current meter. Data was collected at depths of 17m and 96m at a location with a total water depth of 100m. The modelled current speed almost entirely lies within the range of that monitored. There is some variation within the monitored current directions both temporally and spatially through the water column however the principle current directions generally aligned with the more consistent simulated data.

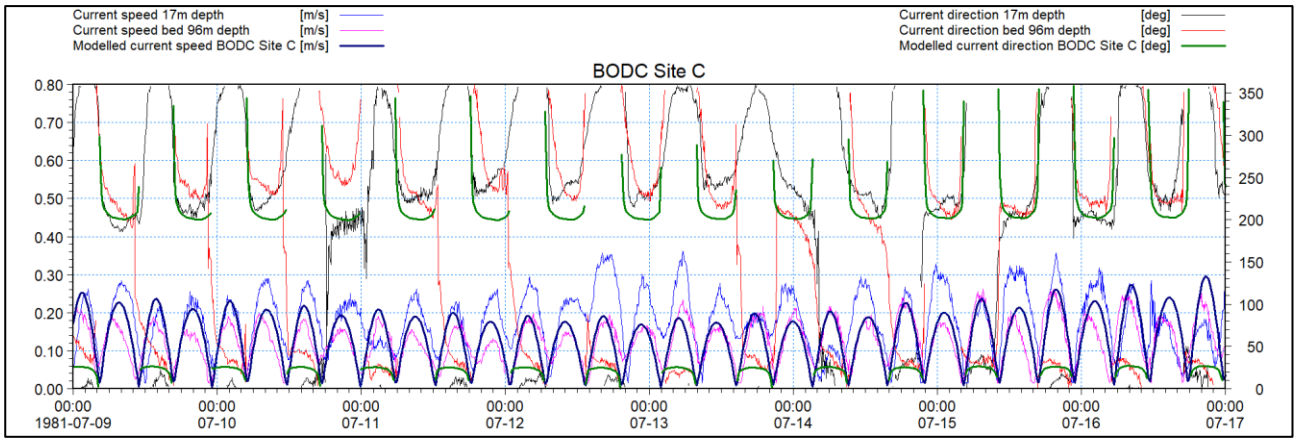

Figure 4A-32: Measured and modelled current speed (left axis) and direction (right axis) BODC Site C.

The BODC Site D data is presented in Figure 4A-33 and was collected during October 1994 using a paddle wheel current meter. Data was collected at depths of 17m and 98m at a location with a total water depth of 108m. The modelled current speed is of the same order of magnitude and largely correlated with the monitored data, whilst the principle current directions are well aligned.

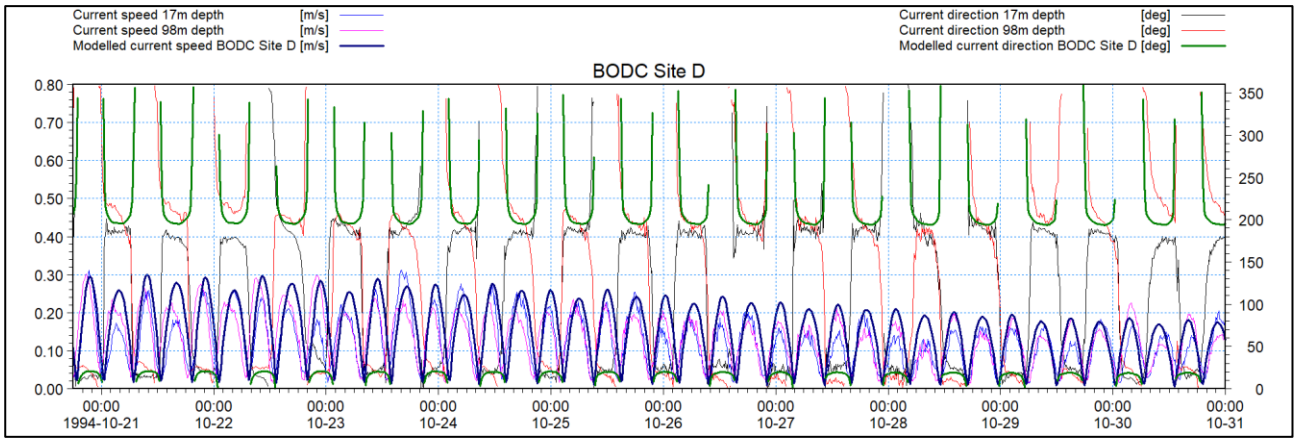

Figure 4A-33: Measured and modelled current speed (left axis) and direction (right axis) BODC Site D.

The BODC Site E data is presented in Figure 4A-34 and was collected during May 1994 using a paddle wheel current meter. Data was collected at a depth of 10m at a location with a total water depth of 22m. The modelled current speed is of the same order of magnitude and principle current directions are largely aligned. It is noted that on occasion, such as 12th May, the monitored current speed is significantly reduced during flood tide. There is a corresponding disturbance in current direction and it likely due to wind conditions running counter to the flood tide, which would be more evident in shallow water locations such as Site E.

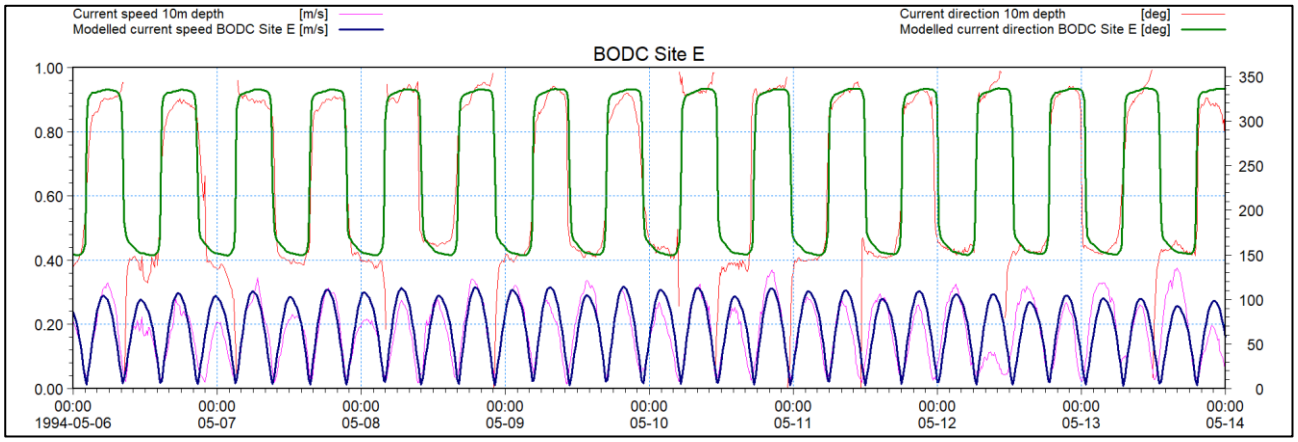

Figure 4A-34: Measured and modelled current speed (left axis) and direction (right axis) BODC Site E.

The BODC Site F data is presented in Figure 4A-35 and was collected during October 1994 using a paddle wheel current meter. Data was collected at a depth of 16m at a location with a total water depth of 26m. The modelled current speed is of the same order of magnitude and principle current directions are largely aligned. As with the previous dataset there are several occasions when the monitored current speed is significantly reduced during part of the tidal cycle. On 16th October this is associated with the two flood tides and 18th October it occurs on ebb tides. There is a corresponding disturbance in current direction on both occasions likely due to northerly and southerly wind conditions respectively. These would not be replicated within the modelled dataset as pure tidal conditions are simulated.

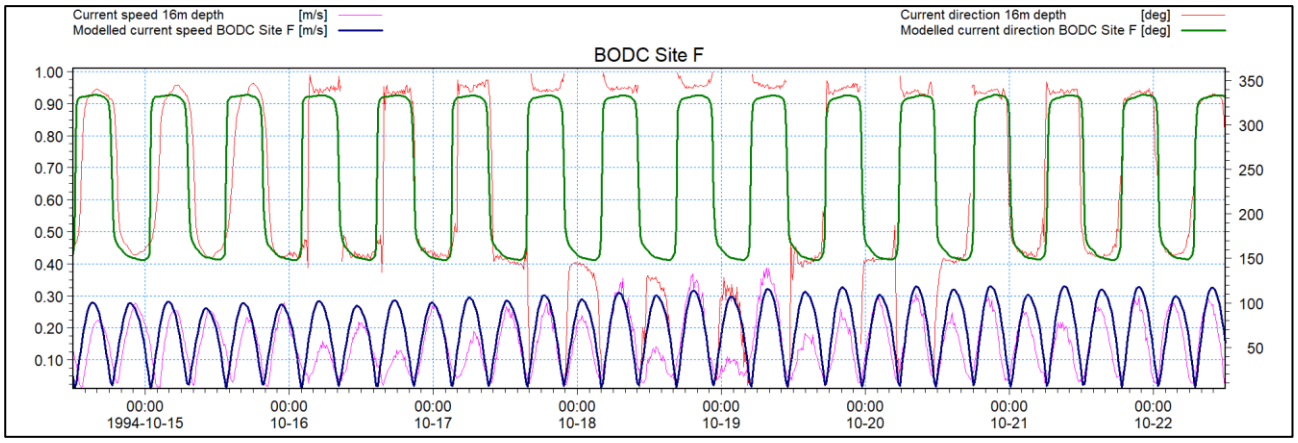

Figure 4A-35: Measured and modelled current speed (left axis) and direction (right axis) BODC Site F.

Overall, across the six locations, where there are not notable effects from meteorological conditions the model is seen to replicate the tidal flow regime in the wider domain.

5 SUMMARY

This Technical Report has quantified the baseline marine processes that characterise the Marine Processes Study Area. This includes tidal current, wave climate and sediment transport under both calm and storm conditions. The numerical modelling has supported the theory that sediment transport in the offshore wind farm area is limited due to the reduced current speed and nature of the seabed material and sediment supply.

Numerical modelling has been used to quantify the changes in tidal currents, wave climate and sediment transport due to the installation of the Project. Results from this modelling programme demonstrated that the presence of the turbine and offshore substation foundation structures has little effect on tidal currents and sediment transport potential. Likewise, the installation of the foundations was found to marginally alter wave heights within the Marine Processes Study Area with little influence beyond the immediate vicinity of the offshore wind farm area.

Finally, suspended sediment plumes associated with foundation drilling and cable installation activities were quantified. In most cases the material released was native to the existing seabed and although average turbidity levels were found to increase for short periods of time during installation, the increased levels were comparable to those experienced during storm conditions. The material released nearshore was subsequently assimilated into the existing sediment transport regime.

The Project is therefore not expected to have a significant effect on marine processes or make a significant change to the existing sediment transport regime.

References

BERR (2008). Review of Cabling Techniques and Environmental Effects applicable to the Offshore Windfarm Industry. Technical Report, Department for Business Enterprise and Regulatory Reform (BERR), in association with Defra, 164pp.

Brown, J., Fernand, L., Hill, A. E., Horsburgh, K. J., Garvine, R. W., Angelico, M. M. P. and Kerrigan, P. C. (2000), Circulation of the western Irish Sea, CEFAS poster, www.cefas.co.uk/Publications/posters/26573-2a.pdf

CEFAS (2016) Suspended Sediment Climatologies around the UK.

Gavin Doherty Geosolutions (2020) Oriel Ground Model Update & Cable Route Interpretation. PARTRAC (2020) Oriel Wind Farm – Floating LiDAR Buoy 12 Month Measurement Campaign Data Report.

Hill, A.E., Brown, J., Fernand, L., (1996) The western Irish Sea gyre: a retention system for Norway lobster (Nephrops norvegicus). Oceanologica Acta 19, 357-368

Hjulstrøm, F., (1939) Transportation of debris by moving water, in Trask, P.D., ed., Recent Marine Sediments; A Symposium: Tulsa, Oklahoma, American Association of Petroleum Geologists, p. 5-31.

Irish Coastal Protection Strategy Study (ICPSS), https://www.gov.ie/en/office-of-public-works/publications/irish-coastal-protection-strategy-study-icpss/

Ladson, A. R. (2008) Hydrology: An Australian Introduction. Oxford University Press.

Nash, J.E., Sutcliffe, J., (1970), River flow forecasting through conceptual models, Part I A discussions of principles, J. Hydrol., 10, 282-290.

Whitehouse, R.J.S., Sutherland, J. & O'Brian D., (2006), Seabed scour assessment for offshore windfarm, 3rd International Conference on Scour and Erosion, CURNET, Gouda, The Netherlands.

Willmott, C.J., Ackleson, S.G., Davis, R.E., Feddema, J.J, Klink, K.M., Legates, D.R., O'Donnell, J., Rowe, C.M., (1985), Statistics for the evaluation and comparison of models, J. Geophys. Res., 90, 8995-9005.